

Programa de Pós Graduação em Ecologia e Conservação

Centro de Ciências Biológicas e da Saúde
Universidade Federal de Mato Grosso Do Sul

**Taquari River Basin: a basin of contrasts, environmental challenges,
and ecosystem opportunities**

Rômulo Oliveira Louzada



Campo Grande
abril 2025

Taquari River Basin: a basin of contrasts, environmental challenges, and ecosystem opportunities

Rômulo Oliveira Louzada

Tese apresentada como requisito para a obtenção do título de **Doutor em Ecologia**, pelo Programa de Pós Graduação em Ecologia e Conservação, Universidade Federal de Mato Grosso do Sul.

Orientador: Fábio de Oliveira Roque

Co-orientador: Ivan Bergier Tavares de Lima

Banca avaliadora

Dr. Mauricio Almeida Gomes
INBIO/UFMS

Dr. Geraldo Alves Damasceno Júnior
INBIO/UFMS

Dr. Michael M. McGlue
University of Kentucky

Dra. Cátia Nunes da Cunha
INPP/UFMT

Dr. Diego Rodrigues Macedo
IGC/UFMG

Agradecimentos

Foram 4 (quatro) anos intensos, com desafios diversos, mas que valeram a pena. Essa caminhada foi assistida a todo momento por Deus e a espiritualidade amiga. Foram os guias espirituais que me deram inspiração e sabedoria para traçar os melhores caminhos. Gratidão eterna por essa missão!

Minha família, Iasmine (esposa) e Pedro Augusto (filho), este nascido durante a jornada do doutorado, foram outros alicerces nessa construção do conhecimento. O apoio incondicional da Iasmine e a inspiração do Pedro Augusto foram meus principais combustíveis. Nunca desisti por vocês meus amores.

Meus pais Vanyr e Pedro, que me ensinaram valores sobre a vida e educação. Educação esta que vale a pena! Só estou aqui por que vocês foram incansáveis no apoio e dedicação. Meu amor por vocês é infinito.

Minha irmã Laila. Minha admiração por você é inexplicável. De alguma forma você me inspira a ser uma pessoa melhor, portanto, essa conquista tem um dedo seu. Isso se estende a minha prima-irmã Ariane, que trouxe o primeiro título de doutorado para nossa família. Você também é exemplo para mim!

Aos meus familiares que me incentivaram de alguma forma e ao longo de toda a minha história, em especial à minha madrinha Tia Didi, Tia vera, meu padrinho Humberto e meu afilhado Pedro Henrique. Essa tese é nossa!

Meus colegas de caminhada no IMASUL, em especial ao presidente André Borges, que sempre me deu condições e apoio para desenvolver as pesquisas. Meu muito obrigado a todos vocês!

As pessoas que contribuíram para os trabalhos desenvolvidos aqui. Vocês nunca serão esquecidos: Michael M. McGlue, Giliane Rasbold, Leandro Luz, Edward Lo, Aguinaldo Silva,

Sidney Kuerten e Glauco Umbelino. Meu muito obrigado pela ajuda de vocês nas orientações, trabalhos de campo e publicações.

Aos meus amigos queridos Amaral e Cesar Sobradie, que sempre me apoiaram nessas idas e vindas pelo Caronal. Sem vocês nada disso seria possível.

Meu co-orientador Ivan Bergier. Obrigado por me mostrar que a ciência vale a pena. Obrigado por apostar em mim sem me conhecer. Obrigado pela dedicação em me fazer um pesquisador. Conseguimos!

Meu orientador Fabio Roque. Obrigado por me aceitar em sua vida e expandir meus horizontes. Creio que sou um profissional mais completo inspirado em você. Sua competência técnica e articulação entre diversos atores são invejáveis. Obrigado por me deixar fazer parte do seu mundo.

Índice

Abstract	7
Introduction	8
Section 1: Upper Taquari River Basin	13
Chapter 1 – Priority Setting for Restoration in Surrounding Savannic Areas of the Brazilian Pantanal Based on Soil Loss Risk and Agrarian Structure	13
Chapter 2 – Combining Optical and Microwave Remote Sensing for Assessing Gullies in Human-Disturbed Vegetated Landscapes	35
Chapter 3 – The First Inventory of Gullies in the Upper Taquari River Basin (Brazil) and Its Agreement with Land Use Classes	54
Chapter 4 – Spatiotemporal patterns of exposed soil in a highly eroded Brazilian river basin in 1985/2024: Is it the worst over?.....	76
Section 2: Lower Taquari River (Pantanal Wetlands)	98
Chapter 5 – River Channel Avulsion in the Taquari River Megafan of the Brazilian Pantanal: Remote Sensing and Modeling Reveal Recent and Future Changes	99
Chapter 6 – Fluvial Avulsions Influence Soil Fertility in the Pantanal Wetlands (Brazil).....	117
Conclusions	143
References	145

Abstract

River basins are geographically defined areas where water drains into a main river. These drainage systems mirror the environment, reflecting the interplay of physical factors such as relief, soil, geology, and hydrography, along with biological elements like vegetation and fauna. Consequently, disturbances in these systems trigger on-site impacts, which can escalate into off-site consequences downstream. Understanding how these impacts evolve over time and space and how they can be mitigated through compensatory ecosystem services (offsets) is the core focus of this study, which provides a comprehensive analysis of the Taquari River Basin in central-western Brazil. The Taquari River Basin is one of the most degraded watersheds in Brazil. It suffers from large-scale erosive processes in its upper region (UTRB) and excessive sedimentation in its lower reaches within the Pantanal wetlands. This sediment accumulation has led to river channel shifts (avulsion) and widespread flooding since the late 20th century. The study was divided into two sections: UTRB and the Pantanal to assess these environmental changes. A broad dataset, including remote sensing, spatial analysis, and statistical modeling, was used to investigate sediment dynamics and their impacts across the basin. A GIS-based Boolean algebra method revealed that 65% of the UTRB is at high or very high risk of soil loss, emphasizing the urgent need to stabilize gullies in the region. A complementary analysis using orbital remote sensing (optical and radar data) identified nearly 3,000 gullies, with 60% still active and only 2% stabilized, highlighting the necessity for immediate restoration efforts. Additionally, datasets from MapBiomas and the Rural Environmental Registry (CAR) underestimate exposed soil areas, suggesting the need for more precise land use classifications. A temporal analysis of exposed soil pixels from 1985 to 2024 revealed that soil exposure peaked in 2021 (3.4% of the UTRB) and decreased to 0.6% in 2024. By 2024, some of areas indicate a negative trend in bare soil pixels as a natural regeneration of vegetation process. However, factors such as commodity prices, climate variability, and environmental policies could influence this recovery trajectory. In the Pantanal, a fluvial avulsion model predicts the formation of a new river channel by 2080, reducing the flooded area and converting it into terrestrial land. This transition enhances soil fertility through organic matter accumulation, but it requires close monitoring to prevent negative outcomes such as deforestation and wildfires. The findings presented here provide a comprehensive assessment of the basin, offering insights for rural landowners facing erosion or flooding while also equipping public authorities with critical data for territorial planning. The study contributes to strategies for erosion control in the upper basin and the preservation of emerging ecosystem services in the Pantanal, particularly in terms of biodiversity conservation and carbon retention.

Introduction

The river basin serves as a mirror of the environment, capturing the interplay between physical drivers, including relief, soil, geology, and hydrography (Lin et al. 2006, Gardon 2021, Annis et al. 2022), biological factors such as vegetation and fauna (Giller & Malmqvist 1998, Wantzen et al. 2016, Chakraborty 2021), and human-induced interactions, commonly by land use, urbanization, or agricultural activities (Allan 2004, Yu et al. 2024). Its environmental conditions directly shape the quality and availability of water resources, making it a crucial unit for understanding a region's ecological and socioeconomic dynamics (Cabello et al. 2015, Cao et al. 2022). As units physically delimited by the relief, the river basins are strategically territorial to reveal the interactions between natural and anthropogenic factors (Warner et al. 2008, Huambachano et al. 2025). Therefore, this characteristic makes the basin essential for assessing environmental impacts, both on-site, at the local level of the intervention, and off-site, in areas downstream or outside the origin of the impact (Majoro et al. 2020). In general, local interventions driven by land use change (e.g. deforestation, soil compaction by machines) result in on-site degradations, including erosion and loss of soil fertility (Osman 2014). Consequently, the loss of particles leads to deposition downstream of watercourses, which can generate siltation and intensification of floods (He et al. 2020), in addition to water contamination by chemical elements transported in on-site erosive processes (Rashmi et al. 2022). The on-site consequences or off-site impacts may be harder to predict and control, yet they are vital for sustainable basin planning.

In examples of mitigating measures, studies show that local interventions, especially the restoration of native vegetation and the adoption of soil and water management and conservation practices, result in compensations/benefits (offsets or trade-offs) downstream of the basin (Singh et al. 2014, Zucca et al. 2021, Meshesha et al. 2024). Mechanisms for controlling soil or stopping soil loss have shown increases in water quality or quantity in China (Tian et al. 2023), Australia (Sonter et al. 2013), the United States (Dobre et al. 2022), as well as successful experiments on

the African continent (Diop et al. 2022). In Brazil, a country marked by intense land use and a history of degraded hydrographic basins, some assertive experiences, including Fonseca et al. (2022) in the savanna biome, Bega et al. (2024) in an Atlantic forest, and dos Santos (2024) in the Brazilian Amazon.

Another common approach in river basin management is the integration of ecosystem services. Well-conserved basins can provide essential regulatory services that sustain life, such as water production (Huang et al. 2022), native vegetation growth and carbon sequestration (Garrastazú et al. 2015), and biodiversity maintenance (Brauman et al. 2014). Additionally, provisioning ecosystem services, such as food production and extractivism (Bruna 2022), as well as cultural services, including contemplation, tourism, and recreation (Wang et al. 2024), contribute to a harmonious arrangement in preserved river basins. However, some services may transform into disservices over time and vary spatially (Xu et al. 2022). For example, grain production can negatively impact bee biodiversity around crops due to the application of agrochemicals (Arpaia et al. 2021), livestock farming can contribute to increased local deforestation (Haddad et al. 2024), and surface runoff and erosion can intensify in downstream waterways (Dampousse et al. 2024). Studies addressing the transformation of an ecosystem service into a disservice are common (see examples in Sun et al. 2020, Petsch et al. 2023, Liu et al. 2024). However, research exploring the opposite process remains scarce, where a disservice is reversed, or a new ecosystem service is generated.

In the central-western region of Brazil, an intriguing case in the Taquari River Basin is an example of how erosion, avulsion, and siltation can positively reflect on soil fertility, biodiversity, and water purification. The Taquari River is an important tributary of the Paraguay River, the main source of the Pantanal, one of the largest wetlands on the globe (Junk & Nunes da Cunha 2005). In its upper part, the Taquari River has relief, soils, geology, and human activities that favor the release of particles in the lower part of the Pantanal (Assine 2005, Couto et al. 2023). For more than 40 years, the silting of the river due to numerous erosion processes

has highlighted this basin. Consequently, the large volume of sediment is the main trigger for bed changes in the lower part of the basin, a phenomenon called river avulsion (Assine 2005).

When relocating the bed, large areas are flooded until the recanalization process matures (Buehler et al. 2011). Furthermore, the colonization of terrestrial environments by aquatic species is evident (Louzada et al. 2020), generating a new ecosystem. Louzada et al. (2021) had already mentioned that the avulsion in the Caronal region in the lower Taquari generated a flood of around 500 thousand hectares and that regulatory ecosystem services such as water purification, retention of sediments and nutrients by macrophytes, in addition to the increase in aquatic biodiversity and possibly carbon sequestration in the soil had been occurring since the beginning of the process in 1997.

In fact, the Taquari River Basin is a dynamic and heterogeneous system, where erosion and sedimentation processes occur in contrasting ways throughout its extension. In the upper part, intense erosion associated with intensive soil use predominates, while in the lower part, in the Pantanal, sediment deposition occurs, resulting in the formation of one of the largest alluvial megafans in the world (Assine, 2005).

Given this complexity, this thesis aimed to evaluate the interaction of these processes over time and space. For this, several sources of information were used, including field data on soil, land use and occupation, and macrophytes, as well as orbital remote sensing images. The analysis was supported by geographic information systems (GIS) tools, regression techniques, and modeling with machine learning algorithms. This broad methodological framework allowed an integrated assessment of past and current conditions and future projections of processes that impact the basin's ecosystem services and disservices, with an emphasis on sediment dynamics (erosion versus sedimentation).

Thus, this thesis was divided into two sections: Section 1 refers to the Upper Taquari (plateau), while Section 2 is the complement of the Lower Taquari (Pantanal). We begin with Chapter 1, Priority setting for restoration in surrounding savannic areas of the Brazilian Pantanal

based on soil loss risk and agrarian structure, published in the *Journal of Environmental Management*, in which the risk of soil loss was assessed through USLE-based map algebra and the identification of ideal points for locating large-scale erosion conservation practices (gullies).

In Chapter 2, *Combining optical and microwave remote sensing for assessing gullies in human-disturbed vegetated landscapes*, published in the journal *Catena*, we sought to create a method to classify gullies according to their degree of stabilization based on the percentage of pixels of exposed soil. This method was applied to a small set of erosions but later replicated for the entire upper Taquari, according to Chapter 3, *The first inventory of gullies in the Upper Taquari River Basin (Brazil) and its agreement with land use classes*, published in *Ecological Informatics*.

In Chapter 4, *Spatiotemporal patterns of exposed soil in a highly eroded Brazilian river basin in 1985/2024: Is it the worst over?* (unpublished) We seek to evaluate the distribution of exposed soil locations in the past and present with a new GIS tool and regressions from soil and vegetation indices from Landsat images, and superimposed on the slope layer, aiming to answer whether the worst is over.

The second section related to the Pantanal begins with Chapter 5, *River channel avulsion in the Taquari River megafan of the Brazilian Pantanal: Remote sensing and modeling reveal recent and future changes*, published in the journal *Applied Geography*, in which an assessment of changes in the landscape flooded by the avulsion was carried out using the R index (Louzada et al. 2020) between 1996 and 2021, and subsequently linear and non-linear modeling in networks until 2080 to evaluate the behavior in terrestrialization.

Finally, considering the results of the previous chapter, which indicated that the flooded area is slowly retreating and will tend to become effectively terrestrial by 2080, we sought to evaluate the impact of this drainage process on the fertility of currently flooded soils. Therefore, in Chapter 6, *Fluvial avulsions influence soil fertility in the Pantanal wetlands (Brazil)*, published in *Science of The Total Environment*, surface soil collections, satellite imagery, and modeling

using the Random Forest algorithm revealed that the rechannelization of the Taquari River is positively influencing carbon and nutrient retention in the soil. These results are strong evidence that the ecosystem disservice in Upper Taquari resulting from soil loss drives the regulatory service of nutrient cycling and the carbon sink in the Pantanal.

Section 1: Upper Taquari River Basin

Chapter 1: Priority setting for restoration in surrounding savannic areas of the Brazilian Pantanal based on soil loss risk and agrarian structure.

Abstract

Soil health is at the core of the sustainability agenda. As in many agroecosystems in the tropics, soil erosion is a major issue in poorly managed pasturelands. A noteworthy case is located in the Upper Taquari River Basin (UTRB), as part of the Upper Paraguay Basin on the plateau with drainage waters for the Taquari megafan in the Brazilian Pantanal. Here we combine slope (S-factor), erodibility (E-factor), rainfall-rainy day ratio (R-factor), and vegetation and soil indices (C-factor) to locate erosion risk and prioritize eco-engineering interventions via palisades and small dams in UTRB. The method consisted of assessing distinct weights between Universal Soil Loss Equation (USLE) factors in a GIS platform, providing 35 combinations of classes as low, moderate, high, and very high erosive risk. The validation of the method was based on the ravine and plain ground truths obtained from high-resolution raster data. The best weight of USLE factors aids to locate critical erosive sites and vegetation patterns. Then, erosion risk and interventions were analyzed according to land use and rural property sizes in the government's Rural Environmental Registry (CAR) database. Overall, the natural factors of slope and erodibility in a proportion of 25% and 75% in GIS algebra provided the best mapping accuracy result. About 65% of the UTRB has high or very high erosion risks, and 70% of the available area can be acknowledged as degraded pasturelands. A total of 4,744 erosion interventions were recorded, with an accuracy of 65.28% and 61.15% for check dams and palisades interventions, respectively. The number of necessary interventions in areas of native vegetation was almost 50% higher than in pasturelands. Even though micro landowners occupy most of the watershed, large properties have about ten times as many areas at high risk of erosion. The mutual cooperation between properties, independently of size, is supported by governmental public policies like incentives for ecosystem services restoration of critical gullies, with CAR compliance and fiscalization.

1. Introduction

Soil erosion is an important issue in implementing a Global Sustainable Agenda (Wuepper et al. 2020). Decreasing land degradation responds positively to six of seventeen UN Sustainable Development Goals (Keesstra et al. 2016). Eroded soils provide ecosystem disservices that refute their natural capital stocks (Dominati et al. 2010). The impact for landowners is direct, given the need for nonrenewable resources for maintaining agricultural production (Telles et al. 2013), but also indirect and cumulative for society due to loss of biodiversity and ecosystem services of support and regulation (García-Ruiz et al. 2017). Land use intensification scenarios associated with climate change estimate erosion rate growth of up to 66% by 2070 worldwide (Borrelli et al. 2020).

Agricultural countries in tropical regions invariably perceive soil loss as an unsolved task. For instance, Wuepper et al. (2020) put Brazil on the top shelf of soil loss at around $4 \text{ t ha}^{-1} \text{ yr}^{-1}$, almost twice the global average of $2.4 \text{ t ha}^{-1} \text{ yr}^{-1}$. Mapping active erosive features (Senanayake et al. 2020) or the location of interventions in severe erosions (Pourghasemi et al. 2020) are issues for conservation and food security, where GIS and RS are widely applied (Sepuru & Dube 2018). Spatialization makes it possible to plan mitigating actions and reduce impacts on and off-site (Boardman et al. 2019). At the landscape scale, the rate of soil erosion is critical for the quantitative assessment of land degradation (Abdulkareem et al. 2019). Models are the most appropriate tools for simulating soil erosion at a relatively large spatial scale (Gao & Wang 2019). Among the most widely used, the Universal Soil Loss Equation (USLE), developed by Wischmeier and Smith (1965) for agricultural sites in the United States, remains valid and commonly applied around the world to assess gross erosion or disaggregated soil sediments in plots (Alewell et al. 2019).

Much of such success of USLE is due to the ease of estimating factors influencing erosion, such as relief, soil erodibility, rainfall erosivity, and land use or cover changes, both by

remote sensing data (RS) and data layers within the Geographical Information System (GIS) platforms (Pruski et al. 2006). In this sense, RS with GIS techniques allows demonstrating a quali-qualitative picture of the risk of soil loss, broadening the view on the management of natural resources (Yesuph & Dagneu 2019). Despite the robustness of mathematical erosion prediction models, there is still room for uncomplex layer algebra techniques for the erosion risk dimension (Ewunetu et al. 2021), which is very appropriate for decision makers to flash allocation of resources for local restoration (Pena et al. 2020).

Spatialization of active erosive alone is not enough for setting priorities for restoration. Although there have been significant advances in increasing ecological resilience on a large scale (Beller et al. 2019), landscape restoration projects need to incorporate socioeconomic dimensions, such as governance, social-political, and financial constraints, and agrarian structure because they are key determinants of restoration success (Armsworth 2014).

Here we use a highly tropical eroded area around the Pantanal, the biggest continuous wetland in the world, as an example to apply a multi-criteria approach based on USLE parameters on a GIS and RS that identifies priority areas at risk of soil loss and land restoration, including drainage criteria from high-resolution RS, through small dams and palisade interventions. Furthermore, we analyze the agrarian structure of the region and discuss possible solutions to mitigate the problem based on the fact that the real agents are the rural landowners. We choose the noteworthy Upper Taquari River Basin (UTRB) as a study case because this region has experienced rapid land cover clearance over the last 30 years (Roque et al. 2016). Gigatonnes of topsoil layers have been transported to the Pantanal by uncontrolled runoff, conjointly with the loss of invaluable biodiversity (Bergier 2013, Lo et al. 2022). As climate changes may alter rainfall and droughts patterns in the Pantanal watersheds (Thielen et al. 2020), one can expect an increase in summer river runoff and sediment load to the plains (Bergier et al. 2018), and an increase in winter wildfire recurrence, both adversely affecting Pantanal's biodiversity and ecological functioning (Silva et al. 2019, Libonati et al. 2020). For the sediment load, Colman et

al. (2019) pointed to up to 40% increased soil loss by 2050 from land-use changes, accompanied by on-site (UTRB) and off-site (Pantanal) pesticide inputs (Roque et al. 2021), and a greater probability of river avulsions of the Taquari River in lowlands (Bergier et al. 2018, Louzada et al. 2020, 2021).

2. Material and methods

2.1 Study Area

As an important watershed of the Upper Paraguay River Basin (UPRB), the Upper Taquari River Basin (UTRB) covers 28,111km² of the states of Mato Grosso and Mato Grosso do Sul in the central-western region of Brazil, bounded by latitudes 17°30'S to 19°30'S and longitudes 53°00'W to 55°00'W (Fig. 1). The elevation ranges from 178 to 921m above sea level. In general, the relief is a mosaic of depressions, isolated planes, and elongated plateaus, highlighting the Maracaju plateau near the city of Coxim, which shares the plateau with the Pantanal (plain). The rivers of the UTRB are geologically stable through bedrocks, but connected to unstable alluvial systems in the Pantanal wetland (Assine 2005). The systematic decrease in the longitudinal gradient in the Pantanal associated with the high sediment load of the uplands determined one of the most notable depositional systems in the world, the Taquari megafan (Assine 2005).

A large part of the UTRB soils originates from sedimentary rocks. Therefore, it presents deep horizons with sandy texture and low natural fertility (Galdino et al. 2005). In terms of precipitation, the summer rainy season runs from November to March (Marengo et al. 2015), ranging from 1,700-1,800mm in the extreme NE to 1,200mm in the S and SW regions (Thielen et al. 2020). Regarding vegetation and land use, the original formation of the Cerrado (Brazilian savanna) was gradually replaced by grazing on sandy soils and agriculture on clay soils after the 1970s (Galdino et al. 2005, Souza et al. 2020).

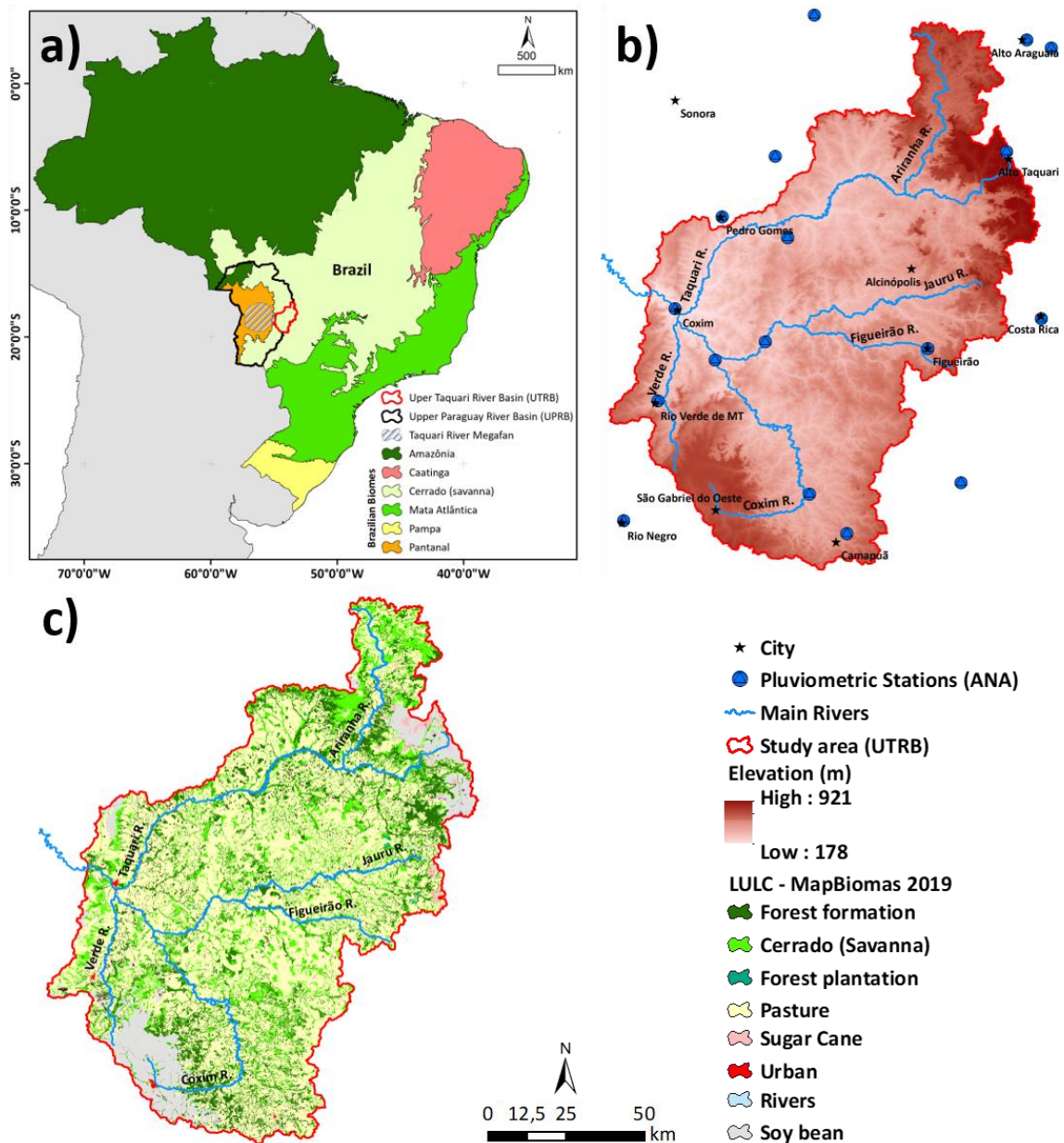


Fig. 1. Location of the Upper Taquari River Basin. (a) official map of Brazilian biomes with emphasis on the UTRB as part of the UPRB and located in the Cerrado, as well as the Taquari megafan in the Pantanal; (b) cities, main rivers of UTRB and rainwater stations of “Agência Nacional das Águas - ANA” used to calculate the rainfall index (item 2.2.1), overlaid by DEM ALOS-PALSAR (item 2.2.3); (c) Land Use/Land Cover from MapBiomas project of 2019 (Souza et al. 2020).

2.2 Soil erosion risk

The erosion process can be suitably represented and modeled in the GIS environment (El Jazouli et al. 2017). Here, we apply the USLE logic with other principles of geospatial analysis on ArcGIS® version 10.4.1. In the original equation of USLE, $A = RKLSCP$, where R is erosivity from rainfall, K is soil erodibility, LS is the topographic factor, and C and P refer to

cover and management. Our set of factors preserved only the erodibility factor (E), replacing the original elements of the USLE, such as rainfall index (R), slope (S), and the best vegetation index (C). Here, conservation practices corresponding to the P-factor were excluded from the multicriteria analysis due to missing updated data. Thus, our final equation was *Erosion risk = RESC*, whose weights for each variable are established in item 2.3.

2.2.1 Rainfall index (R)

In tropical regions, precipitation is the most important driver of the erosive process. Summer heavy rains have been more frequent in the last decade in the UTRB (Bergier et al. 2018, Thielen et al. 2020). Thus, we consider the method of Bergier et al. (2018) more relevant to compose the R factor as it calculates the rain index as a simple ratio of historical total precipitation in mm to the sum of rainy days. The data were collected at ANA pluviometric stations available in the hidroweb (<https://www.snirh.gov.br/hidroweb/>). A total of 21 stations were selected (see Fig. 1b) based on location criteria, within or within 50km of the UTRB seeking to fill the entire study area. The results of the ratio are shown in Supplementary Material (see Table S1). The R factor as raster data was prepared by kriging available on ArcGIS spatial analyst tools applying the default parameters across the watershed boundaries.

2.2.2 Soil erodibility (E)

The spatialization of soil erodibility was based on the recent review of the theme by Godoi et al. (2021) using multilayer soil properties in a cell size of 250m.

2.2.3 Slope (S)

The topographic slope factor was generated from DEM of ALOS-PALSAR images, specifically, the radiometric terrain corrected by resampling of SRTM with a spatial resolution of 12.5m (Laurencelle et al. 2015), available at (<https://search.asf.alaska.edu/#/>). Table S2 shows the list of scenes for the DEMs mosaic (Fig. 1b) and slope (S).

2.2.4 Land Use/Land Cover (C)

Land use and land cover generally vary with the seasons. This is the case of agriculture, whose planting of grains in Brazil has, on average, two harvests interspersed with a fallow period to control Asian soybean rust, which lasts from June to September in the Cerrado biome (Seixas & Godoy 2007). During these months, the soil is exposed to runoff but that practice is made at the apex of the dry season, which would wrongly entail potential erosive risk. In this sense, the vegetation indices of orbital images are useful to extract seasonal surface features to calculate the C factor in the USLE (see applications in Durigon et al. 2014, Chen et al. 2019).

Here, we tested eight vegetation and soil indices two times (Table 1), September 2020 (dry) and April 2021 (wet-dry transition) using Sentinel-2A Level 2 data available from the European Space Agency (<https://scihub.copernicus.eu/>). For the calculations, we use the SNAP software version 8.0.0 (<https://step.esa.int/>) on spectral bands green (G), red (R), and near-infrared (NIR) with a pixel resolution of 10m.

Table 1. List of vegetation and soil radiometric indices applied to the calculation of C. factor.

Type	Index	Equation	Reference
Vegetation	Normalized Difference Vegetation Index (NDVI)	$(NIR - R) / (NIR + R)$	Rouse et al. (1973)
	Transformed Normalized Difference Vegetation Index (TNDVI)	$\sqrt{(NIR - R) / (NIR + R) + 0.5}$	Senseman et al. (1996)
	Enhanced Vegetation Index (EVI)	$2.4 * (NIR - R) / (NIR + R + 1)$	Jiang et al. (2008)
	Soil Adjusted Vegetation Index (SAVI)	$(1 + L) * (NIR - R) / (NIR + R + L)$	Huete (1988)
	Transformed Soil Adjusted Vegetation Index (TSAVI)	$s * (NIR - s * R - a) / (s * NIR + R - a * s + X * (1 + s^2))$	Baret & Guyot (1991)
	Modified Soil Adjusted Vegetation Index (MSAVI)	$(1 + Z) * (NIR - R) / (NIR + R + Z)$	Qi et al. (1994)
	Soil	Brightness Index (BI)	$\sqrt{(R^2) + (G^2) / 2}$
Colour Index (CI)		$(R - G) / (R + G)$	Escadafal (1989)

Terms of the above equations. SAVI: L is the adjustment factor; TSAVI: a is the soil line intercept; s is the soil line slope; X is the adjustment factor to minimize soil noise. For MSAVI, the Z is calculated by $(1 - 2 * NDVI * s * (NIR - s * R)) / (1 + s^2)$, where s is the soil line slope.

The process of choosing the best date and index to obtain the C factor was based on the comparison of the difference of the means between samples of a gully (high risk), obtained at a scale of 1:10,000 of the high-resolution base map ArcGIS, and the opposite flat relief (low risk),

with agricultural areas practice (Fig. S1 in Supplementary Material). Besides, the Sentinel-2 scenes were used to replicate the method and compose the *C-factor* mosaic in the UTRB according to the two possibilities of date imagery (all scenes and multispectral bands information are shown in Table S3).

2.3 Multicriteria analysis and validation

Before multicriteria analysis, spatial factors were resampled to the same 10m *C-factor* resolution. The natural breaking method was applied in the reclassification of all rasters (Gao & Wang 2019), as low risk of erosion (class 1), moderate (class 2), high (class 3), and very high risk of soil erosion (class 4).

In this study, we evaluated the importance of each factor using weights in the raster calculation tools. Thus, a set of possibilities was derived by considering an increase of 25% in the factor, hence totalizing 35 tests (Table 2).

Table 2. Algebra map scheme to calculate soil erosion risk tests. In correspondence to the original USLE elements, S is the topographical factor, E is the soil erodibility, R represents the rainfall index factor and C is the land use/land cover factor.

Test	Algebraic model	Test	Algebraic model	Test	Algebraic model	Test	Algebraic model	Test	Algebraic model
1	S1	8	$S0.5+E0.25+R0.25$	15	$S0.25+E0.5+C0.25$	22	$E0.75+R0.25$	29	$E0.25+R0.75$
2	$S0.75+E0.25$	9	$S0.5+E0.25+C0.25$	16	$S0.25+E0.25+R0.5$	23	$E0.75+C0.25$	30	$E0.25+C0.75$
3	$S0.75+R0.25$	10	$S0.5+R0.25+C0.25$	17	$S0.25+E0.25+C0.5$	24	$E0.5+R0.5$	31	R1
4	$S0.75+C0.25$	11	$S0.25+E0.75$	18	$S0.25+R0.5+C0.25$	25	$E0.5+C0.5$	32	$R0.75+C0.25$
5	$S0.5+E0.5$	12	$S0.25+R0.75$	19	$S0.25+R0.25+C0.5$	26	$E0.5+R0.25+C0.25$	33	$R0.5+C0.5$
6	$S0.5+R0.5$	13	$S0.25+C0.75$	20	$S0.25+E0.25+R0.25+C0.25$	27	$E0.25+R0.5+C0.25$	34	$R0.25+C0.75$
7	$S0.5+C0.5$	14	$S0.25+E0.5+R0.25$	21	E1	28	$E0.25+R0.25+C0.5$	35	C1

To validate the maps, we preserved the method of comparison of eroded to non-eroded themes in item 2.2.4., including 2 preserved flats sites and 32 gullies spatialized in the UTRB (see examples in Figure S2). The selection was done by the average percentage of pixels in class 4 (very high) expected for gullies and class 1 (low) for flat sites. The locations of all validation samples in the UTRB are exhibited in Figure S3 of the Supplementary Material.

2.4 Locations for intervention

An effective gully recovery scheme should consider vegetative, edaphic, and mechanical techniques (Machado et al. 2006), especially on fragile soils primarily composed of sand (Filizola et al. 2011). For quick mitigation of soil losses, we evaluate the best location of recovery techniques for gullies. Hence, the methods of intervention were based on principles of ecohydrology or eco-engineering (e.g., low landscape impacts, organic and in situ materials), in contrast to classical civil engineering (Norris et al. 2008). Within the scope of techniques, we evaluated the palisades represented by perpendicular posts of bamboo or *Eucalyptus sp.* wood installed on sloping lands, which previously have shown promising results (Tardio et al. 2017, Rodrigues 2018). Likewise, checking (small) dams through the soil, sandbags, or stone lines in the gullies' bed have been effective in reducing stream flow (Xu et al. 2020).

To determine the points suitable for palisades and check dams, firstly we vectored all drainage lines in the UTRB in a similar way to gully samples. In total, 31,413 drainages were identified (see Fig. S3 on the Supplementary Material). This step was necessary because ANA's official watercourses are incomplete, displaced, and do not include erosions' ramifications. Palisades were calculated by transforming the starting line into a point, then selecting only combined points in class 4 that pixels are in the appropriate erosion risk test. To avoid false positives, we added another layer of exclusion based on thresholds of the 2019 map of Mapbiomas of savanna and forest formation, which was derived from one of the land use factors in Table 1 that were not applied in the assessment tests.

For check dams, we analyzed the distribution of drainage length in gullies samples, looking for lines in a range equal to the last quartile of erosion lines. The results showed that 22,313 features had an equivalent length (123m ~ 1,623m). In hydrographic basins, the main trunk river is the regional base level. For ravines, the bed is also expected to be at the local minimum, hence an adequate point of sediment impoundment. Sequentially, the nodules of the lines were changed to points with the selection clause where once again lines overlapped by class

4, excluding the points of the palisades and the same vegetation thresholds.

The assessment of eco-engineering interventions was also referenced in the high-resolution image from the base map plugin of the ArcGIS. Using a simple random points sampler, with a 95% confidence interval, at a minimum distance of 1km, it was possible to visually inspect whether palisades and check dams were in erosion (valued 1) or not (valued 0).

2.5 Exploratory analysis of the Forest Code CAR data

The degree of compliance with environmental legislation on farms, established by the Brazilian Forest Code (Law 12,651/2012), is precisely linked to the size of the property (Stefanes et al. 2018). Thus, we searched for the Rural Environmental Registry (CAR) database available on the SICAR website (<https://www.car.gov.br/publico/imoveis/index>), which gathers the main attributes of rural properties, to support a conservation action prioritization plan at the farm scale. Here, we selected the layers of: i) total area; ii) Legal Reserve (RL) area with a minimum of 20% of native vegetation; iii) permanent preservation area (APP) that represents the riparian watercourse; and iv) unrestricted or consolidated area (AC) for economic activities, mainly as providing services of food (meat/grain), timber/fiber (planted wood) and liquid biofuels (sugarcane/grain). An example of layers of property is shown in Figure S4.

The polygons of properties were divided into four categories according to the Forest Code: micro (0 to 4 modules), small (4 to 10 modules), medium (10 to 20 modules), and large (above 20 modules). The modules vary according to the size of the municipality, for which ranges were arbitrarily chosen except for the first category (up to four modules) belonging to a general rule of the forest code for special APP size treatments.

3. Results

3.1 Suitable C-factor

The gully and the flat terrain are close together and located in the same Sentinel-2 scene, therefore sharing the same weather conditions. In addition, their sizes are equivalent, with 5.73

hectares (576 pixels) for the canyon and 5.34 hectares for the plain (538 pixels). Here, we assume the indices are positive and closer to the maximum for photosynthetically active vegetation. In this case, it resembles grasses or plantations in the flat relief area, while in the exposed soil of the gully the values tend to be much lower. The means of indices from the dry period (September 2020), and the transition of wet/dry (April 2021) are shown in Table 3. The vegetation indices for April 2021 were more consistent regarding the differentiation premise between healthy vegetation and exposed soil. In general, the indices presented similar results, but the MSAVI factor was chosen to compose the *C-factor* because it overlaps the others on differences between the antagonistic areas.

Table 3. Mean of vegetation and soil radiometric indices between September 2020 and April 2021.

Index	September 2020		Difference	April 2021		Difference
	high	low		high	low	
NDVI	0.38	0.53	-0.15	0.36	0.59	-0.23
TNDVI	0.40	0.53	-0.13	0.39	0.59	-0.20
EVI	0.38	0.53	-0.15	0.36	0.59	-0.23
SAVI	0.36	0.55	-0.19	0.37	0.61	-0.24
TSAVI	0.79	0.55	0.24	0.52	0.62	-0.10
MSAV I	0.37	0.55	-0.18	0.35	0.61	-0.26
BI	0.40	0.51	-0.11	0.38	0.44	-0.06
CI	0.53	0.49	0.04	0.67	0.47	0.20

3.2 Maps of soil erosion risk in UTRB

The Rainfall Index (*R*), Soil erodibility (*E*), Slope (*S*), and Land Use/Land Cover (*C*) factors are shown in Figure 2. The *R* data, derived from the ANA database, showed a coefficient of variation $CV = 8.9\%$, in which the first class of low erosion risk varied from 13.36 to 15.22, mostly in the center-north area that gathers most of the UTRB. In contrast, higher potential areas for soil erosion (17.82 to 19.35) were restricted to the extreme south and southwest.

The soil erodibility map produced here clearly evidences the predominance of the very high class, determined by quartzarenic neossols and cambisols with 0.020 to $0.042 \text{ t}\cdot\text{ha}^{-1}\cdot\text{MJ}^{-1}\cdot\text{mm}^{-1}$ over 23.58% of the total area. The high class of erodibility was predominant with 40.27%

of UTRB ranging from 0.016 to 0.020 t.ha⁻¹.MJ⁻¹.mm⁻¹, comprising litholic neosols and plinthosols. The least restrictive class of low soil loss (0.002 to 0.011 t.ha⁻¹.MJ⁻¹.mm⁻¹) gathered flat areas with planosols and gleysols in about 11.44%.

An average value of 5.19° or 9.23% of the third factor (*S*) was presented, however, the most important declivity class gathered almost 61% of the pixels distributed between 0° and 4.71°, called low in our soil model, and correlated to 0-3% and 3-8% of Embrapa's flat and smooth wavy relief, respectively. The second prominent class by area was the moderate with 31% of the pixels in a range from 4.71° to 10.54° of the slope. Extremes of mountainous (very high) represented just over 2% of the pixels.

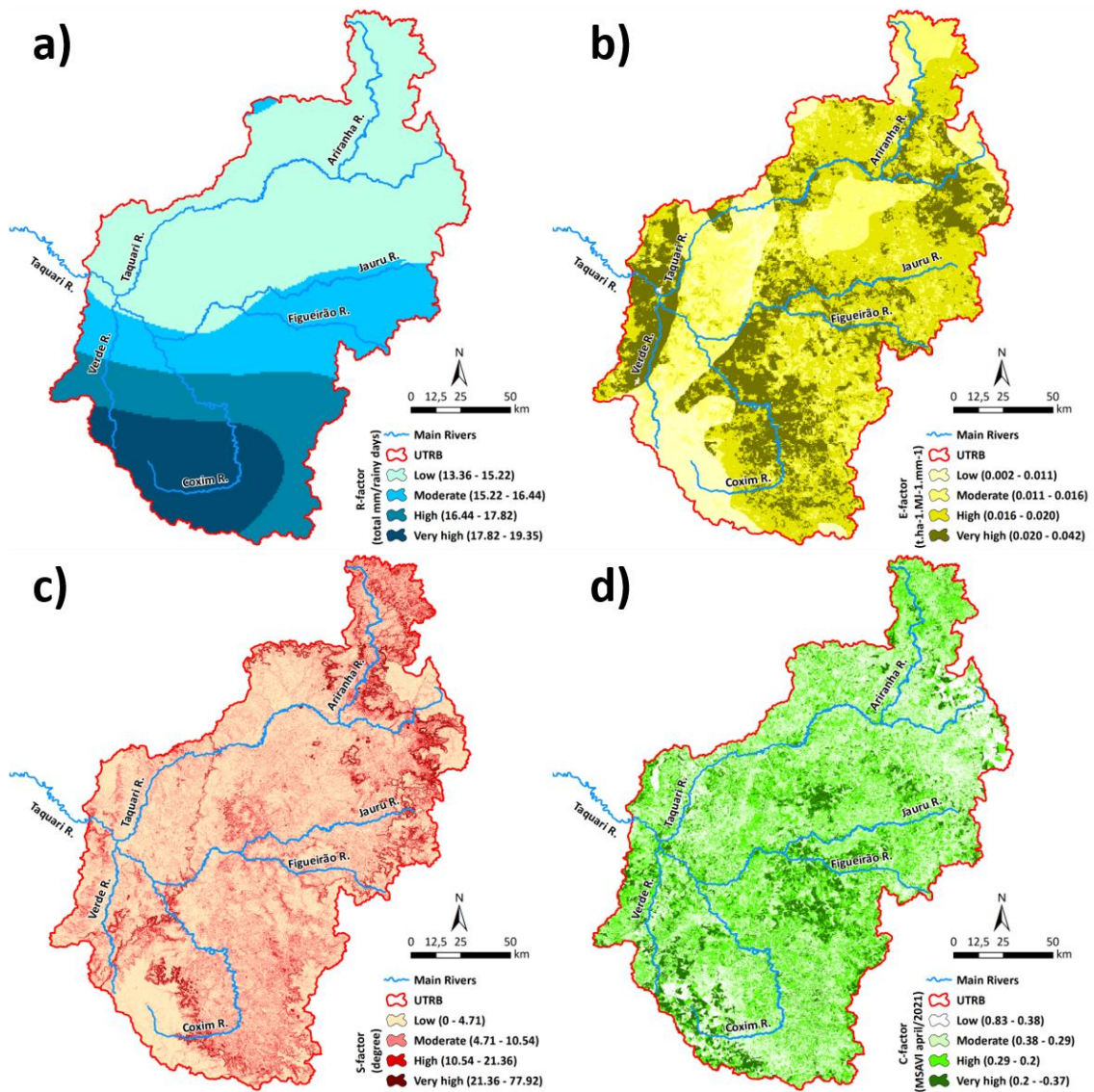


Fig. 2. The sequence of the factors for soil erosion risk evaluation: a) Rainfall index (R), b) Soil erodibility (E), c) Slope (S), and d) Land Use/Land Cover (C).

The MSAVI high values are related to the low probability of soil loss and vice-versa. The map of Figure 2d showed that approximately 76% of the area is included in moderate (41%) and high (35%) classes. The most fragile class ranged from 0.2 to -0.37, occupying approximately 14%.

The thirty-five assessments of soil erosion risk (USLE) were calculated based on the combination of factors and respective weights (Table 2). Altogether, gully and flat samples generated 18,808 and 10,222 pixels. The evaluation was carried out using a percentage of pixels in the most restrictive or very high associated with the flat or low probability of soil loss (Fig. S5). An isolated observation for the two parameters points out in test 13 (S0.25 + C0.75) with 71.15% of the pixels in the very high class for the gully samples. In the flat sample, test 21 (E1) showed 100% of pixels within the low range, nonetheless, the combination of samples brought test 11 (S0.25 + E0.75) with the highest average with 67.43% of pixels with low and/or very high erosive risk.

Test 30, in which all factors have the same 25% weight, was closest to the original USLE. However, the pixel average of 5.03% in the very high and low classes for the ravine and flat area samples did not accredit it for the final map of the erosive risk. The algebraic models in which the *R-factor* was predominant showed the worst outputs in the means, such as test 6 and tests 31 to 34. In summary, the spatial discrepancies between tests 6 and 11 can be verified in Figure 3.

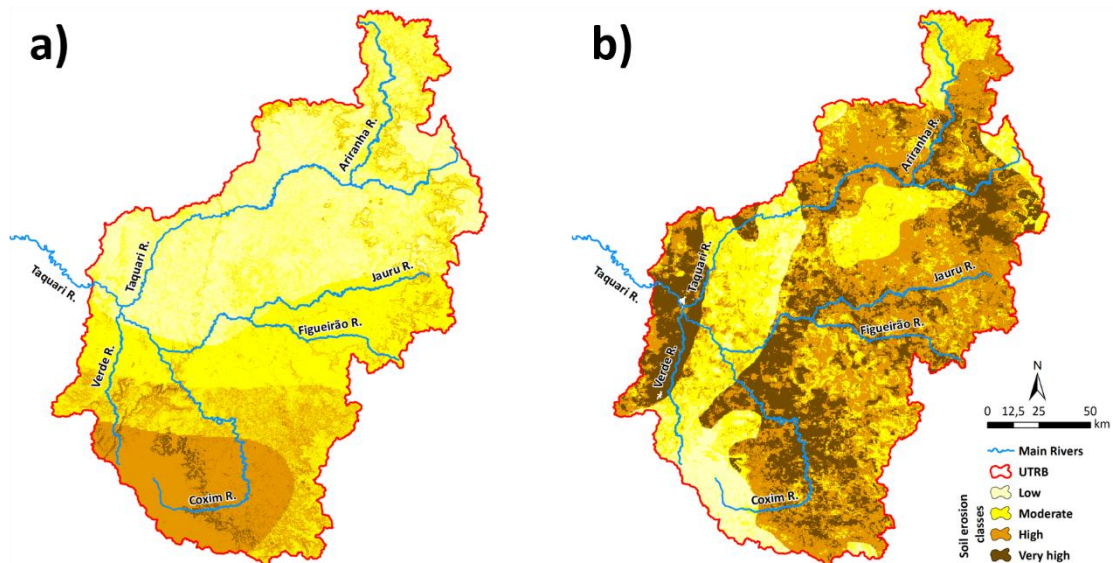


Fig. 3. Comparison map between the worst risk of soil erosion (a) of test 6 for 50% of *S-factor* and *R-factor*, and the best (b) of test 11 for 25% of *S-factor* and 75% of *E-factor*.

3.3 Analysis of interventions in gullies

As expected, the UTRB presented many interventions led by the critical class 4 rate. Based on the land cover results in Table 3, we included the NDVI thresholds from the 2020 image of forest formation (>0.65), savanna (>0.57), and water (<0) to eliminate false positives (Fig. S6). Thus, the spatial algebra identified suitable locations for 3,604 check dams and 1,140 palisades (Fig. 4). The state of MS had 3,598 or 76% of the total interventions, however, both states presented comparable densities of palisades and check dams per area, with 0.15 (MS) and 0.30 intervention/sq.km (MT).

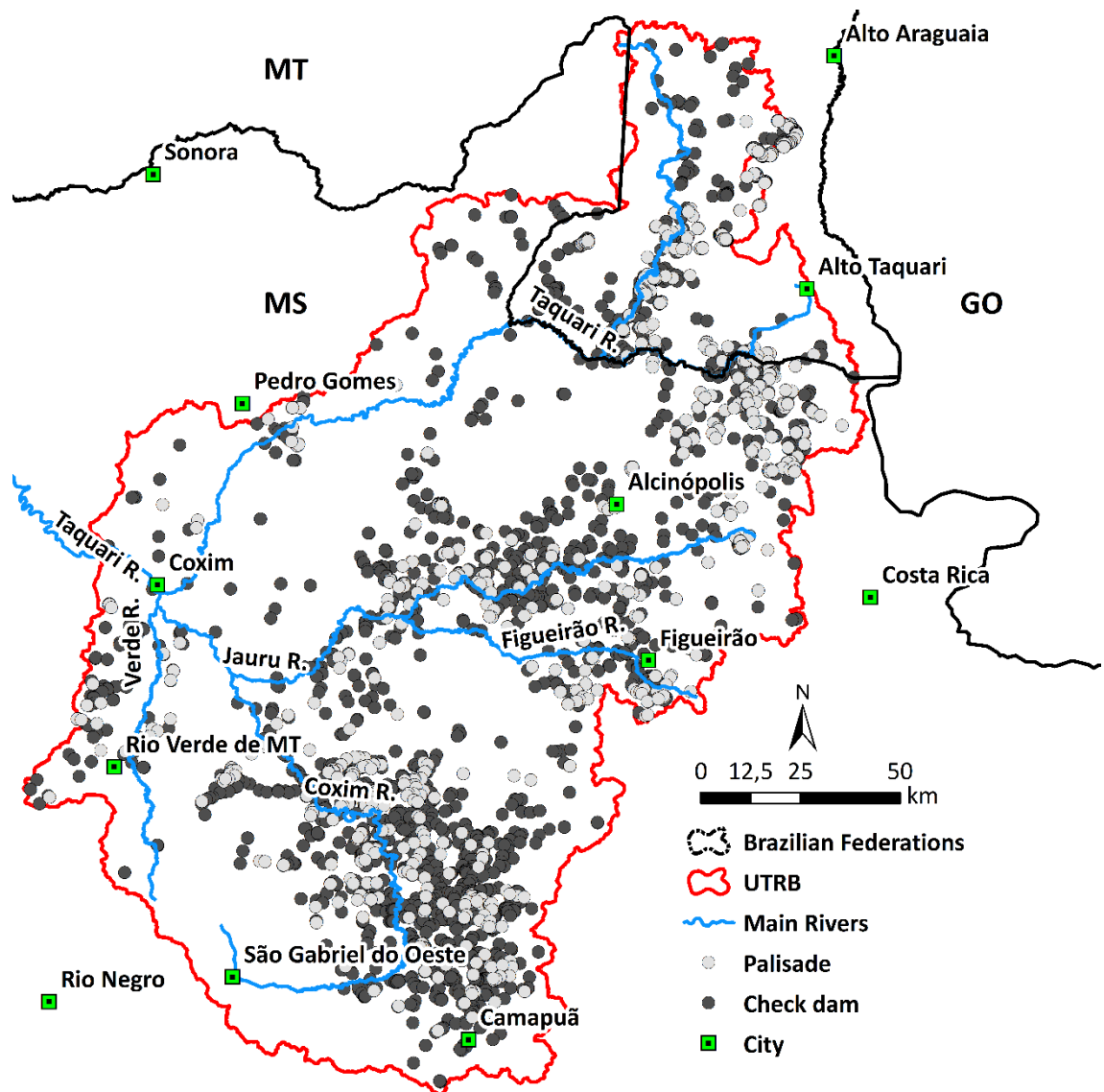


Fig. 4. Suitable areas for interventions with palisades and check dams detected in the UTRB.

The method for finding places for interventions was validated by the random sampler, with 95% CI, resulting in 360 and 296 samples for check dams and palisades, respectively. The validation indicates that 235 points or 65.28% of the check dam were assigned correctly considering the criteria described in item 2.4 (all sample points are shown in Table S4). On the other hand, palisade locations achieved a slightly lower percentage of 61.15%, representing 181 points. Figure 5 depicts examples of the validation process with confirmed/unconfirmed points.

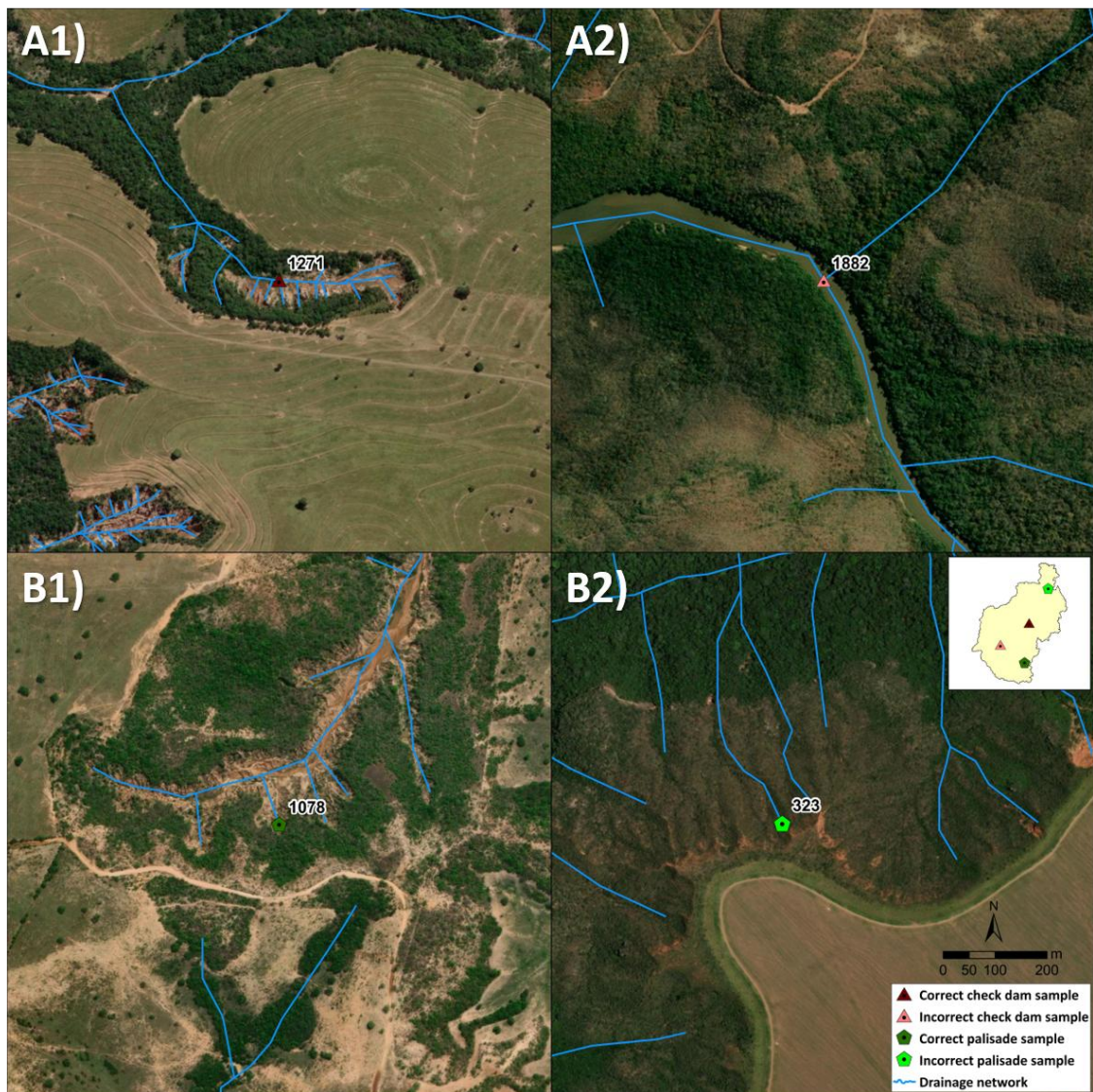


Fig. 5. Examples of check dams (A) and palisades (B) samples overlaid by a high-resolution orbital image available in the ArcGIS plugin. The numbers indicate those correctly (A1 and B1) and incorrectly (A2 and B2) determined by GIS algebra.

The method for the location of dam interventions showed promising accuracy, however, some drainage end points coincided with sandbanks in trunk rivers, such as the Coxim River in A2 in Fig. 5. Overall, the palisades were correlated with the environment ruled by the sloping terrain and unprotected soil, despite some non-exclusions by native gramineous (see example B2 on Fig. 5).

3.4 Integration of soil erosive risk, interventions, and CAR database

About 62.71% of the UTRB is composed of micro properties ranging from 0.24 to 279.9 hectares, including rural settlements, whereas less than 10% represent large properties above

767.9 hectares. In absolute terms, the area at high and very high risk of soil loss in large farms is almost 3 times the sum of micro, small and medium properties. However, the size of the property little influenced the average risk of soil erosion (see Fig. S7a), since all classes were close to 3 (high potential), and one-way ANOVA indicates no significant differences between classes of areas ($p = 0.33$). In comparison to the property's sizes, the features of AC, APP, and RL (Fig. S7b) were also equivalent with a mean erosive risk close to 3 but have significant differences by ANOVA ($p = 1.48E-7$), with RL distinct from AC and APP by Tukey's pairwise test ($p < 0.01$).

By linking the 4,744 intervention points with polygons of 6,571 properties of the SICAR database within the limits of the UTRB, we found that 8.3% of the dams and palisades were in micro properties, followed by 17.4 in small properties, 23.9% in medium size, and 50.3% inside large properties. In terms of internal polygons, AC has demanded 774 interventions, followed by RL with 1,452 and APP with 1,369 intervention points. The number of degraded lands in protected areas by legislation (RL and APP) was almost 50% higher than AC.

4. Discussion

4.1 Main drivers of soil loss in the region

The relative roles of land use and soil properties in shaping patterns of soil loss vary in different landscapes. Here we figured out that relief and erodibility are the main drivers. This finding calls into question the weight of anthropogenic changes in land use as the main factors of soil loss in the basin. On the other hand, recovery strategies directly involve farmers in the correct management of pastures added to the installation of mechanisms to stop the flow of eroding sediments. Our set of multi-criteria rules based on USLE principles, GIS algebra, and RS data allowed us to infer that about 65% of the UTRB area has a high risk of soil loss. Relief and soil properties are commonly highlighted as decisive factors in the erosion rate (Ruiz-Sinoga & Diaz 2010, Lu et al. 2020), however, as a new contribution, we demonstrate that the soil cover factor does not seem to play the main role designed by Galdino et al. (2005), recently updated by

Guerra et al. (2020). This may have occurred due to the fact that the most restrictive class of MSAVI belongs to portions with the total absence of vegetation (Sarparast et al. 2020), belonging to only 0.7% of the basin according to Mapbiomas 2019 (Souza et al. 2020). Even so, considering that the poorly managed pasture is the main villain of the erosive processes of the savanna pastures (Galdino et al. 2016, Colman et al. 2019), future studies maintaining our finest spatial resolution may add a possible correction to these effects by integrating the C-factor to the P-factor for erosion on a regional scale (Panagos et al. 2015).

4.2 Methodological challenges

Easy, fast, and free data for soil resource management is one of the bottlenecks for developing countries (Rosas & Gutierrez 2020). As an open database, our algebra method exploited freely available resources and data. So, it can be a promising alternative for planning the territory of hydrographic basins already degraded by erosion, especially in developing countries (Mennecke & West Jr 2001, Arabameri et al. 2019). Other advancements may provide for the inclusion of accurate relief models (see TanDEM-X performance at Boulton & Stokes 2018). In addition, the analysis of soil spectral responses by RS would provide proxies for new pedological maps (Poppiel et al. 2019), which can contribute to the greater accuracy of the model. In the same way, the role of land cover, more precisely of native vegetation, could be aggregated in the form of historical data. That eliminates, for example, the focus on places with high potential for natural erosion, but the regeneration of vegetation cover has been mitigating the effect of rainfall on the soil (Zhang et al. 2004, Gahrizsangi et al. 2021).

The identification of locations with erosion for recovery interventions is the main outcome of our proposed spatial algebraic rules. We identified 4,744 interventions, 76% of which are suitable for controlling dams. Proportionally, this is much higher than the 327 check dams reported by Rahmati et al. (2019), and 27 by Dash et al. (2021). According to our accuracy assessment, more than 60% of the palisades and check dams had locations related to severe

erosive features, however new layers to false positive exclusion due to the influence of vegetation can be coupled in the method. By putting this into practice, we provide a basis for decision-makers to block more than half of the concentrated flow of sediment in the basin.

We emphasize that the zoning of interventions within erosions was only possible with the vectorization of the drainage lines through visual inspection. Although the current trend of applying machine learning algorithms dominates publications on the spatialization of erosive processes (Ghorbanzadeh et al. 2020) or the detection of ravine edges (Li et al. 2021), here we highlight the importance of human expertise on RS images analysis. In this sense, our algebra of selection and exclusion of false positives can be useful as an attribute for achieving more robust models (Minella et al. 2010), or even for integrating variables in GIS, such as distance to roads, lithology, slope curvatures, and topographic indices (Zabihi et al. 2018, Pourghasemi et al. 2020, Amiri & Pourghasemi 2020), especially regarding the locations suitable for palisades, whose studies are still scarce.

Mapping the structures is the first step toward achieving basin sustainability. Unquestionably, check dams and palisades are effective in controlling sediment flow (Xu et al. 2020), however, this rule is limited to biophysical parameters alone and does not provide an integrated view. Studies have shown that for implementation it is necessary to take into account economic, social, and agrarian structure (Wynants et al. 2019).

4.3 Adding pieces to the puzzle: erosive risk, interventions, and agrarian structure

Based on our analysis of USLE parameters, we could identify priorities for erosion recovery interventions at a landscape scale in the Upper Taquari River Basin, however much work remains to translate it into action. In the real world, it is critical to assess cost, opportunities, economic, social, and policy aspects (Armsworth 2014). By including information on the land structure of the region in our study, we were able to find that an erosion risk area on large properties is about 10 times greater than on micro properties. In this perspective, we agree with

Stefanes et al. (2018) that the recovery of cattle pastures on large properties should be prioritized, as few properties already represent a gain in scale (area) to the renewal of the basin. Although we do not despise the micro properties, which lack technology and resources, this would represent a gain in participation and social engagement in relation to the conservation of natural resources (Tesfahunegn 2019). Thus, we understand that the approaches are different and complementary.

Technically, large properties have an area available to carry out zoning between soil recovery (temporary stoppage) and agricultural production. In addition, they often have access to rural credit and machinery to support conservation activities (see an example in China's land arrangement by Ma et al. 2020). On the other hand, small properties do not have areas available for rotation, access to technology, and credit due to a lack of collateral registration (Carrer et al. 2020). Meanwhile, they may have the manpower to implement conservation practices, including operating machinery or collecting and planting seed species in gullies (Agidew & Singh 2018, Schmidt et al. 2019). Therefore, given the dispersion of erosion points along the basin, we propose to divide the area into smaller projects, probably into micro catchments whose ecological trade-offs (Zhao et al. 2018) and cascading effects downstream on soil retention are measurable. (Sun et al. 2020). The regions of interest are also more favorable for the interaction between micro and large properties in the implementation of recovery actions (Toledo et al. 2018).

But where to start considering that active gullies on all properties are important for land restoration? The prioritization criteria may be constrained by a combination of costs, biodiversity conservation, and climate change mitigation (Strassburg et al. 2020). Indeed, setting restoration priorities is not a consensual issue. Overall, highly degraded areas are prioritized because they need urgent action (Lamb et al. 2005). However, a crescent number of studies also suggest that intermediate degraded areas should be prioritized because the costs and benefits are higher (Tambosi et al. 2014). According to Toledo et al. (2018), active restoration may be complemented by spontaneous regeneration in areas with less adverse conditions. In addition to the criteria

already discussed we suggest to the decision makers an inclusion of a percentage of RL and APP surrounding the erosions to ranking gullies recovery. Basically, gullies permeated by vegetation can be rehabilitated a posteriori, according to their power of self-regeneration (Yang et al. 2018, Prieto et al. 2022). Erosion around the matrices (cattle) will likely be more costly due to the absence of native fragments but should be a priority to increase ecosystem connectivity (Tambosi et al. 2014, Blake et al. 2021).

The solutions for articulating interventions with the agrarian structure permeate the State's performance. We understand that large properties must be provoked by the government to achieve compliance with the Forest Code (Roitman et al. 2018, Stefanos et al. 2018), while structures in small and micro properties can be provided from specific public credit and payment programs for environmental services (Brançalion et al. 2016).

5. Conclusion

The development of multi-criteria can be seen as a first step to planning the basin recovery. Areas of the high potential risk of soil loss in UTRB are evenly distributed between small and large properties, areas of anthropic use, and those reserved for conservation or preservation of natural resources. Similar status has been observed in pastures of savannas in tropical regions; therefore, the widespread degradation requires urgent prioritization for regional stabilization of tropical critical gullies.

The inclusion of agricultural information enriches the visualization of potential implementation opportunities. The weaknesses of one ownership group can be addressed by the strengths of others, as in a collaborative action system. However, the State government is instrumental in invoking, especially with the creation of specific financial resources rooted in public policies for groups of fragile properties in compliance with the Forest Code through the CAR.

Supplementary material available in:

<https://docs.google.com/document/d/1y5IB2XLc8DEcHIeMwmzIuJFJ6v0EFsEk/edit?usp=sharing&oid=110830496409468836501&rtpof=true&sd=true>

Chapter 2: Combining optical and microwave remote sensing for assessing gullies in human-disturbed vegetated landscapes.

Abstract

The accurate assessment of the gully is key to stopping soil loss, especially in agricultural landscapes. This study aims to combine freely distributed remote sensing data for the evaluation of gullies located in a tropical watershed with a history of cattle production. Eighty-four vectorized gullies were defined in the Pirizal River basin, part of the highly eroded Upper Taquari (Brazil). We examined 56 variables from Sentinel-1/2 and ALOS-PALSAR-1 datasets, including SAR products and optical products like textures, water, vegetation, and terrain indices. Following a correlation analysis, 19 variables were selected for mapping in a Random Forest classifier by considering samples of active (soil) and stabilized (vegetation) pixels. The method reached an overall accuracy of 89%, in which soil abundance was responsible for 44% of the overall importance in the classification. Optical indices and texture products outperformed SAR products, whose importance represented only 14%. In the studied river basin, about 63% of the gullies were found stabilized, 30% in the process of stabilization, and only 7% active. The method proved effective, low cost, and promptly replicable to general river basins with gullies, mainly those in the tropics where vegetation has a significant role in soil loss control.

1. Introduction

Permanent gullies are a significant threat to life and property (Ionita et al. 2015). Considering that the soil is an essential resource for the maintenance of terrestrial life and little renewable on a human scale (De Deyn & Kooistra 2021), therefore, preventing the erosion process from advancing through a quick and effective assessment is a service to the ecosystem (Frankl et al. 2021). Until the formation of large pits, the gully usually starts with small furrows, going to the head-cutting phase, then the pit becomes wider and deeper, and may reach the water table (Lal 1992, Tebebu et al. 2010). Natural and anthropic factors such as topography, rainfall, physical and chemical properties of the soil, and vegetation cover influence the generation of gullies (Valentin et al. 2005, Zhao & Hou 2019). In this extensive and complex set of factors, identifying thresholds that indicate whether the gully is expanding or heading toward stabilization is a challenge (Yang et al. 2022).

Mapping gullies is time-consuming and requires extensive field surveys (Rossi et al. 2022). Some of the issues lie in accessing wells, measuring characteristics, and describing the factors that influence the process (Shruthi et al. 2015, Thwaites et al. 2022). Furthermore, the complexity of describing cracks may require work with a group of specialists, making these exercises also costly (Castillo & Gómez 2016). Generally, the most detailed studies focus on single features or a small set of gullies (see examples in Shellberg et al. 2013, Liu et al. 2017). At the basin scale, the studies refer more to the vulnerability of gullies (Arabameri et al. 2018, Gayen et al. 2019) or temporal assessment of size and volume (Eustace et al. 2009, Li et al. 2017, le Roux et al. 2022). Trench development is also studied in the form of the rate of gully head retreat (Vanmaercke et al. 2021, Yibeltal et al. 2021). It is common in all these areas to use robust mathematical models that are provided by high spatial resolution remote sensing mechanisms, including paid orbital imagery, airborne LIDAR, or UAVs (Martins et al. 2020, Conforti et al. 2021, Martín-Velázquez et al. 2022).

For some regions of the world, particularly for poor counties in the Global South, the

analysis and mapping of gullies in large areas can be a challenge, which includes difficulty in accessing paid mapping products (Senanayake et al. 2020). In this context, the development and reach of open-access analytical frameworks are fundamental (Yang et al. 2020, Alexakis et al. 2021). Under this perspective, the Sentinel images are currently the largest constellation of free sensors with multispectral images in the visible, near-infrared (NIR), shortwave infrared (SWIR) (Sentinel 2), and C-band orbital microwave. Synthetic Aperture Radar (Sentinel 1). Therefore, researchers exploit the complementary features of these images in the electromagnetic spectrum to study gullies (Makaya et al. 2019, Guo et al. 2019, Khan et al. 2020). Free data is also a valid option for land use planning in developing countries with high gully density (Senanayake et al. 2020, Olivier et al. 2023).

Indeed, mapping soil erosion in tropical countries is an urgent task, considering their increasing pressure to maintain global food production (Právělie et al. 2021), but also weakened by heavy rains (Godoi et al. 2021) and poor land use management (Borrelli et al. 2020). In addition, tropical soils are poor in the structure that protects against runoff, mainly due to low levels of organic matter and clay (Nair 2019). Not surprisingly, countries with a predominantly hot and humid climate like Brazil are at the forefront of erosion exports through the sale of agricultural commodities to countries with a temperate climate (Cui et al. 2022). Changing this relationship involves recovering severe erosion processes based on assessments that optimize stakeholder decision-making (Castro & Lechthaler 2022).

Here we bring the Pirizal River basin as an example of a tropical Brazilian case containing several gullies, which is part of the greater Upper Taquari River, one of the most eroded basins in the world (Louzada et al. 2022). In this study, we generate a qualitative mapping of the gullies, indicating the active and stabilized features through a wide range of freely remote sensing variables from Sentinel 1/2 and ALOS-PALSAR images. This method goes straight to the point of tropical active gullies and will later be replicated for the rest of Upper Taquari to guide soil/vegetation restoration and inspire other similar initiatives in basins with gullies across

the planet.

2. Material and methods

2.1 Study area and data source

The study was carried out in the Pirizal River basin with an area of 77.23 km² between the geographic coordinates 19°24'30"S, 19°18'30"S and 53°54'30"W, 54°6' 30" W (Fig. 1) in the municipality of Camapuã, state of Mato Grosso do Sul, central-west region of Brazil. Our area belongs to the Cerrado biome, with an Aw (tropical) climate, with rainy summers and dry winters (Peel et al. 2007), and is part of the Upper Taquari River, one impressive eroded basin in Brazil (Galdino et al. 2005, Louzada et al. 2022). Erosions in the upper part are responsible for the silting up of the Taquari River and avulsions in the plains of the Pantanal wetlands (Assine 2005, Louzada et al. 2021).

Surface runoff in the region is significant due to the fragility of sandy soils resulting from quartzitic weathering, long slopes, and wavy relief (Louzada et al. 2022) (see maps of these themes in Figures 1b, 1c and 1d). Additionally, there was a lack of soil conservation practices on land that replaced native vegetation with livestock and grain production since the 1970s (Buller et al. 2016). Anthropogenic gullies, with the exception of geological (natural) gullies, are fissures in the ground easily visible in loco or by satellite images that can go deep until they reach the water table (Valentin et al. 2005, Tebebu et al. 2010). In our study area, the gullies were gradually induced by poor land use in cattle farms, which caused the channels to deepen (Galdino et al. 2005). Mechanical impediments by the advance of erosion forced the abandonment of land for pasture (Buller et al. 2016), so most gullies coincide with remnants of natural vegetation along water courses (Fig. 1e). These fragments are associated with active gullies represent on-site and off-site impacts (Valentin et al. 2005), but also do not meet the legal requirement of the Brazilian Forest Code (Law 12,651 of 2012), which aims to preserve the remnants of native vegetation in 20% of the rural properties.

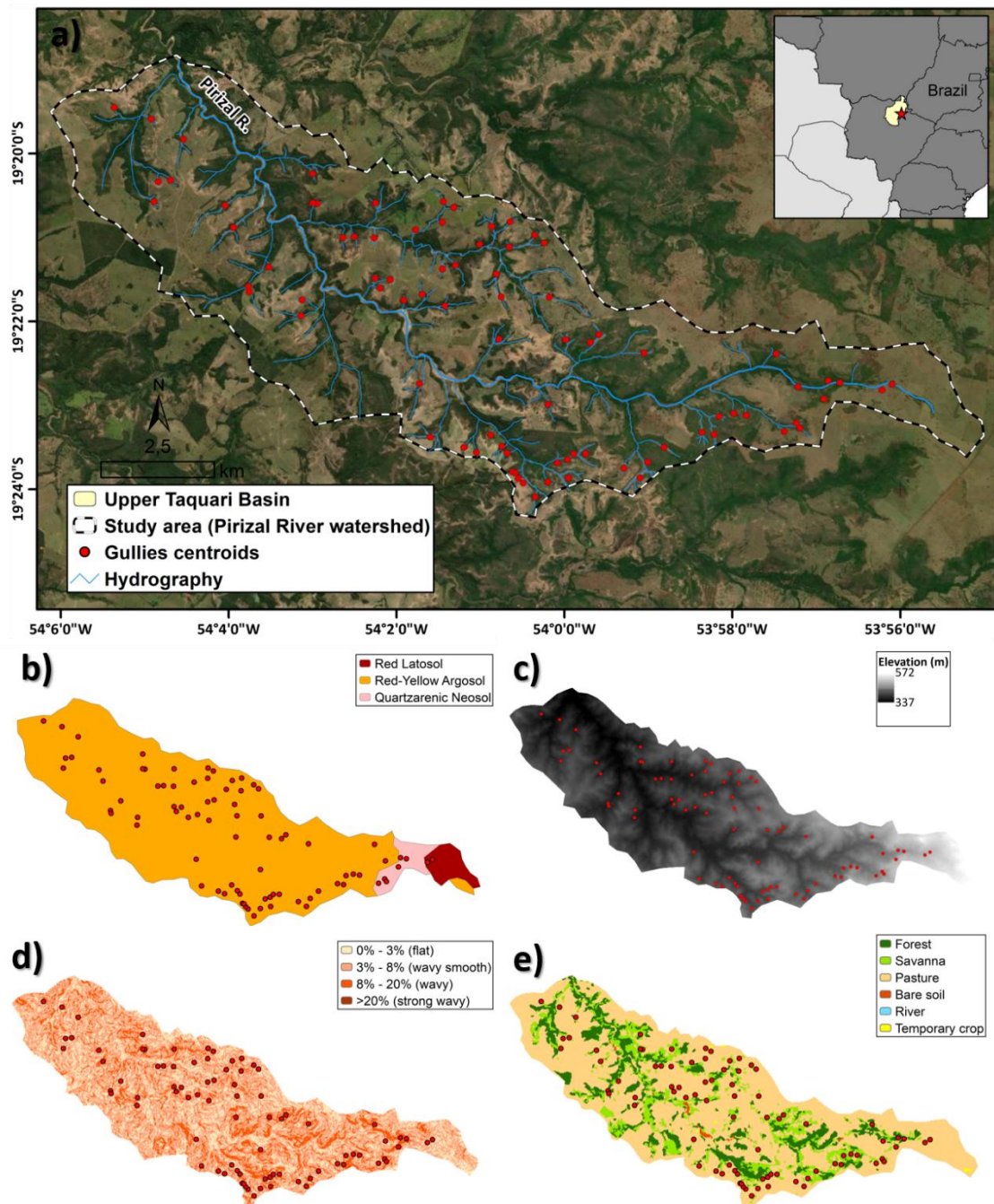


Fig. 1. Location of the Pirizal River watershed (a) in the Upper Taquari River Basin in yellow, with centroids of 84 gullies delimited on the high-resolution base map of ArcGIS. In sequence, (b) official soil layers of 1:250,000 scale map of Brazilian Institute of Geography and Statistics (IGBE); (c) DEM ALOS-PALSAR; (d) slope classes (percentage) according to Embrapa's classification (Santos et al. 2018); (e) Land Use/Land Cover from MapBiomass project of 2019 (Souza et al. 2020).

A freely MAXAR Vivid's Imagery base map layer from 7/14/2016 (0.31m) available on the world imagery plugin from ArcGIS® 10.4.1 was used to vectorize the boundaries of 84 identified gullies (see an example in Fig. 2a). In sequence, the polygons were used as ROI to clip

Sentinel-2A 10m resolution data (True Color Image), and extract 10,303-pixel centroids of gullies (Fig. 2b). The set of centroids also served as the basis for extracting pixel information from variables for further analysis of the Random Forest algorithm (section 2.3).

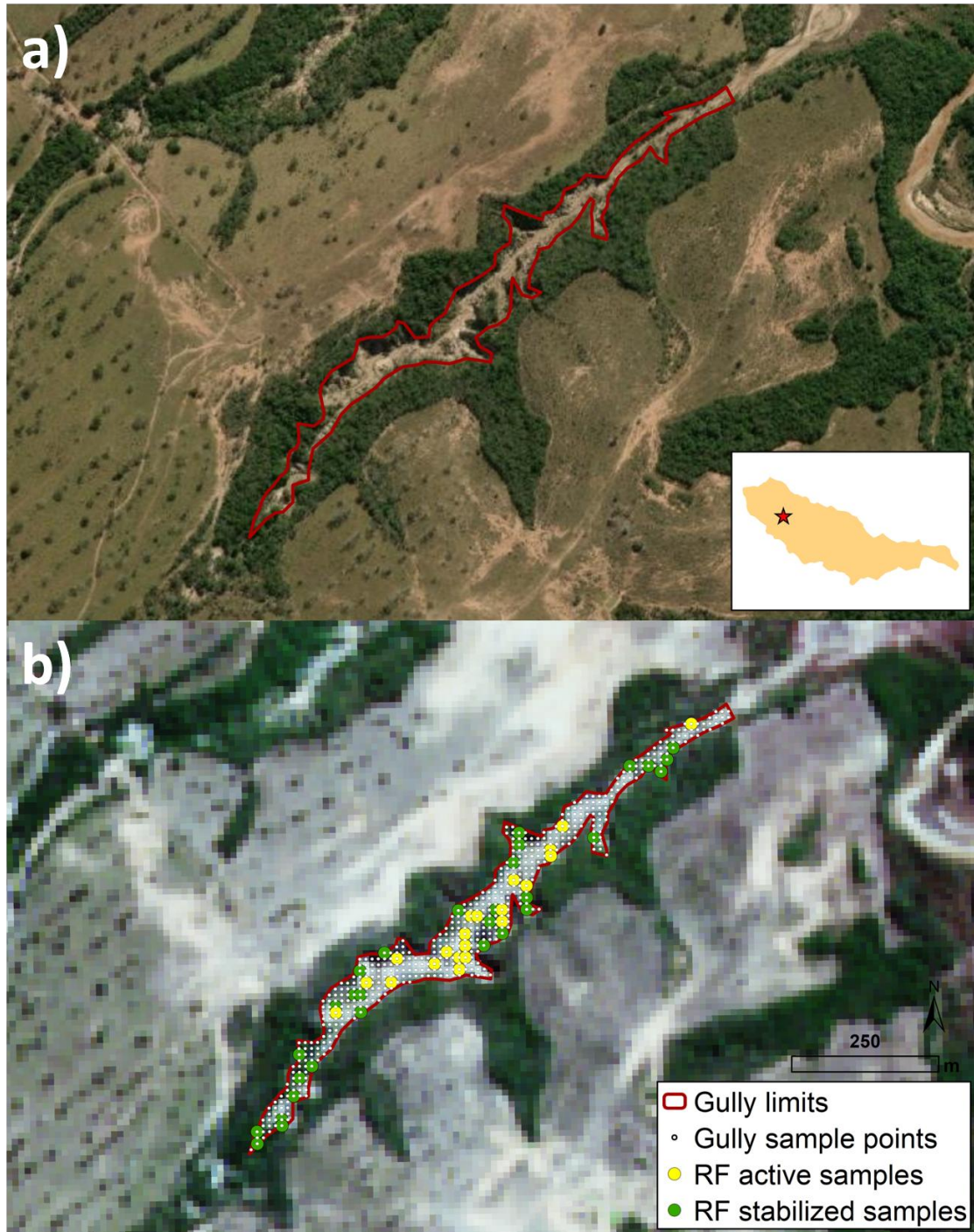


Fig. 2. Example of a gully analysis (Gully G61). (a) pixel centroids overlaid by the Sentinel-2A True Color Image; (b) yellow and green circles correspond to samples of active and stabilized sites, determined by visual interpretation of the high-resolution image.

2.2 Feature extraction from multi-source remote sensing images

Optical and microwave orbital sensors are not concurrent as they explore different electromagnetic spectrum bands (Fu et al. 2020). Thus, we used Sentinel-2A, Sentinel-1B, and ALOS-PALSAR 1 images (data information available in Table 1), to explore 56 variables divided into 10 categories (see all variables and equations in Table 2). The SNAP (Sentinel Application Platform) software and their respective variables were processed in SNAP 8.0., while topographic indices were calculated in ArcGIS 10.4.1. A workflow of processing steps and analysis is presented in Fig. 3.

Table 1. Characteristics of spatial data.

Sensor	Category	Mode	Band	Resolution (m)	Date
Sentinel-2A*	Optical and optical texture	Level 2	B1	60	22/07/2021
			B2	10	
			B3	10	
			B4	10	
			B5	20	
			B6	20	
			B7	20	
			B8	10	
			B8A	20	
			B9	60	
			B10	60	
			B11	20	
B12	20				
Sentinel-1B*	Intensity, intensity texture and polarimetry	SLC_IW	VV & VH	16.69	11/07/2021
	Interferometry				17/06/2021 (master)
					11/07/2021 (slave)
ALOS-PALSAR 1**	Topographic	High-resolution terrain corrected	HH	12.5	16/02/2011

Sources: * Copernicus Open Access Hub (<https://scihub.copernicus.eu/>); ** Alaska Satellite Facility (<https://search.asf.alaska.edu/>).

The choice of variables took into account the practicality of SNAP processing linked to a wide range of variables applicable in soil science. Therefore, we start with soil and vegetation abundance (endmembers) using spectral unmixing techniques (de Asis et al. 2008). Followed the optical vegetation and water indices by the application in soil erosion models at landscape scales (Sepuru & Dube 2018), being Ratio Vegetation Index (RVI), Normalized Difference Vegetation

Index (NDVI), Soil Adjusted Vegetation Index (SAVI), Transformed Soil Adjusted Vegetation Index (TSAVI), Normalized Difference Water Index (NDWI), Modified Normalized Difference Water Index (MNDWI) and Red Edge Position Index (REP). Brightness Index (BI), Color Index (CI), and Redness Index (RI) as radiometric soil indices. Biophysical indices of Leaf Area Index (LAI), Fraction of Absorbed Photosynthetically Active Radiation (FAPAR), and Fraction of Vegetation Cover (FCOVER) by their valuable information on the percentage of canopy cover on degraded lands (Baret 2016). In addition, we include texture variables to reflect land cover morphology (Zhao et al. 2017), being contrast (CON), dissimilarity (DIS), homogeneity (HOM), second angular momentum (ASM), maximum probability (MAX), Entropy (ENT), Mean, Variance (VAR) and Correlation (CORR). Optical texture variables were resampled to 10m resolution (B2), and then we chose the 9x9 window size and select the angles of 0°, 45°, 90°, and 135°.

The group of SAR variables was started by the intensity or backscattering (σ^0), calculated in the polarizations VV and VH from Sentinel-1B. Other metrics extracted were the difference, ratio, mean, and normalized difference. Furthermore, texture variables were applied for each σ_{VV}^0 and σ_{VH}^0 following Jin et al. (2014) methodology and the same parameters of window size and angles of the optical texture. For the polarimetric decomposition, we included entropy (H) and alpha (α) variables. Finishing off the SAR variables, the interferometric coherence was calculated from a pair of Sentinel-1B images in both polarizations (γ_{VV}, γ_{VH}).

Topographic or terrain indices are also applied by their functionalities in erosion risk models (Sharma 2010). Therefore, four classical indices were calculated: Stream Power Index (SPI), Sediment Transport Index (STI), Terrain Roughness Index (TRI), and Topographic Wetness Index (TWI).

Table 2. Variable categories and respective equations.

Category	Variable	Equation	Reference
Spectral unmixing	VEG_ABU	$R_k = \sum_i^n a_i * E_{i,k} + \varepsilon_k$	Keshava & Mustard (2002)
	SOIL_ABU		
Vegetation/water	RVI	B4/B8	Tucker (1979)

indices	NDVI	$(B8-B4) / (B8+B4)$	Rouse Jr. et al. (1973)
	SAVI	$(1 + L) * (B8-B4) / (B8+B4+L)$	Huete (1988)
	TSAVI	$s * (B8 - s * B4 - a) / (s * B8 + B4 - a * s + X * (1 + s * s))$	Baret & Guyot (1991)
	NDWI	$(B8-B12) / (B8+B12)$	Gao (1996)
	MNDWI	$(B3-B11) / (B3+B11)$	Xu (2005)
	REP	$705 + 35 * ((B4 + B7)/2 - B5) / (B6 - B5)$	Clevers et al. (2000)
Soil radiometric indices	BI	$\sqrt{B4^2 + B3^2} / 2$	Mathieu et al. (1998)
	CI	$(B4-B3) / (B4+B3)$	Escadafal (1989)
	RI	$(B4)^2 / (B3)^2$	Barron & Torrent (1986)
Biophysical indices	LAI	Calculation method in the SNAP 8.0. All bands were considered.	Price (1993)
	FAPAR		Liang (2007)
	FCOVER		Kallel et al. (2007)
Texture - optical	CON	$\sum_{n=0}^{N_g-1} n^2 \left\{ \sum_{i=1}^{N_g} \sum_{j=1}^{N_g} p(i,j) \right\}, i-j = n$	Haralick et al. (1973)
	DIS	$\sum_{n=1}^{N_g-1} n \left\{ \sum_{i=1}^{N_g} \sum_{j=1}^{N_g} p(i,j)^2 \right\}, i-j = n$	
	HOM	$\sum_i \sum_j \frac{p(i,j)}{1 + (i-j)^2}$	
	ASM	$\sum_i \sum_j \{p(i,j)\}^2$	
	MAX	$MAX_{i,j} p(i,j)$	
	ENT	$-\sum_i \sum_j p(i,j) \log(p(i,j))$	
	MEAN	$\sum_{i=2}^{2N_g} (ip_{(x+y)}(i))$	
	VAR	$\sum_i \sum_j (i - \mu)^2 * p(i,j)$	
CORR	$\frac{\sum_i \sum_j (i,j)p(i,j) - \mu_x \mu_y}{\sigma_x \sigma_y}$		
Intensity	SIG_VV	$\frac{DN_i^2}{A^2}$	Diniz et al. (2020)
	SIG_VH	$\frac{DN_i^2}{A^2}$	
	DIF_VH_VV	$\sigma_{VH}^0 - \sigma_{VV}^0$	Jin et al. (2014)
	RATIO_VH_VV	$\frac{\sigma_{VH}^0}{\sigma_{VV}^0}$	Diniz et al. (2020)
	MEAN_VH_VV	$(\sigma_{VH}^0 + \sigma_{VV}^0) / 2$	Authors
	ND_VH_VV	$\frac{\sigma_{VH}^0 - \sigma_{VV}^0}{\sigma_{VH}^0 + \sigma_{VV}^0}$	Authors
Texture - SAR intensity	SIG_VV_CON	Calculation method in the SNAP 8.0	Jin et al. (2014)
	SIG_VV_DIS		
	SIG_VV_HOM		
	SIG_VV_ASM		
	SIG_VV_MAX		
	SIG_VV_ENT		
	SIG_VV_MEAN		
	SIG_VV_VAR		
	SIG_VV_CORR		
	SIG_VH_CON		
SIG_VH_DIS			

SIG_VH_HOM
 SIG_VH_ASM
 SIG_VH_MAX
 SIG_VH_ENT
 SIG_VH_MEAN
 SIG_VH_VAR
 SIG_VH_CORR

Polarimetry	H	$-\sum_{i=1}^3 p_i p_i, p_i = \frac{\lambda_i}{\sum_{j=1}^3 \lambda_j}$	Moreira et al. 2013
	Alpha	$\arccos(e_{ii})$	
Interferometry	COH_VV	$\frac{ S_1(x)S_2(x)^* }{\sqrt{\langle S_1(x) ^2 \rangle \langle S_2(x) ^2 \rangle}}$	
	COH_VH		
Topographic indices	SPI	$A_s \tan \beta$	
	STI	$\left(\frac{A_s}{22.13}\right)^{0.6} \left(\frac{\sin \sin \beta}{0.0896}\right)^{1.3}$	
	TRI	$Z \left[\sum (x_{i,j} - x_{00})^2 \right]^{0.5}$	Wilson & Gallant (2000)
	TWI	$\ln \ln \left(\frac{A_s}{\tan \beta}\right)$	

Terms of the above equations. Spectral unmixing: R_k is the reflectance of source at wavelength k ; $E(i,k)$ is the reflectance of endmember i at wavelength k ; n is the number of endmembers; a_i is the abundance of endmember i ; and ϵ_k is the error at wavelength k ; SAVI: L is the adjustment factor; TSAVI: a is the soil line intercept; s is the soil line slope; X is the adjustment factor to minimize soil noise; Texture: $\mu_x, \mu_y, \sigma_x, \sigma_y$ are the means and standard deviations for the row- and column-marginal probabilities of the co-occurrence matrix composed of $p(i, j)$; backscattering intensity: DN_i is the digital number of the pixel i ; A is an absolute calibration constant; Polarimetry H : p_i expresses the appearance probability for each contribution; Interferometry: S_1 and S_2 are the two co-registered complex images; SPI: A_s is the catchment area and β is local slope; TRI: Z is the elevation at central cell.

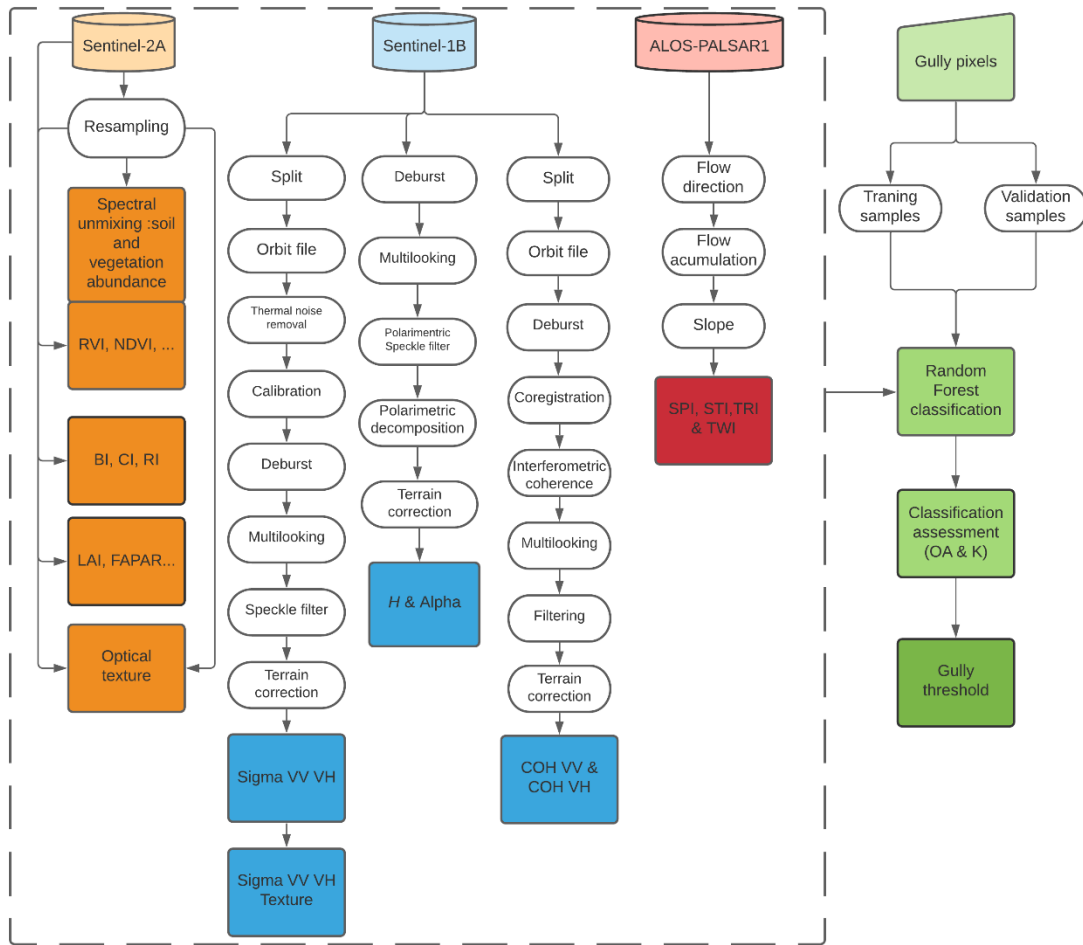


Fig. 3. Workflow of the proposed extraction method of variables.

After collecting the variables and before classifying, we performed a correlation analysis between the data, as some variables have algebraic arrangements in the same spectral bands, which may represent bias in the result (eg: NDVI and RVI). Thus, we submitted the pixel information of the 56 variables to PAST statistical software (Hammer & Harper 2001) and applied a Pearson correlation threshold ≤ -0.5 or ≥ 0.5 to segregate strong autocorrelations. Finally, the choice of a variable within a similar group took into account the one that presented the greatest coefficient of variation, as it is to be expected that the discrepancies represent points of uncovered soil and vegetation presence.

2.3 Random Forest classification and gully threshold activity

The Random Forest (RF) algorithm (Breiman 2001) processed in the R Software for Statistical Computing v.4.0 (R Core Team, 2013) was selected to classify the gully's pixels. For

the training and validation step, we selected 10% of the total pixels. These sampling points were visually inspected as active or stabilized with the help of the ArcGIS base map considering the spectral response of bare soil or vegetation, regardless of the size of vegetation cover (see example in Fig. 2b). Here, vegetation was used as a criterion to define stable soil based on the idea that there is no germination of seeds (tree or bush) as long as there is runoff (Guterman 2000, Zuazo & Pleguezuelo 2009).

Then 70% of the sample was used for training and 30% for validation, with default *n*tree at R (500) and *m*try with the square root of the total number of variables after correlation analysis. In addition, we calculated the importance of the variable by the Mean Decrease Gini index, as an average measure of nodal impurity in classification trees (Khanal et al. 2018). Further assessments of classification agreements were obtained with overall accuracy and the Kappa statistic. Based on the RF results, we propose limits to segregate and categorize gullies by the sum of bare pixels as 'active' (> 50%), 'in stabilization' (20 to 50%), and 'stabilized' (< 20%).

3. Results

We vectored a total of 84 gullies in the studied sub-basin. The tiniest (G41) and the largest (G36) gullies have 0.08 and 5.73 hectares, respectively. The average area per gully is 1.21ha, while most of the gullies in the basin has less than 1 hectare (n = 55). Several forms of gullies were identified in the area such as forked, linear, irregular, and branched, where the majority is closer to or starts new waterways. Looking the land use and occupation map, it was observed that 36% (n=30) of the gullies were in pasture areas, 7% (n=6) in forest formations and most 63% (n=48) were within savannah formations, making it difficult to vectorize the boundaries by the canopy interference.

The correlation results and the descriptive statistics used for the selection of variables are shown in Figure S1 and Table S1 of the Supplementary Material, respectively. After analysis, 37 variables were dropped from the classification process, mainly optical texture and SAR texture

data (all data is shown in Figures S2 to S57). In general, the categories had at least one representative within the final variables in the Gini index (Fig. 4), with emphasis on the first variable SOIL_ABU obtaining 44% representativeness in the classification. Another detail was the difference between the second variable VAR and the last VH_ENT was only 3%. To demonstrate examples of the behavior of pixels in the gullies, we selected the largest G36 by the first six variables (Fig. 5).

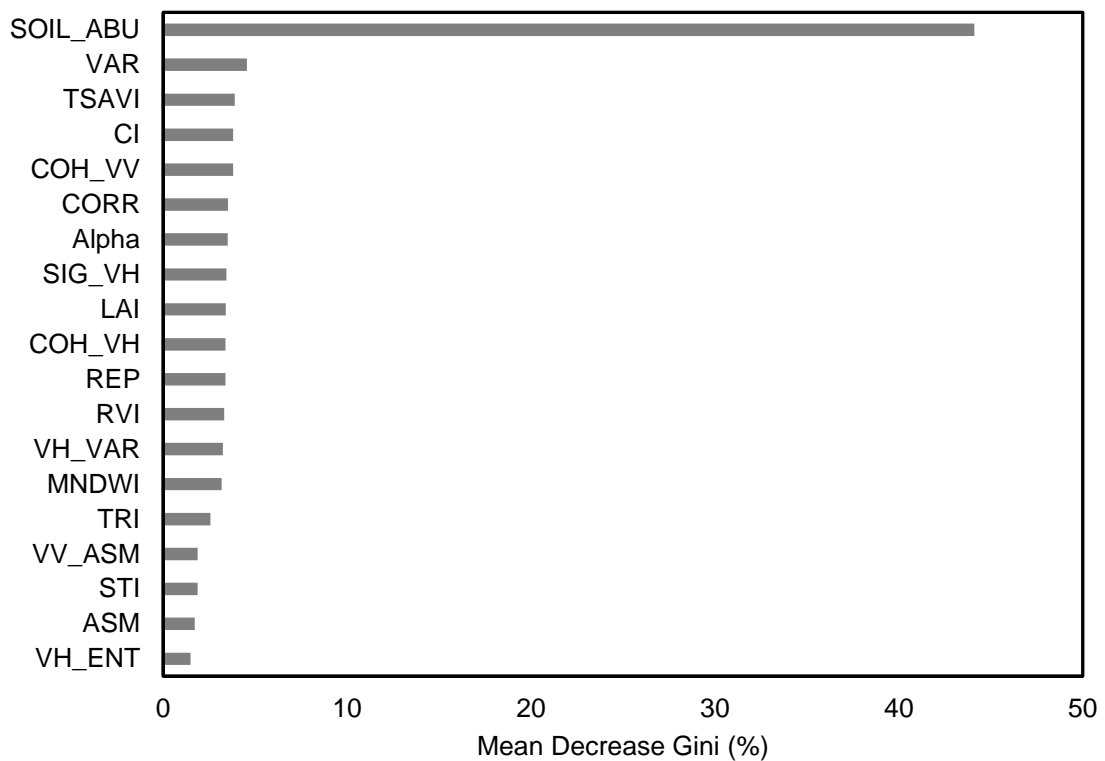


Fig. 4. Importance variables on Random Forest classification based on Gini index.

SOIL_ABU product (Fig. 5a) stood out inside the gully, evidencing pixels with highest values due to exposed soil in the thalweg. The interior of the gully also revealed higher spectral responses for CI (5d). VAR (5b), TSAVI (5c), and CORR (5f) showed similarities with a predominance of high values in almost the entire slit, with the exception of pixels with moderate and low values at the ends. Finally, the variable COH_VV (5e) showed pixels with high responses continuously distributed from the northwest face to the northeast face, while the rest, including the extremities, showed low and moderate values.

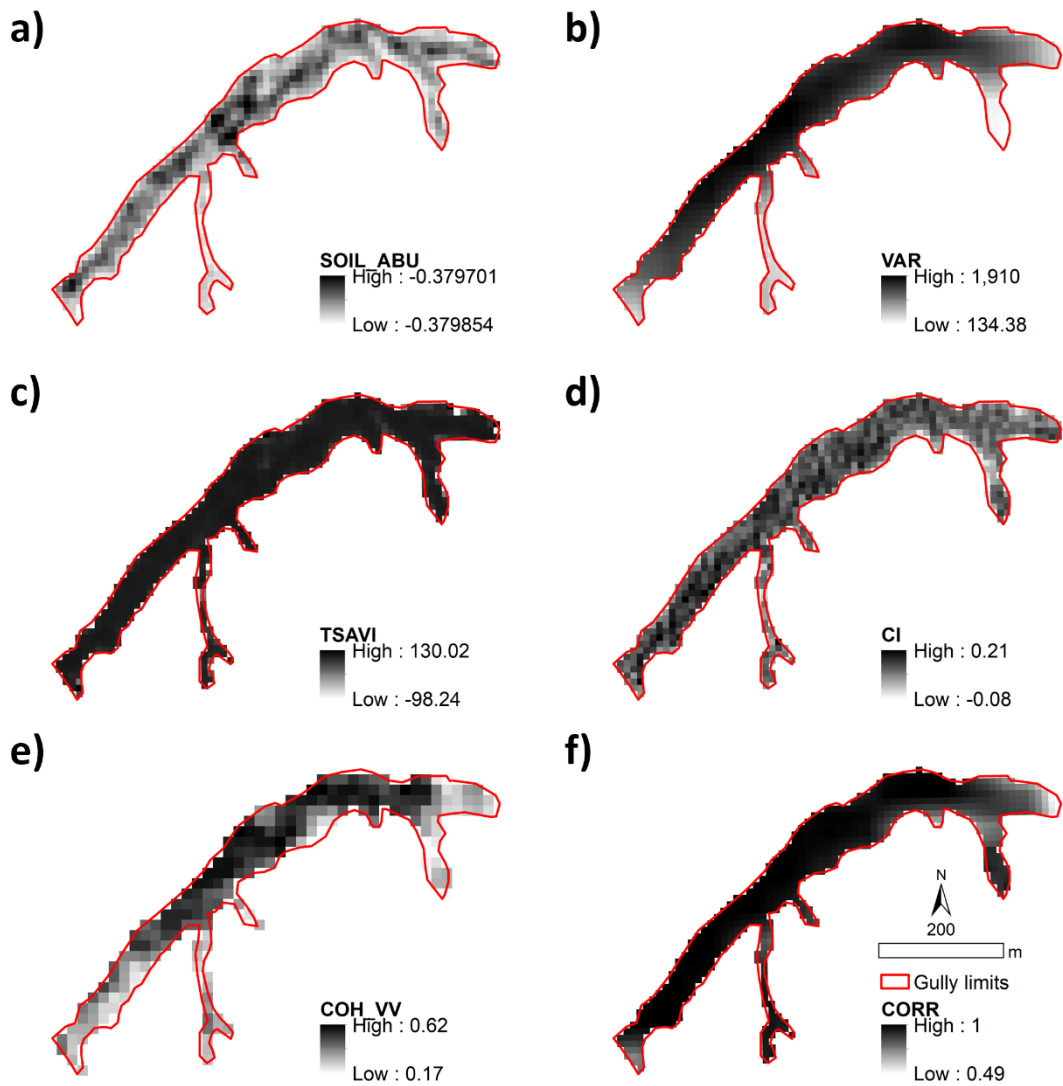


Fig. 5. The six outstanding variables of the Mean Gini for RF classification in gully G36.

For the algorithm validation and training, 1,030 pixels were inspected, with a predominance of vegetation or stabilized points (n=723). The Random Forest (RF) accuracy results are presented in Table 3, with an overall accuracy of 89% and a Kappa index of 74%.

Table 3. Assessment of RF classification.

Classes	Training samples	Validating samples
Active	215	92
Stabilized	506	217
Overall accuracy		0,89
Kappa index		0,74

According to the criteria for classifying gullies by the percentage of active pixels, we observed that the majority of erosions are stabilized n=53 (63%), followed by features in

stabilization n=25 (30%) and active gullies n=6 represented only 7% of the total, as shown in Figure 6. The active erosive features have an average area of 2.56ha, gullies in stabilization 1.85ha and stabilized 0.77ha. The nonparametric analysis of Two-way Kruskal-Wallis followed by the post hoc Dunn-s test indicate significant differences ($p<0.01$) only between stabilized and in stabilization gullies.

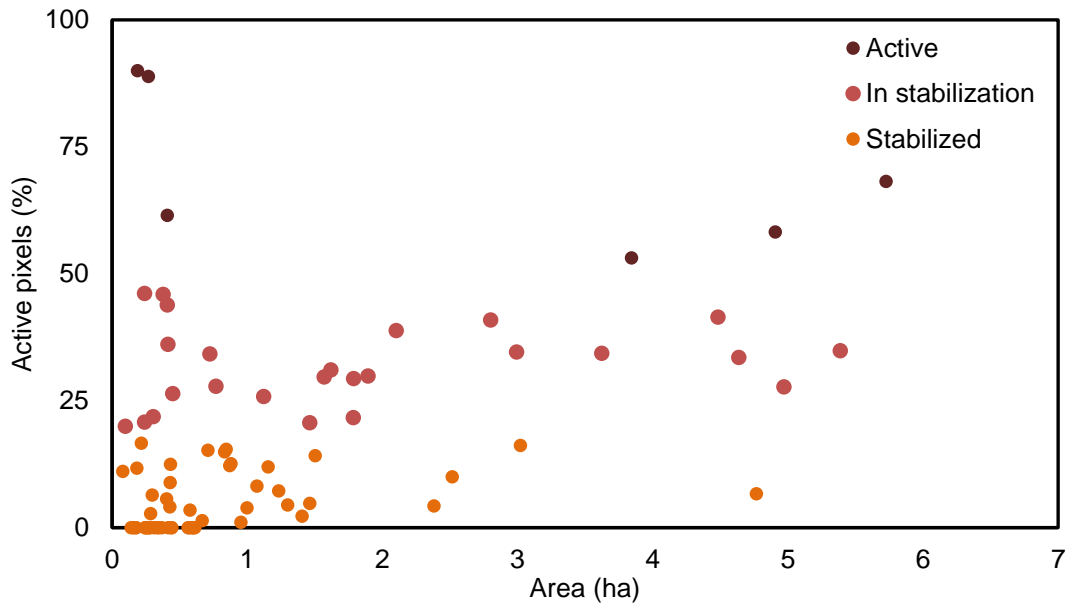


Fig. 6. Thresholds defined for segregating gullies in three major categories according to the percentage of active pixels.

Examples of the distribution of classification results by the three types of gullies are shown in Figure 7. In the stable gully (G81 – Fig. 7ab) there is a significant predominance of vegetation pixels throughout the feature. As for the gully in stabilization (G40 – Fig. 7cd), only the edges and the east and northeast faces have pixels covered by plants, denoting that the inner erosion is still active. This behavior was also similar to the active gully (G36 – Fig. 7ef), but the difference relied on the proportion of active pixels.

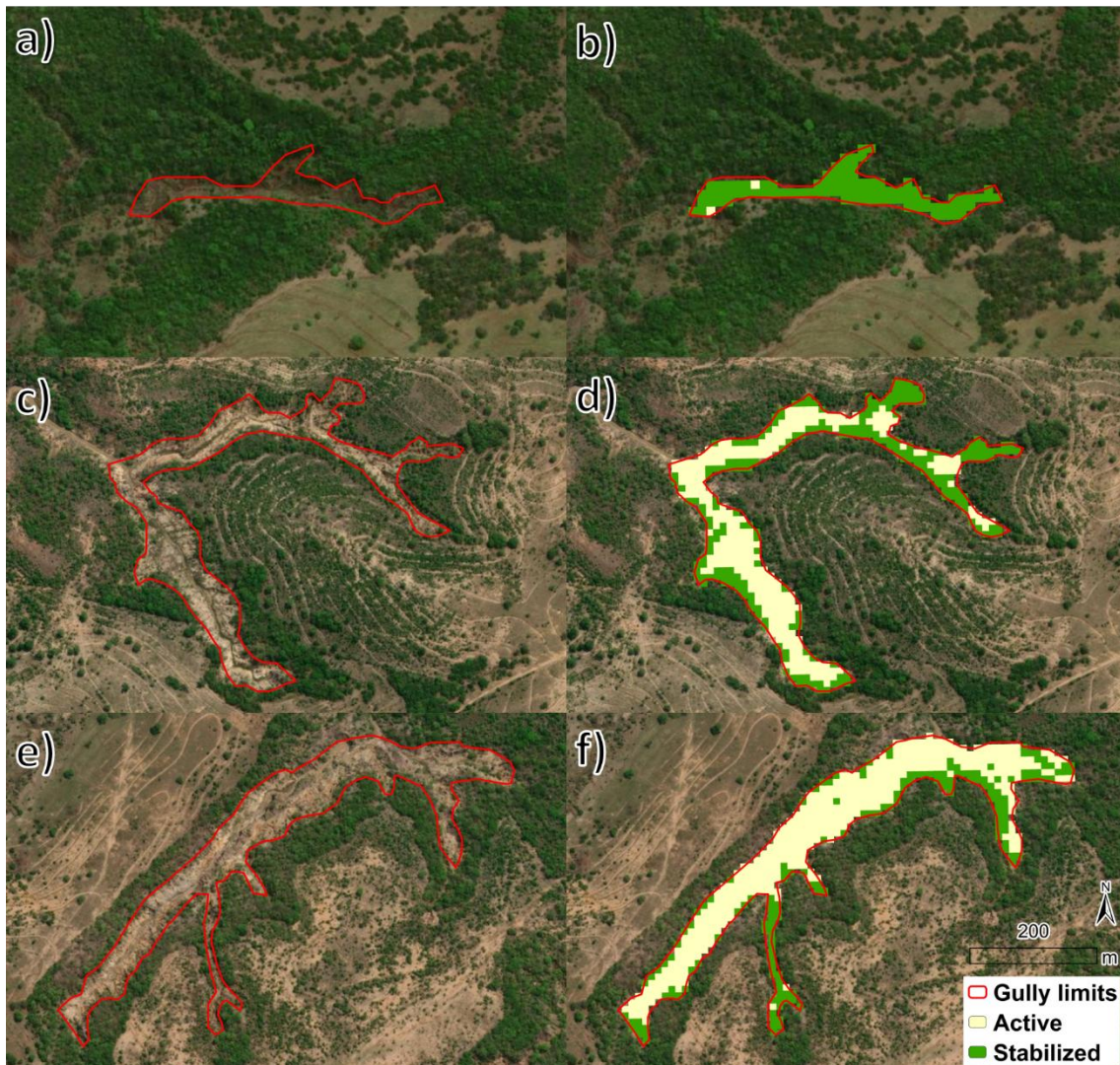


Fig. 7. Examples of useful erosions to discriminate and categorize three major groups of gully conditions: stabilized (G81, a), in stabilization (G40, c) and active (G36, e). Results of RF classifications of the gullies are respectively shown in b, d and f panels.

4. Discussions

4.1 Operation aspects: performance, limitations and implications

The association between multiple orbital remote sensing sources, including radar and optical ranges, proved to be effective in assessing the gullie's stabilization in a tropical system. Previous studies have proposed that condition of an erosion can be identified by analyzing the proportion of soil/vegetation (Dong et al. 2014, Li et al. 2015, Frankl et al. 2021). Our results support partially this idea that soil factors were the major drives to the gullies conditions (eg. SOIL_ABU, TSAVI, and CI), which corroborated other studies (Galang et al. 2007, Laamrani et al. 2020, George et al. 2022). However, we show that it is also important to consider "moisture

content, vegetation cover and topographic aspects to improve the performance of the model (Makaya et al. 2019, Roy et al. 2020, Mohammadifar et al. 2021). Another important observation was the occurrence of stable pixels on the edges of the features and mainly on the heads of the gullies (see detail in Fig. 2b), indicating that stabilization occurs from upstream to downstream after management techniques outside the erosive trench (see signals of terraces in Fig. 7) (Wang et al. 2023).

The wide application of the structure used in this study depends on operational aspects and the availability of orbital data. With regard to the acquisition of SAR variables, we understand that the processing required a technical and computational structure superior to the methods of obtaining optical data (Mandal et al. 2022), however, this routine was not compensated by the results of the Gini index, given that the four final variables accumulated only 14% of importance. Even though, we are analyzing a significative set of basin-scale gullies, and this does not rule out the potential for isolated assessment or a smaller group of features (successful examples in Guo et al. 2019, Vallejo Orti et al. 2021).

The RF classification power added to only two thematic classes was decisive for accuracy (Kwan et al. 2020). Even so, two points for improvement in future work should be highlighted: 1) the base layer date should be as close as possible to the data source to avoid changes in the landscape (see options for the base map of the PlanetScope sensor in Wagner et al. 2023); 2) field trips to guide the classification with the collection of ground truths, especially for the intermediate pixels (in stabilization) which were not included in this exercise. In these specific assessments, recent technologies such as UAVs would also help to perform a complete diagnosis of the feature, including points that are difficult to access due to the sloped terrains (Mohammadifar et al. 2021, Zhou et al. 2023). Thus, calibrating the model with local data would allow one more step in the interpretation of the targets.

Overall, the methods developed here based on the Sentinel family images, in addition to being free, were capable of guiding decision-making for rapid conservation actions at the basin

scale (Fernández et al. 2023). Land use planning in developing countries with tropical climates is almost always precarious (Xie et al. 2020), from scarce resources to purchasing high-resolution images (Radočaj et al. 2020), weak policy implementation from land use by rural landowners (Ariti et al. 2019), and also insufficient resources to implement mitigation measures in the countryside (Higaki et al. 2021). In this sense, practical and inexpensive methods with short-term responses would help to identify erosions in a frank expansion process, reducing on-site and off-site impacts (Das et al. 2023).

4.2 Understanding our case study to scale-up

Our case study can be replicated for the entire Upper Taquari Basin, as it allowed us to reduce field costs and remotely assess all gullies in the basin, defining intervention priorities. Although 63% of the features are stabilized, the remaining 37% still deserve attention to contain sediment loss. From the high-resolution image, we can see that several actions have already been carried out with the implementation of terraces in the pastures and works on the sides of the roads, but these structures must be constantly maintained to avoid ruptures, even more so that climatic scenarios indicate recurrence of rains concentrated in the summer for the coming decades (Bergier et al. 2018, Almazroui et al. 2021).

We also observed that the vast majority of erosions are associated with canopies in watercourses and/or reaching the water table. This is a common characteristic in degraded basins of the Brazilian Cerrado by deep and sandy soils (Fonseca et al. 2022, Louzada et al. 2022). The connection between gullies and watercourses also poses operational obstacles to the adoption of mechanical and vegetative practices (Rodrigues 2018), therefore, actions outside areas of native vegetation are necessary to reduce concentrated runoff inside the erosions, boosting the passive restoration of vegetation (Pereira et al. 2022).

5. Conclusions

The method developed here allows a quick and effective assessment of gully

stabilization conditions at the basin scale, and in regions where the main erosion interruption agent is vegetation. Based on that, optical indices, with an emphasis on spectral unmixing techniques, were the most useful and least complex in such exercise. Even so, more complex SAR products, textures and terrain variables were somewhat helpful in the evaluation. In this methodological framework, the fundamental point seems to be a base image with a date close to the source images of the processing, in order to avoid alterations in the landscape that could influence the precision.

Our method indicated that most gullies were stable in the studied basin, however, stabilization erosions deserve attention so that soil loss is completely circumvented. Our model guides conservation projects through readily available remote sensing products. Therefore, this framework can also be useful in recovery programs for degraded savannas in underdeveloped and developing tropical countries.

Supplementary material available in:

<https://docs.google.com/document/d/1y7n-hGTcZC2NjhoPq-w1Lhc43gOSAmVz/edit?usp=sharing&ouid=110830496409468836501&rtpof=true&sd=true>

Chapter 3: The first inventory of gullies in the Upper Taquari River Basin (Brazil) and its agreement with land use classes.

Abstract

Gully erosion represents the most severe soil loss, with far-reaching consequences beyond the immediate site. Assessing the stability of gullies is particularly challenging in tropical regions with sandy soils and limited accurate data. Nonetheless, initiating gully inventories is a crucial first step in guiding public policies and conservation projects. In this study, we focus on the Upper Taquari River Basin (UTRB) situated on the fringes of the Brazilian Pantanal, where extensive erosion occurs in the upper regions and flooding occurs in the plains. We present the first qualitative and quantitative analysis of gullies in this region. Considering the historical context of the UTRB, it has long suffered from land mismanagement, particularly in livestock activities. Our objective was to evaluate the correspondence between gullies and land use classes in the MapBiomas Project, Brazil's most reliable non-governmental land use map, and the Rural Environmental Registry (CAR), the official information shared between landowners and public authorities. Thirteen remote-sensed indicators encompassing vegetation, water, soil, and terrain indices were assessed for 2022. Gullies were digitized through visual interpretation of a high-resolution Maxar Vivid Basic 2017 image. The classification was performed using the Random Forest (RF) algorithm, wherein pixels were classified into three classes: active, intermediate, and stable, based on the degree of vegetation cover and bare soil. The agreement of the gullies with the features of MapBiomas and CAR was also examined. The results revealed an overall accuracy of 96% and a Kappa index of 93% for the pixel classification. In the study area, 2,960 gullies were digitized, with 60% classified as active features and only 2% as stable. Furthermore, the MapBiomas algorithm misclassified many pixels with active gullies as pasture. Conversely, the CAR data failed to identify gullies as areas demanding restoration. To address these issues, we recommend revising both land use maps to accurately represent the presence of erosions and improve decision-making that favors efficient conservation efforts of the region. As a further result of our actions, the method described here may prove valuable in formulating restoration plans for other tropical savanna regions.

1. Introduction

The consequences of gully erosion extend significantly to the environment and infrastructure (Poesen et al. 2003, Vanmaercke et al. 2021). Within soil erosion, gullies represent a prominent manifestation, primarily instigated by the movement of water runoff (Rahmati et al. 2022). A crucial local effect is the transport of particles and essential nutrients essential for maintaining natural vegetation and agricultural productivity (Powlson et al. 2011, Abbasi et al. 2019). On a larger scale, gullies can disrupt the equilibrium of water within basins, resulting in heightened flooding due to excessive sediment accumulation in rivers (Issaka & Ashraf 2017, Yu et al. 2023). In urban areas, gullies can introduce risks to human life through landslides and slope instability (Guerra et al. 2018, Youssef et al. 2023). Overall, these erosive characteristics tend to undergo rapid transformation under the influence of water dynamics (Wei et al. 2021). Thus, cartography and identifying active gullies (where soil loss occurs) are pivotal in initiating timely restoration initiatives and curbing significant damages (Keesstra et al. 2018).

Gully formation can be ascribed to a blend of natural and human-induced factors. Natural elements encompass steep topography, weathered soils, and intense rainfall events (Blanco & Lal 2008, Anderson et al. 2021). Geological erosion can manifest on steep slopes, irrespective of native vegetation presence (Vanacker et al. 2022). Nevertheless, gullies shaped by human activities exhibit greater prevalence (Kemp et al. 2020). Agricultural practices on steep terrains and overgrazing by livestock notably contribute to erosive characteristics (Merten & Minella 2013, Quintero-Angel & Ospina-Salazar 2023). Moreover, any human land utilization or settlement lacking proper soil and water management as well as conservation strategies (Lepsch 2016), insufficient soil cover relative to rainfall impact (Novara et al. 2021), or the concentration of runoff from rural roads (Rahmati et al. 2022) can foster the development of severe erosion processes.

Due to the complex interplay of various contributing factors, studies on gully susceptibility often entail the fusion of robust machine learning (ML) algorithms with data from

remote sensing (RS) sources. Instances of this integration can be observed in the works of Arabameri et al. (2021), Hitouri et al. (2021), Hitouri et al. (2022), and Chuma et al. (2023). Additionally, Unmanned Aerial Vehicles (UAVs) have emerged as promising instruments in the realms of remote sensing and soil science, as highlighted by Niculiță et al. (2020) and Meinen and Robinson (2021). However, these evaluations typically necessitate fieldwork, which confines the assessment to relatively small watersheds, as Sepuru and Dube (2018) indicated. Consequently, the outstanding challenge pertains to conducting a degree of stability of these gully attributes on a broader regional scale, as articulated by Vanmaercke et al. (2021).

In countries with tropical climates, such as Brazil, where reliance on agricultural commodities is significant, soil erosion poses a notable concern (Cui et al. 2022). This issue is particularly prominent in the Cerrado biome, characterized by fragile soils with a high sand content (Hunke et al. 2015), which face substantial pressures from extensive cattle farming and grain production (Barbosa et al. 2023). Over time, various remote sensing (RS) techniques have been employed to assess gullies within the Cerrado. These approaches encompass the utilization of low-resolution ASTER images for mapping (Vrieling et al. 2007), high-resolution SPOT-5 images for visual interpretation (Jesus et al. 2013), Geographic Object-Based Image Analysis (GEOBIA) with RapidEye for identifying large gullies (Utsumi et al. 2020), and the delineation of gullies through high-resolution constellation imagery sourced from Google Earth Pro (Real et al. 2020).

Additionally, essential tools for environmental management in rural properties in Brazil have emerged, such as institutional land use mapping platforms like MapBiomias and the Rural Environmental Registry (CAR) (Vieira et al. 2023). These platforms offer land use classifications that identify associations with erosion processes, such as bare soil or pasture areas, and guide territorial planning strategies (Perosa et al. 2023). A study conducted by Louzada et al. (2022) examined the correlation between CAR property data, erosion risk, and the implementation of sedimentary barriers in the Upper Taquari River Basin (UTRB), which is a well-known case of

large eroded areas in the Brazilian Cerrado biome (Roque et al. 2021). The UTRB exhibits sandy soils, poorly managed pastures, sinuous relief, and concentrated rainfall during the summer months (December to March), creating an environment favorable for forming numerous gullies (Louzada et al. 2023ab). Furthermore, the presence of sandy sediments contributes to external effects, such as avulsion phenomena in the Pantanal (lower part), caused by the sedimentation of the Taquari River (Assine 2005, Louzada et al. 2021). Hence, we examine numerous RS variables encompassing vegetation, soil, and terrain indices. Our objective is to map and evaluate the status of gullies in the UTRB, serving as an illustration that combines local and external influences. Within this study, we carry out an extensive survey of gullies within the hydrographic basin, seeking to address two central inquiries: firstly, which gullies are actively eroding and require immediate conservation interventions; secondly, how do the mapping techniques of the MapBiomas Project and the management of CAR consider gully features in terms of their respective cartographic attributes.

2. Material and Methods

2.1 Study Area and Gullies Inventory

The UTRB occupies an area of 28,111km² between latitudes 17°30'S to 19°30'S and longitudes 53°00'W to 55°00'W (Fig. 1A) and is located in the center-west of Brazil, covering the states of Mato Grosso and Mato Grosso do Sul. The hydrographic basin is located in the Cerrado biome (Brazilian savannah), where the Taquari River headwaters (Fig. 1B) deliver water and sediment to the depositional system in the Taquari megafan (Assine 2005), the largest of the Pantanal with 50.000km². The relief varies from 178 to 921 (m a.s.l), and the soils are predominantly sandy or of medium texture (clay-sandy-silt) (Galdino et al. 2005). The mean annual precipitation varies between 1,200 mm and 1,800 mm (Marengo et al. 2015), with more significant rainfall events in the austral summer (Bergier et al. 2018, Thielen et al. 2020) and high temperature and reduced humidity in the dry season (Hofmann et al. 2021).

As for land use, we present a 2021 map obtained via MapBiomass (Souza et al. 2020), which summarizes the five most representative classes of the UTRB (Fig. 1C), that is, native vegetation, wetlands, pastures, sugarcane and soybean crops. For them, more than 52% of the land use is about livestock, where areas with significant risk of soil loss have been mapped for restoration strategies (Louzada et al. 2022).

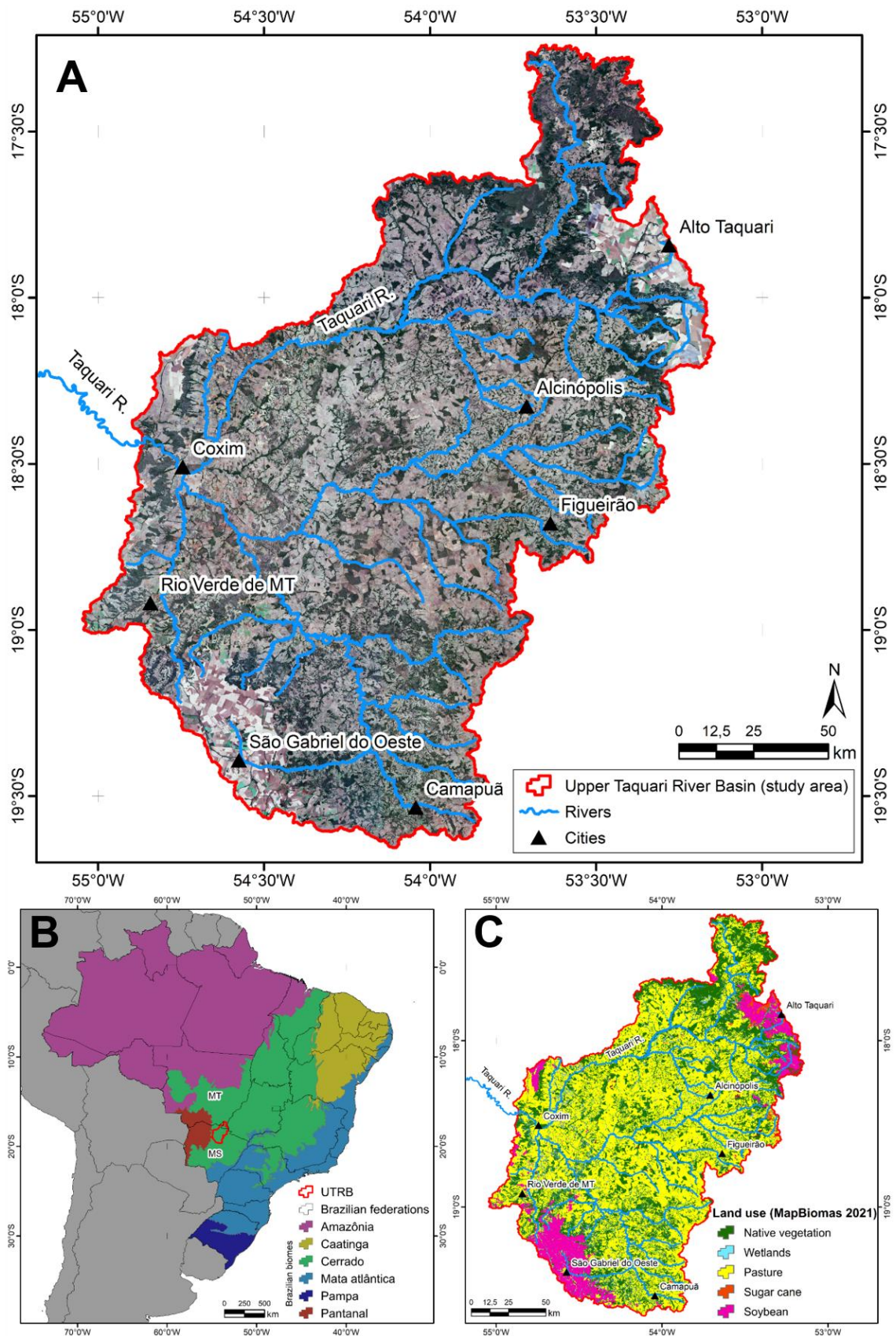


Fig. 1. Location of the Upper Taquari River Basin (UTRB) as the study area (A), superimposed by 2022 Sentinel 2 image mosaic in the True Color composition. (B) Configuration of the Brazilian biomes and respective state federations. (C) Mosaic of the main classes of land use in 2021 from MapBiomas (Souza et al. 2020).

Gullies are linear features in the ground reaching depths greater than 1m, with or without vegetation, dispersed and connected to watercourses (Castillo & Góme 2016, Anderson et al. 2021). While mapping gullies is laborious (Gafurov & Yermolayev 2020) and susceptible to misinterpretation (Thwaites et al. 2022), mitigating costs can be mitigated by reducing field demand. For delimitation to be practical, access to high spatial-resolution images is essential to guarantee greater clarity (Cabral et al. 2020). In this sense, we followed recommendations from Domlija et al. (2019) to use parameters of shape, size, appearance, and texture for visual inspections in gullies inventory based on the Maxar Vivid Basemap 2017-2021 images with a pixel of 0.46 m obtained from the ESRI ArcGIS® at a fixed scale of 1:5,000. For data discussion, we also divided the gullies by size classes into small (up to 1 ha), medium (1 -5 ha), and large (>5 ha).

Furthermore, while conducting the vectorization process, we carefully examined the surroundings of the gullies to determine their classification as either natural/geological formations or as features resulting from anthropogenic activities. Our analysis considered specific conditions within the rugged terrain associated with native vegetation (Vanacker et al. 2019, Wei et al. 2021). Additionally, we considered that the origins of gullies are due to human actions such as constructing unpaved roads, livestock, and unsustainable agricultural practices (van der Waal & Rowntree 2018, Zhang et al. 2019).

2.2 Spatial Patterns of Gullies

We used a mosaic of Sentinel-2A and Sentinel-2B, level 2 images acquired in July 2022 from the European Space Agency (<https://scihub.copernicus.eu/>), accessed on 12/09/2022. The list of scenes and their respective characteristics are in Table S1 in Supplementary Material. Moreover, to obtain the topographic index, we used the DEM ALOS-PALSAR 1 with a resolution of 12.5m (<https://search.asf.alaska.edu/>), accessed on 12/09/2022.

Based on Louzada et al. (2023a), we selected ten features: water, soil, vegetation indices,

biophysical index, optical textures, and topographic index. In addition, three Tasseled Cap indices from Sentinel images were also considered, totaling 13 variables divided into seven major categories (Table 1). Here, we excluded SAR features due to a time-lapse greater than a month between scenes, despite better results on assessments of gully stability (Louzada et al. 2023a). The indices were processed using SNAP software (Sentinel Application Platform) version 9.0, except for the TWI elaborated in ArcGIS version 10.4.1.

Table 1. Categories and variables used in assessing gully stability.

Category	Variable	Equation	Reference
Texture	CORR	$\frac{\sum_i \sum_j (i,j)p(i,j) - \mu_x \mu_y}{\sigma_x \sigma_y}$	Haralick et al. (1973)
	DIS	$\frac{\sum_i \sum_j (i,j)p(i,j) - \mu_x \mu_y}{\sigma_x \sigma_y}$	
	MEAN	$\frac{\sum_i \sum_j (i,j)p(i,j) - \mu_x \mu_y}{\sigma_x \sigma_y}$	
	VAR	$\frac{\sum_i \sum_j (i,j)p(i,j) - \mu_x \mu_y}{\sigma_x \sigma_y}$	
Soil radiometric index	RI	$(B4)^2 / (B3)^2$	Barron & Torrent (1986)
Biophysical index	FCOVER	Calculation method In the SNAP 9.0. All bands were considered.	Kallel et al. (2007)
Vegetation Index	TSAVI	$s * (B8 - s * B4 - a) / (s * B8 + B4 - a * s + X * (1 + s * s))$	Rondeaux et al. (1996)
Water indices	NDWI	$(B8 - B12) / (B8 + B12)$	Gao (1996)
	MNDWI	$(B3 - B11) / (B3 + B11)$	Xu (2005)
Topographic index	TWI	$\ln \left(\frac{A_s}{\tan \beta} \right)$	Wilson & Gallant (2000)
Tasseled Cap	TC_BRI	$0.3037 * B2 + 0.2793 * B3 + 0.4743 * B4 + 0.5585 * B8 + 0.1863 * B12$	Crist & Cicone (1984)
	TC_VEG	$-0.2848 * B2 - 0.2435 * B3 - 0.5436 * B4 + 0.7243 * B8 + 0.0840 * B11 - 0.1800 * B12$	Bannari et al. (1995)
	TC_WET	$0.1509 * B2 + 0.1973 * B3 + 0.3279 * B4 + 0.3406 * B8 - 0.7112 * B11 - 0.4572 * B12$	Crist & Cicone (1984)

Terms of the above equations. Texture: μ_x , μ_y , σ_x , σ_y are the means and standard deviations for the row- and column-marginal probabilities of the co-occurrence matrix composed of $p(i, j)$; TSAVI: a is the soil line intercept; s is the soil line slope; X is the adjustment factor to minimize soil noise; TWI: A_s is the catchment area and β is the local slope. For textures and FCOVER, all bands have been resampled to 10m. The Tasseled Cap calculations preserved the highest spatial resolution (10m). Correlation (CORR), Dissimilarity (DIS), Mean (MEAN), Variance (VAR), Redness Index (RI), Fraction of Vegetation Cover (FCOVER), Transformed Adjusted Soil Vegetation Index (TSAVI), Normalized Difference Water Index (NDWI), Modified Normalized Difference Water Index (MNDWI), Topographic Wetness Index (TWI), Tasseled Cap - Brightness (TC_BRI), Tasseled Cap - Vegetation (TC_VEG), and Tasseled Cap - Wetness (TC_WET).

2.3 Random Forest Classification and Validation

In general, a relationship has been reported between the vegetation cover's complexity

and the degree of stability of severe erosion (Louzada et al. 2023a). Therefore, we selected 1% of the total pixels in the gullies and framed them into stable pixels with the presence of tree vegetation, intermediate pixels with herbaceous-shrub vegetation, and active pixels represented by exposed soils. The adoption of vegetation sizes as a soil stabilization characteristic stems from the relationship between more complex structures (trees) and soils richer in clay and organic matter in the Cerrado (de Souza et al. 2021, Amaral et al. 2022). The selection was done using the ArcGIS random select tool, with a minimum distance of 100m between pixels. The classification was also based on the visual interpretation through the Sentinel-2A and 2-B mosaic in the True Color Image composition in the high-resolution layer of the GIS base map and NDVI (Rouse Jr. et al. 1974) as auxiliary data (see Fig. S1).

Here, we adopted the RF algorithm (Breiman 2001) in R Software for Statistical Computing v.4.0 (R Core Team 2013) for pixel classifications, given its reasonable results in gully mappings compared to other ML methods (Avand et al. 2019, Bachri et al. 2019, Phinzi et al. 2021). We follow the default *n*tree parameters in R (500) and *m*try by the square root of the number of variables (Diniz et al. 2020). From the total pixels evaluated in the visual interpretation, 70% were set for training and 30% for validation through the Overall Accuracy (OA) and Kappa index. Furthermore, we performed the variable importance analysis through the Mean Decrease Gini index.

Based on RF classification, Boolean rules were developed to classify gullies and to guide management and conservation measures. The ratio of pixels categorized as active, intermediate, or stable was used to classify the pixels accordingly as stable ($\geq 70\%$ stable pixels), advanced intermediate ($> 50\%$ intermediate pixels or $> 20\%$ stable pixels, or $< 20\%$ active pixels), initial intermediate (between 20 and 50% active pixels) and active ($\geq 50\%$ active pixels).

2.4 Land use and regulatory legislation analysis

MapBiomass is a notable initiative for mapping land use across national territory. It holds

immense significance in various fields, such as deforestation and regeneration (Coelho-Junior et al. 2022), pasture degradation (Santos et al. 2022), and burned sites (Alencar et al. 2022). The project collaborates with NGOs, universities, and technological companies to research Brazil's land use and climate change. The methodology employs deep learning algorithms and cloud-based image processing from Landsat, Sentinel-2, and Planet, with spatial resolutions of 30m, 10m, and 3m, respectively. Given the project's comprehensive scope, we assessed the agreement between the land use classifications of MapBiomias and our RF classification results at the pixel level.

Concurrently, pixels representing gullies were also compared to the national CAR database, accessed through the SICAR website (<https://www.car.gov.br/publico/imoveis/index>), accessed on 02/02/2023. The CAR is a collection of shapefiles categorized according to the land use types within each rural property. It serves as the primary tool for rural landowners to comply with the legal obligations stipulated by the Brazilian Forestry Code (Law 12.651/2012). Although the system operates on a declaratory basis (owner's responsibility), it undergoes subsequent inspection by each State of Brazil. As a result, it serves as the official platform for exchanging information between rural property owners, public authorities, and the public in general, as a tool for compliance with environmental regulations outlined in the Brazilian Forest Code. This compliance has implications for operation licensing and access to public-private financing (Jung et al. 2017). Table 2 describes the MapBiomias land use classes and the CAR features in our study area.

Pixels classified as active gullies, a higher percentage of correspondence in MapBiomias was expected for other non-vegetated areas (ONV). Those pixels classified as intermediate should correspond to savanna formation (SF), grassland (G), and pasture (P). The remaining classified as stable should be associated with forest formation (FF) and SF. Alternatively, there is no feature related to exposed soil for CAR classes. Nevertheless, considering that most UTRB gullies are connected to watercourses (Louzada et al. 2022,2023a), we assumed these pixels

should correspond to a preservation-protected area (APP). In turn, intermediate pixels could be framed as consolidated area (AC), APP, legal reserves (RL), or ‘vereda’ (V), just like stable pixels, except for the AC class.

Table 2. Land use classes and CAR characteristics were applied in this study.

Source	Item	Description
MapBiomias ¹	Forest formation (FF)	The predominance of tree species, with the formation of continuous canopy
	Savanna formation (SF)	Formations with defined arboreal and shrubby-herbaceous strata
	Forest plantation (FP)	Tree species planted for commercial purposes
	Wetland (W)	Vegetation with a predominance of herbaceous stratum subject to flooding seasonal or under river/lacustrine influence
	Grassland (G)	Native grassland formations with a predominance of herbaceous stratum
	Pasture (P)	Pasture areas, predominantly planted, linked to the activity of agriculture
	Sugarcane (S)	Areas cultivated with the sugarcane crop
	Mosaic of Uses (MU)	Areas of agricultural use where it was impossible to distinguish between pasture and agriculture.
	Urban area (UA)	Areas with significant density of buildings and roads, including accessible areas of buildings and infrastructure.
	Other non-Vegetated Areas (ONV)	Areas of non-permeable surfaces and regions of exposed soil
	Rocky Outcrop (RO)	-
	River, Lake and Ocean (R)	Rivers, lakes, dams, reservoirs, and other bodies of water
	Soybean (SB)	Areas cultivated with soy
	Other Temporary Crops (OTC)	Areas occupied with short- or medium-term crops, usually with a growing season of less than a year
Cotton (C)	Areas cultivated with cotton	
CAR ²	Preservation Protected Area (APP) ³	The protected area, covered or not by native vegetation, has the environmental function of preserving water resources. They are marginal strips of any perennial and intermittent natural watercourse, springs, steep slopes, and plateaus.
	Legal Reserve (RL)	Area covered by native vegetation ranging from 20% to 35% of the total size of the rural property and depending on the state’s biome
	Consolidate Area (AC)	Area of rural property with pre-existing anthropic occupation on July 22, 2008, with buildings, improvements, or integrated crop-livestock activities

Restricted Use (UR)	Areas with use restrictions and protection conditions similar to APP and RL
Vereda (V)	Area with a savannah phytophysiology, found in hydromorphic soils, usually springs of watercourses
Hydrography (H)	Body of water

Sources of descriptions: 1) <https://mapbiomas.org/codigos-de-legenda> accessed on 02/02/2023; 2) Law 12,651/2012; 3) APP polygons may appear in the SICAR database as native vegetation recovery areas.

3. Results

3.1 Gullies inventory and degrees of stability

We identified 2,960 gullies covering an aggregate area of nearly 3,200 hectares during the vectorization process. These gullies constitute 0.1% of the entire study area. On average, each gully had an area of ~1 hectare. Categorizing them by size, it was observed that smaller gullies measuring up to 1 hectare accounted for the majority, comprising 71% of the total (n=2,115). Gullies of medium size, spanning 1 to 5 hectares, constituted 25% (n=746), while larger gullies exceeding 5 hectares made up 3% (n=99). Medium-sized gullies occupied nearly half of the eroded area, representing 46% of the total (1,482.3 hectares). Large-sized gullies covered 28% (898.9 hectares), and small gullies accounted for the remaining 26% (817.6 hectares). The geographical coordinates of the erosion centroids categorized by size groups and corresponding examples of vectorized representations have been overlaid on a high-resolution image. These visualizations are presented in Figure 1, and all geographic coordinates of the centroids are documented in Table S2.

By interpreting neighboring gullies with high-resolution imagery (see results in Table S2), it was noted that only 3% (n=80) of the linear features exhibited characteristics indicative of natural origin, with steep relief in preserved Cerrado vegetation. On the other hand, the remaining 97% (n=2,880) of the gullies were primarily associated with livestock practices and proximity to rural roads. Notably, no erosion has been detected in relatively plain and well-managed soils in grain production areas.

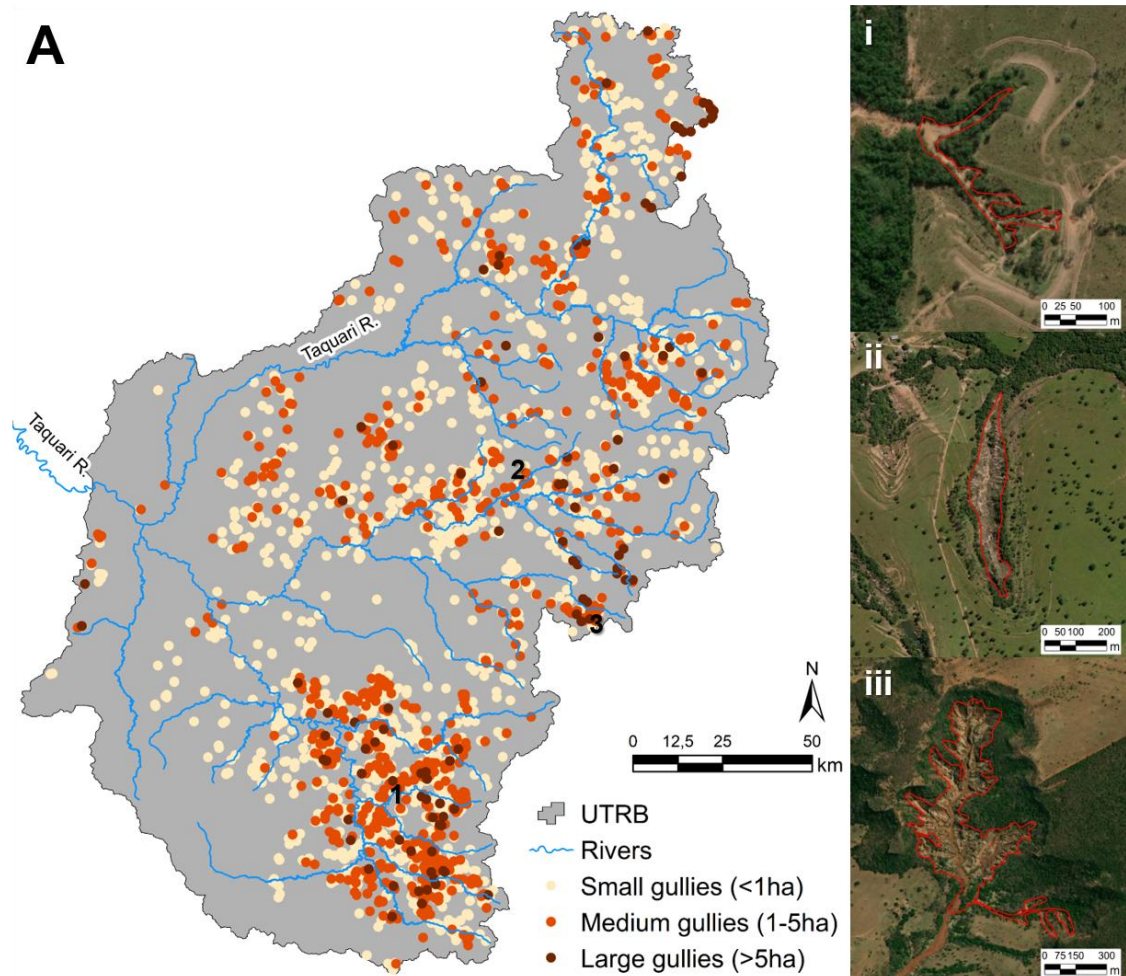


Fig. 2. Map of the distribution of gullies by size groups (A). On the left, there are gullies with red lines. Thus, gully number 173 represents the small erosion group (i), gully 1755 for medium erosions (ii), and gully 1334 for prominent features (iii), both superimposed by high-resolution GIS base map images.

The set of gullies represented 319,806 pixels, and descriptive statistics stratified by variables are presented in Table S3, in addition to the maps of the 13 UTRB variables (see Fig. S2 to S14). From that total, 3,198 pixels (10%) were randomly selected for training and validation, of which 1,888 (59%) were classified as active pixels, 935 (29%) as intermediate pixels, and 375 (12%) pixels were considered stable (see examples in Fig. S15).

The classification results obtained through RF achieved accurate maps depicting different levels of gully stability (Table 3). The OA of the classification was 0.96, with a Kappa index of 0.93, indicating a high level of agreement. Among the three classes, there was minor confusion between intermediate and other classes due to difficulties distinguishing between herbaceous portions and exposed soils. Moreover, shrub stratum pixels are analogous to stable

forest pixels in the Cerrado biome. On the other hand, an essential aspect of this method is the successful separability between extremes represented by stable and active pixels. Regarding spatial variables, the Gini Index (Fig. S16) demonstrated that five variables correspond to more than 83% of the importance in the classification, namely the fraction of Vegetation Cover (FCOVER) with 44%, followed by 16% of Normalized Difference Water Index (NDWI), 14% Tasselled Cap - Vegetation (TC_VEG), 6% of Tasselled Cap - Wetness (TC_WET), and 4% of Redness Index (RI).

Table 3. Confusion matrix of RF classification.

	Active	Intermediate	Stable	Total
Active	556	14	0	570
Intermediate	10	262	6	278
Stable	0	5	107	112
Total	566	281	113	960
OA (%)				96
Kappa index (%)				93

Figure 3 shows the thematic map with the centroid of the gullies and their respective size classes and degrees of stability. Small and medium gullies are commonplace through the four classes of stability, while large gullies neither show erosive features in an advanced stage of stability nor stabilized gullies. The expressive majority of erosion is active (60%), followed by units in the initial intermediate grade (24%) and advanced intermediate grade (15%), and only 2% of gullies are stable. The complete list of erosion by size and stability classes is shown in Table 4.

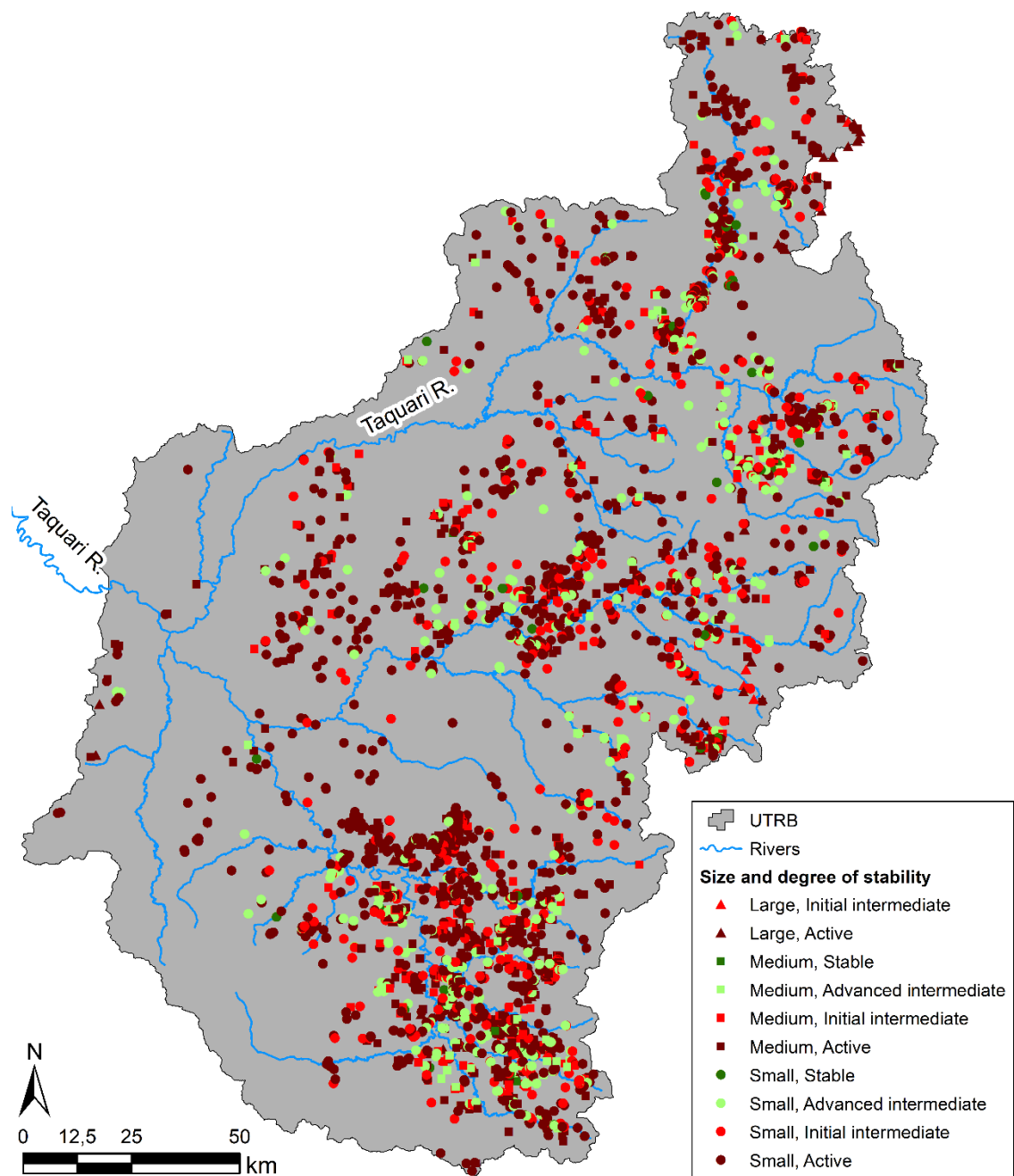


Fig. 3. Map of gully centroids with size classes and degrees of stability.

Table 4. Relationship between degrees of stability and gully class sizes.

Degree of stability	Mediu			Total
	Small	m	Large	
Active	1,193	501	81	1,775
Initial intermediate	508	179	17	704
Advanced intermediate	374	61	0	435
Stable	43	3	0	46
Total	2,118	744	98	2,960

Figure 4 shows several medium-sized gullies (1-5ha) due to their presence across all stability stages. Among these, active gully number 2,603 (depicted in Figure 4A) exhibited over

90% of its pixels as bare soil, transitioning to the early stages of stability towards its endpoint. In the case of the other gully classes, the vegetation pixels corresponding to tree cover matched well with the high-resolution imagery. This alignment is evident from the stabilized gully 1,981 (Figure 4D) along the advanced intermediate gully 1,398 boundaries and initial gully 2,341 (detailed in Figures 4C and 4B).

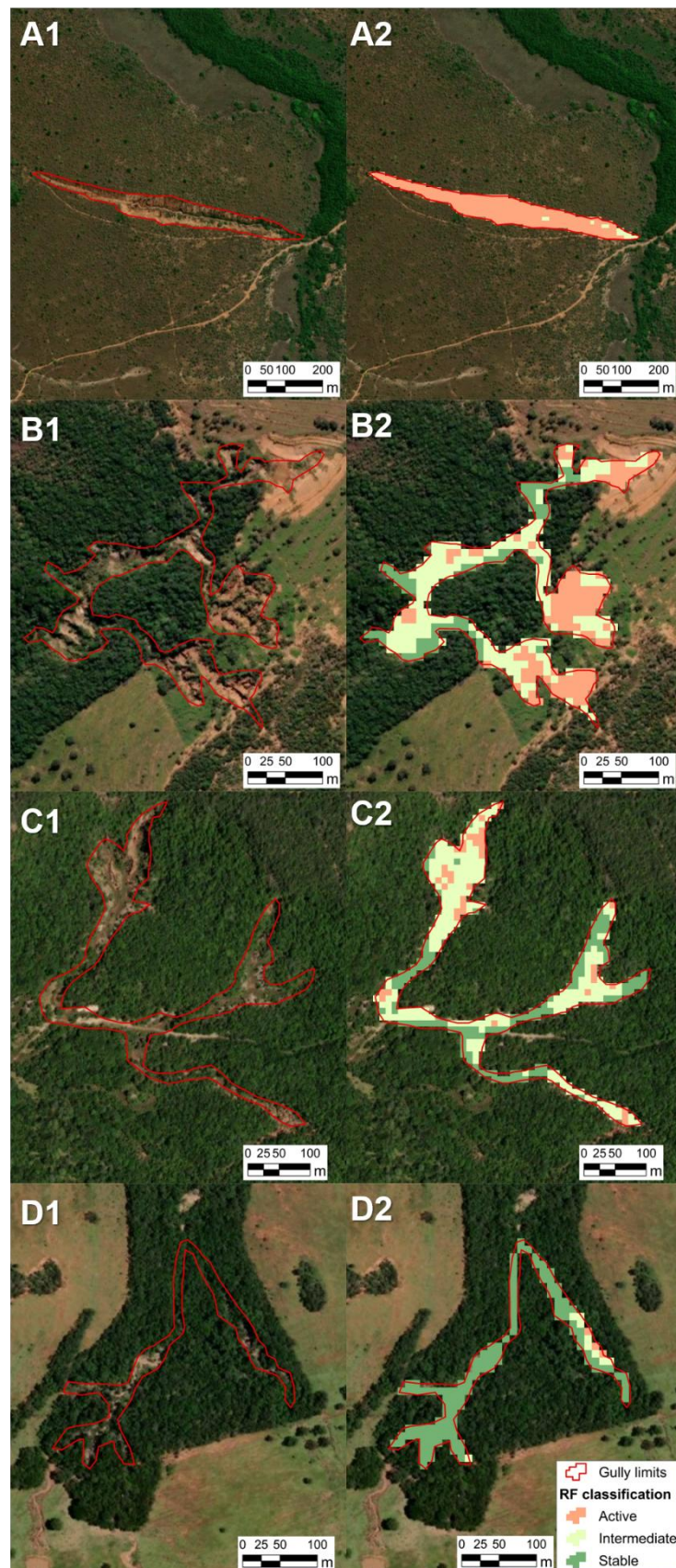


Fig. 4. Samples of medium-sized gullies that are active (A), initial gullies that have intermediate activity (B), advanced gullies that have intermediate activity (C), and stabilized gullies (D). 1) represents the gully boundaries in the high-resolution ArcGIS base map; 2) pixel classification results in the RF algorithm.

3.2 Land use maps and gullies classification

The total gully pixels (n=319,806) were congruent with the MapBiomass land use and occupation raster. However, within the CAR dataset, due to discrepancies in land regularization, only 239,957 pixels (75%) were explicitly identified as erosion within their respective class. Figure 5 portrays the interplay between attributes and gully pixels via bar graphs.

Regarding the MapBiomass data (depicted in Fig. 5A), it was discerned that only 3% of active pixels were categorized under the bared soil classes (ONV). No predominance was observed among intermediate pixels, whereas those stable collectively accounted for 62% relative to FF and SF vegetation pixels. Analyzing the CAR database (as illustrated in Figure 5B), it was verified that no gully pixels could be associated with the category of APP recovery. Alternatively, the prevalence of RL was high, constituting 46% of the entire dataset.

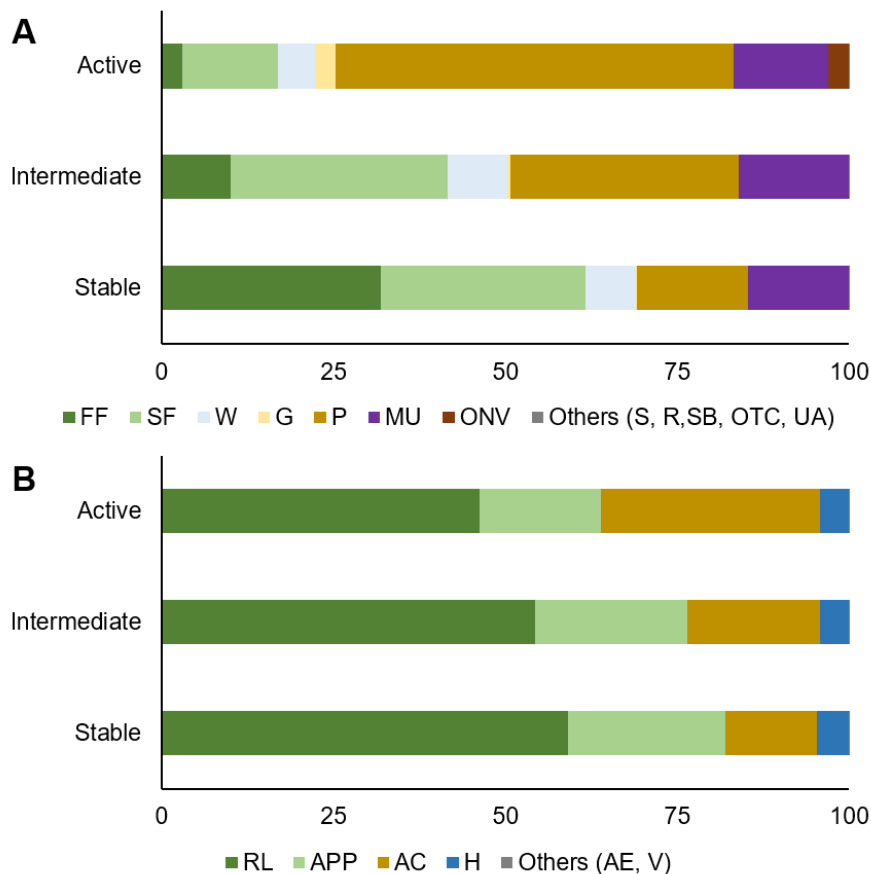


Fig. 5. Relative bar chart depicting the distribution of active, intermediate, and stable pixels concerning MapBiomass (A) and CAR (B) categories.

4. Discussions

4.1 Methodological aspects, challenges, and future perspectives

The UTRB gathers a significant number of gullies (2,960), of which currently 60% are active, corresponding to a density of 9.5 gullies/km². That rate of occurrence is comparable with gully areas on the globe (Vanmaercke et al. 2020). Routinely, gully classification considers each erosive branch as an independent head. Alternatively, our new method considers all related gully heads, hence suitably providing a systemic, interconnected overview.

In our framework, visual inspection plays a crucial role in identifying the boundaries of gullies. Like other studies, scale and high-resolution base image were essential for achieving successful inventories, as highlighted by Vrieling et al. (2008), Đomlija et al. (2019), and Karydas and Panagos (2020). Regarding the variable's importance, FCOVER exhibited a notable relevance in discerning phytophysognomic characteristics within the gully – see equivalent findings by Mudereri et al. (2021) and Li et al. (2023). The present work also evidenced that the most effective stability patterns for gullies involved a combination of multispectral orbital indices like vegetation (FCOVER and TC_VEG), water (NDWI), and soil (RI). Furthermore, substituting complex Synthetic Aperture Radar (SAR) data with optical Tasseled Cap image processing on a regional scale (as discussed in Louzada et al. 2023a) did not compromise results.

Although results are promising, the lack of fieldwork prevents, for example, the separation of active gullies from those stabilized by reaching the bedrock or more resistant parent material (Soares da Silva et al. 2019). Gullies exhibit a heterogeneous nature, resulting in variations in slope characteristics along their length and base (Borja et al. 2018). Therefore, accurate classification always relies on detailed on-site observations and assessments. Field incursions would also add to the delimitation of gullies' perimeter and volume, e.g., with the benefits of UAV technologies (Yang et al. 2019, Soufi et al. 2020). Another issue is obtaining good control points for algorithm training (Arabameri et al. 2019, Chuma et al. 2023) and classification of gully types (Cabral et al. 2020). Altogether, better (historical) remote, aerial, and

local data can be combined to improve our understanding of the evolution of these features over time (Vanmaercke et al. 2021). In that context, fieldwork and the inclusion of new RS data are welcome prior to any restoration interventions.

The current research is among the pioneer studies for evaluating gully stability patterns on a regional scale. Any territory with severe erosion can use our methodological framework based on freely distributed resources (Bell et al. 2021), which optimizes the time and operating costs (Žižala et al. 2019). Besides, the present approach is rather original and thus can enhance earlier studies of gully inventories, e.g., those in Australia (Daley et al. 2021), in semi-arid lands of Iran (Soufi et al. 2020), and in the Loess Plateau in China (Na et al. 2020). For global erosion inventories, as Dube et al. (2020) and Vanmaercke et al. (2021), our findings suggest that the studied region could be regarded as a hotspot in the South America continent, filling part of the research gap (Liu et al. 2021).

4.2 Comparisons with MapBiomias and CAR categories

Upon examining high-resolution images and land use data, significant causes of gullies in the studied region stem from unsustainable practices in pastureland for cattle and the lack of runoff control structures alongside rural roads.

Despite the extensive use of non-governmental initiatives like MapBiomias and governmental systems like the CAR for rural area management (Bonanomi et al. 2019, Heilmayr et al. 2020, Cabral et al. 2022), it is worth noting that neither of these systems includes a specific class for soil erosion. To better understand the non-conformity, we highlight the medium-sized active gully 169 and its respective classification according to the MapBiomias and CAR products (see Fig. S17A to D). The class that is most appropriate for active gullies is other non-vegetated (ONV), but in gully 169 (Fig. S17C), as in most active gullies, there was a large part of the active gully classified as pasture (P). There is no grazing as the top layer has been removed, and the steep, winding relief impedes the area from grazing. With 30 m resolution and multispectral

signatures (Roberts et al. 2019), it is possible to identify erosion features that are larger than 1 hectare if they are well-defined using artificial intelligence (Chowdhuri et al. 2020) or by applying auxiliary data like Sentinel and Planet images. As an outcome, we suggest that MapBiomass add erosion in its category method updates.

The CAR issue is somewhat serious because, under any circumstances, an exposed soil pixel should be considered a fragment of native vegetation (APP or RL). Most critically, there is no specific attribution for gullies. While efficient for law enforcement (Brancalion et al. 2016), mainly to prevent illegal deforestation (Azevedo et al. 2017, Rajão et al. 2020), this work reveals that the CAR deserves an update to directly address active erosion and prevent the onset of new gullies hotspots in the country. Updating features/classes is not simple, as it involves public regulations in various spheres. Another bottleneck is rural landowners, who could be reluctant to report erosion due to eventual land depreciation.

The UTRB is a prime illustration of the discrepancies between existing land use databases and erosion mapping. By focusing on this region, we shed light on the shortcomings in other parts of the country, which could be equally or more severely degraded as other examples of Brazilian soil erosion hotspots (Bezerra et al. 2020, Vieira et al. 2021). Therefore, the land recovery plans might become more practical by incorporating erosion as pivotal in MapBiomass e CAR categorical databases.

5. Conclusions

We developed a novel technique for evaluating gullies by combining visual interpretation and machine learning on readily available remote-sensing images. The findings highlight that 60% of the UTRB gullies are undergoing erosion, emphasizing the urgent requirement for remedial measures. Additionally, only 2% of the gullies have been found stable, indicating substantial room for enhancement. The classes of MapBiomass and CAR neither suitably match nor represent exposed soil characteristics of active erosions, which demand the

effort for creating respective categories.

Despite the satisfactory accuracy demonstrated in this study, combining fieldwork and utilizing more detailed image technologies, such as UAVs, would undoubtedly improve the knowledge of stability thresholds. Our method can reduce field and UAV expedition costs, helping with land use planning and management by providing trustworthy soil erosion information.

Supplementary material available in:

<https://docs.google.com/document/d/1yAJLT8fn-n1auvVs0qljd7WtqawcHak/edit?usp=sharing&ouid=110830496409468836501&rtpof=true&sd=true>

Chapter 4: Spatiotemporal patterns of exposed soil in a highly eroded Brazilian river basin in 1985/2024: Is it the worst over?

Abstract

Soil exposure causes significant environmental degradation through erosion, biodiversity loss, and reduced carbon sequestration, underscoring the importance of spatial monitoring and mitigation strategies. This study employed remote sensing (RS) and geographic information systems (GIS) to analyze the spatiotemporal dynamics of bare soil in the Upper Taquari River Basin (UTRB), Brazil, from 1985 to 2024. A statistical assessment of bare soil separability from other land use and land cover (LULC) classes was conducted using nine vegetation and soil indices derived from Landsat mosaics for 2024. These indices were processed on the Google Earth Engine platform, and ground truth points and orbital image interpretation supported temporal classification. Land use classes from the MapBiomas project were incorporated to examine correlations with bare soil dynamics. Temporal analysis included a breakpoint evaluation of the percentage of exposed soil across the basin, specifically in areas with slopes greater than 8%, with a higher erosion risk. Additionally, the Space Time Cube tool in ArcGIS allowed the assessment of trends in bare soil distribution over time and space. Tasseled Cap Brightness (TC_BRI) exhibited the highest discriminatory power for identifying bare soil among the tested indices. Breakpoint analysis revealed two distinct periods: from 1985 to 2015, there was a linear increase in bare soil (adjusted $R^2 = 0.44$; $p < 0.001$), rising from 0.13% in 1985 to 0.8% in 2015. This trend was strongly correlated with the decline of native vegetation (forest and savanna) and the expansion of anthropogenic land uses such as cotton, soybean, and pasture. In contrast, from 2016 to 2024, no significant trend was detected (adjusted $R^2 = 0.13$; $p > 0.05$), although bare soil peaked in 2021 at 3.36%, followed by a decline to 0.6% in 2024. Correlation analysis indicated that native vegetation loss remained a key driver; however, signs of natural vegetation regeneration were observed, with a transition from bare soil pixels in 2016 to shrub and tree cover by 2024. That agrees with spatial stabilization and localized reduction of bare soil areas, as revealed by the Space Time Cube analysis. Although some areas of the UTRB show stabilization and recovery, the current data are insufficient to model whether the region has surpassed its bare soil exposure and erosion risk peak. Future research should focus on filling these gaps and further evaluating the ecological trajectories of newly vegetated Cerrado areas and the economic factors involved in land use/bare soil oscillations.

1. Introduction

Current soils are at serious risk due to rapid degradation caused by unsustainable human practices, threatening their functionality and ecosystem services (Gomiero, 2016; AbdelRahman, 2023). Although research, techniques, and machinery have advanced in reducing soil loss, erosion remains a serious dilemma today (Feng et al. 2022). Concentrated erosion has significant destructive power, excavating the soil deeply, forming gullies, and causing irreversible loss of fertile land (Singh and Hartsch, 2019). In the same sense, leaf erosion, sometimes less noticeable, leads to the loss of superficial and more fertile soil layers (topsoil) (Osman, 2014; Farooq et al. 2023). In general, this entire rate of degradation begins with the exposure of the soil to the impact of raindrops and surface runoff (Bahddou et al. 2023). Hence, diagnosing degradation sites due to soil exposure is essential, aiming to prevent losses and conserve natural resources.

Another detrimental effect of soil exposure is excessive warming, especially in tropical regions (Sun et al. 2025). Soils disturbed by cover loss or inadequate management tend to absorb more solar radiation and increase their daily temperature (Dawson and Smith, 2007; He et al. 2024). Rising temperatures directly accelerate the decomposition of organic matter by enhancing microbial activity, increasing the release of carbon stored in the soil (Kirschbaum et al. 1995; Barreto et al. 2021). Under these conditions, soils gradually shift from being carbon sinks to becoming net sources of CO₂ emissions (Liu et al., 2022). Although the rapid breakdown of organic matter promotes nutrient cycling, it often occurs without sufficient vegetation to absorb these nutrients (Raza et al. 2023). Consequently, soil degradation contributes to biodiversity loss and the disruption of ecosystem services, posing significant threats to food production and security (Gomiero, 2016).

Therefore, mapping exposed soil sites helps identify areas vulnerable to soil loss due to water action. It also pinpoints areas that may suffer damage from rising temperatures and their interrelationships with the carbon and nutrient cycle (Pregitzer and King, 2005; Macdonald et al. 2018). In this sense, avoiding soil exposure and quickly covering what is exposed avoids impacts

on site (erosion, loss of natural fertility) and even off-site, through siltation of water courses and loss of biodiversity (Majoro et al. 2020; Rashmi et al. 2022). Therefore, the percentage of exposed soil in the landscape can be a valuable metric for assessing the environmental integrity of a watershed scale.

Remote sensing (RS) and GIS emerge as allies in these spatial assessments of landscapes. Several works demonstrate the impacts of anthropogenic activities on natural resources such as water, soil, and biodiversity, applying RS and GIS tools (some examples in Obeidat et al. 2019; Singh and Vyas, 2022; Lv et al. 2025). In this context, vegetation and soil indices from multispectral orbital sensors (e.g., Landsat and Sentinel) are sensitive to changes in land cover and use, making them helpful in interpreting terrestrial targets (Chaves et al. 2020). About exposed soil, several indices have been applied, with emphasis on the bare soil index (BSI) (Salas and Kumaran, 2023), brightness index (BI) (Azabdaftari and Sunar, 2016), and the classics such as the difference normalized vegetation index (NDVI) and soil-adjusted vegetation index (SAVI) (Ul-Haq et al. 2022; Anthony and Emmanuel, 2025). Another promising index is the normalized burn rate (NBR), which has demonstrated good accuracy in identifying agricultural crop residues and is easily misinterpreted as exposed soil (Sousa et al. 2024). In general, orbital sensors like Landsat have limitations regarding spectral clutter due to pixel size (30m) (Hemati et al. 2021); thus, identifying pixels with bare ground patterns is challenging. In addition to field data for identifying spectral patterns, layers such as relief can contribute to the selection of exposed soil pixels and the real potential for soil loss.

Looking at the river basin territory, spatiotemporal analysis can reveal land-use/erosional change patterns that remain undetected when examining time and space in isolation, such as seasonal shifts in erosion hotspots, the persistence of hotspots in time, emerging degradation trends linked to human activities, or yet identifying regions where erosion is accelerating over multiple years. Thus, integrating both spatial and temporal dimensions is crucial to understanding how patterns evolve across locations and time. Translating to tropical

regions, intense rainfall exacerbates soil loss, accelerating biodiversity decline and ecosystem service disruption (Scholes, 2016; Adla et al. 2022). Mapping and long-term erosion monitoring to support cost-effective decision-making for mitigating food production and security impacts are critical (Getahun et al. 2024); it is still rare for most tropical watersheds.

Here, we utilize RS and GIS to conduct a spatiotemporal assessment of the environmental integrity of the tropical Brazilian Upper Taquari River Basin (UTRB). This analysis is based on the proportion of exposed soil pixels detected in Landsat imagery from 1985 to 2024 to determine whether the peak in bare land exposure has already occurred. The UTRB is among the most degraded basins in Brazil, with approximately 3,000 gullies (Louzada et al. 2023) and a landscape characterized by sandy soils and steep slopes, making it highly susceptible to erosion (Ide et al. 2016; Louzada et al. 2022). Understanding the spatiotemporal patterns of exposed soil is essential for assessing erosion trends and their broader impacts, including sedimentation and river avulsion (Assine, 2005). These insights are critical for informing conservation strategies and guiding restoration efforts in the region.

2. Material and Methods

2.1 Study Area

The Upper Taquari River Basin (UTRB) covers 28,111 km² in Mato Grosso and Mato Grosso do Sul, in the central-western region of Brazil (17°30'S – 19°30'S; 53° 00'W–55°00'W – Figure 1a). Altitudes vary from 178 to 921 m, with a landscape of depressions, plains, and plateaus. Considering the slope classes by Santos et al. (2018), around 68% of the area has flat (0-3%) or smoothly undulating relief (3-8%), and 25% of the total falls within the undulating slope range (8 -20%). Only 6% have an upper slope similar to mountains and escarpments or steeps (see slope map in Fig. 1b). Geologically, UTRB rivers flow through stable rocks but connect to unstable alluvial systems in the Pantanal wetland (Assine, 2005). The Taquari megafan, a globally notable depositional system, results from the low longitudinal gradient of the Pantanal and the high sediment loads of the highlands (Assine, 2005; Makaske et al. 2012).

UTRB soils, derived mainly from sedimentary rocks, have sandy textures, deep horizons, and low natural fertility (Galdino et al. 2005). Annual precipitation ranges from 1,700–1,800 mm in the northeast to 1,200 mm in the south and southwest (Thielen et al. 2020), with a rainy season from November to March (Marengo et al. 2015). The original vegetation of the Cerrado has been replaced by grazing on sandy soils and agriculture on clayey soils since the 1970s (Souza et al. 2020), resulting in soil exposure and the formation of huge erosions (gullies) (Louzada et al. 2023). Approximately 62.71% of the UTRB consists of microproperties ranging in size from 0.24 to 279.9 hectares, including rural settlements. In contrast, less than 10% of the area comprises large properties exceeding 767.9 hectares (Louzada et al. 2022).

At the bottom of Figure 1 are examples of photographs obtained in the area of land use and occupation classes that were important for defining the method for extracting bare soil pixels (see details in section 2.3).

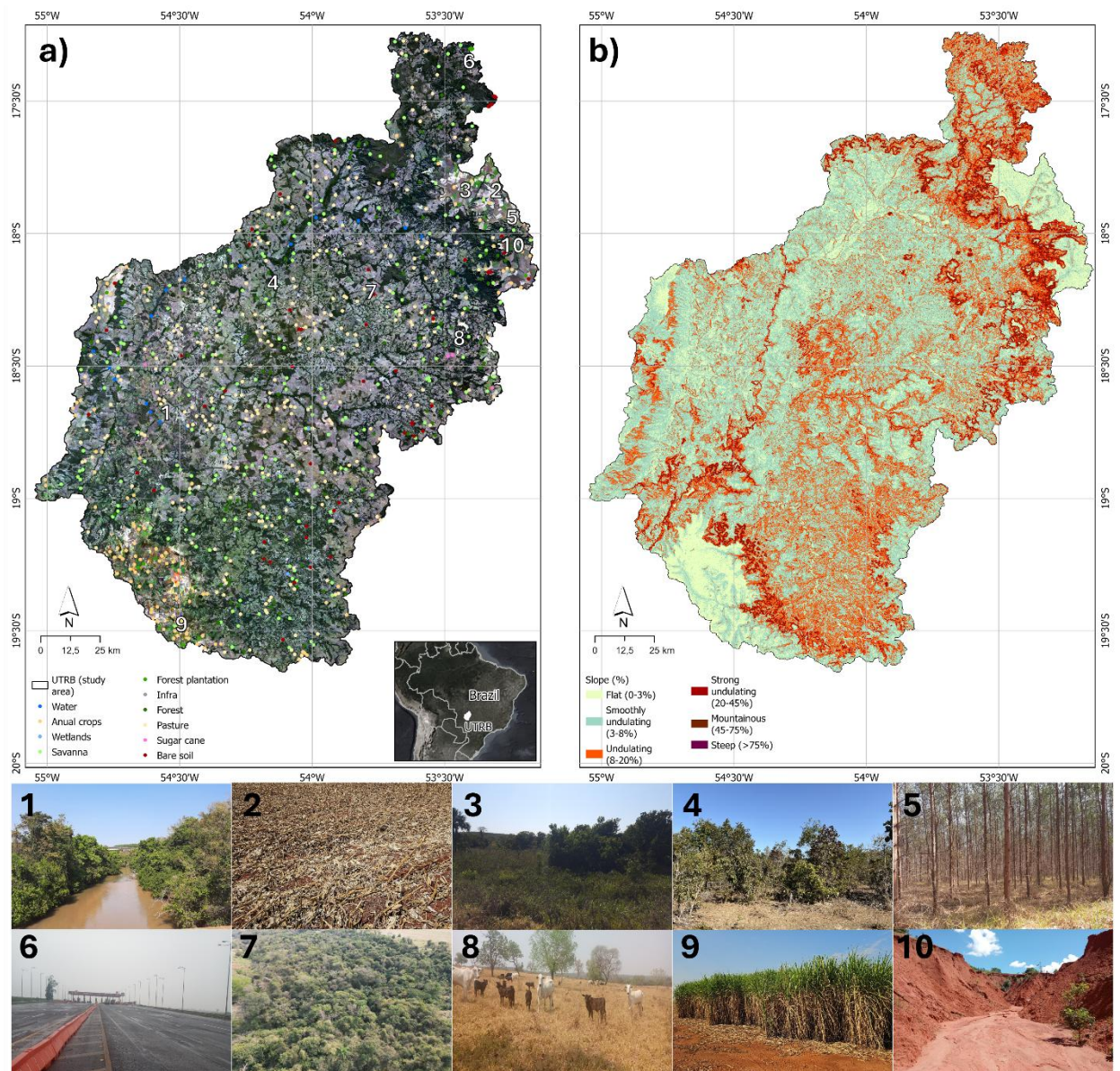


Fig. 1. Map of the Upper Taquari River Basin (UTRB) overlaid on a Landsat 8 (R4G3B2) mosaic as the study area and its location in central-western Brazil (a), as well as the points of 10 land use and occupation classes collected to define the best method for separating bare soil pixels (section 2.3). Slope classes in percentage in the UTRB (b). The numbered photographs are examples of field collections for each land use/occupation class, being: 1) water; 2) annual crops; 3) wetlands; 4) savanna (Cerrado); 5) forest plantation; 6) infrastructure; 7) forest; 8) pasture; 9) sugar cane; and 10) bare soil.

2.2 Data acquisition for bare soil evaluation

The assessment of bare soil pixels used sensors from the Landsat family (30m spatial resolution), given their uninterrupted temporal coverage since 1985, compared to the Sentinel 2 sensor (10m), which has only been available since 2015. At this analysis stage, nine vegetation and soil indices were arbitrarily chosen to define one suitable for segregating pure pixels of

exposed soil in the landscape: the Bare Soil Index (BSI) (Zhao and Chen, 2005), Brightness Index (BI) (Mathieu et al. 1998), Normalized Difference Vegetation Index (NDVI) (Rouse Jr. et al. 1974), Soil-Adjusted Vegetation Index (SAVI) (Huete, 1988), Modified Soil-Adjusted Vegetation Index (MSAVI) (Qi et al. 1994), Transformed Soil-Adjusted Vegetation Index (TSAVI) (Baret and Guyot 1991), Tasseled Cap Vegetation (TC_VEG) (Bannari et al. 1995), Tasseled Cap Brightness (TC_BRI) (Bannari et al. 1995), and Normalized Burn Rate (NBR) (Key and Benson, 2006). Despite not being related to soil or vegetation, NBR was included in the analysis due to its correlation with crop residues (Safanelli et al. 2020).

Index collection was carried out on the Google Earth Engine® (GEE) platform according to the script in Section A of the Supplementary Material. At this stage, images were acquired from the Landsat 8 sensor with median pixels between 06/01/2024 and 08/31/2024, referring to the dry period of the study area. A cloud filter and cloud shadow were also applied to the pure bands before orbital indices calculations.

2.3 Bare soil temporal classification

The classification of exposed ground pixels was carried out by obtaining 152 ground truth points in September 2024, corresponding to the driest period of the year and when soybean planting begins. Additionally, 715 orbital truth points were added through the visual interpretation of an R4G3B2 mosaic of a Landsat 8 image processed at GEE for the same period as the orbital indices (Fig. 1a). 10 classes of land use and occupation (LULC) were collected; they are: water, annual crops (soybean, corn or cotton), humid area, native forest formation, savanna formation or Cerrado, pasture, infrastructure, forest planting (eucalyptus), sugar cane and bare soil (some examples in Fig. 1). The definition of these LULC classes followed the mapping standard carried out by the Mapbiomas project using the same images from the Landsat family (Souza et al. 2020).

The extract values for the points tool in ArcGIS®Pro collected pixel information for each index and LULC class. The data was then normalized to facilitate the comparison of scales and,

finally, the generation of box plots in the R software (R core team, 2013), seeking to visualize distributions and identify patterns in the values.

The index and corresponding ranges that provided the highest separability of exposed soil pixels in the distribution analysis were selected and applied consistently across the entire time series from 2023 to 1985 using the ArcGIS®Pro raster calculator. Nonetheless, years with significant cloud cover and cloud shadows were excluded due to their impact on the study area's total coverage.

2.4 Bare soil pixels affected by high slope

Land slope is one of the main factors of vulnerability to soil loss (Setyawan et al. 2019). As a rule, the hill favors surface runoff to the detriment of infiltration, leaving the land more vulnerable to the loss of particles. Here, we use the relief factor as a mask in the temporal analysis of exposed soil pixels. It was essential to separate the bare pixels related to seasonal agricultural operations, generally carried out on flat or smooth terrain, from those pixels of exposed soil on sloping terrain with a real risk of erosion.

To calculate the slope, the TOPODATA project database was used (<http://www.dsr.inpe.br/topodata/index.php>) from the National Institute for Space Research (INPE), which consists of a refinement of the SRTM images for Brazilian territory (Valeriano, 2005). This study used the percentage slope base with 30m pixels. The original data were stratified into relief classes according to Santos et al. (2018), being: flat (0 to 3%), smoothly undulating (3 to 8%), undulating (8 to 20%), strongly undulating (20 to 45%), mountainous (45 to 75%) and steep (>75%).

2.5 Temporal analysis

The bare soil pixel data of the time series were subjected to a breakpoint analysis in R, using the structchange package (Zeileis et al. 2002), which allows the identification of abrupt changes or transitions in the behavior of the data over time, based on linear regression models. The segments of the time series were defined considering the lowest value of the BIC (Bayesian

Information Criterion), calculated by:

$$\text{BIC} = -2 \times \log(L) + k \times \log(n) \quad (1)$$

where L is the model's probability, k refers to the number of model parameters, and n equals the number of observations. The lowest BIC approach considers the penalties associated with breaks in linear models, helping to reduce overfitting resulting from excessive adjustments. Studies related to land use change, deforestation, and degradation have used this technique to identify breaks in time series (see examples in Jamali et al. 2015; Li et al. 2022; Zhou et al. 2023).

To search for relationships between the percentage of uncovered soil pixels and temporal variations in the UTRB landscape, we correlated the values obtained in the classifications with the land use and occupation classes of the MapBiomas project (<https://brasil.mapbiomas.org/>) in the periods or segments of the breakpoint analysis. MapBiomas is Brazil's main non-governmental effort for mapping natural and anthropogenic land cover features using Landsat images and deep learning algorithms (Souza et al. 2020). This exercise used the classes without human influence: forest formation, savanna formation, wetlands, fields, and rivers. In addition, we included the following anthropogenic use classes: forest plantation, pasture, sugarcane, mosaic of uses, urban area, soybean, corn, and cotton.

In parallel, we used the Sankey diagram, developed in R, to analyze the temporal dynamics of exposed soil pixels. Three thematic classes were defined based on the amplitudes of the land use classes in the analysis of soil and vegetation indices. In this step, we excluded the exposed soil category, which was preserved to track permanent pixels in this condition over time. Thus, the first herbaceous class includes values associated with annual crops, sugarcane, wetlands, and pastures. The second class, shrubs and trees, represents areas corresponding to savannas, forest formations, and forests. Finally, the water class was designated to encompass water bodies. This classification structure provides a clearer understanding of land cover transitions and the persistence of exposed soil in different periods.

2.6 Spatial-temporal analysis of pixels with slope mask

The slope mask was used to separate pixels with real potential for soil loss. To this end, the number of bare soil pixels extracted for each year of the time series (1985/2024) was superimposed on the slope layer to be reclassified according to its relief class.

Subsequently, a spatial analysis of exposed soil pixels in areas with slopes greater than 8% (classified as undulating relief) was conducted using both spatial and temporal dimensions through the Create Space Time Cube By Aggregating Points tool in ArcGIS®Pro. This tool aggregates input point features into spatiotemporal bins, generating a three-dimensional data structure visualized as a cube, where each cell represents dimensions x and y (space) and t (time). The “temporal trends” option was exclusively selected for this analysis, and the results were spatially represented using hexagonal bins. The tool identifies patterns in the time series, classifying each location according to trends over time—upward, downward, or no trend—along with associated confidence levels of 90%, 95%, and 99%.

3. Results

3.1 Bare soil pixel classification and temporal analysis

The years of 1998, 2002, and 2012 did not meet the cloud and cloud shadow criteria and were discarded from the historical series. Among the indices tested to separate bare soil patterns, Tasseled Cap Brightness (TC_BRI) showed the best soil separability concerning pasture, infrastructure, and agricultural crop pixels (see box plot of indices in section B, Fig. S1, in the Supplementary Material). The range for classifying bare soil pixels was arbitrarily defined based on the median of TC_BRI with a value of 37,320 as a minimum limit and no value for a maximum limit, as from this value, there was no overlapping of thematic classes.

The annual classification of exposed soil pixels is presented in Figures S2 to S38. Figure 2 highlights key years in the time series: the 1985 image (Fig. 2a) and its corresponding exposed soil pixels (Fig. 2b), totaling 44,071 pixels; the peak year of 2021, with the TC_BRI image (Fig. 2c) and exposed soil pixels (Fig. 2d), reaching 1,110,801 pixels; and the final year of analysis,

2024, with 198,779 exposed soil pixels shown in Figures 2e and 2f. The maps reveal a marked increase in exposed soil pixels after 1985, particularly concentrated in the central region and along the northern, western, and southern boundaries of the UTRB.

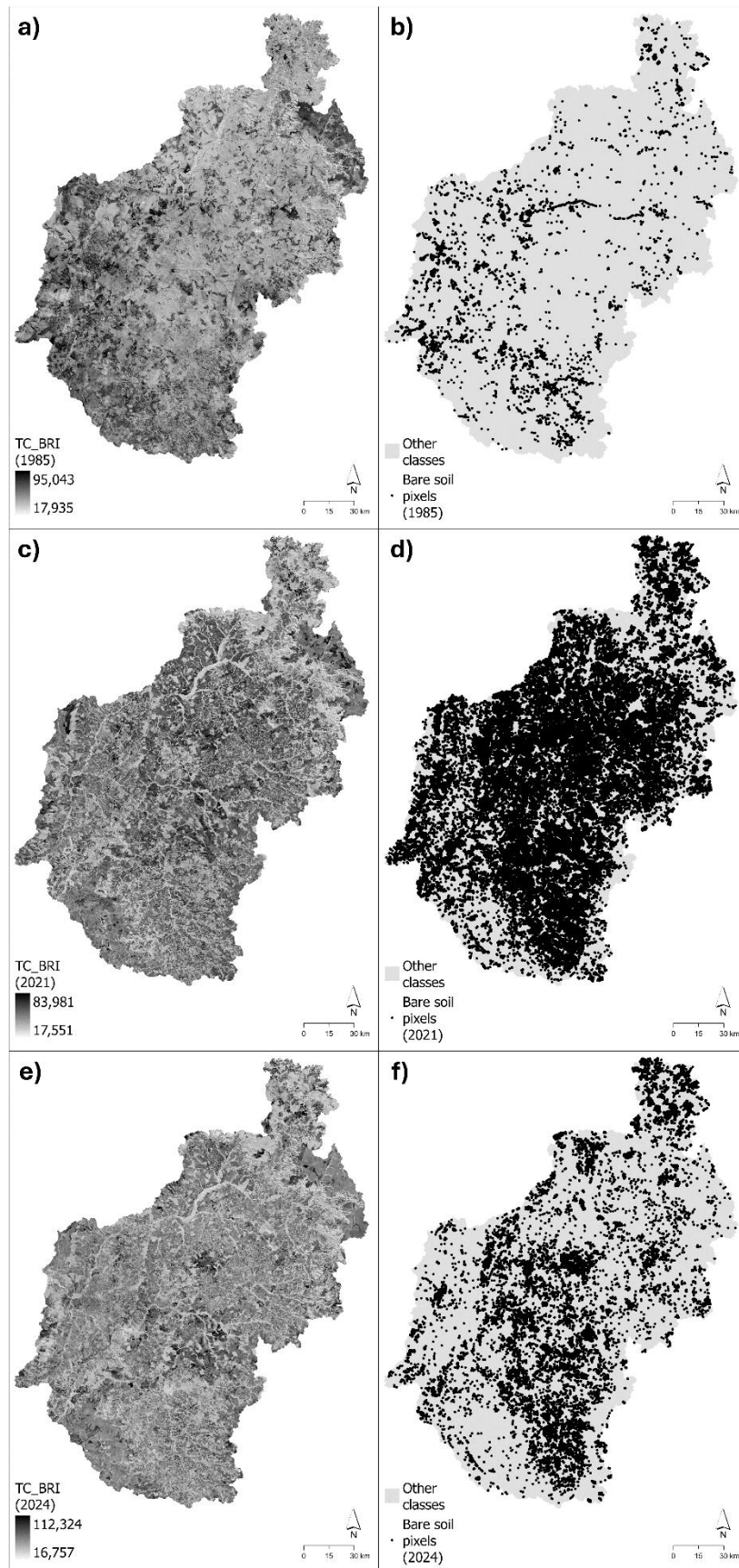


Fig. 2. TC_BRI from observed data from 1985 (a), 2021 (c), and 2024 (e) and the respective classification results of exposed soil pixels for each image (b), (d), and (f).

Figure 3a presents the results of linear regressions between the percentage of exposed soil pixels in the UTRB and time (in years), using the TC_BRI index. Breakpoint analysis indicated that the time series can be segmented into two distinct periods: (A) 1985–2015 and (B) 2016–2023. This segmentation presented the lowest BIC value (67.58) and statistically significant differences between the periods, according to the Kruskal-Wallis and paired Mann-Whitney tests ($p < 0.01$). A clear linear relationship with time was observed in period A, with the percentage of exposed soil pixels increasing from 0.13% in 1985 to 0.8% in 2015 (adjusted $R^2 = 0.44$; $p < 0.001$). In period B, the percentage started at 1.12% in 2016, peaking at 3.36% in 2021. From there, the values decreased, ending at 0.6% in 2024. This "see-saw" behavior in the second period affected the significance of the time trend, resulting in a non-significant linear relationship (adj. $R^2 = 0.13$; $p > 0.05$).

In parallel with the temporal analysis, Figures 3b and 3c present Spearman's correlations between the percentage of exposed soil pixels and the MapBiomas land use and land cover classes from 1985 to 2023. In Period A (1985–2015), all classes showed high and statistically significant correlations ($p < 0.01$). Among the natural classes, savanna ($r = -0.74$) and river ($r = -0.78$) stood out, while among the anthropogenic features, urban area ($r = 0.75$) and cotton ($r = 0.73$). In Period B (2016–2023), only the forest ($r = -0.74$) and grassland ($r = -0.71$) classes maintained significant correlations ($p < 0.05$) with the percentage of exposed soil pixels.

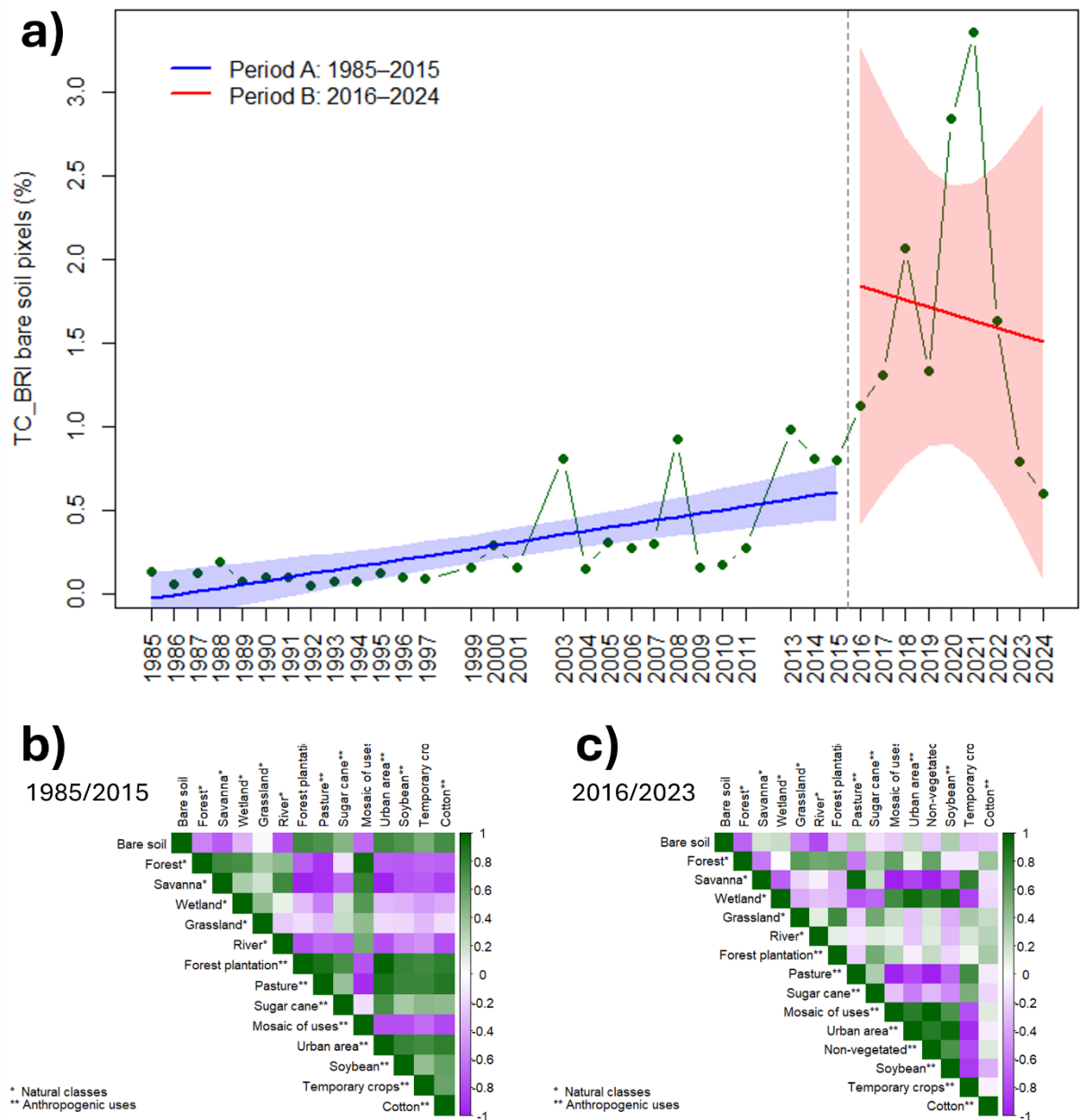


Fig. 3. Linear regressions and 95% confidence intervals (CI) for the percentage of bare soil pixels based on the TC_BRI index from 1985 to 2024 (a), highlighting two distinct periods identified by breakpoint analysis (indicated by the dashed line). Spearman correlation matrices between the percentage of bare soil pixels and land use and land cover classes from the MapBiomas project for 1985–2015 (b) and 2016–2023 (c).

The control points superimposed on the TC_BRI image culminated in defining bare soil pixels and the herbaceous, shrub, tree layers, and water. The limits of these classes were defined arbitrarily through the visual interpretation of the box plot in Figure 4a. The herbaceous class, ranging between 37,320 and 29,370 (25th percentile of pastures), comprised a large part of this class, including sugar cane, annual crops, and infrastructure. The shrubs and trees class, with a

variation between 29,370 and 24,382 (maximum value for the water class), covered the features of the forest, a forest plantation, humid areas, and savanna. Finally, the water class ($<24,382$) has only overlapping outliers from the savanna class.

The Sankey plot (Fig. 4b) present the flows of exposed soil pixels between the cutting years defined by the breakpoint analysis, considering the dynamics of these pixels for the stratified classes shown in Fig. 4a. In 1985, a total of 44,071 exposed soil pixels were identified, of which only 6,426 remained in this condition until 2016. In 2016, of the total exposed soil pixels ($n = 370,121$), 198,726 (53.69%) showed behavior associated with herbaceous vegetation, while 164,387 (44.41%) were related to shrubs and trees. In the second period analyzed, three patterns stand out: the reduction in the total number of exposed soil pixels ($n = 198,779$), a reverse trajectory to that of 1985/2015 with the return of part of the exposed soil pixels to the herbaceous class ($n = 292,769$) pixels and, finally, a significant increase in the transition of these pixels to areas with shrubs and trees ($n = 33,698$). This value was approximately 90% higher than that observed in the previous period ($n = 3,532$).

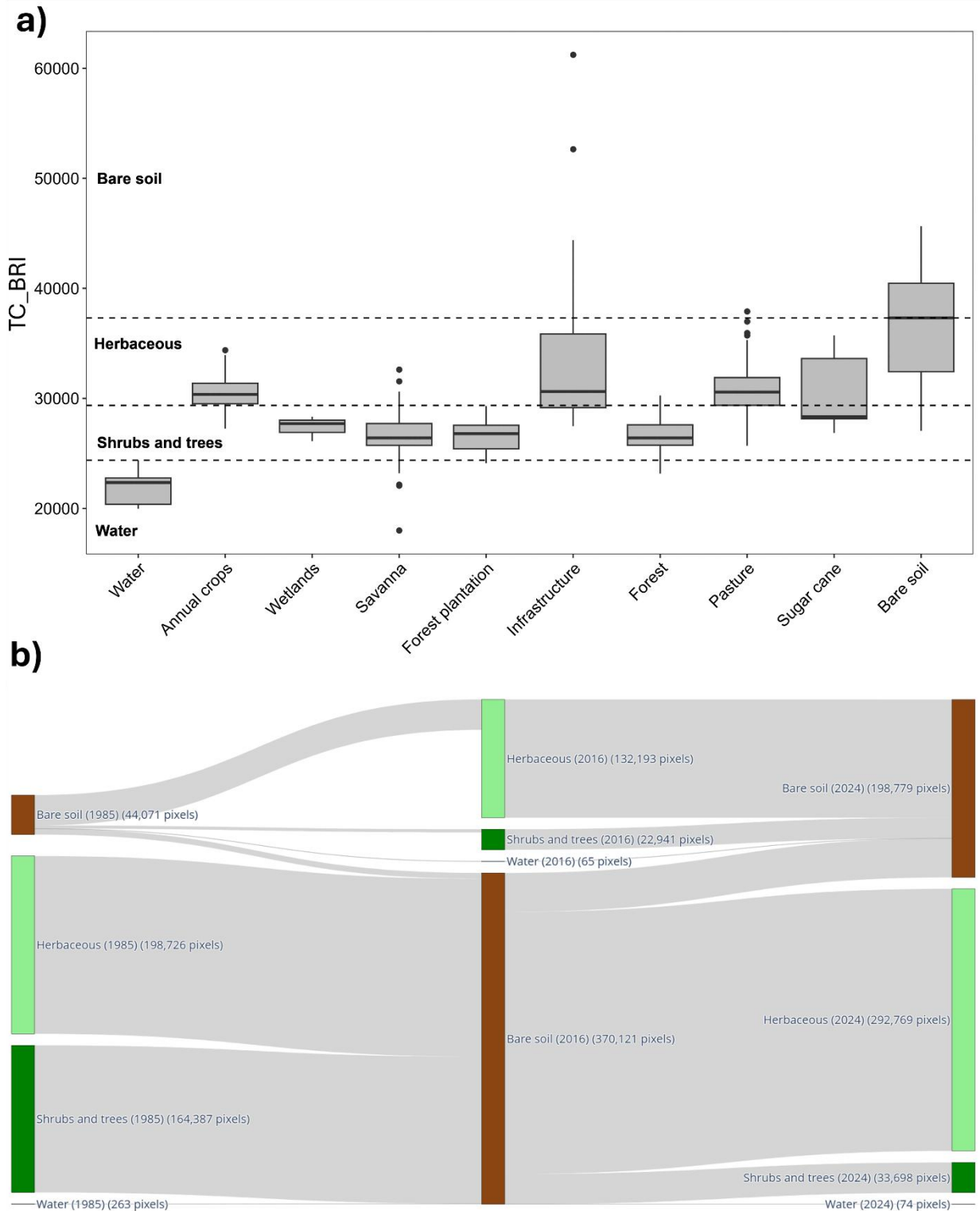


Fig. 4. Box plot of the TC_BRI index for the bare soil, herbaceous, and shrub/tree classes, displayed using a single color scheme and with shaded bands indicating the corresponding spectral ranges (a); (b) Sankey diagram illustrating the transitions of pixel classes in the years 1985, 2016, and 2024, corresponding to the time segments defined by the breakpoint analysis.

3.2 Spatio-temporal and slope mask analysis of bare soil pixels

The dynamic of bare soil pixels located on slopes greater than 8% (Fig. 5a), presented a

similar behavior with total bare soil pixels (Fig. 3a). The breakpoint analysis also revealed the same two periods, 1985–2015 (Period A) and 2016–2024 (Period B), with the lowest BIC value (-27.68), consistent with the results from the analysis of total exposed soil pixels (Fig. 3a). The slope-masked pixels showed statistically significant differences between the periods, according to both the Kruskal-Wallis and paired Mann-Whitney tests ($p < 0.01$). In Period A, the area of exposed soil increased linearly under the influence of rugged terrain (adj. $R^2 = 0.53$; $p < 0.001$), whereas in Period B, no significant trend was observed (adj. $R^2 = 0.13$; $p > 0.05$).

The total number of bare soil pixels overlapping the relief mask showed a slight decrease in the average slope between Period A (11.63%) and Period B (10.88%), as shown in Figure 5b, with these values being significantly different according to Welch's t-test ($p < 0.001$).

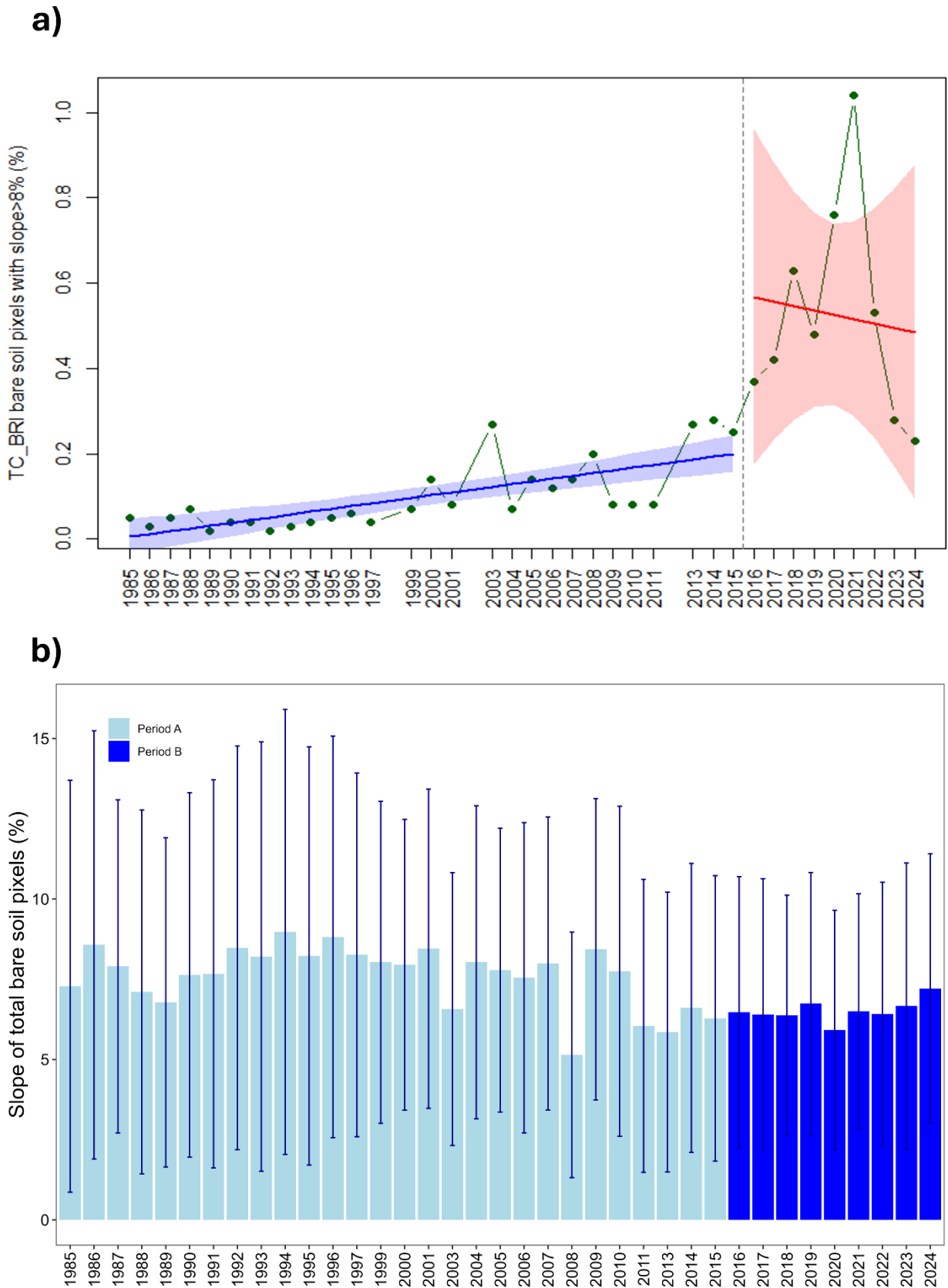


Fig. 5. Linear regressions and 95% confidence intervals (CI) for the percentage of bare soil pixels selected in the slope mask ($>8\%$) from 1985 to 2024 (a), highlighting two distinct periods identified by breakpoint analysis (indicated by the dashed line); (b) Average and standard deviation of slope values for total bare soil pixels, divided according to the two

periods identified in the breakpoint analysis.

Figure 6 presents maps with a spatial analysis of pixel trends for exposed soil in slopes greater than 8% by Space Time Cube in ArcGIS®Pro. During Period A, there is a notable proliferation of hexagons showing a strong increasing trend in exposed soil pixel incidence, in contrast to a few isolated areas with a decreasing trend. In the second period, most sites that previously showed an increasing trend stabilized (showing no significant trend). There was also a substantial rise in the proportion of hexagons with a decreasing trend in exposed soil pixels (green tones), indicating replacement by herbaceous vegetation or shrubs and trees, as illustrated in the Sankey diagram (Fig. 4b).

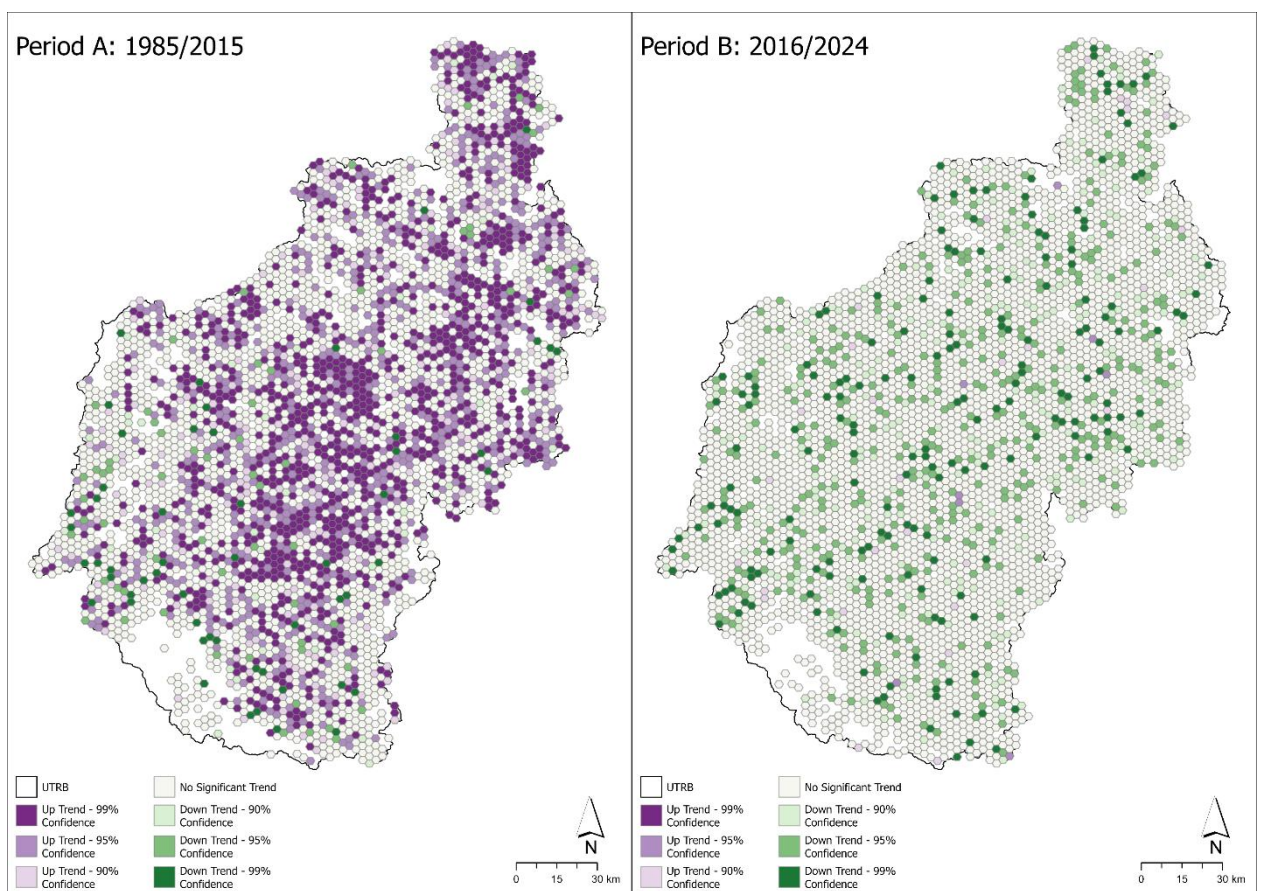


Fig. 6. Spatiotemporal map of trends in the incidence of bare soil pixels with relief equal to or greater than 8% per hexagon between 1985/2015 (period A) and 2016/2024 (period B).

4. Discussion

We applied GIS techniques and analyzed soil and vegetation indices derived from

Landsat imagery to assess the dynamics of bare soil pixels in the UTRB between 1985 and 2024. The temporal analysis of bare soil pixels across the entire basin, specifically in areas with rugged terrain (slopes greater than 8%), revealed a linear increase from 1985 to 2015. Between 2016 and 2024, despite a peak in 2021, when bare soil reached 3.36% of the total area, a trend toward stabilization was observed in exposed soil (Figs. 3a and 5a). Additionally, specific regions within the basin showed localized trends of decreasing bare soil incidence (Fig. 6b). These results suggest that the UTRB may have reached a threshold of maximum soil exposure and is now entering a phase of erosion risk stabilization.

In addition, our findings support previous research highlighting the potential of the Tasseled Cap Brightness (TC_BRI) index for mapping exposed soil areas (e.g., Zhai et al. 2022; Arystanov et al. 2024; Jiang et al. 2024). Our analysis demonstrates that TC_BRI derived from Landsat imagery outperformed both the Bare Soil Index (BSI) (Diek et al. 2017; Nguyen et al. 2021) and the Normalized Burn Ratio (NBR) (Xu et al. 2014; Yilgan et al. 2014) in detecting bare soil. Furthermore, TC_BRI proved to be a valuable indicator for assessing landscape and watershed degradation stages (Valle Júnior et al. 2019; Oñate-Valdivieso et al. 2024; Sousa et al. 2024). Integrating the advanced GIS Space Time Cube tool was also essential in identifying critical areas for restoration—those showing positive trends—and areas requiring minimal or no intervention—those showing negative trends. Previous studies (e.g., Minaei et al. 2018; Wang et al. 2022; Yu et al. 2024) that incorporated spatial and temporal analyses to assess degradation have been instrumental in shaping conservation strategies. Building on this, our approach leveraged GIS tools to integrate both temporal trends and spatial patterns, enabling the identification of space-time clusters that reveal priority pixels for active restoration and zones undergoing passive regeneration.

The comparison with MapBiomass land use classes from 1985 to 2015 revealed that the loss of native vegetation (forest and savanna) and river drying were highly correlated with the increase in bare soil. In parallel, there was a proportional rise in anthropic land use classes such

as soybean, cotton, and pasture. From 2016 to 2023, the only variables that remained significantly correlated were forest and savanna cover declines. This pattern aligns with the historical trajectory of land occupation in the Brazilian Cerrado, marked by deforestation and the replacement of pasturelands with crops (see similar discussions in Garcia and Ballester, 2016; Vieira et al. 2021; Pompeu et al. 2024). Our temporal analysis using the Sankey diagram (Fig. 4b) confirmed this trend, showing that 98.1% of the pixels classified as bare soil in 2016 were originally herbaceous vegetation (53.7%) or shrubs and trees (44.4%) in 1985. Nevertheless, this same analysis also revealed an incipient but notable flow of change from bare soil to shrubs and trees ($n = 33,698$ pixels, or 30.33 km^2). Given that the TC_BRI ranges for these classes are well-defined and distinct, and considering that eight years have passed, we have reasonable confidence that a process of Cerrado regeneration is occurring in previously degraded areas. In this context, our findings reinforce the passive restoration potential of Brazilian savannas (Santos et al., 2020; Silva et al. 2023).

Although our data reveal that variation in exposed soil content over time and space is an environmental indicator in erosion-degraded basins, they do not yet support the hypothesis that the worst-case exposure scenario in the UTRB has already been overcome. The upward trend observed between 2016 and 2021, followed by a decline between 2021 and 2024, remains without conclusive explanations. As in other Cerrado basins, drier years after 2018 may have contributed to the decrease in river flow and the exposure of sandbars in the UTRB (Silva et al. 2018; Salmona et al. 2023). On the economic and behavioral axis, there is evidence that the COVID-19 pandemic (2018-2021) boosted grain exports in Brazil (Schneider et al. 2020), which may have intensified soil disturbance. After 2020, Silva et al. (2025) emphasize that dry years caused declines in agricultural production. In addition, fluctuations in the global commodity market directly influence producers' decisions regarding soil use and management, as exemplified by the recent conflict between Ukraine and Russia, which impacted oil prices, affecting the costs of machinery and fertilizers (Capitani and Gaio, 2024). Given this, uncertainties regarding the

factors that influenced the recent dynamics of exposed soil, combined with the absence of a longer time series, impose limitations on constructing robust predictive models.

Future studies focused on economic and behavioral causes can significantly contribute to understanding sediment dynamics in the basin and predicting new fluctuations. In the short term, promoting the recovery of areas with exposed soil is an essential strategy, primarily through the Rural Environmental Registry (CAR), the central state instrument for territorial management (Louzada et al. 2022). In addition, it is crucial to assess whether areas recently covered by vegetation are restoring the ecosystem functions previously provided, such as water infiltration (Basset et al. 2023), carbon sequestration and nutrient cycling (Colombi et al. 2025), as well as the biodiversity of soil fauna and microorganisms (Pedrinho et al. 2024).

5. *Conclusions*

The effectiveness of the Tasseled Cap Soil Brightness Index (TC_BRI) and the novel Space Time Cube tool from ArcGIS®Pro in identifying bare soil dynamics within the Upper Taquari River Basin (UTRB) highlights their value as key metrics for monitoring landscape degradation. Analysis of bare soil pixel trends from 1985 to 2024 revealed significant temporal variations closely linked to land use changes, particularly the loss of native vegetation such as forests and savannas. A breakpoint analysis of the historical series identified two distinct periods: a phase of linear increase from 1985 to 2015, followed by a stabilization trend between 2016 and 2024. During this latter period, bare soil exposure in the UTRB peaked in 2021, reaching 3.36% of the total area, before declining to 0.6% by 2024. Additionally, slope masking revealed similar patterns in the spatial distribution of bare soil pixels over time.

The Sankey analysis also confirmed that between 1985 and 2015, there was a clear transition from native vegetation pixels (shrubs and trees) to bare soil, indicating deforestation processes aligned with land use classes defined by the MapBiomass project. Although this trend persisted to some extent between 2016 and 2024, an opposite pattern emerged, with signs of regeneration—evident in the transition from bare soil pixels to shrubs and trees.

The variability observed during the second period, particularly between the ascending phase (2016–2021) and the descending phase (2022–2024), lacks clear explanatory factors. However, evidence suggests that fluctuations in grain exports involving large-scale soil disturbance may contribute to increases in bare soil pixels. Additionally, consecutive years of drought and armed conflicts affecting fertilizer imports and oil prices could influence this dynamic. Incorporating economic analyses in future studies may provide valuable insights into the trajectory of bare soil coverage in this heavily erosion-impacted basin. For now, the available data offers decision-makers crucial evidence on where land cover is recovering (downward trend), where degradation is still progressing (upward trend), and where conditions remain stable (no trend).

Supplementary material available in:

https://docs.google.com/document/d/1CJXf9SZ-x7FnRzNn_WKfi4pr3yvyxjNQ/edit?usp=drive_link&oid=110830496409468836501&rtpof=true&sd=true

Section 2: Lower Taquari River (Pantanal wetlands)

Chapter 5: River channel avulsion in the Taquari River megafan of the Brazilian Pantanal: Remote sensing and modeling reveal recent and future changes.

Abstract

The largest crevasse in the Taquari River megafan in the Pantanal, Brazil with a perennial flooded area of ~500,000 hectares, was initiated in 1997 and impacted the environment and people. Here, we spatially characterize and explored a model aiming at predicting the evolution of the rechanneling of the Taquari River within this huge flooded area. Our approach is based on a spatiotemporal dry/wet index (R), which measures the degree of moisture in six major land cover classes. The index was annually estimated from MapBiomas Landsat rasters between 1996 and 2021 and calculated for 142 grid cells (5 x 5 km each). Temporal regressions were then used to predict the state of individual grids in the long term, up to 2080. The results suggest a gradual and slow terrestrialization between 1997 and 2021 as areas returned to pre-avulsion levels, mainly in the eastern and northern limits, closer to the crevasse. Modeling projections suggest that river rechanneling of the Taquari River might be completed by 2080 with its new mouth on the Paraguay-Mirim River. Large areas that are currently aquatic (open water, flooded soils, and flooded vegetation) are predicted to return to terrestrial state (forests and pastures) in the long term.

1. Introduction

As a result of modern climate oscillations and human activities, many wetlands are losing area due to hydrological alterations (Xi et al. 2021). Global inventories point to a decline in coverage of between 30 and 71% over the last century (Davidson 2014, Dixon et al, 2016). Although drought is the main driver, wetland losses are also observed through the expansion of agriculture, urbanization, and industrialization (Ballut-Dajud et al. 2022). Complex processes of runoff, sedimentation, and river avulsions (formation of new channels) based on land use changes have been documented in dynamic wetlands in diverse locations including China (Zheng et al. 2017), India (Singh et al. 2021), and Colombia (Pérez-Consuegra et al. 2021). In Brazil, a current large-scale example occurs in the Taquari River megafan in the Pantanal wetlands, whose area is slowly drying up after the avulsion process at the end of the last century (Assine 2005), partly accelerated by human activities in the upland watershed (Bergier 2013), associated with the recent decrease in rainfall in both the plateau and the floodplain (Ivory et al. 2019, Marengo et al. 2021).

On a generational time scale (~50 years), the Taquari River completely changed course twice (Assine 2005). The largest avulsion remains underway from a perennial crevasse started in 1997 in the Caronal region (Assine 2005, Louzada et al. 2021). In this area, the active depositional lobe in the Taquari River megafan connects to the Paraguay River between two river bottlenecks (Bergier & Assine 2022). The area currently retains water from the two rivers and forms a vast shallow inundated area of more than 500,000 hectares (Figure 1). Despite being an area easily identified in satellite images as one of the wettest in the Pantanal, the Taquari River flow has been gradually shifting into new channels via the crevasse, accompanied by deposition of sand and avulsion progradation (Assine 2005, Assine et al. 2015a, Louzada et al. 2021). In a projection exercise, by conjecturing a nonlinear causal relation between avulsion size and recovery time, Louzada et al. (2021) suggested that river rechannelization in this area may take between 3 and 7 decades.

Geomorphological, climatic, and biogeographic processes influence the structure of wetlands in time and space (Allen et al. 2011), thus influencing ecosystem services (Davidson et al. 2019). In the Taquari River megafan, the recently drained areas provide an increase in ecosystem services by facilitating grazing by livestock (Louzada et al. 2020), while in the flooded portion, ecosystem services include carbon storage via organic matter deposition (Rejmankova 2011), as well as the filtration of water and retention of sediments by aquatic vegetation (Louzada et al. 2021). Moreover, the region experiences an enhancement of biodiversity with aquatic-terrestrial succession or terrestrialization (Coutinho et al. 2018, Junk et al. 2021). Despite the ecological benefits, the permanent flood has brought socioeconomic stresses, mainly due to the impact on 180 livestock farmlands and the exodus of more than 1,000 families from the Pantanal (Ide et al. 2012).

The dynamism of the hydrological system in the Pantanal necessitates socioecological capacities of adaptation (Wantzen 2022), either for local communities that depend on the river for subsistence or transport (Chiaravalloti 2017) or for farmers who yearn for the renewal of pastures and control of invasive species during the flood period (Alho & Sabino 2012). In this sense, the avulsion process interrupted the seasonal and interannual flooding regime in a large part of the South Pantanal through perennial inundation. Previous studies envisaged changes in land use (Guerra et al. 2020, Roque et al. 2021), or in climatic and hydrological behavior (Colman et al. 2019, Bergier et al. 2018,2022). In contrast, attempts to decipher and forecast the evolution from avulsion to terrestrialization are relatively scarce. Therefore, increasing the ability to predict the natural process of shifts in river channels and accompanying changes in inundation can be valuable to guide public policies and strategies for social permanence (Schulz et al. 2019, Tomas et al. 2019).

Based on this context, we sought to simultaneously assess when and where terrestrialization would probably occur in the active and most flooded portion of the Taquari River. For this, we employed the dry/wet ratio index (R) proposed by Louzada et al. (2020), to

identify areas that would be less prone to the formation of the new channel. The approach and the field observational data allowed the creation of a statistical model (regressions) to estimate the terrestrialization time and the probable regions for the new rechanneled main river.

2. Material and Methods

2.1 Study Area

The study area is a region in the heart of the vast floodplain region known as the Pantanal in Brazil, located in the wet/dry tropics between 18°00'S and 19°00'S and longitudes 56°00'W to 57°30'W (Fig. 1), with an area of 4,920 km² in the municipality of Corumbá in the State of Mato Grosso do Sul. The area encompasses the final portion of the Taquari River megafan (Assine 2005), adjoining the floodplains of the Paraguay-mirim River and the Paraguay River, the main river draining the Pantanal region (Assine et al. 2015b, Louzada et al. 2021). Silting by sandy sediments caused the elevation of the bed in periods of flooding and culminated in the rupture of a levee (crevasse) on the right bank of the Taquari River in the Caronal region in 1997/98, making a vast new area of permanent flooding (Assine 2005, Makaske et al. 2012). It was the beginning of the avulsion process and currently, the flooded area is navigable with small boats through ephemeral interconnected streams in the distributary plain with about 175 km of extension, and these channels represent a likely location for the rechannelization of the main river (Louzada et al. 2020,2021).

According to Louzada et al. (2021), there are four distinct sections of the new flow path created by river overflow through the crevasse. The first portion right after the crevasse presents well-defined levees, indicating channel stability (Fig. 1A). As it descends, the drainage loses energy and numerous anastomosed channels appear (Fig. 1B) (Assine 2005), which can be regarded as the initial phase of rechannelization (Louzada et al. 2020). From the middle of the stretch, the number of channels proliferates in such a way that the entire area is flooded (Fig. 1C). In its final portion, the navigable bed takes advantage of a stream (locally called a *corixo*) flowing

into the Paraguay-Mirim River (Fig. 1D).

In general, the flooded areas range in depth from 0.1-5 m and occupy a landscape sculpted by previous fluvial activity and sediment deposition to form a mosaic of grassland, savanna, and gallery forest, characteristic of the Pantanal region (Silva & Abdon 1998). Following the Caronal crevasse formation, many trees in lower-lying areas began dying where they could not tolerate prolonged inundation. Concomitantly, numerous patches of arboreal-shrubby vegetation, locally called *capões* and *cordilheiras* (Pott and Silva 2016), have been preserved because they are slightly above the submerged terrain (see details in Fig. 1C). These effects of changing inundation on landscape vegetation patterns were observed over six field visits at different seasons of the year between 2019 and 2022. Some of these features observed along the course of the navigable bed are presented in the aerial photographs of Figure 1 (A to D).

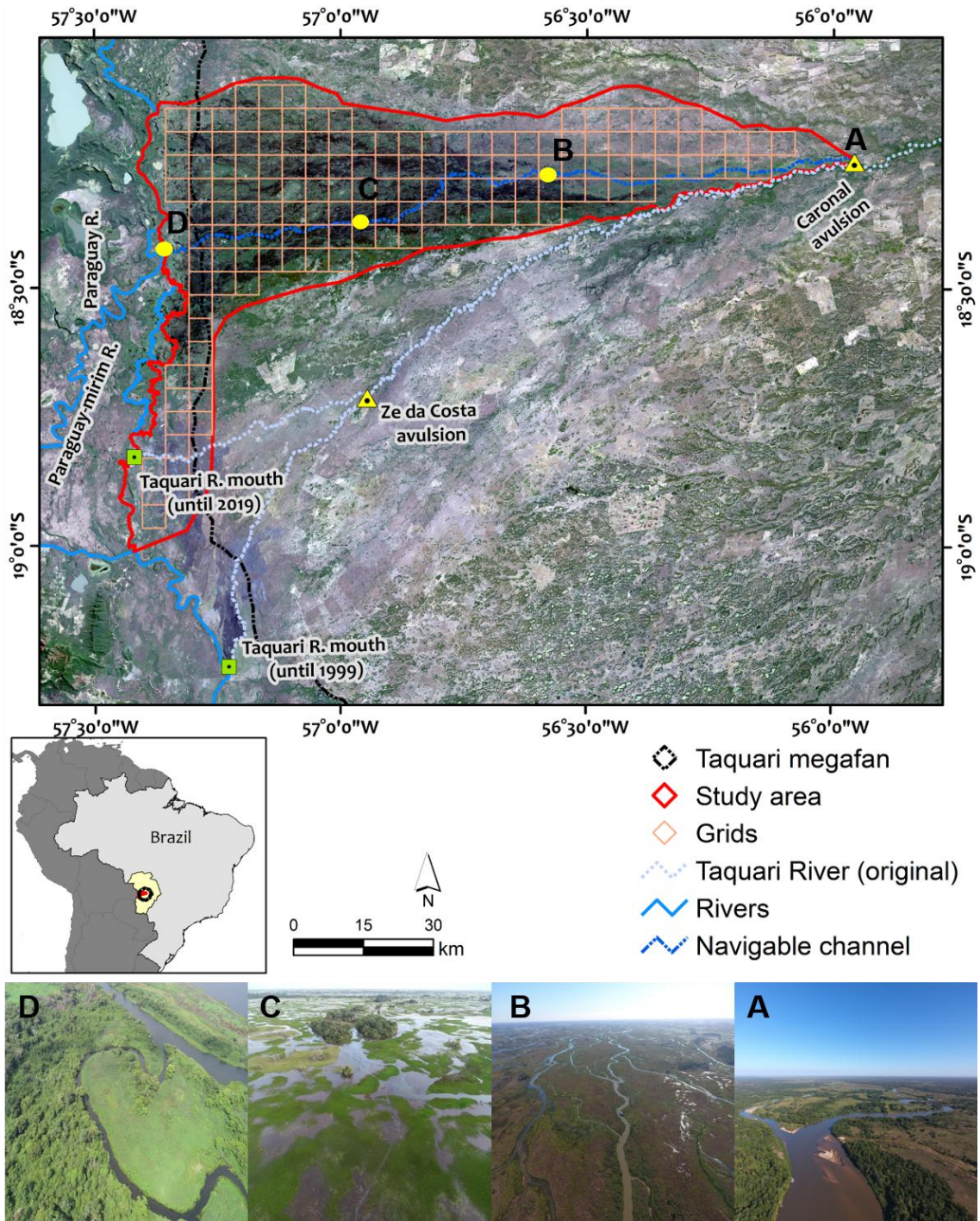


Fig. 1. Location map of the study area in the South American continent and in the Brazilian Pantanal, as well as their position in relation to the Taquari megafan, old mouths (abandoned) by Ze da Costa avulsion, and the floodplain of the Paraguay and Paraguay-Mirim rivers overlaid by a mosaic of Landsat 8 image mosaic from 2021. Three highlights in the map: 1) newly created navigable channel path in dark blue; 2) 5-km grid cells applied as a territorial scale unit for landscape analysis (item 2.3.); 3) original Taquari River channel in process of abandonment by the Caronal avulsion and the earlier Ze da Costa avulsion. At the bottom are aerial figures obtained by drone in 2022, arranged from upstream to downstream: A) Caronal bifurcation (on the right) and abandoned original bed (on the left); B) multiple anastomosed canals (initial rechannelization phase); C) area without remnants of channels close to the terminal end of the flow path; D) end of the navigable course belonging to a *corixo* and its respective mouth with the Paraguay-Mirim River.

2.2 Landscape data collection

Wetlands are important biogeochemical hotspots in nature, largely sustained by the presence of water (McClain et al. 2003). The quantification of water mass loss may indicate a natural process of terrestrialization by the avulsion progress (Louzada et al. 2021, Lo et al. 2022). Here, we use the dry/wet ratio index (R) developed for application in the Taquari megafan by Louzada et al. (2020) as a landscape metric to quantify changes in wetness and dryness in the study area, where values above 1 represent terrestrial terrain (dryness) and below 1 a predominance of the aquatic environment (wetness). This metric was generated from the Mapbiomas project (<https://mapbiomas.org/>), which presented accurate land use/cover (LULC) mapping in Brazilian biomes using the temporal collection of Landsat imagery (Souza et al. 2020, Rosa et al. 2022).

In this study, raster images of the Pantanal biome from 1996 and 2021 were selected and then clipped to our study area. It started in 1996, as this is the last year of the original landscape before the Caronal crevasse and avulsion (Assine 2005). R index was formulated by considering six classes: Forest Formation (FF), Savanna Formation (SF), Wetlands (W), Grassland (G), Pasture (P), and Rivers (Ri). Thus, annual R was calculated by:

$$R = (FF+SF+G +P)/(W+ Ri) \quad (1)$$

2.3 Space-time analysis

To investigate the evolution of spatiotemporal patterns of inundation, we initially divided the study area into grids cells of 5 km x 5 km using the create fishnet tool in ArcGIS 10.4.1. After that, only the polygons that have limits within the area were selected, totaling 142 units. Each cell represented an average of 29,503 pixels, so the maximum positive R was equal to 29,502 (terrestrial) and its opposite extreme 0.00003 (aquatic). To avoid biased results, we transform the original ratio values into a logarithmic scale (Isles 2020), and then, to facilitate the interpretation, the terrestrial and aquatic ranges were subdivided into six thematic classes (Table

1), where values of $R < 1$ are expected for rivers.

The temporal analysis of the data was conducted in ArcGIS and analyzed in the PAST statistical software (Hammer & Harper 2001) with a confidence interval of 99%, considering linear and non-linear regressions. The choice of the adequate equation was made by visual interpretation of the distribution of the plots, prioritizing less complex models (Sivo et al. 2006). Furthermore, the results of statistically significant grid cells were projected for 2030 to 2080 according to the objectives of this work, as well as variations in the dynamics of the Pantanal landscape on a decennial scale (Libonati et al. 2022). Finally, a preliminary exercise was attempted to locate the new river, taking into account the results of the projections, but also considering the current distribution of lowered areas (*corixos* and *vazantes*), free stretches of macrophytes, patches of vegetation (elevated areas), and empirical knowledge acquired from landscape transformations in field expeditions.

Table 1. Six thematic classes of R values and respective logarithmic transformations.

R (pixels)		R (log)		Thematic class
19,668	29,502	4.29	4.47	highly terrestrial
9,834	19,668	3.99	4.29	terrestrial
1	9,834	0	3.99	lightly terrestrial
0.66	1	-0.18	0	lightly aquatic
0.33	0.66	-0.48	-0.18	aquatic
0.00003	0.33	-4.47	-0.48	highly aquatic

3. Results

3.1 1996/2021 time analysis of R index

The annual distribution of thematic classes between 1996 and 2021 for the entire study area is shown in Figure 2. In 1996 wetlands were the most predominant class with 54% followed by grassland with 27% of the area. Pastures, savannahs, and forest formations together comprise 12% of the area, whereas the open water class completes the list of land cover with 7%. After 1997, the percentage of wetlands showed a slight increase with an average percentage above 63% until 2019, when the area dropped to 37% in 2020 and ceased to be predominant in 2021 with 26%, losing ground that year mainly to pastures (32%) and open waters (25%). In the last two

years of the temporal series, increases in the percentage of forest and savanna formations were also observed, while pasture remained below 1% for all years.

The average dry/wet index for the study area never exceeded the limit for terrestrial ($R > 1$), however, the index gradually decreased from 0.63 in 1996 to the peak of the aquatic environment in 2014 with $R = 0.27$. After this series, the values increased sharply until reaching 0.93 in 2021. The increase in the index value after 2019 was accompanied by an increase in the fractional area of river channels and pastures and a decrease in the area of wetlands (Fig. 2). This non-linear behavior presented an R^2 with 0.51 and 0.71 ($p < 0.01$), applying the second and third polynomial equations respectively.

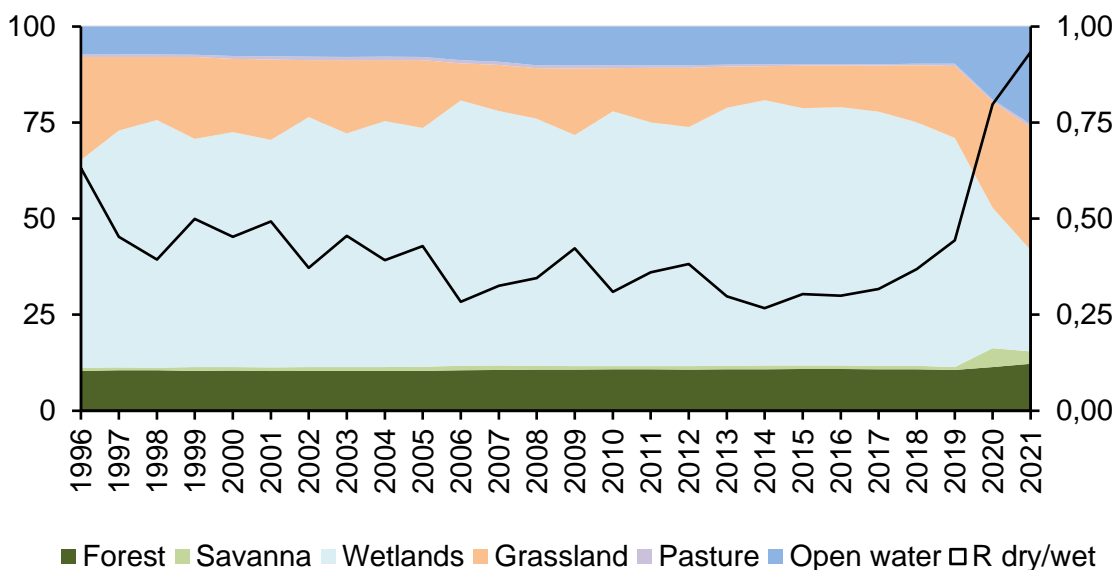


Fig. 2. Percentage of the thematic classes of MapBiomass project between 1996 and 2021 and respective dry/wet index (R) values from the study area.

Figure 3 shows grid cells that at some point in the time series exceeded the pre-avulsion level of 1996, as well as those that remained below that level. Altogether, there seems to be a balanced score of 72 grid cells (51%), and 70 grid cells (49%) above and below the 1996 baseline, respectively. This is expressed geographically in four groups, the largest first in the east in which practically all the meshes exceeded the 1996 threshold (green contours), in addition to two small blocks located parallel to the Paraguay River (red and lilac contours). In the middle and

occupying a large part of the study area, the grid cells with values lower than the beginning of the time series are presented (blue contours). All remaining R's of grid cells over the period are shown in Section A of the supplementary material (see Figures S1 to S25).

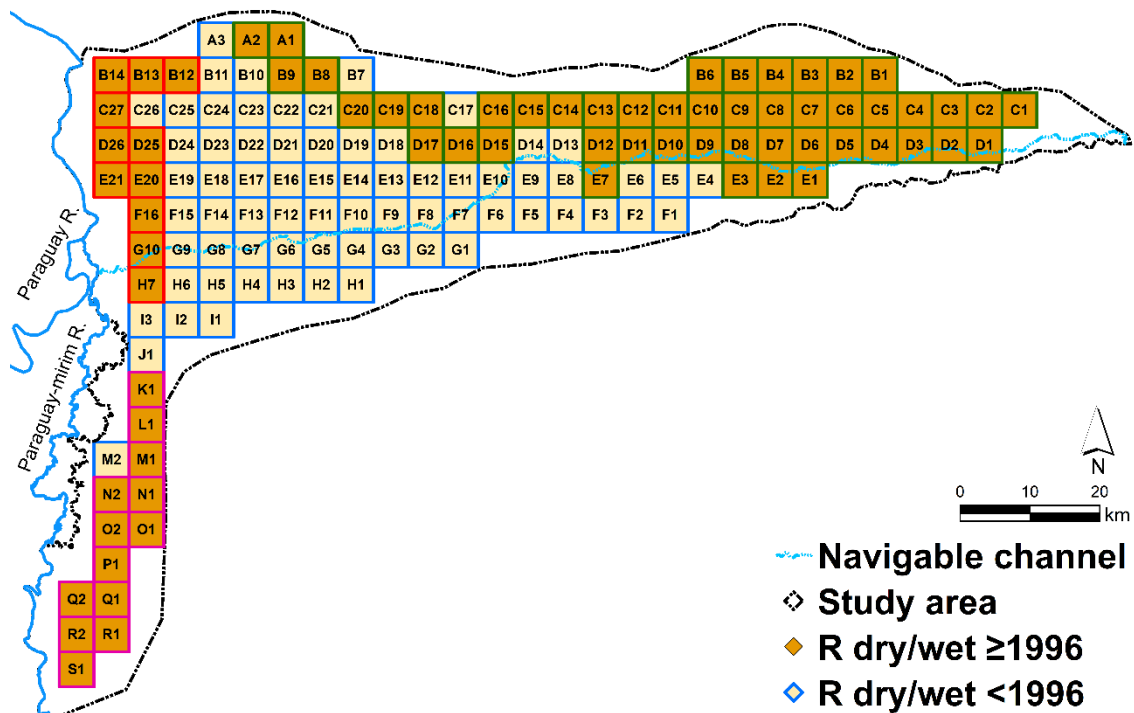


Fig. 3. The grid cells' map highlights the units that present values above and below the original 1996 value (pre-avulsion). Outlines in green, red, lilac and blue make up the four grid blocks discussed in the text.

For regression analyses (Fig. 4), the absolute majority, or 128 grids (80%) showed statistical significance at the 99% confidence interval, with 42 grids (30%) presenting coefficients of determination greater than 0.7. On the other hand, only 28 grids (20%) presented no consistent relationship of R ratio with time, usually for grids far from the crevasse. For the grid cells with significant slopes over time ($p \leq 0.01$), 96 were best fit by quadratic models (yellow grid cells in Fig. 4), and 18 grid cells were fit to linear models (red grid cells). The regressions for the 142 grid cells are shown in section B of the supplemental material (see Figures S26 through S37).

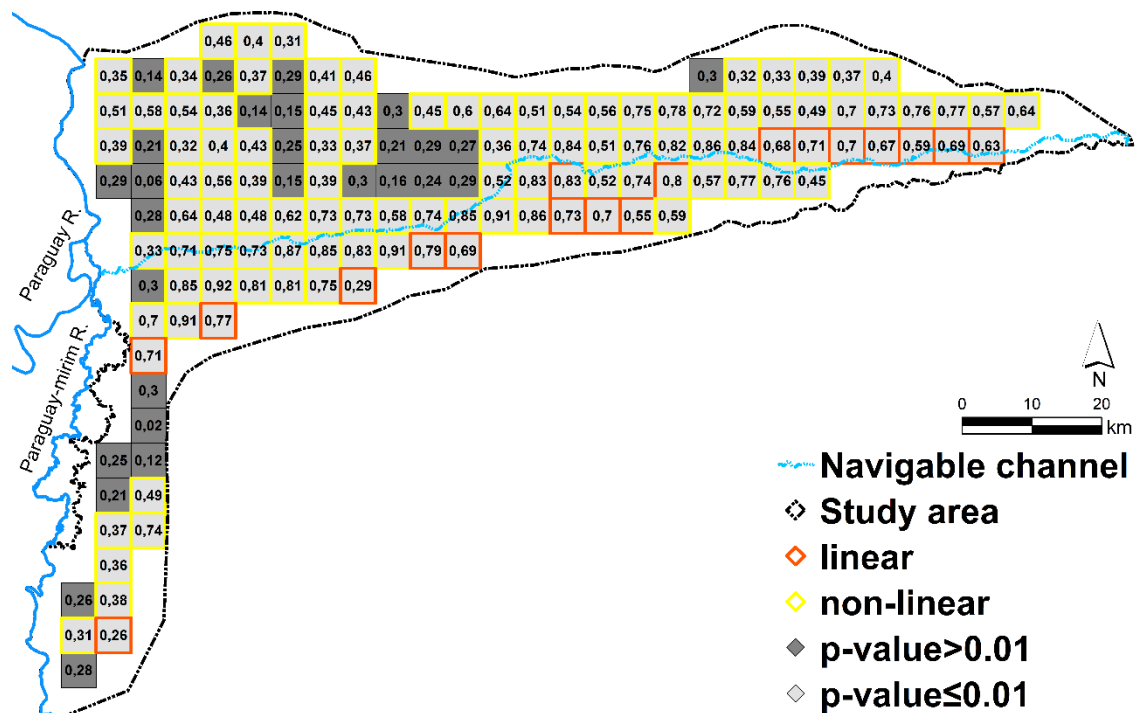


Fig. 4. Geographic distribution of grids labeled by R-squared results in regression analysis.

3.2 Future predictions by R index

By considering the regression models, the projection of the rechannelization process up to 2080 in the study area is shown in Figure 5. Looking initially at the 2021 map, which represents the latest observation, 100 cells (70%) were predominantly aquatic environments, usually far from the crevasse, in 58 (41%) were highly aquatic. Lightly terrestrial environments accounted for 41 grid cells (29%) and were located closer to the crevasse or in the vicinity of the Paraguay River.

From the decadal projections, the rechannelization process effectively begins after 2030. By 2040, 17% of the grid cells shift for the first time to the highly terrestrial class. Alternatively, the highly aquatic class shift toward the center-south and in isolated western portions closer to the Paraguay-Mirim river. These changes continued in 2050, 2060, and 2070, when 32 (22%), 46 (32%), and 55 grids (39%) were highly terrestrial, respectively. Finally, in 2080, the regression models project a predominantly dry environment for the study area, with 102 terrestrial grid cells, of which 70 (49%) are highly terrestrial. The wetland grid cells with only 12 (9%) seem to indicate the region of the new Taquari River will parallel the southern edge of

the study area.

In the new river location exercise, we vectorized the channel using GPS points added to the projections of most aquatic grid cells (Fig. 6). The trajectory was somewhat similar to the current one (navigable channel), but around the geographic coordinate $18^{\circ}20'S/57^{\circ}00'W$ there is an alteration (or change) in the direction of the flow, deviating towards the south. These waters run faster when they follow a deep channel, known locally as “Corixão”. From this region, the flow continues until it meets the Corixo do Cervo, also very deep (detail on the left of Fig. 6), when it finally flows into the Paraguay-Mirim river (future mouth).

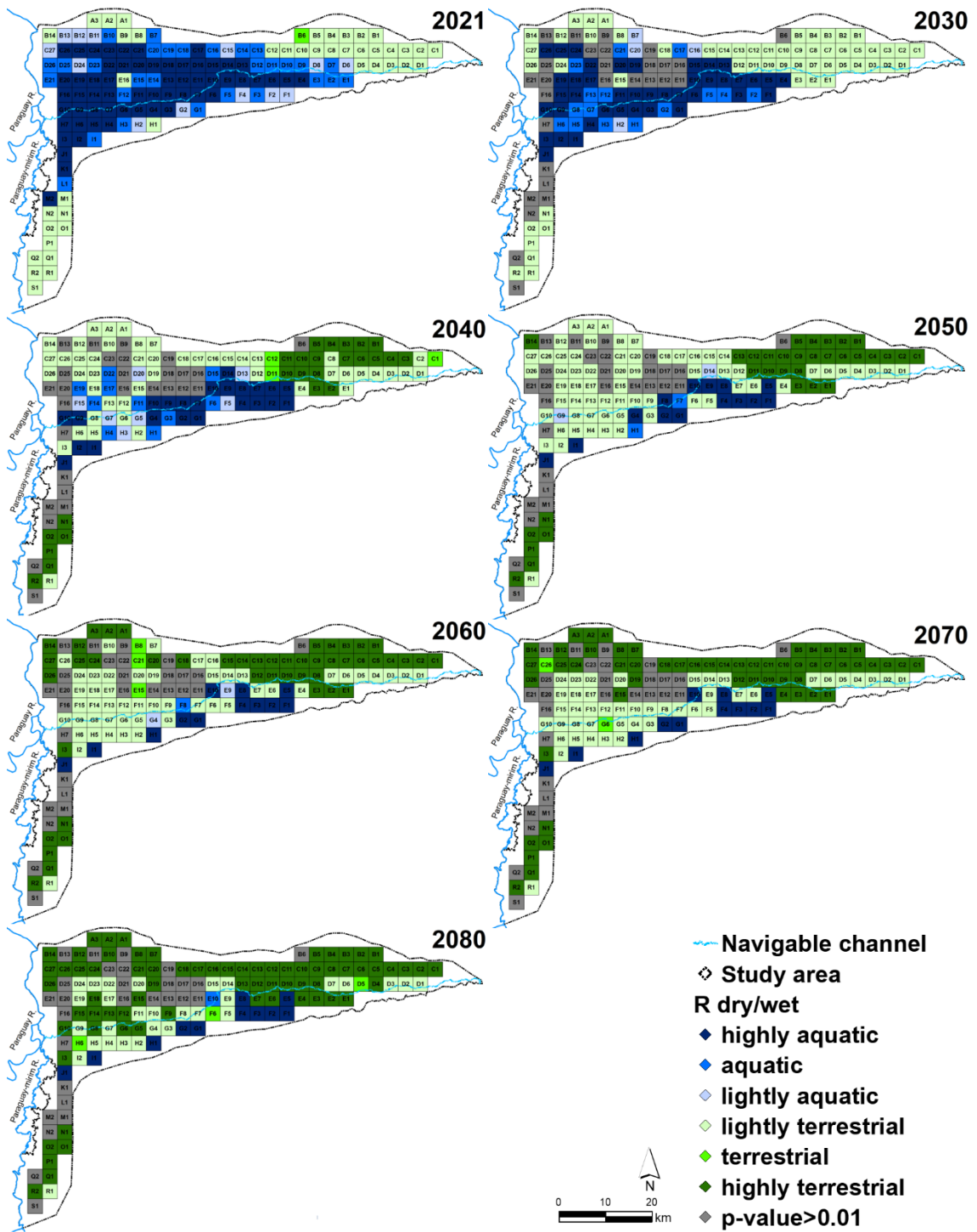


Fig. 5. Map from 2021 (observed) and projected from 2030 to 2080 with the six thematic classes of R values.

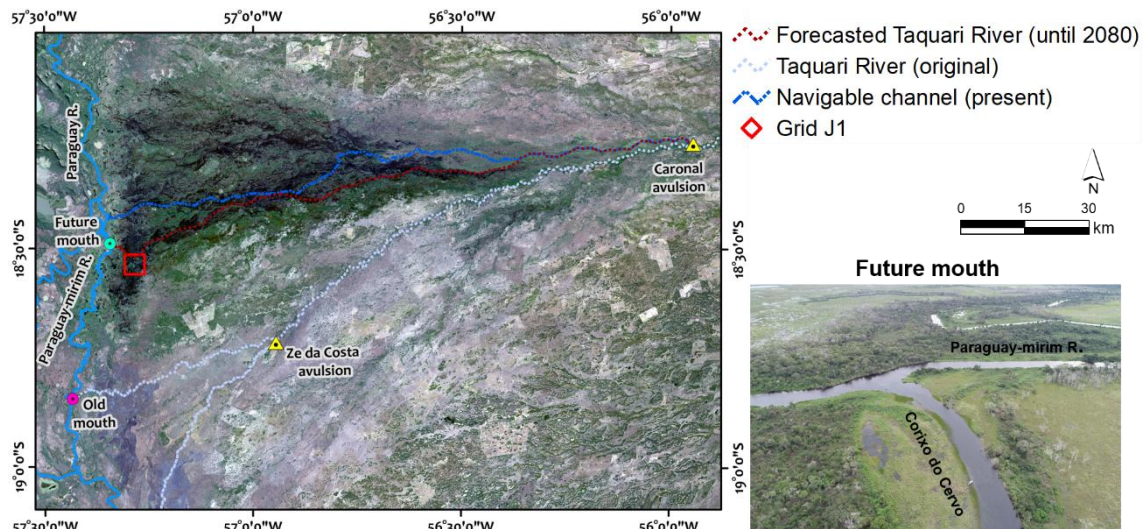


Fig. 6. Projected new course of the Taquari River including its confluence with the Paraguay-Mirim River via a distributary channel presently known as Corixo do Cervo.

4. Discussion

4.1 Rechannelization process in the coming decades

Here we show that in less than 20 years the area will become predominantly terrestrial, confining the aquatic grids southward until forming the new channel of the Taquari River. The channel migration about 40 km northward will be repeating the migration pattern observed by Assine (2005), and reoccupy the paleochannels (Zani et al. 2012). The first portions might become terrestrial by 2040, which coincides with the higher energy of the system dynamics near the Caronal crevasse (Assine et al. 2015b), with a direct relationship with sedimentation, in which sediment accumulation supports marshy and later terrestrial species (Mitsch et al. 2014) while the vegetation cover feedback eases sediment trapping and reinforces the system towards terrestrialization (Nienhuis et al. 2018). At the fringes of the active lobe, terrestrialization is rather slow and is sustained primarily via the balance between evapotranspiration and local rainfall (Freitas et al. 2019). In the medial zone, the aquatic-terrestrial succession is even slower (Louzada et al. 2021), depending on the advance of progradation, evapotranspiration, and the terrestrialization process (Lo et al. 2019), which is promoted by the accumulation of emergent and rooted macrophytes (Pott & Silva 2016).

The rechannelization predicted in less than 60 years will have implications for

biodiversity and socioeconomics. The hydrological stability of nearly untouched floodplains results in the development of high habitat diversity (Junk 2005, Vieira et al. 2015). It is notable that the perennially inundated area is currently an accessible refuge for the terrestrial fauna, especially in times of severe droughts and fires (Tomas et al. 2021). Furthermore, the area has been documented to be an important nursery for fish for over 25 years since the start of the avulsion, including species of economic value, such as Pacu (*Piaractus mesopotamicus*) and Pintado (*Pseudoplatystoma corruscans*) (Frey-Dargas et al. 2014). For terrestrial fauna, the numerous trees killed by the flood, patches of preserved forests, and sites of aquatic-terrestrial succession, have been increasingly attracting birds and mammals including the iconic jaguar (*Panthera onca*) (Harris et al. 2005). Ecosystem services provided by floodplain inundation include groundwater recharge (Wohl 2021), and sediment retention that would cause siltation and interfere with the commercial navigation in the Paraguay River (Schulz et al. 2019, Baigún & Minotti 2021). Moreover, the direct benefits of intense macrophyte proliferation such as water purification (Louzada et al. 2021), temporary retention of heavy metals (Eid et al. 2020), and the role of inundation in enhancing organic carbon storage (Reitsema et al. 2018).

4.2 Discussing opportunities and challenges of the terrestrialization process

Some socioeconomic opportunities along the new river in the coming decades include the resumption of river transport, recreational fishing (Freire et al. 2016), and wildlife tourism (Tortato et al. 2022). The terrestrialization will also influence land values as dry, fertilized soils rich in organic matter should pave the way for the return of traditional livestock (Abreu et al. 2010). However, these opportunities are linked to the challenges of sustainable practices, avoiding [or minimizing] unregulated fishing, deforestation, and fires (Alho et al. 2019, Guerra et al. 2020, Martins et al. 2022). Therefore, assuming the responsibilities for the sustainability of future activities, the government ought to exercise a rigorous regulation of land use and a vigilant supervisory role (Leal Filho et al. 2021). The government should also involve the local

community by bringing its tacit knowledge (Van Dyke 2015) as well as the scientific community (Shirley & Gore 2019, Tomas et al. 2021) to construct a common agenda that optimizes the rational use of natural resources.

Indeed, changes in ecosystem services triggered by avulsive rivers in the Pantanal have been partially explored (Louzada et al. 2021), but need to be better quantified by the scientific community, for example, to support 'glocal' public policies (Gupta et al. 2007, Ostrovszkaya et al. 2013, Brilha et al. 2018). State ambitions of neutrality in greenhouse gas emissions (see www.semagro.ms.gov.br/Geral/estado-carbono-neutro/) and state law 5,235, July 2018 (<https://www.imasul.ms.gov.br/legislacao-ambiental/leis/>) which regulates payments for environmental services, seem to be heading in the right direction. Although our model deserves additional efforts to consider large-scale external forces (Marques et al. 2021), the study area is highly relevant in the context of sustainable food production, climate change mitigation, and carbon sequestration (Ioris 2014). The avulsive nature of the river in the active lobe, however, presents major challenges for choosing an appropriate baseline for additionality (Loisel & Walenta 2022), as Nature's Contribution to People (NCP) from the aquatic phase can be a sink of flooded carbon (Dalmagro et al. 2022), and from the terrestrial phase, the stock of living forest and soil biomass (Borges Pinto et al. 2020). Moreover, effectively capturing carbon will be the biggest challenge, given the lessons from the 2020 fires that brought us evidence of subterranean fires in dry histosols (Damasceno-Junior et al. 2021).

4.3 Limitations and Future Research Directions

This exercise was the first step toward projecting the future location of the new river, but it already opens up large planning windows to avoid environmental losses and promote socioeconomic repairs (see examples of success in China in Liu et al. 2008, Wu et al., 2019). Future work will certainly be able to add value with the inclusion of non-linear drivers such as precipitation and runoff (Bergier & Assine 2022, Louzada et al. 2022), in addition to testing grid

sizes and spatial autocorrelation analysis between units (Zhang et al. 2020), promoting greater accuracy of forecasts. Including anthropic influence is also important, as the terrestrialization of the grid cells post-2020 on the eastern edge near the Caronal is mainly due to the closure of crevasses with hydraulic dredgers, leading to the drainage of several nearby rural properties. Despite this, more robust models do not change the situation that 30 years ago people and the government were completely surprised by the rapid changes in the landscape, and this has generated conflicts that extend to the present day (Schulz et al. 2019). Even with uncertainties associated with climate and sediment supply (Marques et al. 2021, Roque et al. 2021, Wosiacki et al. 2021, Reboita et al. 2022), our results indicate that the new Taquari is undergoing dramatic changes within the generational timeframe, which means that decisions and practices need to be taken with a long-term perspective.

5. Conclusions

In this work, we used the R (dry/wet ratio) index to evaluate the historical spatiotemporal dynamics and to forecast terrestrialization and river rechannelization in the largest avulsion of the Pantanal wetland. The model is based on obtaining statistically significant regressions of spatially gridded R over time, then using these regressions for projecting the future state of each grid. The model is relatively simple and does not take into account large-scale factors that can influence the process such as climate and land-use changes. By assuming the permanence of the current boundary conditions, the steady process of formation of the new channel of the Taquari River might complete by 2080. The geography of the new bed tends to be closer to the abandoned channel, but the outlet may reach the Paraguay-Mirim river 40 km above the last minor and complete avulsion in the Zé da Costa region.

Furthermore, the government, science, and the Pantanal people together can share the responsibility of planning the sustainable use of the territory in the face of real opportunities and challenges brought by Pantanal's avulsive rivers.

Supplementary material available in:

https://docs.google.com/document/d/1yArOjX_WF_QEH8AoYRR45_cNuOoMkLnC/edit?usp=sharing&oid=110830496409468836501&rtpof=true&sd=true

Chapter 6: Fluvial avulsions influence soil fertility in the Pantanal wetlands (Brazil).

Abstract

River avulsions drive important changes in the Pantanal wetlands, owing to their role in the hydro-sedimentology of the region. Although relevant to numerous ecosystem services, few studies have analyzed the influence of river avulsions on soil fertility in the Pantanal. Here, we use the largest ongoing avulsion in the Taquari River (Caronal region) to evaluate the effects on soil fertility, considering two factors: avulsion stage (1) and aquatic-terrestrial succession (2). Since both factors are influenced by macrophyte abundance, an incident map was created through tasseled cap indices from Sentinel 2 images to guide sampling efforts in flooded soils. The mapped area was split into two zones of alluvial processes, the first from the apex of the Caronal lobe corresponding to the Taquari River megafan (TRM), and the second as the distal Paraguay River floodplain (PRF). Soil macro- and micronutrient levels were evaluated from 42 surface samples (0-0.2m) distributed across the two alluvial process zones. The macrophyte map's overall accuracy (OA) was analyzed by a confusion matrix using the Sentinel 2 imagery. Finally, we used Random Forest regressions to determine the influence of response variables on soil attributes, including tassell indices, distance from the Caronal crevasse, macrophyte density, and an existing soil fertility map. The macrophyte map obtained an OA of 93%. Some parameters such as pH ($r=-0.62$; $R^2=0.57$), effective cation exchange capacity ($r=-0.49$; $R^2=0.79$), Mn ($r=-0.71$; $R^2 = 0.6$), Zn ($r=-0.69$; $R^2 =0.54$), and base saturation ($r=-0.7$; $R^2= 0.93$) were influenced by the distance or level of maturation of the avulsion stage in the TRM. Our scattering of soil collections was insufficient to test the terrestrialization hypothesis (2). The study results show that river channel avulsions influence the accumulation of mineral and organic nutrients in tropical floodplain soils, which has implications for fertility and biodiversity.

1. Introduction

Most of the soils in the Brazilian Pantanal, one of the largest continuous wetlands in the world, are infertile, with low levels of organic matter (Couto & Oliveira 2011). Soil fertility maintenance mainly depends on riverine flood pulses (Alho 2008, Petsch et al. 2023), which are responsible for annual inputs of organic matter and mineral particles (Deng et al. 2022, Remor et al. 2022). Small variations in relief determine the soil's susceptibility to flooding (Pereira et al. 2021) and the sediment accumulation rate (Couto et al. 2023). These factors explain the spatial variability of soils and their respective natural fertility in the Pantanal (Couto & Oliveira 2011). Soil type and flooding patterns, in turn, govern vegetation cover (Oliveira et al. 2015) and, consequently, the ecological services associated with them, including primary production, nutrient cycling, and carbon cycling (Maltby & Acreman 2011, Petsch et al. 2023). These seasonal variations between drought and flood generate a balance of elements (Oliveira et al. 2019). Nonetheless, large-scale hydrodynamic events in the Pantanal, such as river avulsions, are responsible for imbalances of soil elements due to prolonged effects that alter the landscape (Louzada et al. 2020,2023a). However, studies evaluating the effect of avulsive processes on biogeochemical attributes in tropical floodplain soils remain scarce (Nascimento et al. 2013, Oliveira Junior et al. 2017).

An avulsion is a process of river channel shifting induced by silting in the channel thalweg (Smith et al. 1989). Generally, the avulsion process is divided into phases, starting with water level and marginal levee elevations about the average plain, thus fissuring (crevasse development) any weakened portion of the marginal levee (Assine et al. 2005, Assine et al. 2015a). Avulsive rivers redistribute sediments over adjacent floodplains (Slingerland & Smith 2004) and promote the total migration of the river channel to a different position within an active lobe. River migration is part of a more extensive process that promotes profound modifications of wetland landscapes, particularly in megafans (Tooth 2018) by flooding extensive areas (Smith et al. 1989, Assine 2005, Assine et al. 2014, Valenza et al. 2020). The roots of terrestrial plants

are asphyxiated by excessive water, and newly flooded areas are gradually replaced by aquatic plants (Tiner 2016, Petsch et al. 2023). In soils, biogeochemical processes are preferentially modulated by the aquatic phase as aeration decreases (Jackson et al. 2014). The rate of degradation of organic matter decreases markedly (Mitsch et al. 2015), and sediment layers are accommodated by channel progradation (Makaske et al. 2012, Valenza et al. 2022).

The most significant avulsion in the Pantanal occurs in the Taquari River, specifically in the Caronal region (Assine 2005, Assine et al. 2005, Louzada et al. 2021). About 30 years ago, the region received diffuse and poorly channelized water and sediment flows covering an area of ~500,000 ha (Louzada et al. 2023a). Over decades, the quasi-perennial flood tends to recede as a new channel emerges (Louzada et al. 2023a), draining adjacent areas and promoting what has been termed an ‘aquatic-terrestrial succession’ (Lo et al. 2017, Ivory et al. 2019). Much of the region remains aquatic, intensively colonized by aquatic vegetation, indicating that river rechannelization could last many decades (Louzada et al. 2023a).

Aquatic vegetation plays a crucial role in the transition of wet and dry environments, whether through terrestrialization that leads to the development of organic soils called histosols (Pott & Silva 2016, Lo et al. 2017) or through the accumulation of nutrients and retention of sediments (Rovira et al. 2016). As pioneers, macrophytes are indicators of altered or disturbed environments that promote ecosystem functions like retaining organic and inorganic sediments and nutrient export (Rovira et al. 2016, Sharma et al. 2021, Morais et al. 2022). In the current avulsion of the Taquari River at Caronal, features such as the continuous inflow of sediments from managed and unmanaged lands in upland areas (Bergier 2013, Roque et al. 2021, Lo et al. 2023), the time duration of the annual flood (Hamilton et al. 1996), and the abundance of aquatic plants (Louzada et al. 2023a) suggest that the active lobe of the Taquari megafan (Zani et al. 2012) could be prone to accumulate nutrients in the upper soil layers (Louzada et al. 2021). The complex interactions between avulsive dynamics, floods, terrestrial-aquatic transitional processes, and vegetation succession are expected to shape soil fertility on a large scale in the

Pantanal; however, little is known about the roles and interactions among these variables.

Here, we explore the Taquari River avulsion stage and its relationship to the spatial distribution of surface soil fertility. Our first hypothesis postulates that crevasse proximity affects the extent of flooding and the abundance of aquatic vegetation, affecting soil nutrient composition. Likewise, aquatic-terrestrial succession, mainly on the edges of the active lobe of Taquari (Louzada et al. 2021), may also affect the stock and distribution of nutrients in topsoil. Based on our results, we explored strategies for both conservation and management of the ongoing avulsion of the Taquari River and its ecosystem services.

To test our hypothesis and track regional-scale landscape changes, such as those in the active lobe of the Taquari megafan, we collected soil samples, adding medium-resolution multispectral imagery (5~30m) to find an appropriate balance between field information and spatial coverage. (Amani et al. 2018, Mishra 2020). In this context, water and vegetation indices play a crucial role in the environmental monitoring of wetlands; these indices are accessible through calculations using collections of freely available Landsat (30m) or Sentinel 2 (10/20m) satellite images (Varghese et al. 2021, Demarquet et al. 2023). Furthermore, we seek to analyze the relationships between spatial variables and soil attributes with the Random Forest machine learning algorithm following the methodological approach of other works (see, for example, Whyte et al. 2018, Amoakoh et al. 2021).

2. Material and Methods

2.1 Study area

The study area has 4,920 km² in the central portion of the Brazilian Pantanal between latitudes 18°00'S and 19°00'S and longitudes 56°00'W to 57°30'W (Fig. 1). The region covers two alluvial depositional zones: the Taquari River megafan (TRM) and the Paraguay River floodplain (PRF). These zones were defined by considering the limits between dry and flooded lands, as well as vectorizations of the geomorphological units presented in Assine (2005), Zani

et al. (2012), and Louzada et al. (2021, 2023a). In short, it comprises an extensive flooded area with an average water column of <1 m extensively colonized by aquatic vegetation. This region transitioned from a terrestrial to an aquatic environment following the Taquari River avulsion in 1997 in the Caronal region (Assine 2005). Currently, the area consists of the most significant active depositional lobe of the Taquari megafan (Makaske et al. 2012, Assine et al. 2015b), incorporating the TRM and PRF zones into a single flooded area (Assine et al. 2015a, Louzada et al. 2023a).

The quasi-perennial aquatic environment peaked in 2014 (Louzada et al. 2023a), and since then, the area has been progressively drying, especially in the recent droughts of 2019 and 2020 (Marengo et al. 2021). In addition, anthropogenic activities like the closing of small crevasses also contribute to river rechannelization (Louzada et al. 2021, Louzada et al. 2023a). Sediment input (Figure 1) is the main factor modulating the environment from east to west. Other factors include the low longitudinal gradient (~0.005 m/km), aquatic and terrestrial vegetation blockages, and excess sand favor deposition (Assine 2005, Hajek & Edmonds 2014). In general, the transformation begins with the occupation of subtle surface voids by layers of sediment (Assine 2005). Then, the surface level is slightly elevated, forming multiple anastomosed channels (Buehler et al. 2011). Maturation of the avulsion occurs when those channels are also sand-filled; then, ‘natural selection’ takes place due to gravity toward a single stream bed. In the study area, the maturation stage of the avulsive process is inversely proportional to the distance from the apex of the lobe in Caronal (Leddy et al. 1993, Louzada et al. 2021).

Sedimentation and terrestrialization are driven by aquatic-terrestrial succession (Pott & Silva 2016, Lo et al. 2017,2019), in which the burial of organic matter from senescent aquatic plants creates suitable conditions for the return of terrestrial plants over an organic soil horizon (Amoros et al. 2000, Bai et al. 2020). In the study region, that process is less intense and slower than sedimentation, occurring more frequently at the lobe edges where the water column is smaller (<1m) and evaporation tends to be higher (Mitsch et al. 2010). The schematic location of

the terrestrialization processes is depicted in green arrows in Figure 1.

The vegetation in the study area consists of grasses (under flooding), rooted and floating macrophytes, and forest and shrub formations distributed on slightly higher terrain with savanna characteristics (Pott et al. 2011). Regarding soils, according to the State's Macrozoning Plan (Mato Grosso do Sul 1989), the predominant soil covering 38.41% of the area is the class dystrophic plintisol (see the reference pedological map in Figure 1), characterized by poor drainage and frequent standing water, low clay content and presence of plinthite or petroplinthite in some of the horizons (Santos et al. 2018), caused by variations in water level. Dystrophic aerosols occupy 32.82%; these are predominantly sandy in texture in all horizons (>90%), as well as low cation exchange capacity (CEC) corresponding with organic matter content (Frazão et al. 2008). With 23.31% coverage, eutrophic planosols stand out due to the difference in clay content between the surface horizon and the B horizon, culminating in the influence of the variation in the water table (Santos et al. 2018). Integrating the remaining soil types are eutrophic fluvisols (2.92%), eutrophic gleisols (2.26%), and eutrophic acrisols, with 0.28% of the area.

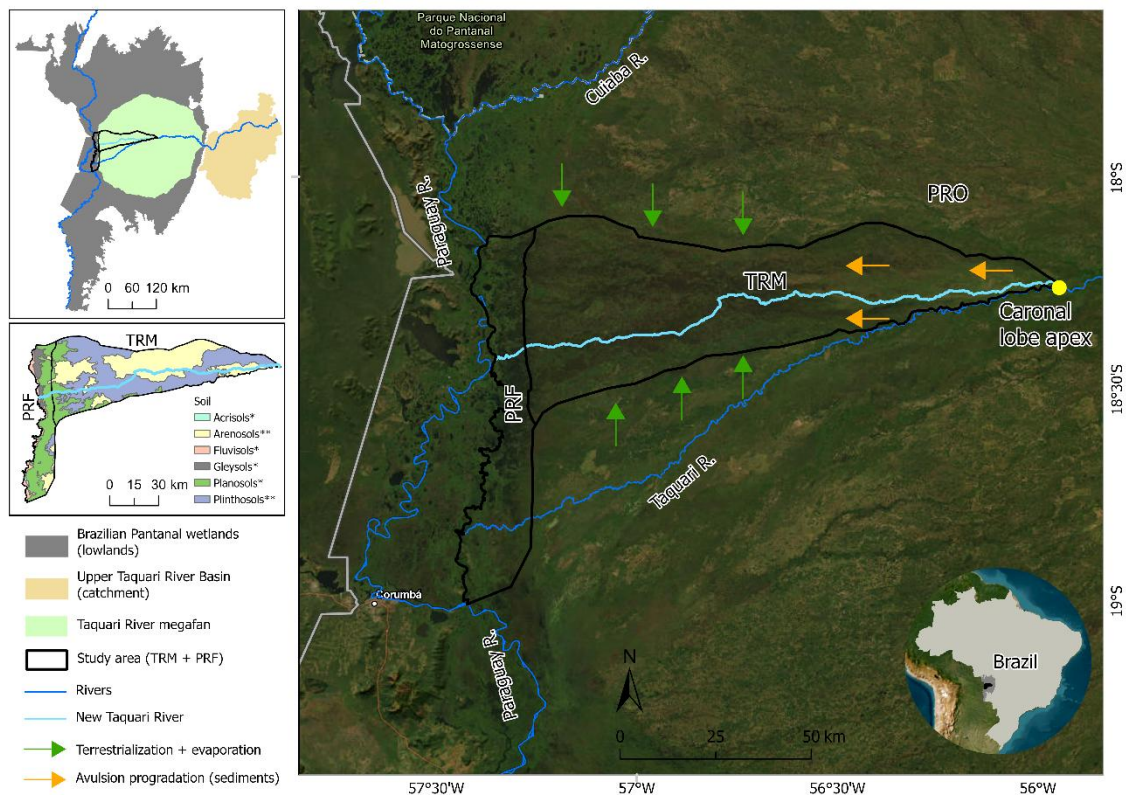


Fig. 1. The Location of the study area in the Pantanal is split into two alluvial depositional zones (item 2.2): Taquari River megafan (TRM) and Paraguay River floodplain (PRF). The arrows correspond to the location and direction of environmental transformation processes from the apex lobe, with the yellow arrow representing sediment accommodation and the green arrow corresponding to interactions between aquatic and terrestrial vegetation and water loss through evaporation. *soils with high natural fertility ($V > 50\%$); **soils with low natural fertility ($V < 50\%$), both parameters analyzed in item 2.6.

2.2 Alluvial depositional zones

To assess the influence of avulsive processes on the chemical properties of soils, it was first necessary to segregate the Taquari River megafan (TRM) and Paraguay River floodplain (PRF) depositional zones. We used satellite images before 1997, highlighting the original Paraguay River floodplain before the Taquari River's avulsion. 1988 is associated with the biggest annual flood, according to the Paraguay River hydrometric station records in Ladário (Brazil) (Bergier & Assine 2022). Therefore, we applied the Modified Normalized Difference Water Index (MNDWI) (Xu 2005) from the Landsat 5, level 2 image (scene 226_073) of July 1988 obtained from the U.S. Geological Survey (<http://earthexplorer.usgs.gov/>). MNDWI is a practical and efficient method for distinguishing aquatic targets, with applications in land use classification work in the TRM (Gil et al. 2019, Pereira et al. 2022).

The delimitation of the flooded areas was vectorized with the aid of visual inspection considering the limits between land ($MNDWI < 0$) and water ($MNDWI > 0$), acquired via the reclassification tool in ArcGIS®PRO (see Figure S1 in the Supplementary Material).

2.3 Aquatic vegetation map

In the last complete avulsion of the Taquari River, Louzada et al. (2020) found that the changes in the landscape after the crevassing began with floods and a predominance of open water, moving to the second stage determined by the predominance of macrophytes. In the third phase, macrophytes share space with waterlogged soils due to multiple channels and the blocking effect of aquatic vegetation (Marcinkowski et al. 2018). Finally, the maturation of the avulsion occurred with the drainage converging towards some channels to the point of starting soil

aeration, leaving the environment conducive to terrestrial vegetation (Mitsch et al. 2005, Coutinho et al. 2018). Here, the avulsion stage and its influence on the chemical properties of the soil were evaluated based on a binary map of the incidence of aquatic vegetation, in which the highest incidence of these plants indicates the initial stage of recanalization.

Aquatic plants are complex targets to be mapped by satellite remote sensing. Spectral confusion is common due to the mixing of patterns with terrestrial plants and fast senescence and photosynthetic activity (Malthus 2017, Mu et al. 2023). As a result, mapping depends on field collections to test and validate the process (Villa et al. 2014). Therefore, we collected basic information through georeferenced photographs ($n=81$) in a region with intense colonization of macrophytes (emergent rooted, submerged, and floating), acquired in January 2023 (see a map of points in Figure 2). Other photographic records are in Figures S2 to S5. Due to the complexity that the targets required, we explored three simultaneous indices: Tasseled Cap Brightness (Crist & Cicone 1984), Tasseled Cap Vegetation (Bannari et al. 1995), and Tasseled Cap Wetness (Crist & Cicone 1984). Tasseled cap indices successfully distinguished floating and submerged aquatic plants by applying all spectral bands compared to 2-band indices (see examples in Samarawickrama et al. 2017, Luo et al. 2023).

In this work, we used Sentinel 2 images, level 2 (scenes T21KXV, T21KVV, and T21KWV), with 10 m and 20 m spatial resolution from November 2022, obtained from the European Space Agency website (<https://dataspace.copernicus.eu/>). The collection date refers to the cloud-free scenes closest to the ground truth field. The indices are here called TC_BRI (1), TC_VEG (2), and TC_WET (3) and are calculated using the following formulas:

$$0.3037*b_2+0.2793*b_3+0.4743*b_4+0.5585*b_8+0.1863*b_{12} \quad (1)$$

$$-0.2848*b_2-0.2435*b_3-0.5436*b_4+0.7243*b_8+0.0840*b_{11}-0.1800*b_{12} \quad (2)$$

$$0.1509*b_2+0.1973*b_3+0.3279*b_4+0.3406*b_8-0.7112*b_{11}-0.4572*b_{12} \quad (3)$$

where b_2 is blue in the electromagnetic spectrum, b_3 is green, b_4 is red, b_8 refers to near-infrared, b_{11} and b_{12} refer to short-wave infrared.

Macrophyte patterns were defined by segmenting the RGB True Color Image using the Segmentation Mean Offset tool in ArcGIS® Pro, applying maximum spatial and spectral detail parameters set to 20 and a minimum set size of pixels of 10. Next, the polygons ($n=43$) that crossed the georeferenced photographs were the basis for selecting the pixels completely inserted into the polygons ($n=9,905$). Using the extract values for points tool, we then collect the values of the three indices for each pixel. Box plots of data made in the R software (R Core Team 2013) were used to select the suitable range of the macrophyte pixels. Finally, we used the ArcGIS® Pro raster calculator tool to generate the binary map according to the box plot analysis's minimum and maximum indices values.

The map's accuracy was generated from 492 random points created by the ArcGIS® Pro spatially balanced points tool, considering 1 point every 10 km². In this evaluation, the confusion matrix was constructed from a visual analysis of the same Sentinel 2 image from November 2022, in the true color R4G3B2 composition, to generate the global accuracy (OA) according to equation 4:

$$OA = \frac{\text{Total number of correctly classified pixels (diagonal)}}{\text{Total number of reference pixels}} \times 100 \quad (4)$$

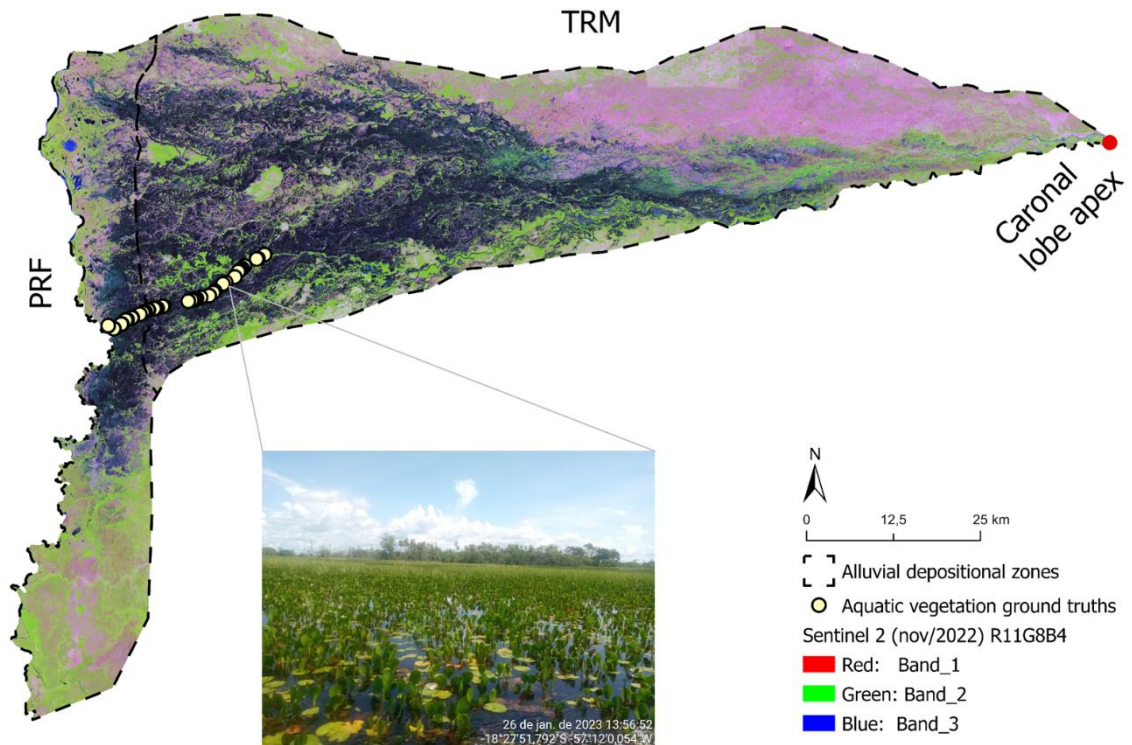


Fig. 2. Map of the distribution of ground truth points collected in January 2023 overlaid on a Sentinel 2 mosaic (R11G8B4), with an example of a georeferenced photograph. The alluvial depositional zones are the Taquari River megafan (TRM) and the Paraguay River floodplain (PRF).

2.4 Sampling design and soil surface collection

The number of soil samples was arbitrarily defined at 75 points, considering the cost-benefit of spending time and resources (~2 weeks). The spatial distribution of the samples was prepared using the ‘create random points tool’ in ArcGIS® Pro, overlapping the macrophyte layer (item 2.3) and at least 1 km apart to increase dispersion. Here we distribute the points over the entire study area to assess the influence of longitudinal variations related to distance from the Caronal apex lobe and likely latitudinal oscillations resulting from terrestrialization.

Sample collection on a small vessel was carried out in June 2023. The soil was collected at a superficial layer (0-0.2 m depth) using an acrylic cylinder 0.3 m deep. This exercise was performed without repetition, and all collected material was homogenized and packaged for laboratory analysis (item 2.5).

2.5 Soil nutrient analysis

We used routine soil analyses in a certified laboratory (Solos Inc., Campo Grande, Mato Grosso do Sul, Brazil) for surveys of the chemical properties of agricultural soils. The macronutrients analyzed were Calcium (Ca), Magnesium (Mg), Phosphorus (P), Potassium (K), Aluminum (Al), and Hydrogen (H). The micronutrients were Iron (Fe), Manganese (Mn), Zinc (Zn), Copper (Cu), and Boron (B). In addition, chemical analyses included organic matter (OM) content and soil pH. Indirectly, the percentage of base saturation (V), the total cation exchange capacity (CEC) by the sum of K, Ca, Mg, Al, and H, and the effective cation exchange capacity (ECEC), the sum of K, Ca, Mg, and Al. All categories of chemical elements, parameters, and units are in Table 1.

Laboratory routines followed the main Brazilian soil analysis methods defined by the manual of the Brazilian Agricultural Research Corporation (EMBRAPA) (Teixeira et al. 2017). Sample preparation began with drying in an oven at 40° C and then sieving to separate fractions above 2 mm. The pH was measured after 1 hour of the solution of 10 g of soil and adding 25 ml of CaCl₂ 0.01 mol L⁻¹. At the same time, the organic matter was obtained by a difference of the weight after oven and incineration in a muffle furnace at 600° C. The P content in the soil was calculated using the Mehlich-1 extraction solution (HCl 0.05 mol L⁻¹ and H₂SO₄ 0.0125 mol L⁻¹) and subsequently read on the ultraviolet spectrometer. A method with flame spectrophotometry was adopted for exchangeable K⁺. The exchangeable bases Ca⁺⁺, Mg⁺⁺, and Al⁺⁺⁺ were analyzed using 1 mol L⁻¹ KCl as extractant and subsequent volumetric measurement. H⁺ was obtained by applying 1 mol L⁻¹ calcium acetate extracting solution at pH 7.

The micronutrients Fe, Mn, Zn, and Cu were obtained through flame atomic absorption spectrometry, preceded by adding Mehlich-1 extracting solution. Finally, B was evaluated from a portion of soil (20 g) and subjected to boiling water for 5 minutes, adding 0.1 mol L⁻¹ CaCl₂ extractor and filtering the solution on filter paper.

Table 1. Soil elements are analyzed as their respective units and extraction methods.

Category	Element/parameter	Unit	Method*
Other	pH	-	CaCl ₂
	Organic Matter (OM)	g/dm ³	-
Macronutrients	Phosphorous (P)	mg/dm ³	Mehlich I
	Potassium (K)	cmol/dm ³	Mehlich I
	Calcium (Ca)	cmol/dm ³	KCL 1M
	Magnesium (Mg)	cmol/dm ³	KCL 1M
	Aluminum (Al)	cmol/dm ³	KCL 1M
	Hydrogen (H)	cmol/dm ³	Acetate 1 and Calcium (pH7.0)
	Cation Exchange Capacity (CEC)	cmol/dm ³	pH (7.0)
	Effective Cation Exchange Capacity (ECEC)	cmol/dm ³	pH (7.0)
	Saturation basis (V)	%	-
Micronutrients	Iron (Fe)	mg/dm ³	Mehlich I
	Manganese (Mn)	mg/dm ³	Mehlich I
	Zinc (Zn)	mg/dm ³	Mehlich I
	Copper (Cu)	mg/dm ³	Mehlich I
	Boron (B)	mg/dm ³	Hot-water-soluble

* The source of the methods is Texeira et al. (2017).

The results of lab analyses were linked to the georeferenced and spatialized collection points using the ArcGIS[®] Pro spline with barriers tool for the macrophyte area obtained in item 2.3. Moreover, R software was used to analyze the data between PRF and TRM using normality tests and respective methods to compare differences.

2.6 Exploratory variables

Considering both deposition zones, we sought to select independent variables that could explain the possible latitudinal and longitudinal variability of all soil chemical attributes. To this end, the following sets of factors were created in ArcGIS[®] Pro: 1) “lobe_apex_distance”, calculated from the straight line distance of the points about the fissured margin, representing the beginning of the avulsion in Caronal; 2) Tasseled Cap indices (item 2.3), obtained from the original values using the extract values for points tool; 3) “macrophytes_density”, based on the transformation of macrophyte pixels into points and subsequent application of the point density tool; 4) “soil_fertility_map”, generated from binary information for dystrophic (0) and eutrophic (1) according to data from the pedological map (detail in Figure 1). After collection, both values

were subjected to correlation analysis in R, discarding autocorrelated variables (>0.4 or <-0.4).

2.7 Random Forest Regression

To explore the response variables of this study, we opted for the Random Forest (RF) algorithm, implemented in the R packages “caret” (Kuhn & Johnson 2013) and “randomForest” (Breiman 2001). The RF machine learning method is non-parametric, highly precise, and less sensitive to outliers and unbalanced, multicollinear data (Belgiu & Drăguț 2016, Antoniadis et al. 2021). Some successful examples of forecasting applying remote sensing techniques are Jeong et al. (2017), evaluating carbon, phosphorus, and nitrogen, and Saidi et al. (2022), measuring the model's responses to the soil's CEC.

Here, we set the parameters ntree=100 and mtry=2 for all regression exercises and select 30% of the data for model testing. In the training process, the purity of each node was evaluated in the construction of decision trees (IncNodePurity) and the mean increase in squared error (IncMSE). Performance was evaluated using the coefficient of determination (R^2), root mean square error (RMSE), and percentage of root mean square error RMSE (%), according to equations 5 to 7:

$$R2 = 1 - \frac{\sum_{i=1}^n (y_i - \hat{y}_i)^2}{\sum_{i=1}^n (y_i - \bar{y})^2} \quad (5)$$

$$RMSE = \sqrt{\frac{1}{n} \sum_{i=1}^n (y_i - \hat{y}_i)^2} \quad (6)$$

$$RMSE (\%) = \left(\frac{RMSE}{\bar{y}} \right) \times 100\% \quad (7)$$

where n is the total number of observations, y_i is the actual observed value, \hat{y}_i is the value predicted by the model, and \bar{y} is the real average of observed values.

3. Results

3.1 Aquatic Vegetation Mapping and Samples Collection

The values of the pixel groups of the TC_BRI, TC_VEG, and TC_WET indices obtained

in the segmentation are presented in Fig. S6, demonstrating that the last two indices largely overlapped. In contrast, the TC_BRI range was quite discrepant from the others. Therefore, it was decided to preserve TC_BRI by adding TC_VEG with great variance. Thus, the final Boolean algebra in the raster calculator was the maximum (1,495.47) and minimum (-860.92) values of TC_VEG, plus the maximum (4,128.6) and minimum (1,889.25) values of TC_BRI. The result is presented in Figure 3, and the original indices in Figures S7 to S9.

The confusion matrix (Table 2) demonstrated that the binary map of macrophytes and non-macrophytes achieved an OA of 93%. The non-macrophyte class performed slightly worse, with an accuracy of 88%. Some classification errors include targets such as open water or mixing with forest canopies. In contrast, the accuracy of the macrophyte class reached 98%. Some examples of the results of the validation process are shown in Figure S10.

Table 2. Confusion matrix and overall accuracy (OA) of the aquatic vegetation map.

	Non_macrophyte	Macrophyte
Non_macrophyte	206	6
Macrophyte	28	252
	OA	93%

Our results revealed that, in 2022, about 56% (2,755 km²) of the study area was covered by macrophytes (see Fig. S11). Aquatic plants accumulate close to the current Taquari River, up to the middle third, approximately 70 km downstream from the apex of the lobe in the Caronal crevasse. Below this region, occupation becomes diffuse, protecting the higher-altitude lands (non-macrophytes). In the final third, near the Paraguay River, aquatic plants are even more dominant, especially in the extreme center-west, close to the mouth of the new Taquari River channel.

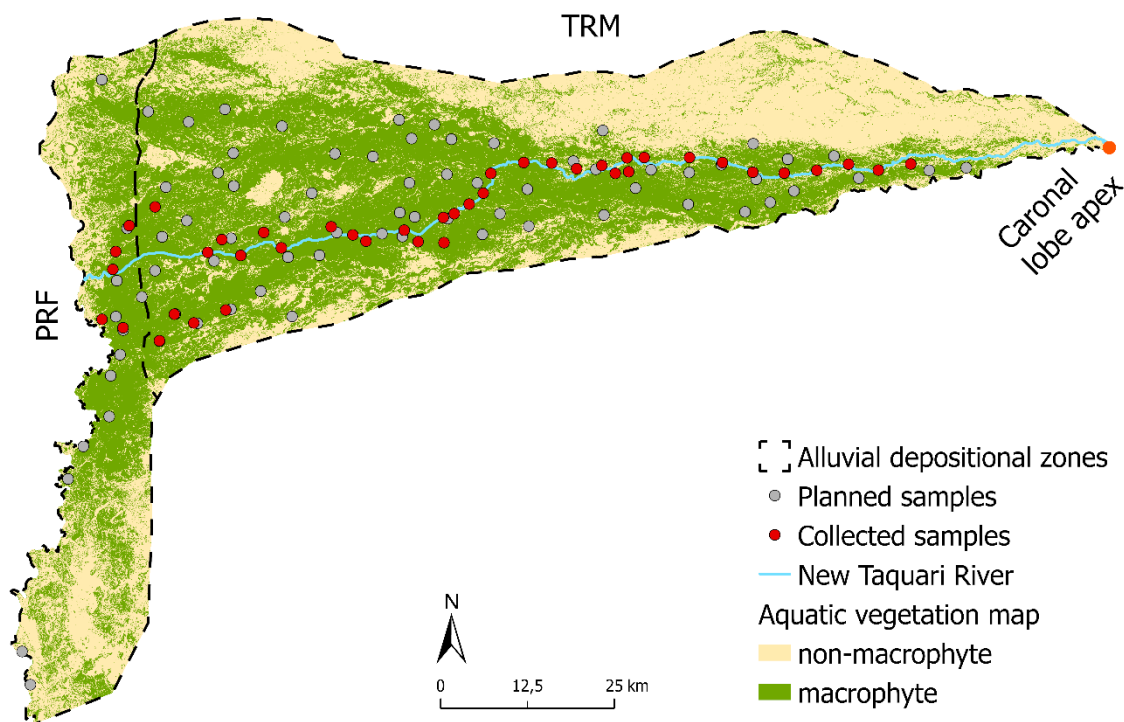


Fig. 3. Distribution map of planned samples and collected samples. Taquari River megafan (TRM), and Paraguay River floodplain (PRF).

42 surface soil samples were collected throughout the investigation, out of the 75 previously designed and planned. The collections were close to the navigable channel, considering the low water level depth (<0.5 m), and the intense colonization of macrophytes prevented lateral dispersion of the sampling. In this final arrangement, 5 samples were collected in the PRF and 37 in the TRM.

3.2 Soil chemical attributes

The results for pH, OM, macro, and micronutrients by alluvial deposition zone are presented in the box plots of Figure 4 (see the complete descriptive statistics of the parameters in Table S1). In general, only the OM ($p < 0.05$) and Mn ($p < 0.01$) parameters showed statistical differences using the Shapiro-Wilk test, followed by the Kruskal-Wallis median analysis. OM in PRF obtained 14.12 g/dm^3 against 5.49 g/dm^3 in TRM, while for Mn, there was the opposite behavior with 5.78 mg/dm^3 (PRF) and 25.99 mg/dm^3 (TRM).

The majority of samples presented an acidic pH below 5 in both zones. Low CEC and

ECEC values were also in both areas, with medians of 5.04 cmol/dm³ and 2.49 cmol/dm³ for PRF and 2.89 cmol/dm³ and 1.59 cmol/dm³ for TRM. The medians of base saturation (V%) demonstrated that the PRF (V=46.63%) was slightly higher than the points in the zone of influence of the Taquari avulsion (V=43.95%); however, proportionally, 35% of the samples in TRM (n=13) presented base saturation values greater than 50%, compared to PRF with 20% (n=1).

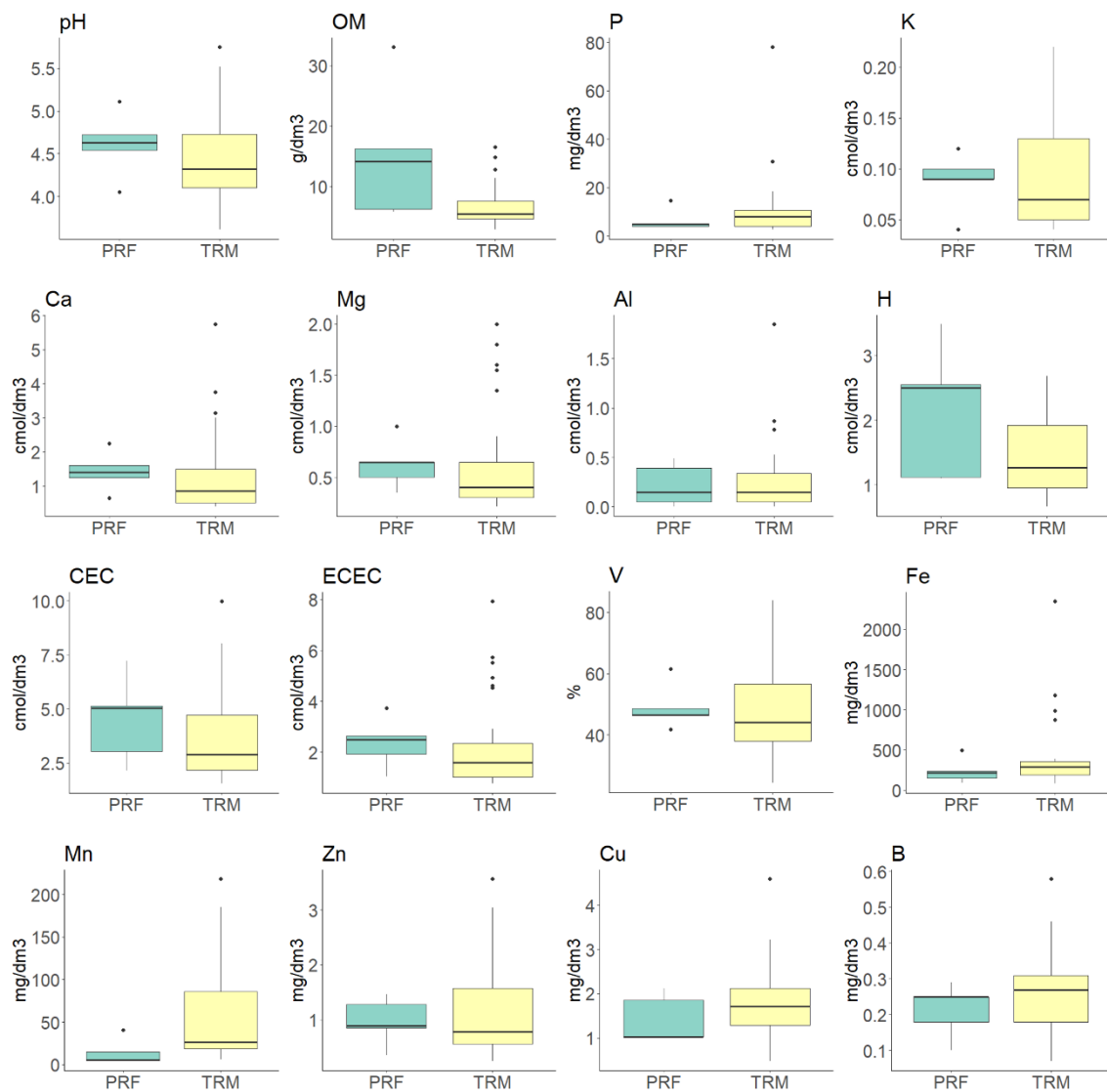


Fig. 4. Box plots of soil parameters in the Paraguay River floodplain (PRF) and Taquari River megafan (TRM). OM=organic matter; P=phosphorous, K=potassium, Ca=calcium, Mg=magnesium, Al=aluminum, H=hydrogen, CEC=cation exchange capacity, ECEC=effective cation exchange capacity, V=saturation basis, Fe=iron, Mn=manganese, Zn=zinc, Cu=copper, and B=boron.

In the mappings of soil parameters and elements (Fig. 5), the macronutrients Ca⁺⁺, Mg⁺⁺,

and the micronutrients Mn and Zn showed a clear decrease in values according to the distance from the apical lobe. The parameters pH (>5.2), V (>67.25%), and ECEC (>4.01 cmol/dm³) record the highest values on the eastern edge close to the crack. Regarding OM, irregular behavior was observed with four isolated spots throughout the area (OM>10.5 g/dm³). Finally, the elements P, K⁺, Fe, Cu, and B had no spatial relationship with the distance of the lobe from the apex; that is, they did not show a pattern in the variation of values along the channel.

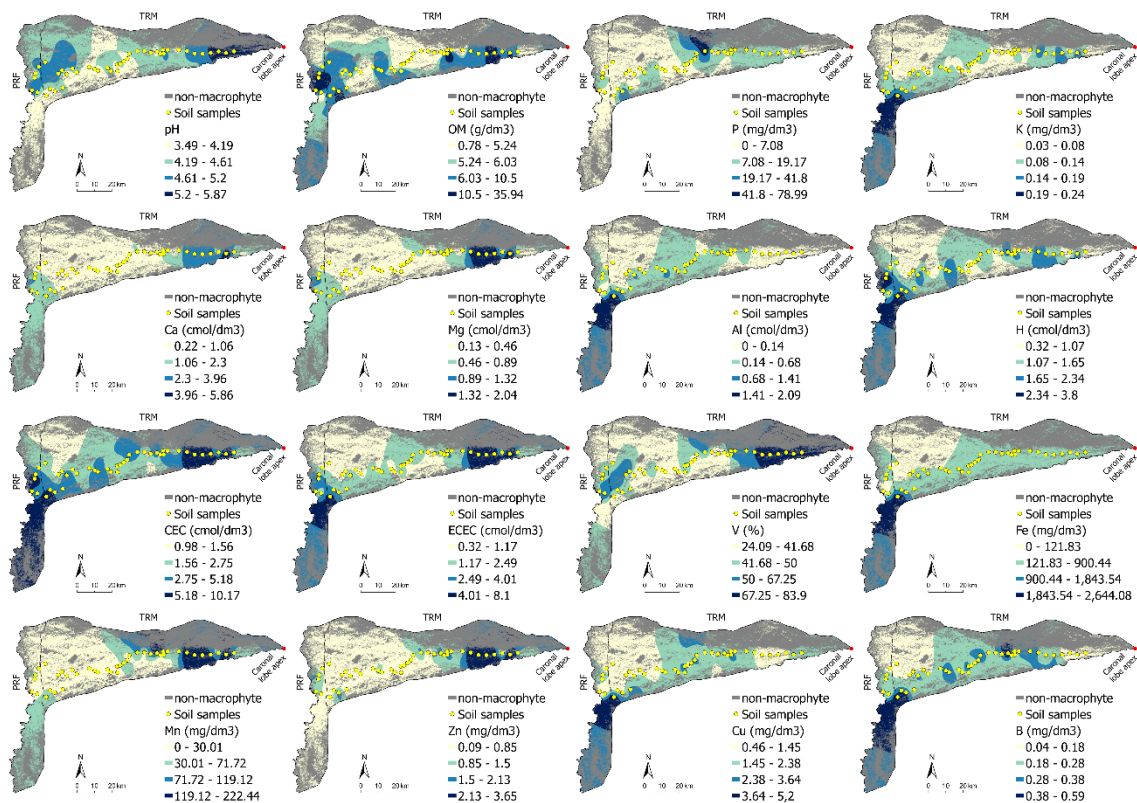


Fig. 5. Results of spatializations of soil parameters and chemical elements of the entire study area. The classes were generated by the geometric interval method, with interference in the V map in which the cut at V=50% was applied in the third class.

3.3 Random Forest Models

Spearman's correlation analysis (Fig. 3) revealed that soil variables are broadly correlated in both zones, with emphasis on relationships between Ca⁺⁺ and Mg⁺⁺ (0.97), and Mn and Zn (0.89). Among associations of variables, TC_BRI and TC_VEG showed the highest correlations (0.83), followed by TC_BRI and macrophyte_intensity (0.63 and 0.59). The factors lobe_apex_distance, TC_BRI, and map_soil_fertility were dismissed due to high collinearity for

the entire study area (PRF+TRM). Alternatively, for the TRM zone, only lobe_apex_distance and map_soil_fertility have been discarded (see data for the original variables in Table S2). As a result, lobe_apex_distance was chosen as a key variable for selection, given its importance in responding to the first hypothesis and the significant correlation with soil properties such as pH, Ca⁺⁺, V, Mn, and Zn levels.

Figures S12 to S15 present graphs on the relevance of response variables in prediction tests of RF models. In 44% of the tests carried out in the total area, the variable TC_VEG predominated in Inc_MSE, while the remaining 56% were attributed to lobe_apex_distance. In relation to Inc_Node_Purity, only two parameters (P and K⁺) presented TC_VEG as the main response variable. In the case of TRM, lobe_apex_distance demonstrated even more influence, as only in the Al⁺⁺⁺ element did the RF model determine that the most suitable variable for Inc_MSE was map_soil_fertility.

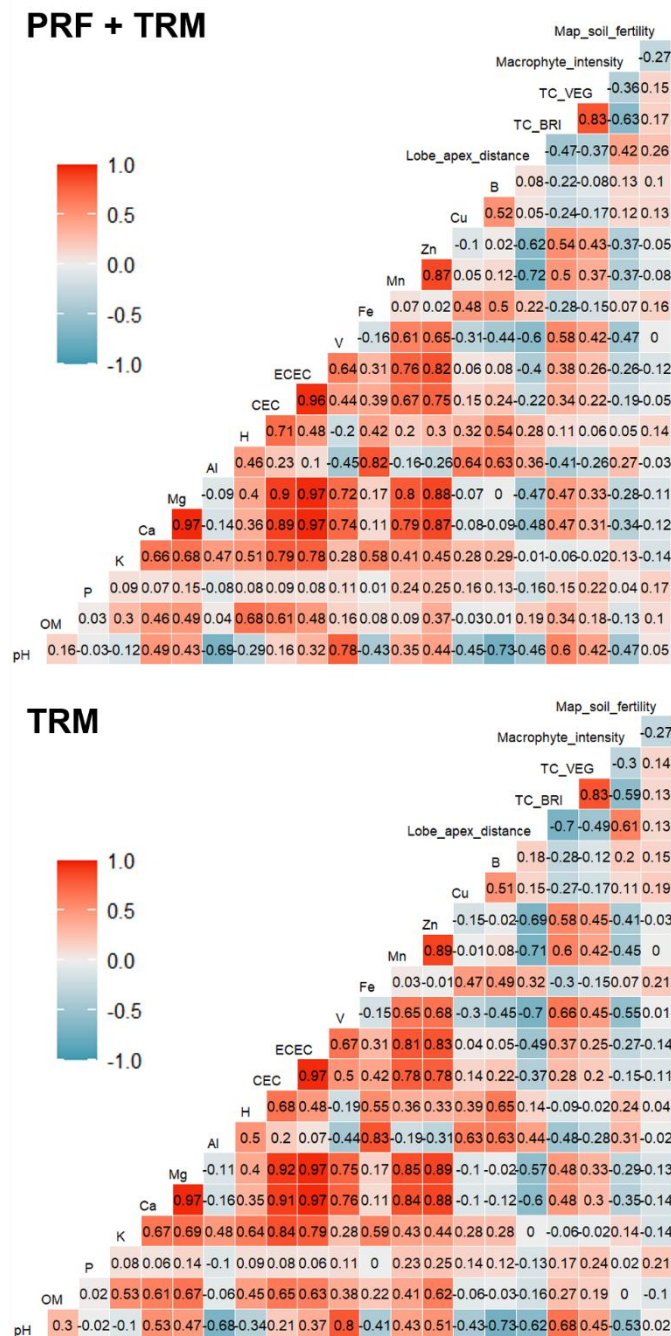


Fig. 6. Comparative results of the Spearman correlation analysis considering the entire study area (PRF and TRM) and the TRM.

The model performance results (Table 3) demonstrate that in the PRF + TRM zones, the pH parameter was the best ($R^2 = 0.57$, RMSE = 0.33, and RMSE % = 7.37), while in the TRM, the V (%) were highlighted ($R^2 = 0.93$, RMSE = 6.12% and RMSE % = 12.14). These two parameters had inverse behavior in the two spatial arrangements, since the pH performance metrics in the total area were higher than the TRM and in V (%) the opposite, with the TRM being higher than the total study area. On the other hand, the parameters OM, P, K⁺, Ca⁺⁺, Al⁺⁺⁺,

H⁺, Fe, and Cu did not present good results for either metrics or in all areas. The elements and parameters Mg⁺⁺, ECEC, Mn, and Zn obtained high R² values. However, there were reservations regarding the high RMSE (%) above 50% in most cases.

Table 3. Performance of regressions in the RF algorithm considering the entire study area (PRF and TRM) and the Taquari River depositional megafan area (TRM). R² = coefficient of determination; RMSE = root mean square error; RMSE (%) = percentage of root mean square error.

Soil elements/ parameters	PRF+TRM			TRM		
	R ²	RMS E	RMSE(%)	R ²	RMSE	RMSE(%)
pH	0.78	0.32	7.28	0.57	0.33	7.37
OM	0.00	8.17	90.08	0.00	4.16	55.88
P	0.11	0.31	141.82	0.01	20.98	146.93
K	0.18	0.03	39.4	0,00	0.06	59.93
Ca	0.17	0.43	53.03	0.01	0.67	79.4
Mg	0.74	0.43	54.23	0.42	0.42	58.4
Al	0.00	0.28	108.13	0.05	0.22	82.48
H	0.09	0.66	54.6	0.02	0.62	40.67
CEC	0.37	1.33	41.09	0.4	1.7	60.69
ECEC	0.18	2.02	69.55	0.79	1.62	73.14
V	0.67	9.32	18.32	0.93	6.12	12.14
Fe	0.1	3	67.52	0.02	530.73	140.55
Mn	0.73	26.12	55.99	0.6	41.91	132.18
Zn	0.47	0.42	44.84	0.54	0.71	63.09
Cu	0.27	0.76	49.02	0,00	1.17	68.69
B	0.41	0.05	22.74	0.04	0.09	33.11

As the metrics presented in Table 3 above, the scatterplot of predicted and actual results used in the RF tests (Fig. 7) demonstrated the best fit for V > pH > Zn. On the other hand, OM, P, K, and Cu obtained the worst fits to the data.

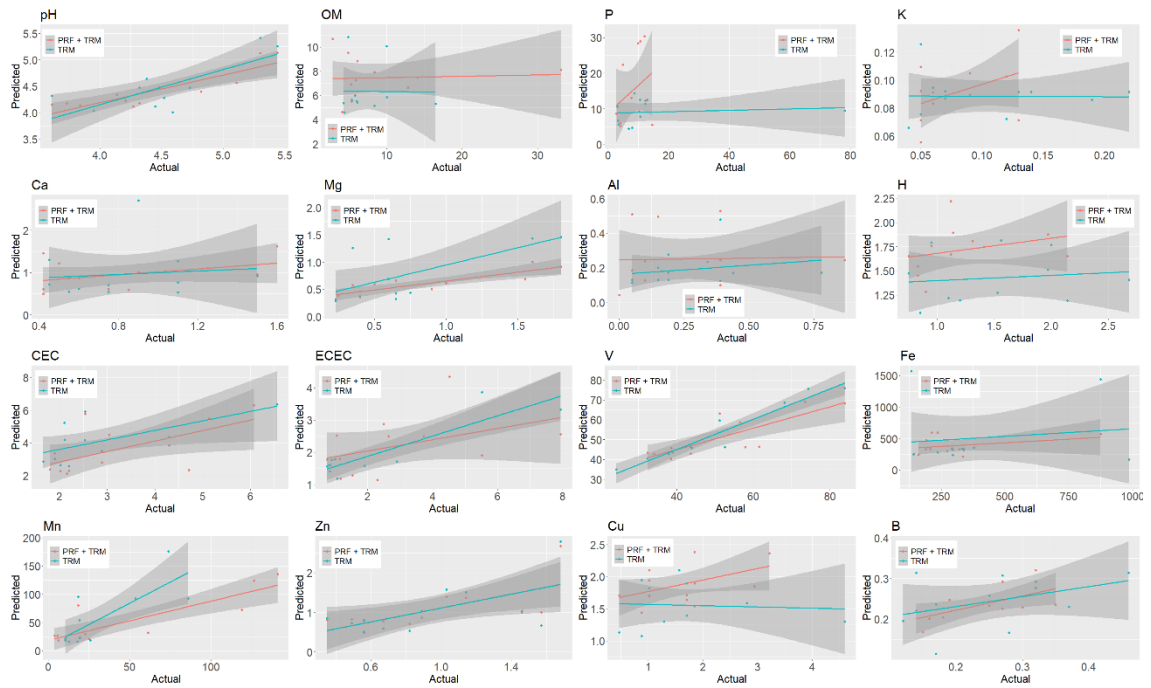


Fig. 7. Distribution graphs of actual and predicted values of soil attributes used in the RF model validation test. Generalized linear models (GLM) were used to fit the trend line with a 95% confidence interval.

4. Discussion

4.1 Considerations of avulsion and soil nutrients

Our evidence, including field investigations, geographic information systems (GIS), remote sensing techniques, and laboratory analyses, sustain the first hypothesis that the avulsion stage is influenced by nutrient concentration and soil fertility indicators. We verified that the distance to the river bifurcation point was preponderant for the decrease in pH values ($r=-0.62$; $R^2=0.57$), ECEC ($r=-0.49$; $R^2=0.79$), Mn ($r=-0.71$; $R^2=0.6$), Zn ($r=-0.69$; $R^2=0.54$), and mainly in base saturation V (%) ($r=-0.7$; $R^2=0.93$). We also identified that PRF presented higher concentrations of OM and was distinct from megafan ($p<0.05$). This was only possible with the adequate separation of the deposition zones, confirming the influence of inputs of dissolved organic carbon into the water by recurrent flood pulses (Wantzen et al. 2005, Oliveira et al. 2019). On the other hand, the second hypothesis on the relationship between terrestrialization and soil fertility could not be suitably tested due to the small latitudinal dispersion of sampling points.

Points up to 50 km from the crevasse recorded average pH and ECEC values of 5.75

and 4.7cmol/dm^3 , respectively, and all values with $V>70\%$ (Table S2). These data are superior to other studies of soils in the Pantanal landscape mosaic, such as river dikes in Babilônia de Souza et al. (2015), non-floodable forests in Cardoso et al. (2017), ephemeral lake and flooded field in Queiroz et al. (2019), or even soils within bays and salines in Nascimento et al. (2023). However, none of these studies considered sites completely flooded and under the constant influence of aquatic vegetation.

The availability of nutrients in lower portions of the Taquari megafan is ruled by pedology and human activities in the Upper Taquari catchment. Generally, soils in the upper portions come from quartz rocks (e.g., sandstones), with distant weathering and leaching processes that culminate in soils with low clay content and activity (Lacerda Filho et al. 2006, Lo et al. 2023). Another essential detail is these weathered soils' low pH (~5) characteristics (Oliveira et al. 2017). The pH influences the soil solution; H^+ ions are the ones that make the most of being absorbed by plant roots, leaving Ca^{++} , Mg^{++} , and K^+ ready to be leached (Frazão et al. 2008). In the Oxisols of Upper Taquari, where highly technical agriculture is developed (Roque et al. 2021), fertilization (e.g., NPK) and liming (CaCO_3) to balance the pH are responsible for the repeated nutrient inputs in each grain harvest. Most of these agrochemicals are transferred to crops, but there are always losses through ion leaching (Ghiberto et al. 2015).

In addition, surface runoff in the poorly managed Upper Taquari Basin may also be responsible for increased nutrient availability for the Pantanal (Bergier 2013, Oliveira et al. 2019). Sandy and poorly structured soils associated with deforestation (Guerra et al. 2020) and land uses without management measures (Louzada et al. 2022), culminated in the formation of around 3,000 gullies (Louzada et al. 2023b).

As Taquari sediments enter the active lobe, they are blocked by the macrophyte mats (Louzada et al. 2021). When sediment flow breaks this barrier, it essentially increases turbidity, interfering with the photosynthetic capacity of aquatic plants with submerged roots (Pedersen et al. 2013). At the same time, floating macrophytes disperse in the newly opened channel.

Therefore, spaces essentially colonized by macrophytes are now channels progressively filled with sediments (Assine 2005, Buehler et al. 2011). Prolonged silt leads to abandonment of the channel, higher than the surrounding area, and colonization by species originating from a seasonal flood environment (Shen et al. 2022). This is part of the aquatic/terrestrial succession or terrestrialization process observed by Louzada et al. (2020) in the oldest avulsion of the Taquari River in the Zé da Costa region.

During this aquatic/terrestrial transition process, aquatic plants retain clay particles, which enhance exchanging charges with the vegetation (Li et al. 2016), promoting the extraction of soluble ions (Greenway 2007, Saralegui et al. 2021). In the wet phase, accumulation predominates over anaerobic decomposition (Passerini et al. 2016, Paccagnella et al. 2020), and net primary productivity is very high (Morais et al. 2022). Proportionally, in the terrestrial phase, the mineralization of organic matter by aerobic decomposition is very effective (Ben-Noah & Friedman 2018, Liu et al. 2023), especially in the low water season (Vourlitis et al. 2017). The most advanced areas of the avulsion corroborate that change of state from vegetation accumulation to mineralization, translating into a change from a regulatory service (e.g., sediment and nutrient retention) to a provisioning service (e.g., soil fertility) (Louzada et al. 2021).

Although our study is limited to a lobe within a large megafan in the Pantanal, our results provide evidence of the important role of avulsion processes in soil formation and the balance of elements/nutrients, as well as how avulsion processes influence soil fertility dynamics through sedimentation and deposition. This is a crucial aspect to consider locally and globally, as similar patterns have been observed in other regions worldwide. For example, in Asia, the processes shaping deltaic landscapes in the Yellow River Delta provide insights into erosion, transportation, and deposition and how the weathering, sorting, and dilution are the main factors altering soil geochemistry in that region (Li et al. 2019). The red clay layer (RCL), characterized by its fine grain size and elevated mineral content, likely originated from highly weathered

sediments, exhibiting significant accumulation of inorganic carbon and fluctuations in elemental ratios that impact nutrient cycling (Li et al. 2019). Additionally, allochthonous materials are used in carbon-nutrient cycling (Li et al. 2023). The accumulation of allochthonous particles further contributes to the persistence of the organic carbon pool and enhances the capacity of minerals to stabilize organic matter (Li et al. 2023). The aquatic vegetation plays a vital role in carbon accumulation and histosol formation through sediment capture, acting as natural barriers that retain sediments, and this process increases soil fertility. It is important to emphasize the need to assess the influence of avulsion processes on soil dynamics in other large wetland areas around the world, such as the Okavango Delta in Botswana (Lisenby et al. 2019), in Bangladesh by Ganges-Brahmaputra Delta Plain (Bomer et al. 2020), and Mamore River in Bolivia (May et al. 2015); since the rate of landscape changes, climate variations, and geomorphological shifts may be key to comprehensively understanding the and generalities/contingencies of large-scale avulsion processes.

4.2 Soil fertility in the Taquari River active lobe: future researches and implications for sustainability

Given the importance of aquatic plants in building and rebuilding the environment, it was necessary to construct an accurate map of aquatic macrophytes. Nevertheless, future research in soil science can add knowledge on the variability and status quo of pasture areas intensely colonized by aquatic plants due to avulsion in the past. In other words, the environmental regulation service during the aquatic phase may have implications for current provisioning processes in the Pantanal, such as those promoted by natural pastures supporting sustainable cattle production in the region (Chiaravalloti et al. 2023). Moreover, improvements in future maps include assessing macrophyte composition and abundance, as these have different hydro-sedimentological responses regarding nutrient retention and carbon dynamics concerning the atmosphere (Pal et al. 2017, Lolu et al. 2019).

In summary, we found that a set of parameters (pH, ECEC, V, Mn, and Zn) are good indicators of soil fertility under the influence of avulsion. With the advancement of drainage due to the maturation of the avulsion and river rechannelization, native pasturelands may benefit from soil fertility, with positive impacts on primary productivity and livestock stocking rate (Cardoso et al. 2010, Santos et al. 2021). Furthermore, in relatively elevated areas, terrestrial plants might be regenerated from native seed banks (Bao et al. 2014, Vourlitis et al. 2015), restoring terrestrial biological diversity (Alho 2008). On the other hand, the emerging precautions with deforestation (Louzada et al. 2020) and the consequent extensive cleaning of areas through wildfires (Damasceno-Junior et al. 2021) threaten both regulatory and provision services of the Taquari avulsion.

5. Conclusions

Remote sensing techniques with soil surface samples allowed us to infer that the avulsion of the Taquari River affects soil fertility dynamics. The evolution of the drainage basin improves pH, ECEC, base saturation, and particular micronutrients. Organic matter takes advantage of flooded regions to accumulate. For the next decades, the benefits of sedimentation and accumulation of aquatic plants are expected to positively affect the soil fertility of nearby depositional zones, following the observed pattern of the proximal crevassing zone.

This study marks the initial endeavor to assess nutrient storage in the soil during the most significant ongoing avulsion in the Pantanal. Subsequent research on these findings is recommended to address how macrophyte species contribute to nutrient accumulation in the soil and assess areas previously inundated by avulsion. Understanding the interplay between aquatic plants and sedimentation is of paramount importance. While avulsion carries ecological benefits in one dimension, it interferes with provisional ecosystem services and is subjected to extreme climate change events. Therefore, implementing conservation strategies, particularly those undertaken with the secular wisdom of “pantaneiros,” is vital to ensure sustainable use of the

active lobe of the Taquari megafan.

Supplementary material available in:

https://docs.google.com/document/d/1yHCOe1H9_u6ih66HcuJdGHb-ip297B4p/edit?usp=sharing&ouid=110830496409468836501&rtpof=true&sd=true

Conclusions

We have taken further steps toward understanding the complexities of the Taquari River. Using an extensive dataset from remote sensing and spatial and statistical analysis techniques, we have advanced our comprehension of the temporal dynamics of sediments in the upper basin and their consequences in the lower Pantanal.

Through a method based on Boolean algebra in a GIS environment, we identified that 65% of the Upper Taquari River Basin (UTRB) is at high or very high risk of soil loss, highlighting the urgent need to stabilize critical gullies in this tropical region. In a subsequent phase, we developed a method for assessing gully stability using orbital remote sensing (optical and radar). Applying this method, we expanded our analysis and found that the UTRB has nearly 3,000 gullies, with approximately 60% still active and only 2% stabilized, requiring urgent restoration measures. Furthermore, data from the MapBiomass project and the Rural Environmental Registry (CAR) do not adequately represent exposed soil areas, suggesting the need for new, more specific land categories.

Looking at the past and present conditions, we conducted a temporal assessment of exposed soil pixels from 1985 to 2024. We observed beyond the breakpoint analysis two distinct periods: from 1985 to 2015, there was a linear increase in bare soil (adjusted $R^2 = 0.44$; $p < 0.001$), rising from 0.13% to 0.8%, mainly associated with native vegetation loss and the expansion of land uses such as cotton, soybean, and pasture. From 2016 to 2024, no significant trend was observed (adjusted $R^2 = 0.13$; $p > 0.05$), although bare soil peaked at 3.36% in 2021 before declining to 0.6% in 2024. Signs of natural regeneration were detected, with bare soil pixels transitioning to shrub and tree cover by 2024, indicating spatial stabilization and localized reduction of degraded areas. However, current data are insufficient to confirm whether the region has surpassed its peak in bare soil exposure and erosion risk. Future studies should address these uncertainties by evaluating the ecological trajectories of regenerating Cerrado areas and the

economic drivers behind land use and bare soil fluctuations.

Regarding the Taquari River in the Pantanal, we developed a model to assess the evolution of avulsion (rechanneling), projecting the formation of a new channel by 2080. Our findings indicate that the fully flooded area is gradually receding and is expected to become predominantly terrestrial by this time. Throughout this drainage process, we also observed that avulsion positively contributes to soil fertility, benefiting from the accumulation of organic matter resulting from macrophyte decomposition. These nutrient cycling and carbon sink services should be closely monitored during the drainage process by authorities and landowners to ensure their long-term benefits, given that deforestation and fires could become recurrent threats in these newly drained fertile lands.

We hope that the results and discussions presented here provide valuable insights for rural landowners—the true stewards of these territories—enabling them to better understand the dynamics of the basin. Likewise, we aim to equip public authorities with the necessary information to monitor erosion restoration in the upper basin and to conserve the newly emerging ecosystem services resulting from avulsion, particularly those related to biodiversity and carbon retention.

References

Introduction

- Allan, J. D. (2004). Landscapes and Riverscapes: The Influence of Land Use on Stream Ecosystems. 35(Volume 35, 2004), 257-284.
- Annis, A., Karpach, M., Morrison, R. R., & Nardi, F. (2022). On the influence of river Basin morphology and climate on hydrogeomorphic floodplain delineations. *Advances in Water Resources*, 159, 104078.
- Arpaia, S., Smagghe, G., & Sweet, J. B. (2021). Biosafety of bee pollinators in genetically modified agro-ecosystems: Current approach and further development in the EU. *Pest Management Science*, 77(6), 2659-2666.
- Assine, M. L. (2005). River avulsions on the Taquari megafan, Pantanal wetland, Brazil. *Geomorphology*, 70(3), 357-371.
- Bega, J. M. M., Saltarelli, W. A., Gücker, B., Boëchat, I. G., Finkler, N. R., & Cunha, D. G. F. (2024). Effects of riparian vegetation restoration and environmental context on ecosystem functioning in tropical streams of southeastern Brazil. *Science of The Total Environment*, 948, 174906.
- Brauman, K. A., van der Meulen, S., & Brils, J. (2014). Ecosystem Services and River Basin Management. In J. Brils, W. Brack, D. Müller-Grabherr, P. Négrel, & J. E. Vermaat (Eds.), *Risk-Informed Management of European River Basins* (pp. 265-294). Berlin, Heidelberg: Springer Berlin Heidelberg.
- Bruna, N. (2022). A climate-smart world and the rise of Green Extractivism. *The Journal of Peasant Studies*, 49(4), 839-864.
- Buehler, H. A., Weissmann, G. S., Scuderi, L. A., & Hartley, A. J. (2011). Spatial and temporal evolution of an avulsion on the Taquari River distributive fluvial system from satellite image analysis. *Journal of Sedimentary Research*, 81(8), 630-640.
- Cabello, V., Willaarts, B. A., Aguilar, M., & del Moral Ituarte, L. (2015). River basins as social-ecological systems linking levels of societal and ecosystem water metabolism in a semiarid watershed. *Ecology and Society*, 20(3).
- Cao, Z., Wang, S., Luo, P., Xie, D., & Zhu, W. (2022). Watershed Ecohydrological Processes in a Changing Environment: Opportunities and Challenges. *Water*, 14(9).
- Chakraborty, S. K. (2021). Ecology of Fishes of Rivers: Functional Roles. In S. K. Chakraborty (Ed.), *Riverine Ecology Volume 2: Biodiversity Conservation, Conflicts and Resolution* (pp. 187-286). Cham: Springer International Publishing.
- Couto, E. G., Corrêa, G. R., Oliveira, V. A., do Nascimento, A. F., Vidal-Torrado, P., Beirigo, R., & Schaefer, C. E. G. R. (2023). Soils of Pantanal: The Largest Continental Wetland. In C. E. G. R. Schaefer (Ed.), *The Soils of Brazil* (pp. 239-267). Cham: Springer International Publishing.
- Damphousse, L., Van Goethem, K., Carroll, E., Stammler, K., & Febria, C. (2024). Ecological impacts of management practices in agricultural drain networks: a literature synthesis. *Canadian Water Resources Journal / Revue canadienne des ressources hydriques*, 49(3), 329-354.
- Diop, M., Chirinda, N., Beniaich, A., El Gharous, M., & El Mejahed, K. (2022). Soil and Water Conservation in Africa: State of Play and Potential Role in Tackling Soil Degradation and Building Soil Health in Agricultural Lands. *Sustainability*, 14(20).
- Dobre, M., Long, J. W., Maxwell, C., Elliot, W. J., Lew, R., Brooks, E. S., & Scheller, R. M. (2022). Water quality and forest restoration in the Lake Tahoe basin: impacts of future management options. *Ecology and Society*, 27(2).
- dos Santos, D. S., Ribeiro, P. G., Andrade, R., Silva, S. H. G., Gastauer, M., Caldeira, C. F., . . . Ramos, S. J. (2024). Clean and accurate soil quality monitoring in mining areas under

- environmental rehabilitation in the Eastern Brazilian Amazon. *Environmental Monitoring and Assessment*, 196(4), 385.
- Fonseca, M. R. S., Elias Soares Uagoda, R., & Marinho Leite Chaves, H. (2023). Runoff, soil loss, and water balance in a restored Karst area of the Brazilian Savanna. *CATENA*, 222, 106878.
- Gardon, F. R. (2021). Land Prioritization: An Approach to the Effective Environmental Planning of Hydrographic Basins. *Environmental Management*, 67(4), 623-631.
- Garrastazú, M. C., Mendonça, S. D., Horokoski, T. T., Cardoso, D. J., Rosot, M. A. D., Nimmo, E. R., & Lacerda, A. E. B. (2015). Carbon sequestration and riparian zones: Assessing the impacts of changing regulatory practices in Southern Brazil. *Land Use Policy*, 42, 329-339.
- Giller, P. S., & Malmqvist, B. (1998). *The biology of streams and rivers*: Oxford University Press.
- Haddad, E. A., Araújo, I. F., Feltran-Barbieri, R., Perobelli, F. S., Rocha, A., Sass, K. S., & Nobre, C. A. (2024). Economic drivers of deforestation in the Brazilian Legal Amazon. *Nature Sustainability*, 7(9), 1141-1148.
- He, Z., Jia, L., Jia, Y., & He, J. (2020). Effects of flood events on sediment transport and deposition in the waterways of Lingding Bay, Pearl River Delta, China. *Ocean & Coastal Management*, 185, 105062.
- Huambachano, M., Nemogá Soto, G. R., & Mwampamba, T. H. (2025). Making room for meaningful inclusion of Indigenous and local knowledge in global assessments: our experiences in the values assessment of the Intergovernmental Science-Policy Platform on Biodiversity and Ecosystem Services. *Ecology and Society*, 30(1).
- Huang, L., Wang, J., & Chen, X. (2022). Ecological infrastructure planning of large river basin to promote nature conservation and ecosystem functions. *Journal of Environmental Management*, 306, 114482. doi:10.1016/j.jenvman.2022.114482.
- Junk, W. J., & Nunes da Cunha, C. (2005). Pantanal: a large South American wetland at a crossroads. *Ecological Engineering*, 24(4), 391-401. doi:10.1016/j.ecoleng.2004.11.012.
- Lin, H., Bouma, J., Pachepsky, Y., Western, A., Thompson, J., van Genuchten, R., . . . Lilly, A. (2006). *Hydropedology: Synergistic integration of pedology and hydrology*. *Water Resources Research*, 42(5).
- Liu, J., Pei, X., Zhu, W., & Jiao, J. (2024). Water-related ecosystem services interactions and their natural-human activity drivers: Implications for ecological protection and restoration. *Journal of Environmental Management*, 352, 120101.
- Louzada, R. O., Bergier, I., & Assine, M. L. (2020). Landscape changes in avulsive river systems: Case study of Taquari River on Brazilian Pantanal wetlands. *Science of The Total Environment*, 723, 138067.
- Louzada, R. O., Bergier, I., Roque, F. O., McGlue, M. M., Silva, A., & Assine, M. L. (2021). Avulsions drive ecosystem services and economic changes in the Brazilian Pantanal wetlands. *Current Research in Environmental Sustainability*, 3, 100057.
- Majoro, F., Wali, U. G., Munyaneza, O., Naramabuye, F.-X., & Mukamwambali, C. (2020). On-site and off-site effects of soil erosion: causal analysis and remedial measures in agricultural land-a review. *Rwanda Journal of Engineering, Science, Technology and Environment*, 3(2).
- Meshesha, T. M., Tsunekawa, A., Haregeweyn, N., Tsubo, M., Fenta, A. A., Berihun, M. L., . . . Kassa, S. B. (2024). Agroecology-based land use/land cover change detection, prediction and its implications for land degradation: A case study in the Upper Blue Nile Basin. *International Soil and Water Conservation Research*, 12(4), 786-797.
- Osman, K. T. (2014). *Soil degradation, conservation and remediation* (Vol. 820): Springer.
- Petsch, D. K., Cionek, V. d. M., Thomaz, S. M., & dos Santos, N. C. L. (2023). Ecosystem services provided by river-floodplain ecosystems. *Hydrobiologia*, 850(12), 2563-2584.
- Rashmi, I., Karthika, K. S., Roy, T., Shinoji, K. C., Kumawat, A., Kala, S., & Pal, R. (2022).

Soil Erosion and Sediments: A Source of Contamination and Impact on Agriculture Productivity. In M. Naeem, J. F. J. Bremont, A. A. Ansari, & S. S. Gill (Eds.), *Agrochemicals in Soil and Environment: Impacts and Remediation* (pp. 313-345). Singapore: Springer Nature Singapore.

Singh, R., Garg, K. K., Wani, S. P., Tewari, R. K., & Dhyani, S. K. (2014). Impact of water management interventions on hydrology and ecosystem services in Garhkundar-Dabar watershed of Bundelkhand region, Central India. *Journal of Hydrology*, 509, 132-149.

Sonter, L. J., Moran, C. J., & Barrett, D. J. (2013). Modeling the impact of revegetation on regional water quality: A collective approach to manage the cumulative impacts of mining in the Bowen Basin, Australia. *Resources Policy*, 38(4), 670-677.

Sun, Y., Hao, R., Qiao, J., & Xue, H. (2020). Function zoning and spatial management of small watersheds based on ecosystem disservice bundles. *Journal of Cleaner Production*, 255, 120285.

Tian, P., Tian, X., Geng, R., Zhao, G., Yang, L., Mu, X., . . . Liu, Y. (2023). Response of soil erosion to vegetation restoration and terracing on the Loess Plateau. *CATENA*, 227, 107103.

Wang, Y., Li, Z., & Deng, X. (2024). Assessment of cultural ecosystem services of the Qinghai-Tibetan Plateau: Guarding the beauty of the Plateau, co-creating a better future. *Ecological Indicators*, 166, 112405.

Wantzen, K. M., Ballouche, A., Longuet, I., Bao, I., Bocoum, H., Cissé, L., . . . Zalewski, M. (2016). River Culture: an eco-social approach to mitigate the biological and cultural diversity crisis in riverscapes. *Ecohydrology & Hydrobiology*, 16(1), 7-18.

Warner, J., Wester, P., & Bolding, A. (2008). Going with the flow: river basins as the natural units for water management? *Water Policy*, 10(S2), 121-138.

Xu, J., Barrett, B., & Renaud, F. G. (2022). Ecosystem services and disservices in the Luanhe River Basin in China under past, current and future land uses: implications for the sustainable development goals. *Sustainability Science*, 17(4), 1347-1364.

Yu, J., Tian, Y., Wang, X., Sun, T., Lancia, M., Andrews, C. B., & Zheng, C. (2024). Integrated Modeling of Flow, Soil Erosion, and Nutrient Dynamics in a Regional Watershed: Assessing Natural and Human-Induced Impacts. *Water Resources Research*, 60(9), e2024WR037531.

Zucca, C., Middleton, N., Kang, U., & Liniger, H. (2021). Shrinking water bodies as hotspots of sand and dust storms: The role of land degradation and sustainable soil and water management. *CATENA*, 207, 105669.

Chapter 1

Abdulkareem, J. H., Pradhan, B., Sulaiman, W. N. A., & Jamil, N. R. (2019). Prediction of Spatial soil loss impacted by long-term land-use/land-cover change in a tropical watershed. *Geoscience Frontiers*, 10(2), 389-403.

Agidew, A.-m. A., & Singh, K. N. (2018). Factors affecting farmers' participation in watershed management programs in the Northeastern highlands of Ethiopia: a case study in the Teleyayen sub-watershed. *Ecological Processes*, 7(1), 15.

Alewell, C., Borrelli, P., Meusburger, K., & Panagos, P. (2019). Using the USLE: Chances, challenges, and limitations of soil erosion modelling. *International Soil and Water Conservation Research*, 7(3), 203-225.

Amiri, M., & Pourghasemi, H. R. (2020). Mapping and Preparing a Susceptibility Map of Gully Erosion Using the MARS Model. In P. K. Shit, H. R. Pourghasemi, & G. S. Bhunia (Eds.), *Gully Erosion Studies from India and Surrounding Regions* (pp. 405-413). Cham: Springer International Publishing.

Arabameri, A., Pradhan, B., & Rezaei, K. (2019). Spatial prediction of gully erosion using ALOS PALSAR data and ensemble bivariate and data mining models. *Geosciences Journal*, 23(4), 669-686.

- Armsworth, P. R. (2014). Inclusion of costs in conservation planning depends on limited datasets and hopeful assumptions. *Annals of the New York Academy of Sciences*, 1322(1), 61-76.
- Assine, M. L. (2005). River avulsions on the Taquari megafan, Pantanal wetland, Brazil. *Geomorphology*, 70(3), 357-371. doi:10.1016/j.geomorph.2005.02.013.
- Baret, F., & Guyot, G. (1991). Potentials and limits of vegetation indices for LAI and APAR assessment. *Remote Sensing of Environment*, 35(2), 161-173.
- Beller, E. E., Spotswood, E. N., Robinson, A. H., Anderson, M. G., Higgs, E. S., Hobbs, R. J., . . . Grossinger, R. M. (2019). Building Ecological Resilience in Highly Modified Landscapes. *BioScience*, 69(1), 80-92.
- Bergier, I. (2013). Effects of highland land-use over lowlands of the Brazilian Pantanal. *Science of The Total Environment*, 463-464, 1060-1066. doi:10.1016/j.scitotenv.2013.06.036.
- Bergier, I., Assine, M. L., McGlue, M. M., Alho, C. J. R., Silva, A., Guerreiro, R. L., & Carvalho, J. C. (2018). Amazon rainforest modulation of water security in the Pantanal wetland. *Science of The Total Environment*, 619-620, 1116-1125.
- Blake, W. H., Kelly, C., Wynants, M., Patrick, A., Lewin, S., Lawson, J., . . . Ndakidemi, P. (2021). Integrating land-water-people connectivity concepts across disciplines for co-design of soil erosion solutions. *Land Degradation & Development*, 32(12), 3415-3430.
- Boardman, J., Vandaele, K., Evans, R., & Foster, I. D. L. (2019). Off-site impacts of soil erosion and runoff: Why connectivity is more important than erosion rates. *Soil Use and Management*, 35(2), 245-256.
- Borrelli, P., Robinson, D. A., Panagos, P., Lugato, E., Yang, J. E., Alewell, C., . . . Ballabio, C. (2020). Land use and climate change impacts on global soil erosion by water (2015-2070). *Proceedings of the National Academy of Sciences*, 117(36), 21994.
- Boulton, S. J., & Stokes, M. (2018). Which DEM is best for analyzing fluvial landscape development in mountainous terrains? *Geomorphology*, 310, 168-187.
- Brancalion, P. H. S., Garcia, L. C., Loyola, R., Rodrigues, R. R., Pillar, V. D., & Lewinsohn, T. M. (2016). A critical analysis of the Native Vegetation Protection Law of Brazil (2012): updates and ongoing initiatives. *Natureza & Conservação*, 14, 1-15.
- Carrer, M. J., Maia, A. G., de Mello Brandão Vinholis, M., & de Souza Filho, H. M. (2020). Assessing the effectiveness of rural credit policy on the adoption of integrated crop-livestock systems in Brazil. *Land Use Policy*, 92, 104468.
- Chen, S., Zha, X., Bai, Y., & Wang, L. (2019). Evaluation of soil erosion vulnerability on the basis of exposure, sensitivity, and adaptive capacity: A case study in the Zhuxi watershed, Changting, Fujian Province, Southern China. *CATENA*, 177, 57-69.
- Colman, C. B., Oliveira, P. T. S., Almagro, A., Soares-Filho, B. S., & Rodrigues, D. B. B. (2019). Effects of Climate and Land-Cover Changes on Soil Erosion in Brazilian Pantanal. *Sustainability*, 11(24), 7053.
- Dash, S. S., Paul, J. C., & Panigrahi, B. (2021). Assessing soil erosion vulnerability and locating suitable conservation structures for agricultural planning using GIS - a case study of Altuma catchment of Brahmani river Basin, Odisha, India. *Arabian Journal of Geosciences*, 14(21), 2201.
- Dominati, E., Patterson, M., & Mackay, A. (2010). A framework for classifying and quantifying the natural capital and ecosystem services of soils. *Ecological Economics*, 69(9), 1858-1868.
- Durigon, V. L., Carvalho, D. F., Antunes, M. A. H., Oliveira, P. T. S., & Fernandes, M. M. (2014). NDVI time series for monitoring RUSLE cover management factor in a tropical watershed. *International Journal of Remote Sensing*, 35(2), 441-453.
- El Jazouli, A., Barakat, A., Ghafiri, A., El Moutaki, S., Ettaqy, A., & Khellouk, R. (2017). Soil erosion modeled with USLE, GIS, and remote sensing: a case study of Ikkour watershed in Middle Atlas (Morocco). *Geoscience Letters*, 4.

- Escadafal, R. (1989). Remote sensing of arid soil surface color with Landsat thematic mapper. *Advances in Space Research*, 9(1), 159-163.
- Ewunetu, A., Simane, B., Teferi, E., & Zaitchik, B. F. (2021). Mapping and Quantifying Comprehensive Land Degradation Status Using Spatial Multicriteria Evaluation Technique in the Headwaters Area of Upper Blue Nile River. *Sustainability*, 13(4).
- Filizola, H. F., Almeida Filho, G. S., Souza, M. D., & Gomes, M. A. F. (2011). Controle dos processos erosivos lineares (ravinas e voçorocas) em áreas de solos arenosos. In (pp. 7). Jaguariúna: Embrapa Meio Ambiente.
- Gahrizangi, H. S., Eslamian, S., Dalezios, N. R., Blanta, A., & Madadi, M. (2021). Vegetation Advantages for Water and Soil Conservation. *Handbook of Water Harvesting and Conservation*, 321-336.
- Galdino, S., Vieira, L. M., & Pellegrin, L. A. (2005). Impactos ambientais e socioeconômicos na Bacia do Rio Taquari-Pantanal: Corumbá: Embrapa Pantanal, 2005.
- Galdino, S., Sano, E. E., Andrade, R. G., Grego, C. R., Nogueira, S. F., Bragantini, C., & Flosi, A. H. G. (2016). Large-scale Modeling of Soil Erosion with RUSLE for Conservationist Planning of Degraded Cultivated Brazilian Pastures. *Land Degradation & Development*, 27(3), 773-784.
- Gao, J., & Wang, H. (2019). Temporal analysis on quantitative attribution of karst soil erosion: A case study of a peak-cluster depression basin in Southwest China. *CATENA*, 172, 369-377.
- García-Ruiz, J. M., Beguería, S., Lana-Renault, N., Nadal-Romero, E., & Cerdà, A. (2017). Ongoing and Emerging Questions in Water Erosion Studies. *Land Degradation & Development*, 28(1), 5-21.
- Ghorbanzadeh, O., Shahabi, H., Mirchooli, F., Valizadeh Kamran, K., Lim, S., Aryal, J., . . . Blaschke, T. (2020). Gully erosion susceptibility mapping (GESM) using machine learning methods optimized by the multi-collinearity analysis and K-fold cross-validation. *Geomatics, Natural Hazards and Risk*, 11(1), 1653-1678.
- Godoi, R. d. F., Rodrigues, D. B. B., Borrelli, P., & Oliveira, P. T. S. (2021). High-resolution soil erodibility map of Brazil. *Science of The Total Environment*, 781, 146673.
- Guerra, A., Oliveira, P. T. S. d., Roque, F. d. O., Rosa, I. M. D., Ochoa-Quintero, J. M., Guariento, R. D., . . . Garcia, L. C. (2020). The importance of Legal Reserves for protecting the Pantanal biome and preventing agricultural losses. *Journal of Environmental Management*, 260, 110128.
- Huete, A. R. (1988). A soil-adjusted vegetation index (SAVI). *Remote Sensing of Environment*, 25(3), 295-309.
- Jiang, Z., Huete, A. R., Didan, K., & Miura, T. (2008). Development of a two-band enhanced vegetation index without a blue band. *Remote Sensing of Environment*, 112(10), 3833-3845.
- Keesstra, S. D., Bouma, J., Wallinga, J., Tiftonell, P., Smith, P., Cerdà, A., . . . Fresco, L. O. (2016). The significance of soils and soil science towards realization of the United Nations Sustainable Development Goals. *SOIL*, 2(2), 111-128.
- Lamb, D., Erskine, P. D., & Parrotta, J. A. (2005). Restoration of Degraded Tropical Forest Landscapes. *Science*, 310(5754), 1628-1632.
- Laurencelle, J., Logan, T., & Gens, R. J. A. S. F. F., Alaska. (2015). ASF radiometrically terrain corrected ALOS PALSAR products. In *Alaska Satellite Facility: Fairbanks, Alaska*.
- Li, S., Xiong, L., Hu, G., Dang, W., Tang, G., & Strobl, J. (2021). Extracting check dam areas from high-resolution imagery based on the integration of object-based image analysis and deep learning. *Land Degradation & Development*, 32(7), 2303-2317.
- Libonati, R., DaCamara, C. C., Peres, L. F., Sander de Carvalho, L. A., & Garcia, L. C. (2020). Rescue Brazil's burning Pantanal wetlands. *588*, 217-219.
- Lo, E. L., Yeager, K. M., Bergier, I., Domingos-Luz, L., Silva, A., & McGlue, M. M. (2022). Sediment Infill of Tropical Floodplain Lakes: Rates, Controls, and Implications for Ecosystem Services. *Frontiers in Earth Science*, 10.

- Louzada, R. O., Bergier, I., & Assine, M. L. (2020). Landscape changes in avulsive river systems: Case study of Taquari River on Brazilian Pantanal wetlands. *Science of The Total Environment*, 723, 138067.
- Louzada, R. O., Bergier, I., Roque, F. O., McGlue, M. M., Silva, A., & Assine, M. L. (2021). Avulsions drive ecosystem services and economic changes in the Brazilian Pantanal wetlands. *Current Research in Environmental Sustainability*, 3, 100057.
- Lu, S., Liu, B., Hu, Y., Fu, S., Cao, Q., Shi, Y., & Huang, T. (2020). Soil erosion topographic factor (LS): Accuracy calculated from different data sources. *CATENA*, 187, 104334.
- Machado, R. L., Resende, A. S., Campello, E. F., Menezes, C. E. G., Souza, C. M., & Franco, A. A. (2006). Recuperação de voçorocas em áreas rurais. In *Embrapa Agrobiologia-Sistema de Produção* (pp. 63). Seropédica: Embrapa Agrobiologia.
- Marengo, J. A., Oliveira, G. S., & Alves, L. M. (2015). Climate change scenarios in the Pantanal. In *Dynamics of the pantanal wetland in South America* (pp. 227-238): Springer.
- Mathieu, R., Pouget, M., Cervelle, B., & Escadafal, R. (1998). Relationships between Satellite-Based Radiometric Indices Simulated Using Laboratory Reflectance Data and Typic Soil Color of an Arid Environment. *Remote Sensing of Environment*, 66(1), 17-28.
- Mennecke, B. E., & West Jr, L. A. (2001). Geographic Information Systems in Developing Countries: Issues in Data Collection, Implementation and Management. *Journal of Global Information Management (JGIM)*, 9(4), 44-54.
- Minella, J. P. G., Merten, G. H., Reichert, J. M., & Cassol, E. A. (2010). Processos e modelagem da erosão: da parcela à bacia hidrográfica. In *Manejo e conservação do solo e da água no contexto das mudanças ambientais*. (pp. 105-135). Rio de Janeiro: Embrapa Solos.
- Norris, J. E., Stokes, A., Mickovski, S. B., Cammeraat, E., Van Beek, R., Nicoll, B. C., & Achim, A. (2008). *Slope stability and erosion control: ecotechnological solutions*: Springer Science & Business Media.
- Panagos, P., Borrelli, P., Meusburger, K., van der Zanden, E. H., Poesen, J., & Alewell, C. (2015). Modelling the effect of support practices (P-factor) on the reduction of soil erosion by water at European scale. *Environmental Science & Policy*, 51, 23-34.
- Pena, S. B., Abreu, M. M., Magalhães, M. R., & Cortez, N. (2020). Water erosion aspects of land degradation neutrality to landscape planning tools at national scale. *Geoderma*, 363, 114093.
- Poppiel, R. R., Lacerda, M. P. C., Demattê, J. A. M., Oliveira, M. P., Gallo, B. C., & Safanelli, J. L. (2019). Pedology and soil class mapping from proximal and remote sensed data. *Geoderma*, 348, 189-206.
- Pourghasemi, H. R., Yousefi, S., Sadhasivam, N., & Eskandari, S. (2020). Assessing, mapping, and optimizing the locations of sediment control check dams construction. *Science of The Total Environment*, 739, 139954.
- Prieto, P. V., Bukoski, J. J., Barros, F. S. M., Beyer, H. L., Iribarrem, A., Brancalion, P. H. S., . . . Crouzeilles, R. (2022). Predicting landscape-scale biodiversity recovery by natural tropical forest regrowth. *Conservation Biology*, 36(3), e13842.
- Pruski, F. F. (2006). *Conservação de solo e água: práticas mecânicas para o controle da erosão hídrica*. Viçosa: Universidade Federal de Viçosa.
- Qi, J., Chehbouni, A., Huete, A. R., Kerr, Y. H., & Sorooshian, S. (1994). A modified soil adjusted vegetation index. *Remote Sensing of Environment*, 48(2), 119-126.
- Rahmati, O., Kalantari, Z., Samadi, M., Uuemaa, E., Moghaddam, D. D., Nalivan, O. A., . . . Tien Bui, D. (2019). GIS-Based Site Selection for Check Dams in Watersheds: Considering Geomorphometric and Topo-Hydrological Factors. *Sustainability*, 11(20).
- Rodrigues, S. C. (2018). Some Practices of Gully Rehabilitation in Central Brazil. In *Ravine Lands: Greening for Livelihood and Environmental Security* (pp. 183-193): Springer.
- Roitman, I., Cardoso Galli Vieira, L., Baiocchi Jacobson, T. K., da Cunha Bustamante, M. M., Silva Marcondes, N. J., Cury, K., . . . Avila, M. L. (2018). *Rural Environmental Registry: An*

innovative model for land-use and environmental policies. *Land Use Policy*, 76, 95-102.

Roque, F. O., Ochoa-Quintero, J., Ribeiro, D. B., Sugai, L. S. M., Costa-Pereira, R., Lourival, R., & Bino, G. (2016). Upland habitat loss as a threat to Pantanal wetlands. *30(5)*, 1131-1134.

Roque, F. d. O., Guerra, A., Johnson, M., Padovani, C., Corbi, J., Covich, A. P., . . . Yon, L. (2021). Simulating land use changes, sediment yields, and pesticide use in the Upper Paraguay River Basin: Implications for conservation of the Pantanal wetland. *Agriculture, Ecosystems & Environment*, 314, 107405.

Rosas, M. A., & Gutierrez, R. R. (2020). Assessing soil erosion risk at national scale in developing countries: The technical challenges, a proposed methodology, and a case history. *Science of The Total Environment*, 703, 135474.

Rouse, J. W., Haas, R. H., Schell, J. A., Deering, D. W., & Harlan, J. C. (1973). Monitoring the vernal advancement and retrogradation (green wave effect) of natural vegetation. NASA/GSFC Type III Final Report, Greenbelt, Md, 371.

Ruiz-Sinoga, J. D., & Diaz, A. R. (2010). Soil degradation factors along a Mediterranean pluviometric gradient in Southern Spain. *Geomorphology*, 118(3), 359-368.

Sarparast, M., Ownegh, M., & Sepehr, A. (2020). Evaluating the impacts of combating-action programs on desertification hazard trends: A case study of Taybad-Bakharz region, northeastern Iran. *Environmental and Sustainability Indicators*, 7, 100043.

Schmidt, I. B., de Urzedo, D. I., Piña-Rodrigues, F. C. M., Vieira, D. L. M., de Rezende, G. M., Sampaio, A. B., & Junqueira, R. G. P. (2019). Community-based native seed production for restoration in Brazil – the role of science and policy. *Plant Biology*, 21(3), 389-397.

Seixas, C. D. S., & Godoy, C. V. (2007). Vazio sanitário: panorama nacional e medidas de monitoramento. Paper presented at the simpósio brasileiro de ferrugem asiática da soja, Londrina.

Senanayake, S., Pradhan, B., Huete, A., & Brennan, J. (2020). A Review on Assessing and Mapping Soil Erosion Hazard Using Geo-Informatics Technology for Farming System Management. *Remote Sensing*, 12(24).

Senseman, G. M., Bagley, C. F., & Tweddale, S. A. (1996). Correlation of rangeland cover measures to satellite-imagery-derived vegetation indices. *Geocarto International*, 11(3), 29-38.

Sepuru, T. K., & Dube, T. (2018). An appraisal on the progress of remote sensing applications in soil erosion mapping and monitoring. *Remote Sensing Applications: Society and Environment*, 9, 1-9.

Silva, P. S., Bastos, A., Libonati, R., Rodrigues, J. A., & DaCamara, C. C. (2019). Impacts of the 1.5 °C global warming target on future burned area in the Brazilian Cerrado. *Forest Ecology and Management*, 446, 193-203.

Souza, C. M., Z. Shimbo, J., Rosa, M. R., Parente, L. L., A. Alencar, A., Rudorff, B. F. T., . . . Azevedo, T. (2020). Reconstructing Three Decades of Land Use and Land Cover Changes in Brazilian Biomes with Landsat Archive and Earth Engine. *12(17)*, 2735.

Stefanes, M., Roque, F. d. O., Lourival, R., Melo, I., Renaud, P. C., & Quintero, J. M. O. (2018). Property size drives differences in forest code compliance in the Brazilian Cerrado. *Land Use Policy*, 75, 43-49.

Strassburg, B. B. N., Iribarrem, A., Beyer, H. L., Cordeiro, C. L., Crouzeilles, R., Jakovac, C. C., . . . Visconti, P. (2020). Global priority areas for ecosystem restoration. *Nature*, 586(7831), 724-729.

Sun, P., Wu, Y., Gao, J., Yao, Y., Zhao, F., Lei, X., & Qiu, L. (2020). Shifts of sediment transport regime caused by ecological restoration in the Middle Yellow River Basin. *Science of The Total Environment*, 698, 134261.

Tambosi, L. R., Martensen, A. C., Ribeiro, M. C., & Metzger, J. P. (2014). A Framework to Optimize Biodiversity Restoration Efforts Based on Habitat Amount and Landscape Connectivity. *Restoration Ecology*, 22(2), 169-177.

Tardio, G., B., M. S., Alexia, S., & Sanjaya, D. (2017). Bamboo structures as a resilient erosion

- control measure. *Proceedings of the Institution of Civil Engineers: Forensic Engineering*, 170(2), 72-83.
- Telles, T. S., Dechen, S. C. F., Souza, L. G. A. d., & Guimarães, M. d. F. (2013). Valuation and assessment of soil erosion costs. *Scientia Agricola*, 70, 209-216.
- Tesfahunegn, G. B. (2019). Farmers' perception on land degradation in northern Ethiopia: Implication for developing sustainable land management. *The Social Science Journal*, 56(2), 268-287.
- Thielen, D., Schuchmann, K.-L., Ramoni-Perazzi, P., Marquez, M., Rojas, W., Quintero, J. I., & Marques, M. I. (2020). Quo vadis Pantanal? Expected precipitation extremes and drought dynamics from changing sea surface temperature. *Plos One*, 15(1), e0227437.
- Toledo, R. M., Santos, R. F., Verheyen, K., & Perring, M. P. (2018). Ecological restoration efforts in tropical rural landscapes: Challenges and policy implications in a highly degraded region. *Land Use Policy*, 75, 486-493.
- Wischmeier, W. H., & Smith, D. D. (1965). Predicting rainfall-erosion losses from cropland east of the Rocky Mountains. Agricultural Research Service, US Department of Agriculture.
- Wuepper, D., Borrelli, P., & Finger, R. (2020). Countries and the global rate of soil erosion. *Nature Sustainability*, 3(1), 51-55.
- Wynants, M., Kelly, C., Mtei, K., Munishi, L., Patrick, A., Rabinovich, A., . . . Ndakidemi, P. (2019). Drivers of increased soil erosion in East Africa's agro-pastoral systems: changing interactions between the social, economic and natural domains. *Regional Environmental Change*, 19(7), 1909-1921.
- Xu, X., Zhu, T., Zhang, H., & Gao, L. (2020). Sediment-Storage Effects of Check-Dam System in the Small Watershed. In *Experimental Erosion* (pp. 113-139): Springer.
- Yang, Y., Wang, L., Yang, Z., Xu, C., Xie, J., Chen, G., . . . Lin, T.-C. (2018). Large Ecosystem Service Benefits of Assisted Natural Regeneration. *Journal of Geophysical Research: Biogeosciences*, 123(2), 676-687.
- Yesuph, A. Y., & Dagne, A. B. (2019). Soil erosion mapping and severity analysis based on RUSLE model and local perception in the Beshillo Catchment of the Blue Nile Basin, Ethiopia. *Environmental Systems Research*, 8(1), 17.
- Zabihi, M., Mirchooli, F., Motevalli, A., Khaledi Darvishan, A., Pourghasemi, H. R., Zakeri, M. A., & Sadighi, F. (2018). Spatial modelling of gully erosion in Mazandaran Province, northern Iran. *CATENA*, 161, 1-13.
- Zhang, B., Yang, Y.-s., & Zepp, H. (2004). Effect of vegetation restoration on soil and water erosion and nutrient losses of a severely eroded clayey Plinthudult in southeastern China. *CATENA*, 57(1), 77-90.
- Zhao, M., Peng, J., Liu, Y., Li, T., & Wang, Y. (2018). Mapping Watershed-Level Ecosystem Service Bundles in the Pearl River Delta, China. *Ecological Economics*, 152, 106-117.

Chapter 2

- Alexakis, D. D., Manoudakis, S., Agapiou, A., & Polykretis, C. (2021). Towards the Assessment of Soil-Erosion-Related C-Factor on European Scale Using Google Earth Engine and Sentinel-2 Images. *Remote Sensing*, 13(24).
- Almazroui, M., Ashfaq, M., Islam, M. N., Rashid, I. U., Kamil, S., Abid, M. A., . . . Sylla, M. B. (2021). Assessment of CMIP6 Performance and Projected Temperature and Precipitation Changes Over South America. *Earth Systems and Environment*, 5(2), 155-183.
- Arabameri, A., Rezaei, K., Pourghasemi, H. R., Lee, S., & Yamani, M. (2018). GIS-based gully erosion susceptibility mapping: a comparison among three data-driven models and AHP knowledge-based technique. *Environmental Earth Sciences*, 77(17), 628.
- Ariti, A. T., van Vliet, J., & Verburg, P. H. (2019). The role of institutional actors and their interactions in the land use policy making process in Ethiopia. *Journal of Environmental Management*, 237, 235-246.

- Assine, M. L. (2005). River avulsions on the Taquari megafan, Pantanal wetland, Brazil. *Geomorphology*, 70(3), 357-371.
- Baret, F. (2016). 2 - Estimation of Biophysical Variables from Satellite Observations. In N. Baghdadi & M. Zribi (Eds.), *Land Surface Remote Sensing in Agriculture and Forest* (pp. 37-80): Elsevier.
- Baret, F., & Guyot, G. (1991). Potentials and limits of vegetation indices for LAI and APAR assessment. *Remote Sensing of Environment*, 35(2), 161-173.
- Barron, V., & Torrent, J. (1986). Use of the Kubelka—Munk theory to study the influence of iron oxides on soil colour. *Journal of Soil Science*, 37(4), 499-510.
- Bergier, I., Assine, M. L., McGlue, M. M., Alho, C. J. R., Silva, A., Guerreiro, R. L., & Carvalho, J. C. (2018). Amazon rainforest modulation of water security in the Pantanal wetland. *Science of The Total Environment*, 619-620, 1116-1125.
- Borrelli, P., Robinson, D. A., Panagos, P., Lugato, E., Yang, J. E., Alewell, C., . . . Ballabio, C. (2020). Land use and climate change impacts on global soil erosion by water (2015-2070). *Proceedings of the National Academy of Sciences*, 117(36), 21994-22001.
- Breiman, L. (2001). Random Forests. *Machine Learning*, 45(1), 5-32.
- Buller, L. S., Bayma-Silva, G., Zanetti, M. R., Ortega, E., de Moraes, A., Goulart, T., & Bergier, I. (2016). Historical Land-Use Changes in São Gabriel do Oeste at the Upper Taquari River Basin. In I. Bergier & M. L. Assine (Eds.), *Dynamics of the Pantanal Wetland in South America* (pp. 191-208). Cham: Springer International Publishing.
- Castillo, C., & Gómez, J. A. (2016). A century of gully erosion research: Urgency, complexity and study approaches. *Earth-Science Reviews*, 160, 300-319.
doi:10.1016/j.earscirev.2016.07.009.
- Castro, L. M., & Lechthaler, F. (2022). The contribution of bio-economic assessments to better informed land-use decision making: An overview. *Ecological Engineering*, 174, 106449.
- Clevers, J., De Jong, S., Epema, G., Addink, E., & Van Der Meer, F. (2000). Meris and the Red-edge index. Paper presented at the Second EARSel Workshop on Imaging Spectroscopy, Enschede.
- Conforti, M., Mercuri, M., & Borrelli, L. (2021). Morphological Changes Detection of a Large Earthflow Using Archived Images, LiDAR-Derived DTM, and UAV-Based Remote Sensing. *Remote Sensing*, 13(1).
- Cui, H., Wang, Z., Yan, H., Li, C., Jiang, X., Wang, L., . . . Shi, Z. (2022). Production-Based and Consumption-Based Accounting of Global Cropland Soil Erosion. *Environmental Science & Technology*, 56(14), 10465-10473.
- Das, P., Saha, T. K., Mandal, I., Debanshi, S., & Pal, S. (2023). Evolution of rills and gullies in lateritic badland region of Indian Rarh tract. *Journal of Earth System Science*, 132(1), 7.
- de Asis, A. M., Omasa, K., Oki, K., & Shimizu, Y. (2008). Accuracy and applicability of linear spectral unmixing in delineating potential erosion areas in tropical watersheds. *International Journal of Remote Sensing*, 29(14), 4151-4171.
- De Deyn, G. B., & Kooistra, L. (2021). The role of soils in habitat creation, maintenance and restoration. *Philosophical Transactions of the Royal Society B: Biological Sciences*, 376(1834), 20200170.
- Diniz, J. M. F. d. S., Gama, F. F., & Adami, M. (2020). Evaluation of polarimetry and interferometry of sentinel-1A SAR data for land use and land cover of the Brazilian Amazon Region. *Geocarto International*, 1-19.
- Dong, Y., Xiong, D., Su, Z. a., Li, J., Yang, D., Shi, L., & Liu, G. (2014). The distribution of and factors influencing the vegetation in a gully in the Dry-hot Valley of southwest China. *CATENA*, 116, 60-67. doi:10.1016/j.catena.2013.12.009.
- Escadafal, R. (1989). Remote sensing of arid soil surface color with Landsat thematic mapper. *Advances in Space Research*, 9(1), 159-163.
- Eustace, A., Pringle, M., & Witte, C. (2009). Give Me the Dirt: Detection of Gully Extent and Volume Using High-Resolution Lidar. In S. Jones & K. Reinke (Eds.), *Innovations in Remote*

- Sensing and Photogrammetry (pp. 255-269). Berlin, Heidelberg: Springer Berlin Heidelberg.
- Fernández, D., Adermann, E., Pizzolato, M., Pechenkin, R., Rodríguez, C. G., & Taravat, A. (2023). Comparative Analysis of Machine Learning Algorithms for Soil Erosion Modelling Based on Remotely Sensed Data. *Remote Sensing*, 15(2).
- Fonseca, C. A., Al-Ansari, N., Silva, R. M., Santos, C. A., Zerouali, B., Oliveira, D. B., & Elbeltagi, A. (2022). Investigating Relationships between Runoff–Erosion Processes and Land Use and Land Cover Using Remote Sensing Multiple Gridded Datasets. *ISPRS International Journal of Geo-Information*, 11(5).
- Frankl, A., Nyssen, J., Vanmaercke, M., & Poesen, J. (2021). Gully prevention and control: Techniques, failures and effectiveness. *Earth Surface Processes and Landforms*, 46(1), 220-238.
- Fu, W., Ma, J., Chen, P., & Chen, F. (2020). Remote sensing satellites for digital earth. In *Manual of digital earth* (pp. 55-123): Springer, Singapore.
- Galang, M. A., Markewitz, D., Morris, L. A., & Bussell, P. (2007). Land use change and gully erosion in the Piedmont region of South Carolina. *Journal of Soil and Water Conservation*, 62(3), 122.
- Galdino, S., Vieira, L. M., & Pellegrin, L. A. (2005). *Impactos ambientais e socioeconômicos na Bacia do Rio Taquari-Pantanal: Corumbá: Embrapa Pantanal*, 2005.
- Gao, B. (1996). NDWI—A normalized difference water index for remote sensing of vegetation liquid water from space. *Remote Sensing of Environment*, 58(3), 257-266.
- Gayen, A., Pourghasemi, H. R., Saha, S., Keesstra, S., & Bai, S. (2019). Gully erosion susceptibility assessment and management of hazard-prone areas in India using different machine learning algorithms. *Science of The Total Environment*, 668, 124-138.
- George, E. B., Gomez, C., Nagesh Kumar, D., Dharumarajan, S., & Lalitha, M. (2022). Impact of bare soil pixels identification on clay content mapping using airborne hyperspectral AVIRIS-NG data: spectral indices versus spectral unmixing. *Geocarto International*, 1-23.
- Godoi, R. d. F., Rodrigues, D. B. B., Borrelli, P., & Oliveira, P. T. S. (2021). High-resolution soil erodibility map of Brazil. *Science of The Total Environment*, 781, 146673.
- Guo, S., Bai, X., Chen, Y., Zhang, S., Hou, H., Zhu, Q., & Du, P. (2019). An Improved Approach for Soil Moisture Estimation in Gully Fields of the Loess Plateau Using Sentinel-1A Radar Images. *Remote Sensing*, 11(3).
- Gutterman, Y. (2000). Environmental factors and survival strategies of annual plant species in the Negev Desert, Israel. *Plant Species Biology*, 15(2), 113-125.
- Hammer, Ø., Harper, D. A., & Ryan, P. D. J. P. e. (2001). PAST: Paleontological statistics software package for education and data analysis. 4(1), 9.
- Haralick, R. M., Shanmugam, K., & Dinstein, I. (1973). Textural Features for Image Classification. *IEEE Transactions on Systems, Man, and Cybernetics*, SMC-3(6), 610-621.
- Higaki, D., Karki, K. K., Koiwa, N., Takahashi, M., & Ghimire, S. K. (2021). Rehabilitation of Gully-Dominant Hill Slopes by Using Low-Cost Measures—A Case Study in Nepal. In Ž. Arbanas, P. T. Bobrowsky, K. Konagai, K. Sassa, & K. Takara (Eds.), *Understanding and Reducing Landslide Disaster Risk: Volume 6 Specific Topics in Landslide Science and Applications* (pp. 347-353). Cham: Springer International Publishing.
- Huete, A. R. (1988). A soil-adjusted vegetation index (SAVI). *Remote Sensing of Environment*, 25(3), 295-309.
- Ionita, I., Fullen, M. A., Zgłobicki, W., & Poesen, J. (2015). Gully erosion as a natural and human-induced hazard. *Natural Hazards*, 79(1), 1-5.
- Jin, H., Mountrakis, G., & Stehman, S. V. (2014). Assessing integration of intensity, polarimetric scattering, interferometric coherence and spatial texture metrics in PALSAR-derived land cover classification. *ISPRS Journal of Photogrammetry and Remote Sensing*, 98, 70-84.
- Kallel, A., Le Hégarat-Mascle, S., Otlé, C., & Hubert-Moy, L. (2007). Determination of

vegetation cover fraction by inversion of a four-parameter model based on isoline parametrization. *Remote Sensing of Environment*, 111(4), 553-566.

Keshava, N., & Mustard, J. F. (2002). Spectral unmixing. *IEEE Signal Processing Magazine*, 19(1), 44-57.

Khan, A., Govil, H., Kumar, G., & Dave, R. (2020). Synergistic use of Sentinel-1 and Sentinel-2 for improved LULC mapping with special reference to bad land class: a case study for Yamuna River floodplain, India. *Spatial Information Research*, 28(6), 669-681.

Khanal, S., Fulton, J., Klopfenstein, A., Douridas, N., & Shearer, S. (2018). Integration of high resolution remotely sensed data and machine learning techniques for spatial prediction of soil properties and corn yield. *Computers and Electronics in Agriculture*, 153, 213-225.

Kwan, C., Gribben, D., Ayhan, B., Li, J., Bernabe, S., & Plaza, A. (2020). An Accurate Vegetation and Non-Vegetation Differentiation Approach Based on Land Cover Classification. *Remote Sensing*, 12(23).

Laamrani, A., Joosse, P., McNairn, H., Berg, A. A., Hagerman, J., Powell, K., & Berry, M. (2020). Assessing Soil Cover Levels during the Non-Growing Season Using Multitemporal Satellite Imagery and Spectral Unmixing Techniques. *Remote Sensing*, 12(9).

Lal, R. (1992). Restoring Land Degraded by Gully Erosion in the Tropics. In R. Lal & B. A. Stewart (Eds.), *Soil Restoration: Soil Restoration Volume 17* (pp. 123-152). New York, NY: Springer New York.

le Roux, J., Morake, L., van der Waal, B., Leigh Anderson, R., & Hedding, D. W. (2022). Intra-gully mapping of the largest documented gully network in South Africa using UAV photogrammetry: Implications for restoration strategies. *Progress in Physical Geography: Earth Environment International*, 46(5), 772-789.

Li, Z., Zhang, Y., Zhu, Q., He, Y., & Yao, W. (2015). Assessment of bank gully development and vegetation coverage on the Chinese Loess Plateau. *Geomorphology*, 228, 462-469.

Li, Z., Zhang, Y., Zhu, Q., Yang, S., Li, H., & Ma, H. (2017). A gully erosion assessment model for the Chinese Loess Plateau based on changes in gully length and area. *CATENA*, 148, 195-203. doi:10.1016/j.catena.2016.04.018.

Liang, S. (2007). Recent developments in estimating land surface biogeophysical variables from optical remote sensing. *Progress in Physical Geography: Earth and Environment*, 31(5), 501-516.

Liu, K., Ding, H., Tang, G., Zhu, A. X., Yang, X., Jiang, S., & Cao, J. (2017). An object-based approach for two-level gully feature mapping using high-resolution DEM and imagery: a case study on hilly loess plateau region, China. *Chinese Geographical Science*, 27(3), 415-430.

Louzada, R. O., Bergier, I., Roque, F. O., McGlue, M. M., Silva, A., & Assine, M. L. (2021). Avulsions drive ecosystem services and economic changes in the Brazilian Pantanal wetlands. *Current Research in Environmental Sustainability*, 3, 100057.

Louzada, R. O., Bergier, I., Diniz, J. M. F. d. S., Guerra, A., & Roque, F. d. O. (2022). Priority setting for restoration in surrounding savannic areas of the Brazilian Pantanal based on soil loss risk and agrarian structure. *Journal of Environmental Management*, 323, 116219.

Makaya, N. P., Mutanga, O., Kiala, Z., Dube, T., & Seutloali, K. E. (2019). Assessing the potential of Sentinel-2 MSI sensor in detecting and mapping the spatial distribution of gullies in a communal grazing landscape. *Physics and Chemistry of the Earth, Parts A/B/C*, 112, 66-74.

Mandal, D., Kumar, V., Lopez-Sanchez, J. M., Rao, Y. S., McNairn, H., Bhattacharya, A., & Mitchell, S. (2022). Chapter 16 - A processing chain for estimating crop biophysical parameters using temporal Sentinel-1 synthetic aperture radar data in cloud computing framework. In P. K. Srivastava, D. K. Gupta, T. Islam, D. Han, & R. Prasad (Eds.), *Radar Remote Sensing* (pp. 309-325): Elsevier.

Martins, B. H., Suzuki, M., Yastika, P. E., & Shimizu, N. (2020). Ground Surface Deformation Detection in Complex Landslide Area—Bobonaro, Timor-Leste—Using SBAS DInSAR, UAV Photogrammetry, and Field Observations. *Geosciences*, 10(6).

- Martín-Velázquez, S., Rodríguez-Santalla, I., Roperó-Szymańska, N., Gomez-Ortiz, D., Martín-Crespo, T., & de Ignacio-San José, C. (2022). Geomorphological Mapping and Erosion of Abandoned Tailings in the Hiendelaencina Mining District (Spain) from Aerial Imagery and LiDAR Data. *Remote Sensing*, 14(18).
- Mathieu, R., Pouget, M., Cervelle, B., & Escadafal, R. (1998). Relationships between Satellite-Based Radiometric Indices Simulated Using Laboratory Reflectance Data and Typic Soil Color of an Arid Environment. *Remote Sensing of Environment*, 66(1), 17-28.
- Mohammadifar, A., Gholami, H., Comino, J. R., & Collins, A. L. (2021). Assessment of the interpretability of data mining for the spatial modelling of water erosion using game theory. *CATENA*, 200, 105178.
- Moreira, A., Prats-Iraola, P., Younis, M., Krieger, G., Hajnsek, I., & Papathanassiou, K. P. (2013). A tutorial on synthetic aperture radar. *IEEE Geoscience and Remote Sensing Magazine*, 1(1), 6-43.
- Nair, K. P. (2019). Soil Fertility and Nutrient Management. In K. P. Nair (Ed.), *Intelligent Soil Management for Sustainable Agriculture: The Nutrient Buffer Power Concept* (pp. 165-189). Cham: Springer International Publishing.
- Olivier, G., Van De Wiel, M. J., & De Clercq, W. P. (2023). Intersecting views of gully erosion in South Africa. *Earth Surface Processes and Landforms*, 48(1), 119-142.
- Peel, M. C., Finlayson, B. L., & McMahon, T. A. (2007). Updated world map of the Köppen-Geiger climate classification. *Hydrol. Earth Syst. Sci.*, 11(5), 1633-1644.
- Pereira, L. C., Balbinot, L., Matus, G. N., Dias, H. C. T., & Tonello, K. C. (2021). Aspects of forest restoration and hydrology: linking passive restoration and soil–water recovery in Brazilian Cerrado. *Journal of Forestry Research*, 32(6), 2301-2311.
- Právělie, R., Patriche, C., Borrelli, P., Panagos, P., Roșca, B., Dumitrașcu, M., . . . Bandoș, G. (2021). Arable lands under the pressure of multiple land degradation processes. A global perspective. *Environmental Research*, 194, 110697.
- Price, J. C. (1993). Estimating leaf area index from satellite data. *IEEE Transactions on Geoscience and Remote Sensing*, 31(3), 727-734.
- R Core Team, R. (2013). *R: A language and environment for statistical computing*. In: R foundation for statistical computing Vienna, Austria.
- Radočaj, D., Obhodaš, J., Jurišić, M., & Gašparović, M. (2020). Global Open Data Remote Sensing Satellite Missions for Land Monitoring and Conservation: A Review. *Land*, 9(11).
- Rodrigues, S. C. (2018). Some Practices of Gully Rehabilitation in Central Brazil. In J. C. Dagar & A. K. Singh (Eds.), *Ravine Lands: Greening for Livelihood and Environmental Security* (pp. 183-193). Singapore: Springer Singapore.
- Rossi, M., Torri, D., De Geeter, S., Cremer, C., & Poesen, J. (2022). Topographic thresholds for gully head formation in badlands. *Earth Surface Processes and Landforms*, 47(15), 3558-3587.
- Rouse, Jr. W., Haas, R. H., Schell, J. A., Deering, D. W., & Harlan, J. C. J. N. G. T. I. F. R., Greenbelt, Md. (1974). Monitoring the vernal advancement and retrogradation (green wave effect) of natural vegetation. 371.
- Roy, P., Chakraborty, R., Chowdhuri, I., Malik, S., Das, B., & Pal, S. C. (2020). Development of Different Machine Learning Ensemble Classifier for Gully Erosion Susceptibility in Gandheswari Watershed of West Bengal, India. In J. K. Rout, M. Rout, & H. Das (Eds.), *Machine Learning for Intelligent Decision Science* (pp. 1-26). Singapore: Springer Singapore.
- Santos, H. G. d., Tito, P. K., Anjos, L. H. C. d., Oliveira, V. A., Lumbreras, J. F., Coelho, M. R., . . . Solos, E. (2018). *Sistema brasileiro de classificação de solos*. Brasília, DF: Embrapa.
- Senanayake, S., Pradhan, B., Huete, A., & Brennan, J. (2020). A Review on Assessing and Mapping Soil Erosion Hazard Using Geo-Informatics Technology for Farming System Management. *Remote Sensing*, 12(24).
- Sepuru, T. K., & Dube, T. (2018). An appraisal on the progress of remote sensing applications

in soil erosion mapping and monitoring. *Remote Sensing Applications: Society and Environment*, 9, 1-9.

Sharma, A. (2010). Integrating terrain and vegetation indices for identifying potential soil erosion risk area. *Geo-spatial Information Science*, 13(3), 201-209.

Shellberg, J. G., Brooks, A. P., & Rose, C. W. (2013). Sediment production and yield from an alluvial gully in northern Queensland, Australia. *Earth Surface Processes and Landforms*, 38(15), 1765-1778.

Shruthi, R. B. V., Kerle, N., Jetten, V., Abdellah, L., & Machmach, I. (2015). Quantifying temporal changes in gully erosion areas with object oriented analysis. *CATENA*, 128, 262-277.

Souza, C. M., Z. Shimbo, J., Rosa, M. R., Parente, L. L., A. Alencar, A., Rudorff, B. F. T., . . . Azevedo, T. (2020). Reconstructing Three Decades of Land Use and Land Cover Changes in Brazilian Biomes with Landsat Archive and Earth Engine. 12(17), 2735.

Tebebu, T. Y., Abiy, A. Z., Zegeye, A. D., Dahlke, H. E., Easton, Z. M., Tilahun, S. A., . . . Steenhuis, T. S. (2010). Surface and subsurface flow effect on permanent gully formation and upland erosion near Lake Tana in the northern highlands of Ethiopia. *Hydrol. Earth Syst. Sci.*, 14(11), 2207-2217.

Tucker, C. J. (1979). Red and photographic infrared linear combinations for monitoring vegetation. *Remote Sensing of Environment*, 8(2), 127-150.

Thwaites, R. N., Brooks, A. P., Pietsch, T. J., & Spencer, J. R. (2022). What type of gully is that? The need for a classification of gullies. *Earth Surface Processes and Landforms*, 47(1), 109-128.

Vallejo Orti, M., Winiwarter, L., Corral-Pazos-de-Provens, E., Williams, J. G., Bubenzer, O., & Höfle, B. (2021). Use of TanDEM-X and Sentinel Products to Derive Gully Activity Maps in Kunene Region (Namibia) Based on Automatic Iterative Random Forest Approach. *IEEE Journal of Selected Topics in Applied Earth Observations and Remote Sensing*, 14, 607-623.

Valentin, C., Poesen, J., & Li, Y. (2005). Gully erosion: Impacts, factors and control. *CATENA*, 63(2), 132-153.

Vanmaercke, M., Panagos, P., Vanwalleghem, T., Hayas, A., Foerster, S., Borrelli, P., . . . Poesen, J. (2021). Measuring, modelling and managing gully erosion at large scales: A state of the art. *Earth-Science Reviews*, 218, 103637.

Wagner, F. H., Dalagnol, R., Silva-Junior, C. H. L., Carter, G., Ritz, A. L., Hirye, M. C. M., . . . Saatchi, S. (2023). Mapping Tropical Forest Cover and Deforestation with Planet NICFI Satellite Images and Deep Learning in Mato Grosso State (Brazil) from 2015 to 2021. *Remote Sensing*, 15(2).

Wang, N., Luo, J., He, S., Li, T., Zhao, Y., Zhang, X., . . . Zheng, Z. (2023). Characterizing the rill erosion process from eroded morphology and sediment connectivity on purple soil slope with upslope earthen dike terraces. *Science of The Total Environment*, 860, 160486.

Wilson, J. P., & Gallant, J. C. (2000). Digital Terrain Analysis. In *Terrain Analysis: Principles and Applications* (Vol. 6, pp. 1-27).

Xie, H., Zhang, Y., Wu, Z., & Lv, T. (2020). A Bibliometric Analysis on Land Degradation: Current Status, Development, and Future Directions. *Land*, 9(1).

Xu, H.-Q. (2005). A study on information extraction of water body with the modified normalized difference water index (MNDWI). *Journal of Remote Sensing*, 5, 589-595.

Yang, Q., Zhu, M., Wang, C., Zhang, X., Liu, B., Wei, X., . . . Yang, L. (2020). Study on a soil erosion sampling survey in the Pan-Third Pole region based on higher-resolution images. *International Soil and Water Conservation Research*, 8(4), 440-451.

Yang, A., Wang, C., Yang, Q., Pang, G., Long, Y., Wang, L., . . . Cruse, R. M. (2022). Choosing the Right Horizontal Resolution for Gully Erosion Susceptibility Mapping Using Machine Learning Algorithms: A Case in Highly Complex Terrain. *Remote Sensing*, 14(11).

Yibeltal, M., Tsunekawa, A., Haregeweyn, N., Adgo, E., Meshesha, D. T., Masunaga, T., . . . Liyew Berihun, M. (2021). Effect of subsurface water level on gully headcut retreat in tropical highlands of Ethiopia. *Earth Surface Processes and Landforms*, 46(6), 1209-1222.

- Zhao, H., Fang, X., Ding, H., Josef, S., Xiong, L., Na, J., & Tang, G. (2017). Extraction of Terraces on the Loess Plateau from High-Resolution DEMs and Imagery Utilizing Object-Based Image Analysis. *ISPRS International Journal of Geo-Information*, 6(6).
- Zhao, L., & Hou, R. (2019). Human causes of soil loss in rural karst environments: a case study of Guizhou, China. *Scientific Reports*, 9(1), 1-11. doi:10.1038/s41598-018-35808-3.
- Zhou, X., Wei, Y., He, J., & Cai, C. (2023). Estimation of gully erosion rate and its determinants in a granite area of southeast China. *Geoderma*, 429, 116223.
- Zuazo, V. c. H. D., & Pleguezuelo, C. R. o. R. (2009). Soil-Erosion and Runoff Prevention by Plant Covers: A Review. In E. Lichtfouse, M. Navarrete, P. Debaeke, S. Véronique, & C. Alberola (Eds.), *Sustainable Agriculture* (pp. 785-811). Dordrecht: Springer Netherlands.

Chapter 3

- Abbasi, N. A., Xu, X., Lucas-Borja, M. E., Dang, W., & Liu, B. (2019). The use of check dams in watershed management projects: Examples from around the world. *Science of The Total Environment*, 676, 683-691.
- Alencar, A. A. C., Arruda, V. L. S., Silva, W. V., Conciani, D. E., Costa, D. P., Crusco, N., . . . Véléz-Martin, E. (2022). Long-Term Landsat-Based Monthly Burned Area Dataset for the Brazilian Biomes Using Deep Learning. *Remote Sensing*, 14(11).
- Amaral, A. G., Bijos, N. R., Moser, P., & Munhoz, C. B. R. (2022). Spatially structured soil properties and climate explain distribution patterns of herbaceous shrub species in the Cerrado. *Plant Ecology*, 223(1), 85-97.
- Anderson, R. L., Rowntree, K. M., & Le Roux, J. J. (2021). An interrogation of research on the influence of rainfall on gully erosion. *CATENA*, 206, 105482.
- Arabameri, A., Cerda, A., & Tiefenbacher, J. P. (2019). Spatial Pattern Analysis and Prediction of Gully Erosion Using Novel Hybrid Model of Entropy-Weight of Evidence. *Water*, 11(6).
- Arabameri, A., Chandra Pal, S., Costache, R., Saha, A., Rezaie, F., Seyed Danesh, A., . . . Hoang, N.-D. (2021). Prediction of gully erosion susceptibility mapping using novel ensemble machine learning algorithms. *Geomatics, Natural Hazards and Risk*, 12(1), 469-498.
- Assine, M. L. (2005). River avulsions on the Taquari megafan, Pantanal wetland, Brazil. *Geomorphology*, 70(3), 357-371.
- Avand, M., Janizadeh, S., Naghibi, S. A., Pourghasemi, H. R., Khosrobeigi Bozchaloei, S., & Blaschke, T. (2019). A Comparative Assessment of Random Forest and k-Nearest Neighbor Classifiers for Gully Erosion Susceptibility Mapping. *Water*, 11(10).
- Azevedo, A. A., Rajão, R., Costa, M. A., Stabile, M. C. C., Macedo, M. N., dos Reis, T. N. P., . . . Pacheco, R. (2017). Limits of Brazil's Forest Code as a means to end illegal deforestation. *Proceedings of the National Academy of Sciences*, 114(29), 7653-7658.
- Bachri, I., Hakdaoui, M., Raji, M., Teodoro, A. C., & Benbouziane, A. (2019). Machine Learning Algorithms for Automatic Lithological Mapping Using Remote Sensing Data: A Case Study from Souk Arbaa Sahel, Sidi Ifni Inlier, Western Anti-Atlas, Morocco. 8(6), 248.
- Bannari, A., Morin, D., Bonn, F., & Huete, A. R. (1995). A review of vegetation indices. *Remote Sensing Reviews*, 13(1-2), 95-120.
- Barbosa, F. R. G. M., Duarte, V. N., Staduto, J. A. R., & Kreter, A. C. (2023). Land-Use Dynamics for Agricultural and Livestock in Central-West Brazil and its Reflects on the Agricultural Frontier Expansion. *Cleaner and Circular Bioeconomy*, 4, 100033.
- Barron, V., & Torrent, J. (1986). Use of the Kubelka—Munk theory to study the influence of iron oxides on soil colour. *Journal of Soil Science*, 37(4), 499-510.
- Bell, W. D., Hoffman, M. T., & Visser, V. (2021). Regional land degradation assessment for dryland environments: The Namaqualand Hardeveld bioregion of the Succulent Karoo biome as a case-study. *Land Degradation & Development*, 32(7), 2287-2302. doi:10.1002/ldr.3900.
- Bergier, I., Assine, M. L., McGlue, M. M., Alho, C. J. R., Silva, A., Guerreiro, R. L., & Carvalho, J. C. (2018). Amazon rainforest modulation of water security in the Pantanal

wetland. *Science of The Total Environment*, 619-620, 1116-1125.

Bezerra, M. O., Baker, M., Palmer, M. A., & Filoso, S. (2020). Gully formation in headwater catchments under sugarcane agriculture in Brazil. *Journal of Environmental Management*, 270, 110271.

Blanco, H., & Lal, R. (2008). *Principles of soil conservation and management* (Vol. 167169): Springer New York.

Bonanomi, J., Tortato, F. R., Gomes, R. d. S. R., Penha, J. M., Bueno, A. S., & Peres, C. A. (2019). Protecting forests at the expense of native grasslands: Land-use policy encourages open-habitat loss in the Brazilian cerrado biome. *Perspectives in Ecology and Conservation*, 17(1), 26-31.

Borja, P., Molina, A., Govers, G., & Vanacker, V. (2018). Check dams and afforestation reducing sediment mobilization in active gully systems in the Andean mountains. *CATENA*, 165, 42-53.

Brancalion, P. H. S., Garcia, L. C., Loyola, R., Rodrigues, R. R., Pillar, V. D., & Lewinsohn, T. M. (2016). A critical analysis of the Native Vegetation Protection Law of Brazil (2012): updates and ongoing initiatives. *Natureza & Conservação*, 14, 1-15.

Breiman, L. (2001). Random Forests. *Machine Learning*, 45(1), 5-32.

Cabral, T. L., Nummer, A. V., & Bateira, C. (2020). Indicadores morfométricos como suporte para a classificação de voçorocas em sub-bacias hidrográficas no Município de Cacequi, RS. *Revista Brasileira de Geomorfologia*, v. 21, nº 1, 139-154.

Cabral, A. I. R., Laques, A. E., & Saito, C. H. (2022). Assessment of the effect of landowner type on deforestation in the Brazilian Legal Amazon using remote sensing data. *Environmental Conservation*, 49(4), 225-233.

Castillo, C., & Gómez, J. A. (2016). A century of gully erosion research: Urgency, complexity and study approaches. *Earth-Science Reviews*, 160, 300-319.

Chowdhuri, I., Pal, S. C., Arabameri, A., Saha, A., Chakraborty, R., Blaschke, T., . . . Band, S. S. (2020). Implementation of Artificial Intelligence Based Ensemble Models for Gully Erosion Susceptibility Assessment. *Remote Sensing*, 12(21).

Chuma, G. B., Mugumaarhahama, Y., Mond, J. M., Bagula, E. M., Ndeko, A. B., Lucungu, P. B., . . . Schmitz, S. (2023). Gully erosion susceptibility mapping using four machine learning methods in Luzinzi watershed, eastern Democratic Republic of Congo. *Physics and Chemistry of the Earth, Parts A/B/C*, 129, 103295.

Coelho-Junior, M. G., Valdiones, A. P., Shimbo, J. Z., Silgueiro, V., Rosa, M., Marques, C. D. L., . . . Azevedo, T. (2022). Unmasking the impunity of illegal deforestation in the Brazilian Amazon: a call for enforcement and accountability. *Environmental Research Letters*, 17(4), 041001.

Crist, E. P., & Cicone, R. C. (1984). A Physically-Based Transformation of Thematic Mapper Data---The TM Tasseled Cap. *Geoscience and Remote Sensing, IEEE Transactions on*, GE-22(3), 256-263.

Cui, H., Wang, Z., Yan, H., Li, C., Jiang, X., Wang, L., . . . Shi, Z. (2022). Production-Based and Consumption-Based Accounting of Global Cropland Soil Erosion. *Environmental Science & Technology*, 56(14), 10465-10473.

Daley, J., Stout, J., Curwen, G., Brooks, A., Spencer, J., Pietsch, T., . . . Rainforest Research Centre Limited, C. (2021). Development and application of automated tools for high resolution gully mapping and classification from lidar data. Report to the National Environmental Science Program: Reef Rainforest Research Centre Limited, Cairns.

de Souza, G. F., Almeida, R. F., Bijos, N. R., Fagg, C. W., & Munhoz, C. B. R. (2021). Herbaceous-shrub species composition, diversity and soil attributes in moist grassland, shrub grassland and savanna in Central Brazil. *Brazilian Journal of Botany*, 44(1), 227-238.

Diniz, J. M. F. d. S., Gama, F. F., & Adami, M. (2020). Evaluation of polarimetry and interferometry of sentinel-1A SAR data for land use and land cover of the Brazilian Amazon

- Region. Geocarto International, 1-19.
- Domlija, P., Bernat Gazibara, S., Arbanas, Ž., & Mihalić Arbanas, S. (2019). Identification and Mapping of Soil Erosion Processes Using the Visual Interpretation of LiDAR Imagery. *ISPRS International Journal of Geo-Information*, 8(10).
- Dube, H. B., Mutema, M., Muchaonyerwa, P., Poesen, J., & Chaplot, V. (2020). A global analysis of the morphology of linear erosion features. *CATENA*, 190, 104542.
- Gafurov, A. M., & Yermolayev, O. P. (2020). Automatic gully detection: Neural networks and computer vision. *Remote Sensing*, 12(11), 1743.
- Galdino, S., Vieira, L. M., & Pellegrin, L. A. (2005). *Impactos ambientais e socioeconômicos na Bacia do Rio Taquari-Pantanal: Corumbá: Embrapa Pantanal*, 2005.
- Gao, B. (1996). NDWI—A normalized difference water index for remote sensing of vegetation liquid water from space. *Remote Sensing of Environment*, 58(3), 257-266.
- Guerra, A. J. T., Fullen, M. A., Bezerra, J. F. R., & Jorge, M. d. C. O. (2018). Gully Erosion and Land Degradation in Brazil: A Case Study from São Luís Municipality, Maranhão State. In J. C. Dagar & A. K. Singh (Eds.), *Ravine Lands: Greening for Livelihood and Environmental Security* (pp. 195-216). Singapore: Springer Singapore.
- Haralick, R. M., Shanmugam, K., & Dinstein, I. (1973). Textural Features for Image Classification. *IEEE Transactions on Systems, Man, and Cybernetics*, SMC-3(6), 610-621.
- Heilmayr, R., Rausch, L. L., Munger, J., & Gibbs, H. K. (2020). Brazil's Amazon Soy Moratorium reduced deforestation. *Nature Food*, 1(12), 801-810.
- Hitouri, S., Varasano, A., Mohajane, M., Ijlil, S., Essahlaoui, N., Ali, S. A., . . . Teodoro, A. C. (2022). Hybrid Machine Learning Approach for Gully Erosion Mapping Susceptibility at a Watershed Scale. *ISPRS International Journal of Geo-Information*, 11(7).
- Hofmann, G. S., Cardoso, M. F., Alves, R. J. V., Weber, E. J., Barbosa, A. A., de Toledo, P. M., . . . de Oliveira, L. F. B. (2021). The Brazilian Cerrado is becoming hotter and drier. *Global Change Biology*, 27(17), 4060-4073.
- Hunke, P., Roller, R., Zeilhofer, P., Schröder, B., & Mueller, E. N. (2015). Soil changes under different land-uses in the Cerrado of Mato Grosso, Brazil. *Geoderma Regional*, 4, 31-43.
- Issaka, S., & Ashraf, M. A. (2017). Impact of soil erosion and degradation on water quality: a review. *Geology, Ecology, and Landscapes*, 1(1), 1-11.
- Jesuz, C. R. d., Ito, J. B. B., & Zeilhofer, P. (2013). Erosões mecânicas na bacia hidrográfica do rio Tenente Amaral, Jaciara—MT, e suas determinantes socioambientais. *Revista Mato-Grossense de Geografia*, 16(01).
- Jung, S., Rasmussen, L. V., Watkins, C., Newton, P., & Agrawal, A. (2017). Brazil's National Environmental Registry of Rural Properties: Implications for Livelihoods. *Ecological Economics*, 136, 53-61.
- Kallel, A., Le Hégarat-Masclé, S., Ottlé, C., & Hubert-Moy, L. (2007). Determination of vegetation cover fraction by inversion of a four-parameter model based on isoline parametrization. *Remote Sensing of Environment*, 111(4), 553-566.
- Karydas, C., & Panagos, P. (2020). Towards an Assessment of the Ephemeral Gully Erosion Potential in Greece Using Google Earth. *Water*, 12(2).
- Keesstra, S., Mol, G., De Leeuw, J., Okx, J., Molenaar, C., De Cleen, M., & Visser, S. (2018). Soil-Related Sustainable Development Goals: Four Concepts to Make Land Degradation Neutrality and Restoration Work. *Land*, 7(4).
- Kemp, D. B., Sadler, P. M., & Vanacker, V. (2020). The human impact on North American erosion, sediment transfer, and storage in a geologic context. *Nature Communications*, 11(1), 6012.
- Lepsch, I. F. (2016). *Formação e conservação dos solos: Oficina de textos*.
- Li, L., Mu, X., Jiang, H., Chianucci, F., Hu, R., Song, W., . . . Yan, G. (2023). Review of ground and aerial methods for vegetation cover fraction (fCover) and related quantities estimation: definitions, advances, challenges, and future perspectives. *ISPRS Journal of*

Photogrammetry and Remote Sensing, 199, 133-156. Liu, G., Zheng, F., Wilson, G. V., Xu, X., & Liu, C. (2021). Three decades of ephemeral gully erosion studies. *Soil and Tillage Research*, 212, 105046.

Louzada, R. O., Bergier, I., Roque, F. O., McGlue, M. M., Silva, A., & Assine, M. L. (2021). Avulsions drive ecosystem services and economic changes in the Brazilian Pantanal wetlands. *Current Research in Environmental Sustainability*, 3, 100057.

Louzada, R. O., Bergier, I., Diniz, J. M. F. d. S., Guerra, A., & Roque, F. d. O. (2022). Priority setting for restoration in surrounding savannic areas of the Brazilian Pantanal based on soil loss risk and agrarian structure. *Journal of Environmental Management*, 323, 116219.

Louzada, R. O., Reis, L. K., Diniz, J. M. F. d. S., Roque, F. d. O., Gama, F. F., & Bergier, I. (2023a). Combining optical and microwave remote sensing for assessing gullies in human-disturbed vegetated landscapes. *CATENA*, 228, 107127.

Louzada, R. O., Roque, F. d. O., Diniz, J. M. F. d. S., & Bergier, I. (2023b). River channel avulsion in the Taquari River megafan of the Brazilian Pantanal: Remote sensing and modeling reveal recent and future changes. *Applied Geography*, 155, 102955.

Marengo, J. A., Oliveira, G. S., & Alves, L. M. (2015). Climate change scenarios in the Pantanal. In *Dynamics of the pantanal wetland in South America* (pp. 227-238): Springer.

Meinen, B. U., & Robinson, D. T. (2021). Agricultural erosion modelling: Evaluating USLE and WEPP field-scale erosion estimates using UAV time-series data. *Environmental Modelling & Software*, 137, 104962.

Merten, G. H., & Minella, J. P. G. (2013). The expansion of Brazilian agriculture: Soil erosion scenarios. *International Soil and Water Conservation Research*, 1(3), 37-48.

Mudereri, B. T., Chitata, T., Mukanga, C., Mupfiga, E. T., Gwahirisa, C., & Dube, T. (2021). Can biophysical parameters derived from Sentinel-2 space-borne sensor improve land cover characterisation in semi-arid regions? *Geocarto International*, 36(19), 2204-2223.

Na, J., Yang, X., Tang, G., Dang, W., & Strobl, J. (2020). Population Characteristics of Loess Gully System in the Loess Plateau of China. *Remote Sensing*, 12(16).

Niculită, M., Mărgărint, M. C., & Tarolli, P. (2020). Chapter 10 - Using UAV and LiDAR data for gully geomorphic changes monitoring. In P. Tarolli & S. M. Mudd (Eds.), *Developments in Earth Surface Processes* (Vol. 23, pp. 271-315): Elsevier.

Novara, A., Cerda, A., Barone, E., & Gristina, L. (2021). Cover crop management and water conservation in vineyard and olive orchards. *Soil and Tillage Research*, 208, 104896.

Perosa, B., Newton, P., & da Silva, R. F. B. (2023). A monitoring, reporting and verification system for low carbon agriculture: A case study from Brazil. *Environmental Science & Policy*, 140, 286-296.

Phinzi, K., Holb, I., & Szabó, S. (2021). Mapping Permanent Gullies in an Agricultural Area Using Satellite Images: Efficacy of Machine Learning Algorithms. *Agronomy*, 11(2).

Poesen, J., Nachtergaele, J., Verstraeten, G., & Valentin, C. (2003). Gully erosion and environmental change: importance and research needs. *CATENA*, 50(2), 91-133.

Powlson, D. S., Gregory, P. J., Whalley, W. R., Quinton, J. N., Hopkins, D. W., Whitmore, A. P., . . . Goulding, K. W. T. (2011). Soil management in relation to sustainable agriculture and ecosystem services. *Food Policy*, 36, S72-S87.

Quintero-Angel, M., & Ospina-Salazar, D. I. (2023). Agricultural Soil Degradation in Colombia. In P. Pereira, M. Muñoz-Rojas, I. Bogunovic, & W. Zhao (Eds.), *Impact of Agriculture on Soil Degradation I: Perspectives from Africa, Asia, America and Oceania* (pp. 177-218). Cham: Springer International Publishing.

R Core Team, R. (2013). *R: A language and environment for statistical computing*. In: R foundation for statistical computing Vienna, Austria.

Rahmati, O., Kalantari, Z., Ferreira, C. S., Chen, W., Soleimanpour, S. M., Kapović-Solomon, M., . . . Kazemi Kazemabady, N. (2022). Contribution of physical and anthropogenic factors to gully erosion initiation. *CATENA*, 210, 105925.

- Rajão, R., Soares-Filho, B., Nunes, F., Börner, J., Machado, L., Assis, D., . . . Figueira, D. (2020). The rotten apples of Brazil's agribusiness. *Science*, 369(6501), 246-248. Real, L. S. C., Crestana, S., Ferreira, R. R. M., Sígolo, J. B., & Rodrigues, V. G. S. (2020). Proposition for a new classification of gully erosion using multifractal and lacunarity analysis: A complex of gullies in the Palmital stream watershed, Minas Gerais (Brazil). *CATENA*, 186, 104377.
- Roberts, D., Wilford, J., & Ghattas, O. (2019). Exposed soil and mineral map of the Australian continent revealing the land at its barest. *Nature Communications*, 10(1), 5297.
- Rondeaux, G., Steven, M., & Baret, F. (1996). Optimization of soil-adjusted vegetation indices. *Remote Sensing of Environment*, 55(2), 95-107.
- Roque, F. d. O., Guerra, A., Johnson, M., Padovani, C., Corbi, J., Covich, A. P., . . . Yon, L. (2021). Simulating land use changes, sediment yields, and pesticide use in the Upper Paraguay River Basin: Implications for conservation of the Pantanal wetland. *Agriculture, Ecosystems & Environment*, 314, 107405.
- Rouse, Jr. W., Haas, R. H., Schell, J. A., Deering, D. W., & Harlan, J. C. J. N. G. T. I. F. R., Greenbelt, Md. (1974). Monitoring the vernal advancement and retrogradation (green wave effect) of natural vegetation. 371.
- Santos, C. O., Mesquita, V. V., Parente, L. L., Pinto, A. D., & Ferreira, L. G. (2022). Assessing the Wall-to-Wall Spatial and Qualitative Dynamics of the Brazilian Pasturelands 2010–2018, Based on the Analysis of the Landsat Data Archive. *Remote Sensing*, 14(4).
- Sepuru, T. K., & Dube, T. (2018). An appraisal on the progress of remote sensing applications in soil erosion mapping and monitoring. *Remote Sensing Applications: Society and Environment*, 9, 1-9.
- Soares da Silva, A., Seliger, R., Sattler, D., & Heinrich, J. (2019). Soil Degradation in Southeast Brazil: A Challenge for Restoration and Rehabilitation. In U. Nehren, S. Schlüter, C. Raedig, D. Sattler, & H. Hissa (Eds.), *Strategies and Tools for a Sustainable Rural Rio de Janeiro* (pp. 377-389). Cham: Springer International Publishing.
- Soufi, M., Bayat, R., & Charkhabi, A. H. (2020). Gully Erosion in I. R. Iran: Characteristics, Processes, Causes, and Land Use. In P. K. Shit, H. R. Pourghasemi, & G. S. Bhunia (Eds.), *Gully Erosion Studies from India and Surrounding Regions* (pp. 357-368). Cham: Springer International Publishing.
- Souza, C. M., Z. Shimbo, J., Rosa, M. R., Parente, L. L., A. Alencar, A., Rudorff, B. F. T., . . . Azevedo, T. (2020). Reconstructing Three Decades of Land Use and Land Cover Changes in Brazilian Biomes with Landsat Archive and Earth Engine. 12(17), 2735.
- Thwaites, R. N., Brooks, A. P., Pietsch, T. J., & Spencer, J. R. (2022). What type of gully is that? The need for a classification of gullies. *Earth Surface Processes and Landforms*, 47(1), 109-128.
- Thielen, D., Schuchmann, K.-L., Ramoni-Perazzi, P., Marquez, M., Rojas, W., Quintero, J. I., & Marques, M. I. (2020). Quo vadis Pantanal? Expected precipitation extremes and drought dynamics from changing sea surface temperature. *Plos One*, 15(1), e0227437.
- Utsumi, A. G., Pissarra, T. C. T., Rosalen, D. L., Martins Filho, M. V., & Rotta, L. H. S. (2020). Gully mapping using geographic object-based image analysis: A case study at catchment scale in the Brazilian Cerrado. *Remote Sensing Applications: Society and Environment*, 20, 100399.
- van der Waal, B., & Rowntree, K. (2018). Landscape Connectivity in the Upper Mzimvubu River Catchment: An Assessment of Anthropogenic Influences on Sediment Connectivity. *Land Degradation & Development*, 29(3), 713-723.
- Vanacker, V., Ameijeiras-Mariño, Y., Schoonejans, J., Cornélis, J.-T., Minella, J. P. G., Lamouline, F., . . . Opfergelt, S. (2019). Land use impacts on soil erosion and rejuvenation in Southern Brazil. *CATENA*, 178, 256-266.
- Vanacker, V., Molina, A., Rosas, M. A., Bonnesoeur, V., Román-Dañobeytia, F., Ochoa-Tocachi, B. F., & Buytaert, W. (2022). The effect of natural infrastructure on water erosion

- mitigation in the Andes. *SOIL*, 8(1), 133-147.
- Vanmaercke, M., Chen, Y., De Geeter, S., Poesen, J., & Campforts, B. (2020). A first data-driven gully head density map of the world. Paper presented at the EGU General Assembly Conference Abstracts.
- Vanmaercke, M., Panagos, P., Vanwalleghem, T., Hayas, A., Foerster, S., Borrelli, P., . . . Poesen, J. (2021). Measuring, modelling and managing gully erosion at large scales: A state of the art. *Earth-Science Reviews*, 218, 103637.
- Vieira, R. M. d. S. P., Tomasella, J., Barbosa, A. A., Polizel, S. P., Ometto, J. P. H. B., Santos, F. C., . . . Toledo, P. M. d. (2021). Land degradation mapping in the MATOPIBA region (Brazil) using remote sensing data and decision-tree analysis. *Science of The Total Environment*, 782, 146900.
- Vieira, R. M., Tomasella, J., Cunha, A. P., Barbosa, A. A., Pompeu, J., Ferreira, Y., . . . Ometto, J. (2023). Socio-Environmental Vulnerability to Drought Conditions and Land Degradation: An Assessment in Two Northeastern Brazilian River Basins. *Sustainability*, 15(10).
- Vrieling, A., Rodrigues, S. C., Bartholomeus, H., & Sterk, G. (2007). Automatic identification of erosion gullies with ASTER imagery in the Brazilian Cerrados. *International Journal of Remote Sensing*, 28(12), 2723-2738.
- Vrieling, A., de Jong, S. M., Sterk, G., & Rodrigues, S. C. (2008). Timing of erosion and satellite data: A multi-resolution approach to soil erosion risk mapping. *International Journal of Applied Earth Observation and Geoinformation*, 10(3), 267-281.
- Wei, Y., Liu, Z., Wu, X., Zhang, Y., Cui, T., Cai, C., . . . Cheng, D. (2021). Can Benggang be regarded as gully erosion? *CATENA*, 207, 105648.
- Wilson, J. P., & Gallant, J. C. (2000). Digital Terrain Analysis. In *Terrain Analysis: Principles and Applications* (Vol. 6, pp. 1-27).
- Xu, H.-Q. (2005). A study on information extraction of water body with the modified normalized difference water index (MNDWI). *Journal of Remote Sensing*, 5, 589-595.
- Yang, S., Guan, Y., Zhao, C., Zhang, C., Bai, J., & Chen, K. (2019). Determining the influence of catchment area on intensity of gully erosion using high-resolution aerial imagery: A 40-year case study from the Loess Plateau, northern China. *Geoderma*, 347, 90-102.
- Youssef, A. M., Mahdi, A. M., Al-Katheri, M. M., Pouyan, S., & Pourghasemi, H. R. (2023). Multi-hazards (landslides, floods, and gully erosion) modeling and mapping using machine learning algorithms. *Journal of African Earth Sciences*, 197, 104788.
- Yu, S.-Y., Li, W.-J., Zhou, L., Yu, X., Zhang, Q., & Shen, Z. (2023). Human disturbances dominated the unprecedentedly high frequency of Yellow River flood over the last millennium. *Science Advances*, 9(8), eadf8576.
- Zhang, Y., Zhao, Y., Liu, B., Wang, Z., & Zhang, S. (2019). Rill and gully erosion on unpaved roads under heavy rainfall in agricultural watersheds on China's Loess Plateau. *Agriculture, Ecosystems & Environment*, 284, 106580.
- Žižala, D., Juřicová, A., Zádorová, T., Zelenková, K., & Minařík, R. (2019). Mapping soil degradation using remote sensing data and ancillary data: South-East Moravia, Czech Republic. *European Journal of Remote Sensing*, 52(sup1), 108-122.

Chapter 4

- AbdelRahman, M. A. E. (2023). An overview of land degradation, desertification and sustainable land management using GIS and remote sensing applications. *Rendiconti Lincei. Scienze Fisiche e Naturali*, 34(3), 767-808. doi:10.1007/s12210-023-01155-3.
- Adla, K., Dejan, K., Neira, D., & Dragana, Š. (2022). Chapter 9 - Degradation of ecosystems and loss of ecosystem services. In J. C. Prata, A. I. Ribeiro, & T. Rocha-Santos (Eds.), *One Health* (pp. 281-327): Academic Press.
- Anthony, T., & Emmanuel, A. (2025). Geomodeling soil quality using remote sensing and land

- use metrics in Abeokuta, Nigeria. *Discover Geoscience*, 3(1), 3. doi:10.1007/s44288-025-00112-x.
- Arystanov, A., Karabkina, N., Sagin, J., Nurguzhin, M., King, R., & Bekseitova, R. (2024). Use of Indices Applied to Remote Sensing for Establishing Winter–Spring Cropping Areas in the Republic of Kazakhstan. *Sustainability*, 16(17). doi:10.3390/su16177548.
- Assine, M. L. (2005). River avulsions on the Taquari megafan, Pantanal wetland, Brazil. *Geomorphology*, 70(3), 357-371. doi:10.1016/j.geomorph.2005.02.013.
- Azabdaftari, A., & Sunar, F. (2016). SOIL SALINITY MAPPING USING MULTITEMPORAL LANDSAT DATA. *Int. Arch. Photogramm. Remote Sens. Spatial Inf. Sci.*, XLI-B7, 3-9. doi:10.5194/isprs-archives-XLI-B7-3-2016.
- Bahddou, S., Otten, W., Whalley, W. R., Shin, H.-C., El Gharous, M., & Rickson, R. J. (2023). Changes in soil surface properties under simulated rainfall and the effect of surface roughness on runoff, infiltration and soil loss. *Geoderma*, 431, 116341. doi:10.1016/j.geoderma.2023.116341.
- Bannari, A., Morin, D., Bonn, F., & Huete, A. R. (1995). A review of vegetation indices. *Remote Sensing Reviews*, 13(1-2), 95-120. doi:10.1080/02757259509532298.
- Baret, F., & Guyot, G. (1991). Potentials and limits of vegetation indices for LAI and APAR assessment. *Remote Sensing of Environment*, 35(2), 161-173. doi:10.1016/0034-4257(91)90009-U.
- Barreto, M. S. C., Ramlogan, M., Oliveira, D. M. S., Verburg, E. E. J., Elzinga, E. J., Rouff, A. A., . . . Alleoni, L. R. F. (2021). Thermal stability of soil organic carbon after long-term manure application across land uses and tillage systems in an oxisol. *CATENA*, 200, 105164. doi:10.1016/j.catena.2021.105164.
- Basset, C., Abou Najm, M., Ghezzehei, T., Hao, X., & Daccache, A. (2023). How does soil structure affect water infiltration? A meta-data systematic review. *Soil and Tillage Research*, 226, 105577. doi:10.1016/j.still.2022.105577.
- Capitani, D. H. D., & Gaio, L. E. (2024). Dynamic connectedness and volatility spillover in the Brazilian agricultural market in the context of the Covid-19 pandemic. *Estudos Econômicos*, 54(04), e53575446. doi:10.1590/1980-53575446dclg.
- Chaves, M. E. D., Picoli, M. C. A., & Sanches, I. D. (2020). Recent Applications of Landsat 8/OLI and Sentinel-2/MSI for Land Use and Land Cover Mapping: A Systematic Review. *Remote Sensing*, 12(18). doi:10.3390/rs12183062.
- Colombi, G., Martani, E., & Fornara, D. (2025). Regenerative organic agriculture and soil ecosystem service delivery: A literature review. *Ecosystem Services*, 73, 101721. doi:10.1016/j.ecoser.2025.101721.
- Dawson, J. J. C., & Smith, P. (2007). Carbon losses from soil and its consequences for land-use management. *Science of The Total Environment*, 382(2), 165-190. doi:10.1016/j.scitotenv.2007.03.023.
- Diek, S., Fornallaz, F., Schaepman, M. E., & De Jong, R. (2017). Barest Pixel Composite for Agricultural Areas Using Landsat Time Series. *Remote Sensing*, 9(12). doi:10.3390/rs9121245.
- Farooq, O., Imran, M., Awan, M. I., Sarwar, N., Mubeen, K., Ahmed, M., & Ahmad, S. (2023). Causes of Soil Erosion, Its Measurements, and Management. In M. Ahmed & S. Ahmad (Eds.), *Disaster Risk Reduction in Agriculture* (pp. 211-232). Singapore: Springer Nature Singapore.
- Feng, S., Zhao, W., Zhan, T., Yan, Y., & Pereira, P. (2022). Land degradation neutrality: A review of progress and perspectives. *Ecological Indicators*, 144, 109530. doi:10.1016/j.ecolind.2022.109530.
- Galdino, S., Vieira, L. M., & Pellegrin, L. A. (2005). Impactos ambientais e socioeconômicos na Bacia do Rio Taquari-Pantanal: Corumbá: Embrapa Pantanal, 2005.
- Garcia, A. S., & Ballester, M. V. R. (2016). Land cover and land use changes in a Brazilian Cerrado landscape: drivers, processes, and patterns. *Journal of Land Use Science*, 11(5), 538-559. doi:10.1080/1747423X.2016.1182221.
- Getahun, S., Kefale, H., & Gelaye, Y. (2024). Application of Precision Agriculture Technologies

- for Sustainable Crop Production and Environmental Sustainability: A Systematic Review. *The Scientific World Journal*, 2024(1), 2126734. doi:10.1155/2024/2126734.
- Gomiero, T. (2016). Soil Degradation, Land Scarcity and Food Security: Reviewing a Complex Challenge. *Sustainability*, 8(3). doi:10.3390/su8030281.
- He, S., Zhang, C., Meng, F.-R., Bourque, C. P. A., Huang, Z., Li, X., . . . Liu, C. (2024). Vegetation-cover control of between-site soil temperature evolution in a sandy desertland. *Science of The Total Environment*, 908, 168372. doi:10.1016/j.scitotenv.2023.168372.
- Hemati, M., Hasanlou, M., Mahdianpari, M., & Mohammadimanesh, F. (2021). A Systematic Review of Landsat Data for Change Detection Applications: 50 Years of Monitoring the Earth. *Remote Sensing*, 13(15). doi:10.3390/rs13152869.
- Huete, A. R. (1988). A soil-adjusted vegetation index (SAVI). *Remote Sensing of Environment*, 25(3), 295-309. doi:10.1016/0034-4257(88)90106-X.
- Ide, C. N., Gonçalves, F. V., Latoria, G., Val, H. C., Silva, J. B., Steffen, J. L., . . . Broch, S. A. (2016). Soil and water conservation in the Upper Paraguay River Basin: examples from Mato Grosso do Sul, Brazil. In *Tropical Wetland Management* (pp. 99-133): Routledge.
- Jamali, S., Jönsson, P., Eklundh, L., Ardö, J., & Seaquist, J. (2015). Detecting changes in vegetation trends using time series segmentation. *Remote Sensing of Environment*, 156, 182-195. doi:10.1016/j.rse.2014.09.010.
- Jiang, N., Dou, C., Tang, Y., Galdies, C., Yan, L., & Ding, H. (2024). Derivation of tasseled cap transformation coefficients for SDGSAT-1 Multispectral Imager at-sensor reflectance data. *International Journal of Digital Earth*, 17(1), 2413885. doi:10.1080/17538947.2024.2413885.
- Key, C.H.; Benson, N.C. (2006). Landscape Assessment (LA): Sampling and Analysis Methods. In *Firemon: Fire Effects Monitoring and Inventory System*; Lutes, D., Keane, R.E., Caratti, J.F., Key, C.H., Benson, N.C., Sutherland, S., Gangi, L., Eds.; RMRS-GTR-164; Rocky Mountain Research Station, US Department of Agriculture, Forest Service: Fort Collins, CO, USA. pp. LA-1-LA-51.
- Kirschbaum, M. U. F. (1995). The temperature dependence of soil organic matter decomposition, and the effect of global warming on soil organic C storage. *Soil Biology and Biochemistry*, 27(6), 753-760. doi:10.1016/0038-0717(94)00242-S.
- Li, D., Dengsheng, L., Yunzhong, W., & Luo, K. (2022). Retrieval of eucalyptus planting history and stand age using random localization segmentation and continuous land-cover classification based on Landsat time-series data. *GIScience & Remote Sensing*, 59(1), 1426-1445. doi:10.1080/15481603.2022.2118440.
- Liu, X., Wang, S., Zhuang, Q., Jin, X., Bian, Z., Zhou, M., . . . Zhang, Y. (2022). A Review on Carbon Source and Sink in Arable Land Ecosystems. *Land*, 11(4). doi:10.3390/land11040580.
- Louzada, R. O., Bergier, I., Diniz, J. M. F. d. S., Guerra, A., & Roque, F. d. O. (2022). Priority setting for restoration in surrounding savannic areas of the Brazilian Pantanal based on soil loss risk and agrarian structure. *Journal of Environmental Management*, 323, 116219. doi:10.1016/j.jenvman.2022.116219.
- Louzada, R. O., Bergier, I., & Roque, F. d. O. (2023). The first inventory of gullies in the Upper Taquari River Basin (Brazil) and its agreement with land use classes. *Ecological Informatics*, 78, 102365. doi:10.1016/j.ecoinf.2023.102365.
- Lv, W., Yang, L., Xu, Z., & Zhang, Q. (2025). Spatiotemporal evolution of farmland ecosystem stability in the Fenhe River Basin China based on perturbation-resistance-response framework. *Ecological Informatics*, 86, 102977. doi:10.1016/j.ecoinf.2024.102977.
- Macdonald, C. A., Delgado-Baquerizo, M., Reay, D. S., Hicks, L. C., & Singh, B. K. (2018). Chapter 6 - Soil Nutrients and Soil Carbon Storage: Modulators and Mechanisms. In B. K. Singh (Ed.), *Soil Carbon Storage* (pp. 167-205): Academic Press.
- Majoro, F., Wali, U. G., Munyaneza, O., Narambuye, F.-X., & Mukamwambali, C. (2020). On-site and off-site effects of soil erosion: causal analysis and remedial measures in agricultural land-a review. *Rwanda Journal of Engineering, Science, Technology and Environment*, 3(2).

doi:10.4314/rjeste.v3i2.1.

Makaske, B., Maathuis, B. H. P., Padovani, C. R., Stolker, C., Mosselman, E., & Jongman, R. H. G. (2012). Upstream and downstream controls of recent avulsions on the Taquari megafan, Pantanal, south-western Brazil. *Earth Surface Processes and Landforms*, 37(12), 1313-1326. doi:10.1002/esp.3278.

Marengo, J. A., Oliveira, G. S., & Alves, L. M. (2015). Climate change scenarios in the Pantanal. In *Dynamics of the pantanal wetland in South America* (pp. 227-238): Springer.

Mathieu, R., Pouget, M., Cervelle, B., & Escadafal, R. (1998). Relationships between Satellite-Based Radiometric Indices Simulated Using Laboratory Reflectance Data and Typic Soil Color of an Arid Environment. *Remote Sensing of Environment*, 66(1), 17-28. doi:10.1016/S0034-4257(98)00030-3.

Minaei, M., Shafizadeh-Moghadam, H., & Tayyebi, A. (2018). Spatiotemporal nexus between the pattern of land degradation and land cover dynamics in Iran. *Land Degradation & Development*, 29(9), 2854-2863. doi:10.1002/ldr.3007.

Nguyen, C. T., Chidthaisong, A., Kieu Diem, P., & Huo, L.-Z. (2021). A Modified Bare Soil Index to Identify Bare Land Features during Agricultural Fallow-Period in Southeast Asia Using Landsat 8. *Land*, 10(3). doi:10.3390/land10030231.

Obeidat, M., Awawdeh, M., & Lababneh, A. (2019). Assessment of land use/land cover change and its environmental impacts using remote sensing and GIS techniques, Yarmouk River Basin, north Jordan. *Arabian Journal of Geosciences*, 12(22), 685. doi:10.1007/s12517-019-4905-z.

Oñate-Valdivieso, F., Oñate-Paladines, A., & Díaz, R. (2024). Soil degradation in andean watersheds: a case study using remote sensing. *12*. doi:10.3389/feart.2024.1325189.

Osman, K. T. (2014). Soil Erosion by Water. In K. T. Osman (Ed.), *Soil Degradation, Conservation and Remediation* (pp. 69-101). Dordrecht: Springer Netherlands.

Pedrinho, A., Mendes, L. W., de Araujo Pereira, A. P., Araujo, A. S. F., Vaishnav, A., Karpouzias, D. G., & Singh, B. K. (2024). Soil microbial diversity plays an important role in resisting and restoring degraded ecosystems. *Plant and Soil*, 500(1), 325-349. doi:10.1007/s11104-024-06489-x.

Pompeu, J., Assis, T. O., & Ometto, J. P. (2024). Landscape changes in the Cerrado: Challenges of land clearing, fragmentation and land tenure for biological conservation. *Science of The Total Environment*, 906, 167581. doi:10.1016/j.scitotenv.2023.167581.

Pregitzer, K., & King, J. (2005). Effects of soil temperature on nutrient uptake. In *Nutrient acquisition by plants: an ecological perspective* (pp. 277-310): Springer.

Qi, J., Chehbouni, A., Huete, A. R., Kerr, Y. H., & Sorooshian, S. (1994). A modified soil adjusted vegetation index. *Remote Sensing of Environment*, 48(2), 119-126. doi:10.1016/0034-4257(94)90134-1.

R Core Team, R, 2013. R: A language and environment for statistical computing. In: R Foundation for Statistical Computing Vienna, Austria.

Rashmi, I., Karthika, K. S., Roy, T., Shinoji, K. C., Kumawat, A., Kala, S., & Pal, R. (2022). Soil Erosion and Sediments: A Source of Contamination and Impact on Agriculture Productivity. In M. Naeem, J. F. J. Bremont, A. A. Ansari, & S. S. Gill (Eds.), *Agrochemicals in Soil and Environment: Impacts and Remediation* (pp. 313-345). Singapore: Springer Nature Singapore.

Raza, T., Qadir, M. F., Khan, K. S., Eash, N. S., Yousuf, M., Chatterjee, S., . . . Oetting, J. N. (2023). Unraveling the potential of microbes in decomposition of organic matter and release of carbon in the ecosystem. *Journal of Environmental Management*, 344, 118529. doi:10.1016/j.jenvman.2023.118529.

Rouse, Jr. W., Haas, R. H., Schell, J. A., Deering, D. W., & Harlan, J. C. J. N. G. T. I. F. R., Greenbelt, Md. (1974). Monitoring the vernal advancement and retrogradation (green wave effect) of natural vegetation. 371.

Safanelli, J. L., Chabrillat, S., Ben-Dor, E., & Demattê, J. A. M. (2020). Multispectral Models from Bare Soil Composites for Mapping Topsoil Properties over Europe. *Remote Sensing*, 12(9).

doi:10.3390/rs12091369.

Salas, E. A. L., & Kumaran, S. S. (2023). Hyperspectral Bare Soil Index (HBSI): Mapping Soil Using an Ensemble of Spectral Indices in Machine Learning Environment. *Land*, 12(7). doi:10.3390/land12071375.

Salmona, Y. B., Matricardi, E. A., Skole, D. L., Silva, J. F., Coelho Filho, O. D., Pedlowski, M. A., . . . Souza, S. A. (2023). A Worrying Future for River Flows in the Brazilian Cerrado Provoked by Land Use and Climate Changes. *Sustainability*, 15(5). doi:10.3390/su15054251.

Santos, H. G. d., Jacomine, P. K. T., Anjos, L. d., Oliveira, V. d., Lumberras, J. F., Coelho, M. R., . . . Cunha, T. J. F. (2018). *Sistema brasileiro de classificação de solos* (Vol. 5 ed.). Embrapa: Brasília, DF.

Santos, G. L. d., Pereira, M. G., Delgado, R. C., Torres, J. L. R., da Silva Cravo, M. D., Barreto, A. C., & Magistrali, I. C. (2020). Evaluation of natural regeneration and recovery of environmental services in a watershed in the Cerrado-Brazil. *Environment, Development and Sustainability*, 22(6), 5571-5583. doi:10.1007/s10668-019-00440-2.

Schneider, S., Cassol, A., Leonardi, A., & Marinho, M. d. M. J. E. a. (2020). Os efeitos da pandemia da Covid-19 sobre o agronegócio ea alimentação. 34(100), 167-188. doi:10.1590/s0103-4014.2020.34100.011.

Scholes, R. J. (2016). Climate change and ecosystem services. *WIREs Climate Change*, 7(4), 537-550. doi:10.1002/wcc.404.

Setyawan, C., Lee, C.-Y., & Prawitasari, M. (2019). Investigating spatial contribution of land use types and land slope classes on soil erosion distribution under tropical environment. *Natural Hazards*, 98(2), 697-718. doi:10.1007/s11069-019-03725-x.

Silva, V. d. P. R. d., Silva, M. T., Singh, V. P., de Souza, E. P., Braga, C. C., de Holanda, R. M., . . . Braga, A. C. R. (2018). Simulation of stream flow and hydrological response to land-cover changes in a tropical river basin. *CATENA*, 162, 166-176. doi:10.1016/j.catena.2017.11.024.

Silva, T. R., Silva, T. R., Sano, E. E., & Vieira, D. L. M. (2023). Mapping the regeneration potential of native vegetation in cultivated pastures of the Brazilian Cerrado. *Environmental Monitoring and Assessment*, 195(9), 1038. doi:10.1007/s10661-023-11606-x.

Silva, R. F. B., Viña, A., de Castro Victoria, D., Batistella, M., Martha, G. B., Moran, E. F., & Liu, J. (2025). Compound effects of drought and COVID-19 on soybean production in Brazil: Challenges and policy responses. *Science of The Total Environment*, 971, 179047. doi:10.1016/j.scitotenv.2025.179047.

Singh, M., & Hartsch, K. (2019). Basics of soil erosion. In *Watershed Hydrology, Management and Modeling* (pp. 1-61): CRC Press.

Singh, A., & Vyas, V. (2022). A Review on remote sensing application in river ecosystem evaluation. *Spatial Information Research*, 30(6), 759-772. doi:10.1007/s41324-022-00470-5.

Souza, C. M., Z. Shimbo, J., Rosa, M. R., Parente, L. L., A. Alencar, A., Rudorff, B. F. T., . . . Azevedo, T. (2020). Reconstructing Three Decades of Land Use and Land Cover Changes in Brazilian Biomes with Landsat Archive and Earth Engine. 12(17), 2735. doi:10.3390/rs12172735.

Sousa, G. P. B. d., Bellinaso, H., Rosas, J. T. F., Mello, D. C. d., Rosin, N. A., Amorim, M. T. A., . . . Demattê, J. A. M. (2024). Assessing soil degradation in Brazilian agriculture by a remote sensing approach to monitor bare soil frequency: impact on soil carbon. *Soil Advances*, 2, 100011. doi:10.1016/j.soilad.2024.100011.

Sun, S., Lü, Y., Feng, X., Maestre, F. T., & Fu, B. (2025). Optimizing soil conservation through comprehensive benefit assessment in river basins. *Environmental Science and Ecotechnology*, 23, 100496. doi:10.1016/j.ese.2024.100496.

Thielen, D., Schuchmann, K.-L., Ramoni-Perazzi, P., Marquez, M., Rojas, W., Quintero, J. I., & Marques, M. I. (2020). Quo vadis Pantanal? Expected precipitation extremes and drought dynamics from changing sea surface temperature. *Plos One*, 15(1), e0227437. doi:10.1371/journal.pone.0227437.

- Ul Haq, Y., Shahbaz, M., Asif, H. M. S., Al-Laith, A., Alsabban, W., & Aziz, M. H. (2022). Identification of soil type in Pakistan using remote sensing and machine learning. *PeerJ Computer Science*, 8, e1109. doi:10.7717/peerj-cs.1109.
- Valeriano, M. M. (2005). Modelo digital de variáveis morfométricas com dados SRTM para o território nacional: o projeto TOPODATA. In: XII Simpósio Brasileiro de Sensoriamento Remoto, 2005, Goiânia, GO. Anais do XII Simpósio Brasileiro de Sensoriamento Remoto. p. 1-8.
- Valle Júnior, R. F. d., Siqueira, H. E., Valera, C. A., Oliveira, C. F., Sanches Fernandes, L. F., Moura, J. P., & Pacheco, F. A. L. (2019). Diagnosis of degraded pastures using an improved NDVI-based remote sensing approach: An application to the Environmental Protection Area of Uberaba River Basin (Minas Gerais, Brazil). *Remote Sensing Applications: Society and Environment*, 14, 20-33. doi:10.1016/j.rsase.2019.02.001.
- Vieira, R. M. d. S. P., Tomasella, J., Barbosa, A. A., Polizel, S. P., Ometto, J. P. H. B., Santos, F. C., . . . Toledo, P. M. d. (2021). Land degradation mapping in the MATOPIBA region (Brazil) using remote sensing data and decision-tree analysis. *Science of The Total Environment*, 782, 146900. doi:10.1016/j.scitotenv.2021.146900.
- Wang, N., Naz, I., Aslam, R. W., Quddoos, A., Soufan, W., Raza, D., . . . Ahmed, B. (2024). Spatio-Temporal Dynamics of Rangeland Transformation using machine learning algorithms and Remote Sensing data. *Rangeland Ecology & Management*, 94, 106-118. doi:10.1016/j.rama.2024.02.008.
- Xu, D., Guo, X., Li, Z., Yang, X., & Yin, H. (2014). Measuring the dead component of mixed grassland with Landsat imagery. *Remote Sensing of Environment*, 142, 33-43. doi:10.1016/j.rse.2013.11.017.
- Yilgan, F., Miháliková, M., Kara, R. S., & Ustuner, M. (2024). Analysis of the forest fire in the 'Bohemian Switzerland' National Park using Landsat-8 and Sentinel-5P in Google Earth Engine. *Natural Hazards*. doi:10.1007/s11069-024-07052-8.
- Yu, B., Zang, Y., Wu, C., & Zhao, Z. (2024). Spatiotemporal dynamics of wetlands and their future multi-scenario simulation in the Yellow River Delta, China. *Journal of Environmental Management*, 353, 120193. doi:10.1016/j.jenvman.2024.120193.
- Zeileis, A., Leisch, F., Hornik, K., & Kleiber, C. (2002). strucchange: An R Package for Testing for Structural Change in Linear Regression Models. *Journal of Statistical Software*, 7(2), 1 - 38. doi:10.18637/jss.v007.i02.
- Zhai, Y., Roy, D. P., Martins, V. S., Zhang, H. K., Yan, L., & Li, Z. (2022). Conterminous United States Landsat-8 top of atmosphere and surface reflectance tasseled cap transformation coefficients. *Remote Sensing of Environment*, 274, 112992. doi:10.1016/j.rse.2022.112992.
- Zhao, H., & Chen, X. (2005). *Use of normalized difference bareness index in quickly mapping bare areas from TM/ETM+*. Paper presented at the International geoscience and remote sensing symposium.
- Zhou, M., Dengqiu, L., Kuo, L., & Lu, D. (2023). Integration of Landsat time-series vegetation indices improves consistency of change detection. *International Journal of Digital Earth*, 16(1), 1276-1299. doi:10.1080/17538947.2023.2200040.

Chapter 5

- Abreu, U. G. P., McManus, C., & Santos, S. (2010). Cattle ranching, conservation and transhumance in the Brazilian Pantanal. *Pastoralism*, 1(1), 99-114.
- Alho, C. J., & Sabino, J. (2012). Seasonal Pantanal flood pulse: implications for biodiversity. *Oecologia Australis*, 16(4), 958-978.
- Alho, C. J., Mamede, S. B., Benites, M., Andrade, B. S., & Sepulveda, J. J. (2019). Threats to the biodiversity of the Brazilian Pantanal due to land use and occupation. *Ambiente & Sociedade*, 22.
- Allen, C. R., Cumming, G. S., Garmestani, A. S., Taylor, P. D., & Walker, B. H. (2011).

- Managing for resilience. *Wildlife Biology*, 17(4), 337-349.
- Assine, M. L. (2005). River avulsions on the Taquari megafan, Pantanal wetland, Brazil. *Geomorphology*, 70(3), 357-371.
- Assine, M. L., Merino, E. R., Pupim, F. d. N., Macedo, H. d. A., & Santos, M. G. M. d. (2015a). The Quaternary alluvial systems tract of the Pantanal Basin, Brazil. *Brazilian Journal of Geology*, 45, 475-489.
- Assine, M. L., Macedo, H. A., Stevaux, J. C., Bergier, I., Padovani, C. R., & Silva, A. (2015b). Avulsive rivers in the hydrology of the pantanal wetland Dynamics of the Pantanal wetland in South America (pp. 83-110): Springer.
- Baigún, C. R., & Minotti, P. G. (2021). Conserving the Paraguay-Paraná Fluvial Corridor in the XXI Century: Conflicts, Threats, and Challenges. *Sustainability*, 13(9).
- Ballut-Dajud, G. A., Sandoval Herazo, L. C., Fernández-Lambert, G., Marín-Muñiz, J. L., López Méndez, M. C., & Betanzo-Torres, E. A. (2022). Factors Affecting Wetland Loss: A Review. *Land*, 11(3).
- Bergier, I. (2013). Effects of highland land-use over lowlands of the Brazilian Pantanal. *Science of The Total Environment*, 463-464, 1060-1066.
- Bergier, I., Assine, M.L., McGlue, M.M., Alho, C.J., Silva, A., Guerreiro, R.L., Carvalho, J. C. (2018). Amazon rainforest modulation of water security in the Pantanal wetland. *Science of The Total Environment*. 619, 1116–1125.
- Bergier, I., & Assine, M. L. (2022). Functional fluvial landforms of the Pantanal: Hydrologic trends and responses to climate changes. *Journal of South American Earth Sciences*, 119, 103977.
- Borges Pinto, O., Marques, A. C., & Vourlitis, G. L. (2020). Aboveground Carbon Storage and Cycling of Flooded and Upland Forests of the Brazilian Pantanal. *Forests*, 11(6).
- Brilha, J., Gray, M., Pereira, D. I., & Pereira, P. (2018). Geodiversity: An integrative review as a contribution to the sustainable management of the whole of nature. *Environmental Science & Policy*, 86, 19-28.
- Chiaravalloti, R. M. (2017). Overfishing or Over Reacting? Management of Fisheries in the Pantanal Wetland, Brazil. *Conservation and Society*, 15(1), 111-122.
- Colman, C. B., Oliveira, P. T. S., Almagro, A., Soares-Filho, B. S., & Rodrigues, D. B. B. (2019). Effects of Climate and Land-Cover Changes on Soil Erosion in Brazilian Pantanal. *Sustainability*, 11(24).
- Coutinho, B. A., Pott, V. J., Arrua, B. A., Aoki, C., & Pott, A. (2018). Ecological succession of aquatic macrophytes on floating meadows in the Pantanal wetland. *Brazilian Journal of Botany*, 41(1), 65-75.
- Dalmagro, H. J., de Souza, P. J., Engelbrecht, M. M., de Arruda, P. H. Z., Sallo, F. d. S., Vourlitis, G. L., . . . Couto, E. G. (2022). Net carbon dioxide exchange in a hyperseasonal cattle pasture in the northern Pantanal wetland of Brazil. *Agricultural and Forest Meteorology*, 324, 109099.
- Damasceno-Junior, G., Roque, F. d. O., Garcia, L., Ribeiro, D., Tomas, W., Scremin-Dias, E., . . . Pott, A. (2021). Lessons to be Learned from the Wildfire Catastrophe of 2020 in the Pantanal Wetland. *Wetland Sci. Pract*, 38, 107-115.
- Davidson, N. C. (2014). How much wetland has the world lost? Long-term and recent trends in global wetland area. *Marine and Freshwater Research*, 65(10), 934-941.
- Davidson, N. C., van Dam, A. A., Finlayson, C. M., & McInnes, R. J. (2019). Worth of wetlands: revised global monetary values of coastal and inland wetland ecosystem services. *Marine and Freshwater Research*, 70(8), 1189-1194.
- Dixon, M. J. R., Loh, J., Davidson, N. C., Beltrame, C., Freeman, R., & Walpole, M. (2016). Tracking global change in ecosystem area: The Wetland Extent Trends index. *Biological Conservation*, 193, 27-35.
- Eid, E. M., Galal, T. M., Sewelam, N. A., Talha, N. I., & Abdallah, S. M. (2020).

Phytoremediation of heavy metals by four aquatic macrophytes and their potential use as contamination indicators: a comparative assessment. *Environmental Science and Pollution Research*, 27(11), 12138-12151.

Freire, K. M. F., Tubino, R. A., Monteiro-Neto, C., Andrade-Tubino, M. F., Belruss, C. G., Tomás, A. R. G., . . . Vieira, J. P. (2016). Brazilian recreational fisheries: current status, challenges and future direction. *Fisheries Management and Ecology*, 23(3-4), 276-290.

Freitas, J. G., Furquim, S. A. C., Aravena, R., & Cardoso, E. L. (2019). Interaction between lakes' surface water and groundwater in the Pantanal wetland, Brazil. *Environmental Earth Sciences*, 78(5), 139.

Frey-Dargas, J. H.; Aoki, C.; Rosa, F. R.; Resende, E. K. (2014). Composição e distribuição de comunidades de peixes na planície de inundação do rio Taquari, Pantanal, MS. *Boletim de Pesquisa e Desenvolvimento (Embrapa Pantanal)*, v. unico, p. 01.

Guerra, A., Roque, F. d. O., Garcia, L. C., Ochoa-Quintero, J. M., Oliveira, P. T. S. d., Guariento, R. D., & Rosa, I. M. D. (2020). Drivers and projections of vegetation loss in the Pantanal and surrounding ecosystems. *Land Use Policy*, 91, 104388.

Gupta, J., van der Leeuw, K., & de Moel, H. (2007). Climate change: a 'glocal' problem requiring 'glocal' action. *Environmental Sciences*, 4(3), 139-148.

Hammer, Ø., Harper, D. A., & Ryan, P. D. J. P. e. (2001). PAST: Paleontological statistics software package for education and data analysis. 4(1), 9.

Harris, M. B., Tomas, W., Mourão, G., Da Silva, C. J., Guimarães, E., Sonoda, F., & Fachim, E. (2005). Safeguarding the Pantanal Wetlands: Threats and Conservation Initiatives. *Conservation Biology*, 19(3), 714-720.

Ide, C. N., Gonçalves, F. V., Latoria, G., Val, H. C., Silva, J. B., Steffen, J. L., . . . Broch, S. A. (2012). Soil and water conservation in the Upper Paraguay River Basin: examples from Mato Grosso do Sul, Brazil. In *Tropical Wetland Management: The South-American Pantanal and the International Experience* (pp. 99-133): Ashgate Publishing Farnham, UK.

Ioris, A. A. R. (2014). Approaches and Responses to Climate Change: Challenges for the Pantanal and the Upper Paraguay River Basin. In *Alternate Routes: A Journal of Critical Social Research* (Vol. 25).

Isles, P. D. F. (2020). The misuse of ratios in ecological stoichiometry. *Ecology*, 101(11), e03153.

Ivory, S. J., McGlue, M. M., Spera, S., Silva, A., & Bergier, I. (2019). Vegetation, rainfall, and pulsing hydrology in the Pantanal, the world's largest tropical wetland. *Environmental Research Letters*, 14(12), 124017.

Junk, W. J. (2005). Flood pulsing and the linkages between terrestrial, aquatic, and wetland systems. *SIL Proceedings, 1922-2010*, 29(1), 11-38.

Junk, W. J., Cunha, N. d., Thomaz, S. M., Agostinho, A. A., Ferreira, F. A., Filho, E. E. d. S., . . . Kawakita, K. (2021). Macrohabitat classification of wetlands as a powerful tool for management and protection: The example of the Paraná River floodplain, Brazil. *Ecohydrology & Hydrobiology*, 21(3), 411-424.

Leal Filho, W., Azeiteiro, U. M., Salvia, A. L., Fritzen, B., & Libonati, R. (2021). Fire in Paradise: Why the Pantanal is burning. *Environmental Science & Policy*, 123, 31-34.

Libonati, R., Geirinhas, J. L., Silva, P. S., Russo, A., Rodrigues, J. A., Belém, L. B., . . . Nunes, A. M. (2022). Assessing the role of compound drought and heatwave events on unprecedented 2020 wildfires in the Pantanal. *Environmental Research Letters*, 17(1), 015005.

Liu, J., Li, S., Ouyang, Z., Tam, C., & Chen, X. (2008). Ecological and socioeconomic effects of China's policies for ecosystem services. *Proceedings of the National Academy of Sciences*, 105(28), 9477-9482.

Lo, E. L., McGlue, M. M., Silva, A., Bergier, I., Yeager, K. M., de Azevedo Macedo, H., . . . Assine, M. L. (2019). Fluvio-lacustrine sedimentary processes and landforms on the distal Paraguay fluvial megafan (Brazil). *Geomorphology*, 342, 163-175.

- Lo, E. L., Yeager, K. M., Bergier, I., Domingos-Luz, L., Silva, A., & McGlue, M. M. (2022). Sediment Infill of Tropical Floodplain Lakes: Rates, Controls, and Implications for Ecosystem Services. *Frontiers in Earth Science*, 10.
- Loisel, J., & Walenta, J. (2022). Carbon parks could secure essential ecosystems for climate stabilization. *Nature Ecology & Evolution*, 6(5), 486-488.
- Louzada, R. O., Bergier, I., & Assine, M. L. (2020). Landscape changes in avulsive river systems: Case study of Taquari River on Brazilian Pantanal wetlands. *Science of The Total Environment*, 723, 138067.
- Louzada, R. O., Bergier, I., Roque, F. O., McGlue, M. M., Silva, A., & Assine, M. L. (2021). Avulsions drive ecosystem services and economic changes in the Brazilian Pantanal wetlands. *Current Research in Environmental Sustainability*, 3, 100057.
- Louzada, R. O., Bergier, I., Diniz, J. M. F. d. S., Guerra, A., & Roque, F. d. O. (2022). Priority setting for restoration in surrounding savannic areas of the Brazilian Pantanal based on soil loss risk and agrarian structure. *Journal of Environmental Management*, 323, 116219.
- Makaske, B., Maathuis, B. H., Padovani, C. R., Stolker, C., Mosselman, E., & Jongman, R. H. (2012). Upstream and downstream controls of recent avulsions on the Taquari megafan, Pantanal, south-western Brazil. *Earth Surface Processes and Landforms*, 37(12), 1313-1326.
- Marengo, J. A., Cunha, A. P., Cuartas, L. A., Deusdará Leal, K. R., Broedel, E., Seluchi, M. E., . . . Bender, F. (2021). Extreme Drought in the Brazilian Pantanal in 2019–2020: Characterization, Causes, and Impacts. 3.
- Marques, J. F., Alves, M. B., Silveira, C. F., Amaral e Silva, A., Silva, T. A., dos Santos, V. J., & Calijuri, M. L. (2021). Fires dynamics in the Pantanal: Impacts of anthropogenic activities and climate change. *Journal of Environmental Management*, 299, 113586.
- Martins, P. I., Belém, L. B. C., Szabo, J. K., Libonati, R., & Garcia, L. C. (2022). Prioritising areas for wildfire prevention and post-fire restoration in the Brazilian Pantanal. *Ecological Engineering*, 176, 106517.
- McClain, M. E., Boyer, E. W., Dent, C. L., Gergel, S. E., Grimm, N. B., Groffman, P. M., . . . Pinay, G. (2003). Biogeochemical Hot Spots and Hot Moments at the Interface of Terrestrial and Aquatic Ecosystems. *Ecosystems*, 6(4), 301-312.
- Mitsch, W. J., Nedrich, S. M., Harter, S. K., Anderson, C., Nahlik, A. M., & Bernal, B. (2014). Sedimentation in created freshwater riverine wetlands: 15 years of succession and contrast of methods. *Ecological Engineering*, 72, 25-34.
- Nienhuis, J. H., Törnqvist, T. E., & Esposito, C. R. (2018). Crevasse Splays Versus Avulsions: A Recipe for Land Building With Levee Breaches. *Geophysical Research Letters*, 45(9), 4058-4067.
- Ostrovskaya, E., Douven, W., Schwartz, K., Pataki, B., Mukuyu, P., & Kagwa, R. C. (2013). Capacity for sustainable management of wetlands: Lessons from the WETwin project. *Environmental Science & Policy*, 34, 128-137.
- Pérez-Consuegra, N., Hoyos, N., Restrepo, J. C., Escobar, J., & Hoke, G. D. (2021). Contrasting climate controls on the hydrology of the mountainous Cauca River and its associated sedimentary basin: Implications for interpreting the sedimentary record. *Geomorphology*, 377, 107590.
- Pott, A., & Silva, J. S. V. d. (2016). Terrestrial and Aquatic Vegetation Diversity of the Pantanal Wetland. In I. Bergier & M. L. Assine (Eds.), *Dynamics of the Pantanal Wetland in South America* (pp. 111-131). Cham: Springer International Publishing.
- Reboita, M. S., Kuki, C. A. C., Marrafon, V. H., de Souza, C. A., Ferreira, G. W. S., Teodoro, T., & Lima, J. W. M. (2022). South America climate change revealed through climate indices projected by GCMs and Eta-RCM ensembles. *Climate Dynamics*, 58(1), 459-485.
- Reitsemá, R. E., Meire, P., & Schoelynck, J. (2018). The Future of Freshwater Macrophytes in a Changing World: Dissolved Organic Carbon Quantity and Quality and Its Interactions With Macrophytes. *Frontiers in Plant Science*, 9.

- Rejmankova, E. (2011). The role of macrophytes in wetland ecosystems. *Journal of Ecology and Environment*, 34(4), 333-345.
- Roque, F. d. O., Guerra, A., Johnson, M., Padovani, C., Corbi, J., Covich, A. P., . . . Yon, L. (2021). Simulating land use changes, sediment yields, and pesticide use in the Upper Paraguay River Basin: Implications for conservation of the Pantanal wetland. *Agriculture, Ecosystems & Environment*, 314, 107405.
- Rosa, M. R., Brancalion, P. H. S., Crouzeilles, R., Tambosi, L. R., Piffer, P. R., Lenti, F. E. B., . . . Metzger, J. P. Hidden destruction of older forests threatens Brazil's Atlantic Forest and challenges restoration programs. *Science Advances*, 7(4), eabc4547.
- Schulz, C., Whitney, B. S., Rossetto, O. C., Neves, D. M., Crabb, L., de Oliveira, E. C., . . . Saito, C. H. (2019). Physical, ecological and human dimensions of environmental change in Brazil's Pantanal wetland: Synthesis and research agenda. *Science of The Total Environment*, 687, 1011-1027.
- Shirley, E. A., & Gore, M. L. (2019). Trust in scientists and rates of noncompliance with a fisheries rule in the Brazilian Pantanal. *PLOS ONE*, 14(3), e0207973.
- Silva, J., & Abdon, M. d. M. (1998). Delimitação do Pantanal Brasileiro e suas sub-regiões. *Pesqui. Agropecu. Bras*, 33, 1703–1711.
- Singh, M., Sinha, R., & Tandon, S. K. (2021). Geomorphic connectivity and its application for understanding landscape complexities: a focus on the hydro-geomorphic systems of India. *Earth Surface Processes and Landforms*, 46(1), 110-130.
- Sivo, S. A., Fan, X., Witta, E. L., & Willse, J. T. (2006). The Search for "Optimal" Cutoff Properties: Fit Index Criteria in Structural Equation Modeling. *The Journal of Experimental Education*, 74(3), 267-288.
- Souza, C. M., Z. Shimbo, J., Rosa, M. R., Parente, L. L., A. Alencar, A., Rudorff, B. F. T., . . . Azevedo, T. (2020). Reconstructing Three Decades of Land Use and Land Cover Changes in Brazilian Biomes with Landsat Archive and Earth Engine. *12(17)*, 2735.
- Tomas, W. M., de Oliveira Roque, F., Morato, R. G., Medici, P. E., Chiaravalloti, R. M., Tortato, F. R., . . . Junk, W. J. (2019). Sustainability Agenda for the Pantanal Wetland: Perspectives on a Collaborative Interface for Science, Policy, and Decision-Making. *Tropical Conservation Science*, 12, 1940082919872634.
- Tortato, F., Ribas, C., Concone, H., & Hoogesteijn, R. (2022). Turismo de observação de mamíferos no Pantanal. *Boletim Do Museu Paraense Emílio Goeldi - Ciências Naturais*, 16(3), 351-370.
- Van Dyke, C. (2015). Boxing daze – using state-and-transition models to explore the evolution of socio-biophysical landscapes. *Progress in Physical Geography: Earth and Environment*, 39(5), 594-621.
- Vieira, L. C. G., Padial, A. A., Velho, L. F. M., Carvalho, P., & Bini, L. M. (2015). Concordance among zooplankton groups in a near-pristine floodplain system. *Ecological Indicators*, 58, 374-381.
- Wantzen, K. M. (2022). River culture: How socio-ecological linkages to the rhythm of the waters develop, how they are lost, and how they can be regained. *The Geographical Journal*, n/a(n/a). doi:10.1111/geoj.12476.
- Wohl, E. (2021). An Integrative Conceptualization of Floodplain Storage. *Reviews of Geophysics*, 59(2), e2020RG000724.
- Wosiacki, L. F. K., Suekame, H. K., Wood, M. S., Gonçalves, F. V., & Bleninger, T. (2021). Mapping of suspended sediment transport using acoustic methods in a Pantanal tributary. *Environmental Monitoring and Assessment*, 193(8), 493.
- Wu, X., Wang, S., Fu, B., Feng, X., & Chen, Y. (2019). Socio-ecological changes on the Loess Plateau of China after Grain to Green Program. *Science of The Total Environment*, 678, 565-573.
- Xi, Y., Peng, S., Ciais, P., & Chen, Y. (2021). Future impacts of climate change on inland

Ramsar wetlands. *Nature Climate Change*, 11(1), 45-51.

Zani, H., Assine, M. L., & McGlue, M. M. (2012). Remote sensing analysis of depositional landforms in alluvial settings: Method development and application to the Taquari megafan, Pantanal (Brazil). *Geomorphology*, 161-162, 82-92.

Zhang, W., Chang, W. J., Zhu, Z. C., & Hui, Z. (2020). Landscape ecological risk assessment of Chinese coastal cities based on land use change. *Applied Geography*, 117, 102174.

Zheng, S., Wu, B., Wang, K., Tan, G., Han, S., & Thorne, C. R. (2017). Evolution of the Yellow River delta, China: Impacts of channel avulsion and progradation. *International Journal of Sediment Research*, 32(1), 34-44.

Chapter 6

Alho, C. J. R. (2008). Biodiversity of the Pantanal: response to seasonal flooding regime and to environmental degradation. *Brazilian journal of biology*, 68, 957-966.

Amani, M., Salehi, B., Mahdavi, S., & Brisco, B. (2018). Spectral analysis of wetlands using multi-source optical satellite imagery. *ISPRS Journal of Photogrammetry and Remote Sensing*, 144, 119-136.

Amoakoh, A. O., Aplin, P., Awuah, K. T., Delgado-Fernandez, I., Moses, C., & Alonso, C. P. (2021, 11-16 July 2021). Tropical Peatland Classification Using Multi-Sensor Sentinel Imagery and Random Forest Algorithm in Greater Amanzule, Ghana. Paper presented at the 2021 IEEE International Geoscience and Remote Sensing Symposium IGARSS.

Amoros, C., Bornette, G., & Henry, C. P. (2000). A vegetation-based method for ecological diagnosis of riverine wetlands. *Environmental Management*, 25(2).

Antoniadis, A., Lambert-Lacroix, S., & Poggi, J.-M. (2021). Random forests for global sensitivity analysis: A selective review. *Reliability Engineering & System Safety*, 206, 107312.

Assine, M. L. (2005). River avulsions on the Taquari megafan, Pantanal wetland, Brazil. *Geomorphology*, 70(3), 357-371.

Assine, M. L., Padovani, C. R., Zacharias, A. A., Angulo, R. J., & de Souza, M. C. (2005). Compartimentação geomorfológica, processos de avulsão fluvial e mudanças de curso do Rio Taquari, Pantanal Mato-Grossense. *Revista Brasileira de Geomorfologia*, 6, 97-108.

Assine, M. L., Corradini, F. A., Pupim, F. d. N., & McGlue, M. M. (2014). Channel arrangements and depositional styles in the São Lourenço fluvial megafan, Brazilian Pantanal wetland. *Sedimentary Geology*, 301, 172-184.

Assine, M.L., Macedo, H.A., Stevaux, J.C., Bergier, I., Padovani, C.R., Silva, A. (2015a). Avulsive Rivers in the Hydrology of the Pantanal Wetland. In: Bergier, I., Assine, M. (eds) *Dynamics of the Pantanal Wetland in South America. The Handbook of Environmental Chemistry*, vol 37. Springer, Cham.

Assine, M. L., Merino, E. R., Pupim, F. D. N., Macedo, H. D. A., & Santos, M. G. M. D. (2015b). The Quaternary alluvial systems tract of the Pantanal Basin, Brazil. *Brazilian Journal of Geology*, 45, 475-489.

Babilônia de Sousa, J., Aparecida Pereira Pierangeli, M., Evaldo Serafim, M., & Alves de Souza, C. (2015). atributos morfológicos, físicos e químicos de solos e processos erosivos nas margens do Rio Paraguai, Pantanal Superior, Mato Grosso, Brasil. *Boletim de Geografia*, 33(1).

Bai, J., Guan, Y., Liu, P., Zhang, L., Cui, B., Li, X., & Liu, X. (2020). Assessing the safe operating space of aquatic macrophyte biomass to control the terrestrialization of a grass-type shallow lake in China. *Journal of Environmental Management*, 266, 110479.

Bannari, A., Morin, D., Bonn, F., & Huete, A. R. (1995). A review of vegetation indices. *Remote Sensing Reviews*, 13(1-2), 95-120.

Bao, F., Pott, A., Ferreira, F. A., & Arruda, R. (2014). Soil seed bank of floodable native and cultivated grassland in the Pantanal wetland: effects of flood gradient, season and species invasion. *Brazilian Journal of Botany*, 37(3), 239-250.

Belgiu, M., & Drăguț, L. (2016). Random forest in remote sensing: A review of applications

and future directions. *ISPRS Journal of Photogrammetry and Remote Sensing*, 114, 24-31.

Ben-Noah, I., & Friedman, S. P. (2018). Review and Evaluation of Root Respiration and of Natural and Agricultural Processes of Soil Aeration. *Vadose Zone Journal*, 17(1), 1701-19.

Bergier, I. (2013). Effects of highland land-use over lowlands of the Brazilian Pantanal. *Science of The Total Environment*, 463-464, 1060-1066.

Bergier, I., & Assine, M. L. (2022). Functional fluvial landforms of the Pantanal: Hydrologic trends and responses to climate changes. *Journal of South American Earth Sciences*, 119, 103977.

Bomer, E. J., Wilson, C. A., Hale, R. P., Hossain, A. N. M., & Rahman, F. M. A. (2020). Surface elevation and sedimentation dynamics in the Ganges-Brahmaputra tidal delta plain, Bangladesh: Evidence for mangrove adaptation to human-induced tidal amplification. *CATENA*, 187, 104312.

Breiman, L. (2001). Random Forests. *Machine Learning*, 45(1), 5-32.

Buehler, H. A., Weissmann, G. S., Scuderi, L. A., & Hartley, A. J. (2011). Spatial and Temporal Evolution of an Avulsion on the Taquari River Distributive Fluvial System from Satellite Image Analysis. *Journal of Sedimentary Research*, 81(8), 630-640.

Cardoso, E. L., Silva, M. L. N., Silva, C. A., Curi, N., & Freitas, D. A. F. d. (2010). Estoques de carbono e nitrogênio em solo sob florestas nativas e pastagens no bioma Pantanal. *Pesquisa Agropecuária Brasileira*, 45, 1028-1035.

Cardoso, E., Salis, S. d., Crispim, S., Fernandes, F., & Fernandes, A. (2017). Regeneração natural de áreas utilizadas como roça no Pantanal da Nhecolândia. In *Boletim de Pesquisa e Desenvolvimento. Embrapa Pantanal: Corumba/MS*.

Chiaravalloti, R. M., Tomas, W. M., Akre, T., Morato, R. G., Camilo, A. R., Giordano, A. J., & Leimgruber, P. (2023). Achieving conservation through cattle ranching: The case of the Brazilian Pantanal. *Conservation Science and Practice*, n/a(n/a). doi:10.1111/csp2.13006.

Coutinho, B. A., Pott, V. J., Arrua, B. A., Aoki, C., & Pott, A. (2018). Ecological succession of aquatic macrophytes on floating meadows in the Pantanal wetland. *Brazilian Journal of Botany*, 41(1), 65-75.

Couto, E. G., & Oliveira, M. D. d. (2011). The soil diversity of the Pantanal. In W. J. Junk, Da Silva, C.J., Nunes da Cunha, C., Wantzen, K.M. (Ed.), *The Pantanal: Ecology, biodiversity and sustainable management of a large neotropical seasonal wetland* (pp. 40-64): Pensoft Publishers, Sofia–Moscow.

Couto, E. G., Corrêa, G. R., Oliveira, V. A., do Nascimento, A. F., Vidal-Torrado, P., Beirigo, R., & Schaefer, C. E. G. R. (2023). Soils of Pantanal: The Largest Continental Wetland. In C. E. G. R. Schaefer (Ed.), *The Soils of Brazil* (pp. 239-267). Cham: Springer International Publishing.

Crist, E. P., & Cicone, R. C. (1984). A Physically-Based Transformation of Thematic Mapper Data---The TM Tasseled Cap. *Geoscience and Remote Sensing, IEEE Transactions on*, GE-22(3), 256-263.

Damasceno-Junior, G. A., Pereira, A. d. M. M., Oldeland, J., Parolin, P., & Pott, A. (2021). Fire, Flood and Pantanal Vegetation. In G. A. Damasceno-Junior & A. Pott (Eds.), *Flora and Vegetation of the Pantanal Wetland* (pp. 661-688). Cham: Springer International Publishing.

Demarquet, Q., Rapinel, S., Dufour, S., & Hubert-Moy, L. (2023). Long-Term Wetland Monitoring Using the Landsat Archive: A Review. *Remote Sensing*, 15(3).

Deng, Z., Huang, D., He, Q., & Chassagne, C. (2022). Review of the action of organic matter on mineral sediment flocculation. 10. doi:10.3389/feart.2022.965919.

Frazão, L. A., Píccolo, M. d. C., Feigl, B. J., Cerri, C. C., & Cerri, C. E. P. (2008). Propriedades químicas de um Neossolo Quartzarênico sob diferentes sistemas de manejo no Cerrado mato-grossense. *Pesquisa Agropecuária Brasileira*, 43, 641-648.

Ghiberto, P. J., Libardi, P. L., & Trivelin, P. C. O. (2015). Nutrient leaching in an Ultisol cultivated with sugarcane. *Agricultural Water Management*, 148, 141-149.

Gil, A. P., Padovani, C. R., & Coelho, A. L. N. (2019). Comparação entre NDWI e MNDWI para o mapeamento de áreas inundadas no Pantanal do Taquari. Paper presented at the XIX

- Simpósio Brasileiro de Sensoriamento Remoto (INPE), Santos.
- Greenway, M. (2007). The Role of Macrophytes in Nutrient Removal using Constructed Wetlands. In S. N. Singh & R. D. Tripathi (Eds.), *Environmental Bioremediation Technologies* (pp. 331-351). Berlin, Heidelberg: Springer Berlin Heidelberg.
- Guerra, A., Roque, F. d. O., Garcia, L. C., Ochoa-Quintero, J. M., Oliveira, P. T. S. d., Guariento, R. D., & Rosa, I. M. D. (2020). Drivers and projections of vegetation loss in the Pantanal and surrounding ecosystems. *Land Use Policy*, 91, 104388.
- Hajek, E. A., & Edmonds, D. A. (2014). Is river avulsion style controlled by floodplain morphodynamics? *Geology*, 42(3), 199-202.
- Hamilton, S. K., Sippel, S. J., & Melack, J. M. (1996). Inundation patterns in the Pantanal wetland of South America determined from passive microwave remote sensing. *Archiv für Hydrobiologie*, 137, 1-23.
- Ivory, S. J., McGlue, M. M., Spera, S., Silva, A., & Bergier, I. (2019). Vegetation, rainfall, and pulsing hydrology in the Pantanal, the world's largest tropical wetland. *Environmental Research Letters*, 14(12), 124017.
- Jackson, C. R., Thompson, J. A., & Kolka, R. K. (2014). Wetland soils, hydrology and geomorphology. In C. U. o. C. P.-C. Berkeley (Ed.), In: Batzer, D. Sharitz, R., eds. *Ecology of freshwater estuarine wetlands*. (pp. 23-60).
- Jeong, G., Oeverdieck, H., Park, S. J., Huwe, B., & Ließ, M. (2017). Spatial soil nutrients prediction using three supervised learning methods for assessment of land potentials in complex terrain. *CATENA*, 154, 73-84.
- Kuhn, M., Johnson, K., 2013. *Applied Predictive Modeling*. Springer, New York.
- Lacerda Filho, J. V. d., Brito, R. S. C. d., Silva, M. d. G. d., Oliveira, C. C. d., Moreton, L. C., Martins, E. G., . . . Valente, C. R. (2006). *Geologia e recursos minerais do estado de Mato Grosso do Sul*. CPRM; SEPROTUR/MS; EGRHP/MS.
- Leddy, J. O., Ashworth, P. J., & Best, J. L. (1993). Mechanisms of anabranch avulsion within gravel-bed braided rivers: observations from a scaled physical model. *Geological Society, London, Special Publications*, 75(1), 119-127.
- Li, F., Pan, Y., Xie, Y., Chen, X., Deng, Z., Li, X., . . . Tang, Y. (2016). Different roles of three emergent macrophytes in promoting sedimentation in Dongting Lake, China. *Aquatic Sciences*, 78(1), 159-169.
- Li, Y., Zhang, H., Fu, C., Tu, C., Luo, Y., & Christie, P. (2019). A red clay layer in soils of the Yellow River Delta: Occurrence, properties and implications for elemental budgets and biogeochemical cycles. *CATENA*, 172, 469-479.
- Li, Y., Fu, C., Hu, J., Zeng, L., Tu, C., & Luo, Y. (2023). Soil Carbon, Nitrogen, and Phosphorus Stoichiometry and Fractions in Blue Carbon Ecosystems: Implications for Carbon Accumulation in Allochthonous-Dominated Habitats. *Environmental Science & Technology*, 57(14), 5913-5923.
- Lisenby, P. E., Tooth, S., & Ralph, T. J. (2019). Product vs. process? The role of geomorphology in wetland characterization. *Science of The Total Environment*, 663, 980-991.
- Liu, C., Shen, Q., Gu, X., Zhang, L., Han, C., & Wang, Z. (2023). Burial or mineralization: Origins and fates of organic matter in the water-suspended particulate matter-sediment of macrophyte- and algae-dominated areas in Lake Taihu. *Water Research*, 243, 120414.
- Lo, E. L., Silva, A., Bergier, I., McGlue, M. M., de Paula Silva, B. L., Silva, A. P. S., . . . da Silva, E. R. d. S. (2017). Spatiotemporal evolution of the margins of Lake Uberaba, Pantanal floodplain (Brazil). *Geografia*, 42(3), 159-173.
- Lo, E. L., McGlue, M. M., Silva, A., Bergier, I., Yeager, K. M., de Azevedo Macedo, H., . . . Assine, M. L. (2019). Fluvio-lacustrine sedimentary processes and landforms on the distal Paraguay fluvial megafan (Brazil). *Geomorphology*, 342, 163-175.
- Lo, E. L., Silva, A., Kuerten, S., Louzada, R. O., Rasbold, G. G., & McGlue, M. M. (2023). Source-to-sink controls on modern fluvial sands in the Pantanal back-bulge basin (Brazil).

Sedimentologia, 1(1).

- Lolu, A. J., Ahluwalia, A. S., Sidhu, M. C., & Reshi, Z. A. (2019). Carbon Sequestration Potential of Macrophytes and Seasonal Carbon Input Assessment into the Hokersar Wetland, Kashmir. *Wetlands*, 39(3), 453-472.
- Louzada, R. O., Bergier, I., & Assine, M. L. (2020). Landscape changes in avulsive river systems: Case study of Taquari River on Brazilian Pantanal wetlands. *Science of The Total Environment*, 723, 138067.
- Louzada, R. O., Bergier, I., Roque, F. O., McGlue, M. M., Silva, A., & Assine, M. L. (2021). Avulsions drive ecosystem services and economic changes in the Brazilian Pantanal wetlands. *Current Research in Environmental Sustainability*, 3, 100057.
- Louzada, R. O., Bergier, I., Diniz, J. M. F. d. S., Guerra, A., & Roque, F. d. O. (2022). Priority setting for restoration in surrounding savannic areas of the Brazilian Pantanal based on soil loss risk and agrarian structure. *Journal of Environmental Management*, 323, 116219.
- Louzada, R. O., Roque, F. d. O., Diniz, J. M. F. d. S., & Bergier, I. (2023a). River channel avulsion in the Taquari River megafan of the Brazilian Pantanal: Remote sensing and modeling reveal recent and future changes. *Applied Geography*, 155, 102955.
- Louzada, R. O., Bergier, I., & Roque, F. d. O. (2023b). The first inventory of gullies in the Upper Taquari River Basin (Brazil) and its agreement with land use classes. *Ecological Informatics*, 78, 102365.
- Luo, J., Ni, G., Zhang, Y., Wang, K., Shen, M., Cao, Z., . . . Duan, H. (2023). A new technique for quantifying algal bloom, floating/emergent and submerged vegetation in eutrophic shallow lakes using Landsat imagery. *Remote Sensing of Environment*, 287, 113480.
- Makaske, B., Maathuis, B. H. P., Padovani, C. R., Stolker, C., Mosselman, E., & Jongman, R. H. G. (2012). Upstream and downstream controls of recent avulsions on the Taquari megafan, Pantanal, south-western Brazil. *Earth Surface Processes and Landforms*, 37(12), 1313-1326.
- Maltby, E., & Acreman, M. C. (2011). Ecosystem services of wetlands: pathfinder for a new paradigm. *Hydrological Sciences Journal*, 56(8), 1341-1359.
- Malthus, T. J. (2017). Chapter 9 - Bio-optical Modeling and Remote Sensing of Aquatic Macrophytes. In D. R. Mishra, I. Ogashawara, & A. A. Gitelson (Eds.), *Bio-optical Modeling and Remote Sensing of Inland Waters* (pp. 263-308): Elsevier.
- Marengo, J. A., Cunha, A. P., Cuartas, L. A., Deusdará Leal, K. R., Broedel, E., Seluchi, M. E., . . . Bender, F. (2021). Extreme Drought in the Brazilian Pantanal in 2019–2020: Characterization, Causes, and Impacts. 3.
- Marcinkowski, P., Kiczko, A., & Okruszko, T. (2018). Model-Based Analysis of Macrophytes Role in the Flow Distribution in the Anastomosing River System. *Water*, 10(7).
- Mato Grosso do Sul. (1989). *Macrozoneamento Geoambiental do Estado de Mato Grosso do Sul*. SECRETARIA DE PLANEJAMENTO E COORDENAÇÃO GERAL-SEPLAN-MS.
- May, J.-H., Plotzki, A., Rodrigues, L., Preusser, F., & Veit, H. (2015). Holocene floodplain soils along the Río Mamoré, northern Bolivia, and their implications for understanding inundation and depositional patterns in seasonal wetland settings. *Sedimentary Geology*, 330, 74-89.
- Mishra, N. B. (2020). Wetlands: remote sensing. In *Wetlands and Habitats* (pp. 201-212): CRC Press.
- Mitsch, W. J., Zhang, L., Anderson, C. J., Altor, A. E., & Hernández, M. E. (2005). Creating riverine wetlands: Ecological succession, nutrient retention, and pulsing effects. *Ecological Engineering*, 25(5), 510-527.
- Mitsch, W. J., Nahlik, A., Wolski, P., Bernal, B., Zhang, L., & Ramberg, L. (2010). Tropical wetlands: seasonal hydrologic pulsing, carbon sequestration, and methane emissions. *Wetlands Ecology and Management*, 18(5), 573-586.
- Mitsch, W. J., Bernal, B., & Hernandez, M. E. (2015). Ecosystem services of wetlands. *International Journal of Biodiversity Science, Ecosystem Services & Management*, 11(1), 1-4.

- Morais, M. d., Abdo, M. S. A., dos Santos, C., Sander, N. L., da Silva Nunes, J. R., Lázaro, W. L., & da Silva, C. J. (2022). Long-term analysis of aquatic macrophyte diversity and structure in the Paraguay river ecological corridor, Brazilian Pantanal wetland. *Aquatic Botany*, 178, 103500.
- Mu, S., You, K., Song, T., Li, Y., Wang, L., & Shi, J. (2023). Identification for the species of aquatic higher plants in the Taihu Lake basin based on hyperspectral remote sensing. *Environmental Monitoring and Assessment*, 195(8), 989. doi:10.1007/s10661-023-11523-z.
- Nascimento, A. F. d., Furquim, S. A. C., Couto, E. G., Beirigo, R. M., Oliveira Júnior, J. C. d., Camargo, P. B. d., & Vidal-Torrado, P. (2013). Genesis of textural contrasts in subsurface soil horizons in the Northern Pantanal-Brazil. *Revista Brasileira de Ciência do Solo*, 37, 1113-1127.
- Nascimento, D. C., Corrêa, G. R., Gradella, F. d. S., Campos, P. V., Koch, V. A., & Vasconcelos, B. N. F. (2023). Solos de ambientes lacustres do Pantanal Sul-Mato-Grossense. *Sociedade & Natureza*, 35, e67560.
- Oliveira, P. C. d., Torezan, J. M. D., & Cunha, C. N. d. (2015). Effects of flooding on the spatial distribution of soil seed and spore banks of native grasslands of the Pantanal wetland. *Acta Botanica Brasilica*, 29, 400-407.
- Oliveira, M. D. d., Calheiros, D. F., & Hamilton, S. K. (2019). Mass balances of major solutes, nutrients and particulate matter as water moves through the floodplains of the Pantanal (Paraguay River, Brazil). *Revista Brasileira de Recursos Hídricos*, 24.
- Oliveira Junior, J. C. d., Beirigo, R. M., Chiapini, M., do Nascimento, A. F., Couto, E. G., & Vidal-Torrado, P. (2017). Origin of mounds in the Pantanal wetlands: An integrated approach between geomorphology, pedogenesis, ecology and soil micromorphology. *PLOS ONE*, 12(7), e0179197.
- Paccagnella, Y. C., Bianchini, I., & da Cunha-Santino, M. B. (2020). Decomposition dynamics of two aquatic macrophytes: response of litter interaction with temperature and dissolved oxygen availability. *Brazilian Journal of Botany*, 43(4), 1047-1059.
- Pal, S., Chattopadhyay, B., Datta, S., & Mukhopadhyay, S. K. (2017). Potential of Wetland Macrophytes to Sequester Carbon and Assessment of Seasonal Carbon Input into the East Kolkata Wetland Ecosystem. *Wetlands*, 37(3), 497-512.
- Passerini, M. D., Cunha-Santino, M. B., & Bianchini, I. (2016). Oxygen availability and temperature as driving forces for decomposition of aquatic macrophytes. *Aquatic Botany*, 130, 1-10.
- Pedersen, O., Colmer, T. D., & Sand-Jensen, K. (2013). *Underwater Photosynthesis of Submerged Plants – Recent Advances and Methods*. 4.
- Pereira, G., Ramos, R. d. C., Rocha, L. C., Brunzell, N. A., Merino, E. R., Mataveli, G. A. V., & Cardozo, F. d. S. (2021). Rainfall patterns and geomorphological controls driving inundation frequency in tropical wetlands: How does the Pantanal flood? *Progress in Physical Geography: Earth and Environment*, 45(5), 669-686.
- Pereira, L. E., Lo, E. L., & Paranhos Filho, A. C. (2022). Analysis of the Taquari Megafan through radiometric indices. *Journal of South American Earth Sciences*, 119, 104034.
- Petsch, D. K., Cionek, V. d. M., Thomaz, S. M., & dos Santos, N. C. L. (2023). Ecosystem services provided by river-floodplain ecosystems. *Hydrobiologia*, 850(12), 2563-2584.
- Pott, A., Oliveira, A. K., Damasceno-Junior, G. A., & Silva, J. S. (2011). Plant diversity of the Pantanal wetland. *Brazilian journal of biology*, 71, 265-273.
- Pott, A., & Silva, J. S. V. d. (2016). Terrestrial and Aquatic Vegetation Diversity of the Pantanal Wetland. In I. Bergier & M. L. Assine (Eds.), *Dynamics of the Pantanal Wetland in South America* (pp. 111-131). Cham: Springer International Publishing.
- Queiroz, R. F. P. d., Corrêa, G. R., dos Santos Gradella, F., & Rosa, G. P. (2019). Gradiente edáfico define as fitofisionomias do pantanal do abobral, Brasil. *Oecologia Australis*, 23(4).
- R Core Team, R, 2013. R: A language and environment for statistical computing. In: R Foundation for Statistical Computing Vienna, Austria.

- Remor, M. B., Vilas Boas, M. A., Sampaio, S. C., Damatto, S. R., Stevaux, J. C., & dos Reis, R. R. (2022). Sedimentation rate and accumulation of nutrients in the Upper Paraná river floodplain. *Journal of Radioanalytical and Nuclear Chemistry*, 331(2), 1019-1027.
- Roque, F. d. O., Guerra, A., Johnson, M., Padovani, C., Corbi, J., Covich, A. P., . . . Yon, L. (2021). Simulating land use changes, sediment yields, and pesticide use in the Upper Paraguay River Basin: Implications for conservation of the Pantanal wetland. *Agriculture, Ecosystems & Environment*, 314, 107405.
- Rovira, A., Alcaraz, C., & Trobajo, R. (2016). Effects of plant architecture and water velocity on sediment retention by submerged macrophytes. *Freshwater Biology*, 61(5), 758-768.
- Saidi, S., Ayoubi, S., Shirvani, M., Azizi, K., & Zeraatpisheh, M. (2022). Comparison of Different Machine Learning Methods for Predicting Cation Exchange Capacity Using Environmental and Remote Sensing Data. *Sensors*, 22(18).
- Santos, H. G. d., Jacomine, P. K. T., dos;, A. L. H. C., Oliveira, V. A. d., Lumbrreras, J. F., Coelho, M. R., . . . Cunha, T. J. F. (2018). *Sistema brasileiro de classificação de solos*. Embrapa Solos: Centro Nacional de Pesquisa de Solos: Rio de Janeiro.
- Santos, S. A., Cardoso, E. L., Valls, J. F. M., & Pott, A. (2021). Natural Pastures of the Pantanal: Diversity, Productive Potential and Dynamics. In G. A. Damasceno-Junior & A. Pott (Eds.), *Flora and Vegetation of the Pantanal Wetland* (pp. 471-489). Cham: Springer International Publishing.
- Samarawickrama, U., Piyaratne, D., & Ranagalage, M. (2017). Relationship between NDVI with Tasseled cap indices: A remote sensing based analysis. *International Journal of Innovative Research in Technology*, 3(12), 13-19.
- Saralegui, A. B., Willson, V., Caracciolo, N., Piol, M. N., & Boeykens, S. P. (2021). Macrophyte biomass productivity for heavy metal adsorption. *Journal of Environmental Management*, 289, 112398.
- Sharma, R., Vymazal, J., & Malaviya, P. (2021). Application of floating treatment wetlands for stormwater runoff: A critical review of the recent developments with emphasis on heavy metals and nutrient removal. *Science of The Total Environment*, 777, 146044.
- Shen, R., Yang, H., Rinklebe, J., Bolan, N., Hu, Q., Huang, X., . . . Shi, L. (2022). Seasonal flooding wetland expansion would strongly affect soil and sediment organic carbon storage and carbon-nutrient stoichiometry. *Science of The Total Environment*, 828, 154427.
- Slingerland, R., & Smith, N. D. (2004). River avulsions and their deposits. *Annual Review of Earth and Planetary Sciences*, 32(1), 257-285. doi:10.1146/annurev.earth.32.101802.120201.
- Smith, N. D., Cross, T. A., Dufficy, J. P., & Clough, S. R. (1989). Anatomy of an avulsion. *Sedimentology*, 36(1), 1-23.
- Teixeira, P. C., Donagemma, G. K., Fontana, A., & Teixeira, W. G. (2017). *Manual de métodos de análise de solo*. In: Embrapa Brasília, DF.
- Tiner, R. W. (2016). *Wetland indicators: A guide to wetland formation, identification, delineation, classification, and mapping*: CRC press.
- Tooth, S. (2018). The geomorphology of wetlands in drylands: Resilience, nonresilience, or . . .? *Geomorphology*, 305, 33-48.
- Valenza, J. M., Edmonds, D. A., Hwang, T., & Roy, S. (2020). Downstream changes in river avulsion style are related to channel morphology. *Nature Communications*, 11(1), 2116.
- Valenza, J. M., Edmonds, D. A., & Weissmann, G. S. (2022). Quantifying river avulsion activity from satellite remote sensing: Implications for how avulsions contribute to floodplain stratigraphy in foreland basins. *Journal of Sedimentary Research*, 92(6), 487-502.
- Varghese, D., Radulović, M., Stojković, S., & Crnojević, V. (2021). Reviewing the Potential of Sentinel-2 in Assessing the Drought. *Remote Sensing*, 13(17).
- Villa, P., Mousivand, A., & Bresciani, M. (2014). Aquatic vegetation indices assessment through radiative transfer modeling and linear mixture simulation. *International Journal of Applied Earth Observation and Geoinformation*, 30, 113-127.

- Vourlitis, G. L., de Almeida Lobo, F., Pinto, O. B., Zappia, A., Dalmagro, H. J., de Arruda, P. H. Z., & de Souza Nogueira, J. (2015). Variations in aboveground vegetation structure along a nutrient availability gradient in the Brazilian pantanal. *Plant and Soil*, 389(1), 307-321.
- Vourlitis, G. L., Hentz, C. S., Pinto, O. B., Carneiro, E., & de Souza Nogueira, J. (2017). Soil N, P, and C dynamics of upland and seasonally flooded forests of the Brazilian Pantanal. *Global Ecology and Conservation*, 12, 227-240.
- Xu, H.-Q. (2005). A study on information extraction of water body with the modified normalized difference water index (MNDWI). *Journal of Remote Sensing*, 5, 589-595.
- Zani, H., Assine, M. L., & McGlue, M. M. (2012). Remote sensing analysis of depositional landforms in alluvial settings: Method development and application to the Taquari megafan, Pantanal (Brazil). *Geomorphology*, 161-162, 82-92.
- Wantzen, K. M., Drago, E., & Da Silva, C. J. (2005). Aquatic habitats of the Upper Paraguay River-Floodplain-System and parts of the Pantanal(Brazil). *Ecohydrology & Hydrobiology*, 5(2), 107-126.
- Whyte, A., Ferentinos, K. P., & Petropoulos, G. P. (2018). A new synergistic approach for monitoring wetlands using Sentinels -1 and 2 data with object-based machine learning algorithms. *Environmental Modelling & Software*, 104, 40-54.

